

# Cementitious Grouts for ILW Encapsulation – Composition, Hydration and Performance.

Joshua Dean Hawthorne

Submitted in accordance with the requirements for the degree of  
Doctor of Philosophy

The University of Leeds  
School of Chemical and Process Engineering

September 2016

The candidate confirms that the work submitted is his own and that appropriate credit has been given where reference has been made to the work of others.

This copy has been supplied on the understanding that it is copyright material and that no quotation from the thesis may be published without proper acknowledgement.

© 2016. The University of Leeds and Joshua D. Hawthorne.



## Acknowledgements

I'd like to start by expressing my gratitude to my supervisor, Dr. Leon Black. His passion, support and guidance have been constant throughout this project, I'll be forever grateful for his help and encouragement. More than that though, I'll take with me a passion to share knowledge and experience in an effort to engender co-operation and generosity throughout my future working life, in very much the way Leon has, and continues to do.

I am grateful to the other academics of the University of Leeds who have provided insight and ideas as well as technical support and cross-disciplinary experience. Dr. Xiaodong Jia for his help with X-ray CT and post-processing techniques; Prof. Bruce Hanson for providing great industrial context and helping with promoting links with industrial support; the other academic members of the Leeds Nuclear Group – Dr. Tim Hunter, Dr. David Harbottle and Prof. Mike Fairweather for their thought-provoking and stimulating input at group meetings.

Thanks must go to Gavin Cann of the National Nuclear Laboratory, who has been a part of this project from shortly after its conception. His insight and knowledge have helped to keep the project as relevant as possible in what is a quickly and constantly changing landscape for the industry. I am also indebted to Dr. Adam Qaisar, also of NNL, for his help and support in performing X-ray computational tomography and helping me to gain access to the great facilities at NNL Central Lab. I am highly indebted to Dr. Yoshito Nakashima, whose generosity and guidance allowed me to complete analysis which would have otherwise not been possible; going out of his way to be of help someone he had never met and with no personal gain to be made really resonated with me and embodies the spirit of research and academic study.

Realising this PhD would not have been possible were it not for the help and support of a number of students, past and present, who have been very generous in their sharing of experience, knowledge and patient teaching on a range of techniques and sample preparation. Julia, Mark, Wei, Robin, James, Sam, Roland and Rodrigo; thank you for sharing your time and your knowledge with me, it's made this journey a great deal easier! Thanks also to the extended nuclear group and the engineering materials group for their involvement in the project through discussions and conversations both in group meetings and in what have been a number of stimulating and productive offices over the years.

I must also thank the technical staff who have aided me massively in gaining competence in a wide range of techniques. Stuart Micklethwaite and John Harrington

for sharing their knowledge of SEM and providing support with any technical issues; Suzanne Patel for assisting with powder characterisation and to Becky Harrison for help with a whole host of challenges and issues. I'd also like to thank Pete, Steve, Ryan and Les for their help and support over the years.

I'd like to thank Kenny and Ian, with whom I shared a lift to and from Leeds throughout much of the past 4 years, making the long commute much easier and the 6am starts more bearable. Sharing the driving, saving money on fuel and reducing my carbon footprint made the whole process much easier both physically and mentally.

There are a number of other people who have contributed in some way to this project who I must acknowledge. Simon Chudley and Paul Rounce of Hanson cement for their help in sourcing materials and corroborating results of physical properties. Dr. Nick Collier of the University of Sheffield for providing help, support and advice during the early stages of the project and, subsequently, whenever our paths have crossed. I'd also like to express my gratitude to the wider research community, whether aiding me and this research through conversations or discussions at conferences and meetings, or through providing knowledge within the numerous publications that have taught me so much.

I would like to acknowledge the EPSRC, the University of Leeds, the Nuclear Decommissioning Authority and Sellafield Ltd. For their financial support throughout this project, without which none of this would have been possible.

Finally, I want to thank my wife Jade and my family for their constant support and encouragement. The last 4 years have afforded me an amazing opportunity to grow and develop in research, but more importantly as a person. I've learned a great number of skills which I'll carry forward and I'll be forever grateful for my time at Leeds and look back at it with great fondness.

## Abstract

The preferred route to treatment of the vast majority of intermediate level nuclear waste (ILW) within the UK is via encapsulation within a composite cement system. The integrity of these conditioned waste packages must be maintained for hundreds to thousands of years since they will eventually be stored deep below ground in a geological disposal facility (GDF), with this expected to be a permanent route to disposal.

A thorough and clear understanding of the hydration, microstructural development, and hence performance, of grouting materials is essential in providing confidence in the suitability of the technology and ensuring that structural integrity is maintained.

This project comes at a time of significant uncertainty for the cement industry, as well as the steel industry which has significant ramifications on the availability of blastfurnace slag (BFS, hereafter referred to as slag). Through quantifying the ramifications of changes to supply of either of these materials it will be possible to determine the resilience of the technique to chemical and physical variations, in an effort to futureproof supply.

Within this study, grouts prepared with slag and ordinary Portland cement (OPC), at a ratio of 3:1 slag: OPC at a water to binder ratio (w/b) of 0.35, were analysed at 20°C. The impact of OPC composition, slag composition and slag fineness on rate and degree of hydration were assessed. Microstructural development was followed by a number of techniques in 2 and 3 dimensions, with the engineering performance of samples also quantified via a range of testing protocols. Resilience to potential fire scenarios was also investigated through simulated heat-testing of samples and subsequent analysis.

Slag fineness is the most significant factor in controlling rate and degree of its hydration within both young and mature pastes at these high replacement levels. Availability of pore space into which hydrates may grow appears to be the limiting factor in continued hydration; significant quantities of CH remain after 1 year of hydration, intermixed with C-S-H in a densely filled microstructure.

## Table of Contents

Acknowledgements .....	i
Abstract.....	iii
Table of Contents.....	iv
List of Tables.....	vii
List of Figures .....	viii
Nomenclature.....	xii
1. Introduction.....	1
1.1 Background .....	1
1.2 Aims and objectives .....	2
2. Literature review .....	5
2.1 Cement chemistry.....	5
2.1.1 Ordinary Portland cement (OPC).....	5
2.1.2 Composite cements.....	13
2.2 Treatment and disposal technologies for nuclear waste.....	20
2.2.1 Classification of wastes and preferred routes to treatment.....	20
2.2.2 Cementitious systems for ILW encapsulation .....	25
2.3 Microstructural development and durability considerations .....	31
2.3.1 Techniques to probe microstructure in two and three-dimensions .....	31
2.3.2 Techniques to follow degree of hydration of SCMs .....	37
2.4 Previous studies involving grouts for ILW encapsulation.....	41
2.4.1 Published works from the nuclear industry.....	42
2.4.2 The works of Glasser and Atkins .....	43
2.4.3 Research from the University of Sheffield.....	44
2.5 Summary.....	45
3. Materials and methods .....	47
3.1 Characterisation of Raw Materials .....	48
3.1.1 XRF.....	48

3.1.2	Determination of Particle Size Distribution (PSD) .....	48
3.1.3	Methods to determine density .....	49
3.1.4	Methods to determine Specific Surface Area (SSA).....	49
3.2	Materials.....	52
3.2.1	Ordinary Portland Cement (OPC) .....	54
3.2.2	Blastfurnace Slag (slag).....	55
3.3	Experimental Techniques .....	59
3.3.1	Mix Designs and Sample Preparation.....	59
3.3.2	Dilatometry .....	59
3.3.3	Isothermal Conduction Calorimetry (ICC) .....	61
3.3.4	Drying of samples for secondary analysis techniques.....	64
3.3.5	Thermogravimetric Analysis (TGA/DTA).....	65
3.3.6	X-ray Diffraction (XRD).....	69
3.3.7	Scanning Electron Microscopy (SEM).....	70
3.3.8	X-ray micro-Computational Tomography (X- $\mu$ CT).....	74
3.3.9	Gas Permeability (Leeds cell) .....	87
3.3.10	Sorptivity.....	90
3.4	Summary.....	92
4.	Hydration, microstructural development and engineering performance of cementitious grouts for ILW encapsulation.....	94
4.1	Early age grout hydration .....	94
4.1.1	Bound water and portlandite content determined via thermogravimetric analysis (TGA).....	94
4.1.2	Determination of degree of hydration and microstructural development from BSE-IA.....	97
4.1.3	Following early age hydration by means of chemical shrinkage (dilatometry) and isothermal conduction calorimetry.....	110
4.1.4	Corroboration of methods to determine hydration kinetics.....	117
4.2	XRD analysis.....	124

4.3 Assessing impact of hydration on microstructural development and transport properties .....	128
4.3.1 Intrinsic gas permeability.....	128
4.3.2 X-ray micro-computed tomography and random walk simulation .....	129
4.4 Summary.....	138
5. Impact of heat-treatment upon microstructure, phase assemblage and engineering performance of cementitious grouts for ILW encapsulation.....	140
5.1 Visual observations of heat-treated samples .....	140
5.2 Physical properties of heat-treated samples .....	144
5.2.1 Intrinsic gas permeability.....	144
5.2.2 Sorptivity .....	147
5.3 X-ray micro-computed tomography and random walk simulation.....	149
5.4 Phase assemblage following exposure to elevated temperatures.....	159
5.4.1 Portlandite content and mass loss determined via TGA .....	159
5.4.2 XRD analysis .....	161
5.5 Summary.....	163
5.5.1 Industrial ramifications .....	164
6. Conclusions and further work .....	166
7. References .....	178

## List of Tables

Table 2-1: Typical ranges of slag composition (%), modified from Lang (2002) .....	16
Table 2-2: Reactions between cementitious grout and radwaste species, from (Glasser, 2011). .....	27
Table 3-1: Chemical composition of as received materials determined via XRF .....	53
Table 3-2: Clinker phases as determined via Bogue analysis .....	53
Table 3-3: Physical properties of anhydrous materials at time of mixing .....	54
Table 3-4: Legend of mix designs of powder compositions studied.....	57
Table 3-5: Selection of techniques for arresting hydration (Zhang and Scherer, 2011) .....	64
Table 3-6: Details of samples analysed via X-ray $\mu$ CT .....	77
Table 4-1: Rate of slag hydration (% of 28 day hydration).....	101
Table 4-2: Calibration factors correlating chemical shrinkage with degree of hydration as determined via BSE-IA at 28 days.....	118
Table 4-3: Calibration factors relating isolated heat release due to slag hydration with degree of hydration as determined via BSE-IA at 28 days .....	121
Table 4-4: Impact of resolution on pore connectivity and subsequent determined tortuosity.....	133
Table 5-1: Sorptivity coefficients of oven-dried and heat-treated grout samples.....	147
Table 5-2: Mass loss at target temperatures from samples analysed via TGA .....	150
Table 5-3: Mass loss at 550°C of samples from the centre of specimens previously heated to 800°C.....	159

## List of Figures

Figure 2-1: Heat evolution curve of a typical modern portland cement [From (Bye, 1999)] .....	11
Figure 2-2: CaO-Al <sub>2</sub> O <sub>3</sub> -SiO <sub>2</sub> ternary diagram of cementitious materials (Lothenbach et al., 2011) .....	14
Figure 2-3: Modelled changes in hydrates formed within an OPC: slag blended system, with materials of typical composition and assuming 75% hydration of the slag component (Lothenbach et al., 2011).....	18
Figure 2-4: Composition of treated and untreated ILW streams within the UK waste inventory, modified from (NDA, 2013b) .....	22
Figure 2-5: Schematic of a generic conditioned ILW waste package within a 500L stainless steel drum (NDA, 2013d). .....	23
Figure 2-6: Limitations of extrapolation from two to three dimensions with respect to feature sizes and interconnectivity (Scrivener, 2004) .....	35
Figure 3-1: Particle size distribution of cements .....	55
Figure 3-2: Particle size distribution of slag powders and quartz .....	58
Figure 3-3: Segmentation of heat of hydration from reaction of slag .....	63
Figure 3-4: Heat released due to slag hydration in the system C1S2f .....	63
Figure 3-5: TGA, DTA and $\delta$ DTA for C1S2c system hydrated for 28 days .....	66
Figure 3-6: Determination of CH content from tangent method .....	68
Figure 3-7: SEM micrograph of C1S2c system at 28 days with corresponding grey level histogram.....	72
Figure 3-8: (a) C1S2c system hydrated for 28 days, (b). Associated Mg map and (c). anhydrous slag fraction isolated.....	73
Figure 3-9: Example reconstructed slice through X-ray $\mu$ CT scan. Sample shown is C1S2c following heat-treatment to 800°C at 7 days .....	75
Figure 3-10: segmentation of VOI to yield porosity - (left). Section through untreated VOI (right). Same section of VOI following thresholding and (bottom). Corresponding histogram with threshold point highlighted. ....	80
Figure 3-11: simplified representation of the mirror boundary condition employed. (a). A simple periodic boundary condition (b). a mirrored boundary condition yielding a continuous percolated pore network to ensure accurate estimation of tortuosity (Nakashima and Kamiya, 2007).....	82
Figure 3-12: Example trajectory (400,000 timesteps) in 3 orthogonal planes of random walker in segmented pore space within C1S2c system at 28 days .....	83

Figure 3-13: Trajectories of walkers within the digitized pore networks of segmented VOIs in 3 dimensions, representing the C1S1 system at 7 days, 28 days and at 28 days following heat-treatment to 800°C.....	86
Figure 3-14: Components of the Leeds cell.....	88
Figure 3-15: Determination of intrinsic permeability for sample C1S3c hydrated for 28 days and hydration stopped via oven drying at 50°C .....	90
Figure 3-16: experimental setup for sorptivity testing, modified from (Tasdemir, 2003) .....	91
Figure 4-1: Bound water content as a function of time .....	95
Figure 4-2: CH content as a function of time, determined via TGA.....	96
Figure 4-3: Evolution of clinker hydration from BSE-IA.....	98
Figure 4-4: Evolution of slag hydration with time from BSE-IA .....	99
Figure 4-5: Evolution of slag hydration of selected mixes from BSE-IA compared to the results of Whittaker (2014) and Kocaba (2010).....	102
Figure 4-6: Weighted degree of hydration of all blends as a function of time.....	103
Figure 4-7: Microstructural development of C1S1 system at ages 2-365 days imaged at 800x magnification.....	104
Figure 4-8: Microstructural development of C1S2c system at ages 2-365 days imaged at 800x magnification .....	106
Figure 4-9: Microstructural development of C1S2f system at ages 2-365 days imaged at 800x magnification.....	107
Figure 4-10: Coarse porosity as a function of time, determined via BSE-IA .....	108
Figure 4-11: Evolution of chemical shrinkage for all project mixes up to 28 days .....	110
Figure 4-12: Isolated shrinkage as a result of slag hydration for all mix designs .....	111
Figure 4-13: Evolution of chemical shrinkage for C1S2c and C1S2f and associated quartz blends over 56 days.....	112
Figure 4-14: Chemical shrinkage as a function of slag chemistry and fineness.....	113
Figure 4-15: Heat evolution of C1 systems over 3 days .....	114
Figure 4-16: Heat evolution of C2 systems over 3 days .....	116
Figure 4-17: Isolated heat due to slag hydration within all grouts .....	117
Figure 4-18: Chemical shrinkage calibrated with BSE-IA for all systems up to 28 days .....	119
Figure 4-19: Chemical shrinkage due to slag hydration, calibrated with BSE-IA for C1S2c and C2S1f systems up to 56 days.....	120
Figure 4-20: Heat evolution due to slag hydration, calibrated with BSE-IA for all systems up to 28 days .....	122

Figure 4-21: Correlation between calorimetry and chemical shrinkage for all mix designs .....	123
Figure 4-22: XRD patterns of all samples, showing hydration of the clinker phases from 2 to 365 days .....	125
Figure 4-23: XRD patterns of all samples showing AFt and AFm phases .....	127
Figure 4-24: Intrinsic permeability of samples at 28 days, which have not been dried nor exposed to elevated temperatures .....	128
Figure 4-25: 3D rendering of 28 day aged samples from X-ray CT. a). C1S2c and b). C2S1 .....	130
Figure 4-26: Cross-section through VOI of C1S2c and C2S1 samples at 28 days ...	131
Figure 4-27: Impact of X-ray CT resolution on determined diffusion tortuosity .....	132
Figure 4-28: Cross-sections highlighting porosity in C1S2c system at high-resolution (left) and lower-resolution (right) .....	132
Figure 4-29: Diffusion tortuosity as a function of segmented porosity for all non-heat-treated samples analysed during first run (1.2-1.6 $\mu$ m) .....	135
Figure 4-30: Diffusion tortuosity as a function of segmented porosity for C1S2c and C1S2f systems at 7, 28 and 60 days (second run at 0.53 $\mu$ m). .....	136
Figure 4-31: Evolution of microstructure and porosity of C1S2c grout at 7 days (top), 28 days (middle) and 60 days (bottom) at a resolution of 0.53 $\mu$ m .....	137
Figure 5-1: C1S1 and C1S2c samples before and after heat-treatment at 800°C ....	142
Figure 5-2: SEM micrographs of heat-treated samples at 800x magnification. A). C1S1 at 400°C. B). C1S1 at 800°C. C). C1S2c at 400°C & D). C1S2c at 800°C. ....	143
Figure 5-3: Intrinsic permeability of grout samples as a function of exposure conditions .....	145
Figure 5-4: Sorptivity indices for all mixes following exposure to elevated temperatures .....	148
Figure 5-5: diffusive tortuosity of C1S1 and C1S2c samples at 28 days with and without heat-treatment .....	151
Figure 5-6: Visual representation of damage induced through heating to C1S1 grouting formulation. Untreated grout at 28 days (top), heat-treated to 400°C (middle) and heat-treated to 800°C (bottom) .....	153
Figure 5-7: Diffusive tortuosity of C1S2c and C1S2f samples at 7 days with and without heat-treatment .....	154
Figure 5-8: Visual representation of damage induced through heating to C1S2c grouting formulation. Untreated grout at 7 days (top), heat-treated to 200°C (middle) and heat-treated to 800°C (bottom) .....	157

Figure 5-9: Visual representation of damage induced through heating to C1S2f grouting formulation. Untreated grout at 7 days (top), heat-treated to 200°C (middle) and heat-treated to 800°C (bottom) .....	158
Figure 5-10: CH content at centre of samples (27mm diameter) following heat-treatment .....	160
Figure 5-11: XRD patterns of heat-treated samples at 7-70° 2θ (Ms – monosulfate, Hc - hemicarboaluminate, Ht - hydrotalcite, g - gehlenite). .....	162

## Nomenclature

BFS	Blast furnace slag
BNFL	British nuclear fuels Ltd.
BSE	Backscattered electron
BSI	British standards institute
DECC	Department of Energy and Climate Change
EDX	Energy dispersive x-ray spectroscopy
GDF	Geological disposal facility
GGBS	Ground granulated blastfurnace slag
ICC	Isothermal conduction calorimetry
ILW	Intermediate level waste
IPA	Isopropyl alcohol
LOI	Loss on ignition
MACs	Minor additional constituents
NMR	Nuclear magnetic resonance
OPC	Ordinary Portland cement
PSD	Particle size distribution
SCM	Supplementary cementitious material
SEM: BSE- IA	Scanning electron microscopy: backscattered electron image analysis
S/S	Solidification/Stabilisation
TGA	Thermogravimetric analysis
UKAEA	UK Atomic Energy Authority
VOI	Volume of interest
W/B	Water to binder ratio

W/C	Water to cement ratio
wt%	Weight percent
XRD	X-ray diffraction
XRF	X-ray fluorescence
X- $\mu$ CT	X-ray micro computational tomography

# 1. Introduction

## 1.1 Background

2016 marks the 60<sup>th</sup> anniversary of civil nuclear power in the UK, over this time there has been a great deal of pioneering development in terms of reactor design and operation as well as reprocessing of fuels. One by-product of this long period of development and utilisation has been the unavoidable production of a large volume of waste. This waste is of great variability in terms of radioactivity content, the states in which it exists and subsequently the ways in which it is managed and treated; within the UK, the safe storage, treatment and ultimate disposal of nuclear waste poses arguably the greatest engineering challenge of the coming century.

Variations in composition, levels of radioactivity and state (liquid, solid, slurry, sludge etc.) define the most suitable treatment and disposal routes for each waste stream; as a result it is essential to have a 'toolbox' of approaches, techniques and formulations of encapsulating materials to provide suitable pre-treatment (Milestone et al., 2006).

UK government strategy, as outlined by the Nuclear Decommissioning Authority (NDA, 2016a) is for the vast majority of treated intermediate level waste (ILW) to be stored in a geological disposal facility (GDF) at a depth of 200-1000m below ground (DECC, 2014). Until the date that a suitable site is identified, licenced and a facility constructed; treated waste packages are to be kept in interim storage. The total length of this storage period is as yet not certain, but is likely to be in the region of decades as the implementation of a GDF may not occur within this century.

Conditioned waste packages must therefore be constructed with durability and longevity in mind since their future is uncertain and their suitability to both interim storage and ultimate placement within a GDF is of paramount importance.

This project aims to provide significant insight into the hydration, microstructural development and subsequent engineering performance of a number of cementitious grouts used in the treatment of the high volume and highly variable ILW streams produced in the UK.

The current and legacy standard specification grouts along with a number of potential replacement mixes were studied. Grout formulations were prepared with 75% blastfurnace slag (BFS/slag) and 25% ordinary Portland cement (OPC), i.e. 3:1 BFS: OPC systems. Grouts were prepared using a range of BFS and OPC compositions, with chemical composition and physical properties (fineness) assessed both independently and dependently.

Grouts for the treatment of ILW have been studied fairly extensively over the years with countless industrial trials and investigations. A number of more in depth PhD projects, similar to this in a number of ways, have provided significant further insight (Utton, 2006, Collier, 2006) with a number of similar or related projects currently ongoing at a number of universities across the UK.

This project marks the first time in which significant investigation has been made into grout hydration using the most up-to-date methods, in addition to engineering performance testing. The research presented herein is further enhanced through microstructural investigation via X-ray micro-computed tomography and Monte Carlo based 'random walk' simulations, the first time that such a technique has been used to study ILW grouting matrices.

## **1.2 Aims and objectives**

The aims of this project were three fold;

- 1. To quantify hydration, understand how it is impacted by the chemical and physical attributes of the constituent materials and to link this to microstructural development.**

Previous research has shown that the chemistry and physical properties of both clinker and slag have significant ramifications on their rate and overall degree of hydration. This project aimed to identify the degree to which these parameters affect hydration within grouts prepared for the treatment of ILW, in which the replacement level by slag is significantly high and the properties of the constituent materials are of notable importance.

To this end, a number of objectives needed to be satisfied:

1. Use a range of suitable techniques to quantify hydration of both slag and clinker within the studied composite systems at a range of ages; assessing the suitability of each and using results to corroborate one another.
  2. Quantify the degree to which the chemical composition and physical properties (critically, particle size distribution) of blastfurnace slag control or limit hydration at different ages.
  3. Probe microstructural development through application of a number of appropriate techniques and methodologies. Particularly, apply microcomputed x-ray tomography and subsequent random walk simulations on untreated samples to provide statistically meaningful results,
- 2. To understand how variations in hydration impact upon engineering performance, with a key focus on the impact of damage caused at elevated temperatures, in line with potential fire scenario regulations.**

Permeability of waste packages will play a key role in determining their long-term durability and suitability for proposed storage and disposal scenarios. Understanding the impacts of composition upon microstructural development and ultimately engineering performance is crucial in ensuring that the treatment technology is fit for purpose and that a future GDF is safe and poses no danger to its surrounding biosphere. Clearly, leaching of waste species into the surrounding environment is the most significant concern with regards waste treatment and long-term suitability of conditioned waste packages.

One of the key concerns in the safe storage, transport and ultimate placement of waste packages into a GDF is the potential for the occurrence of scenarios in which damage may be caused. The most significant of these concerns relate to potential fire scenarios and the subsequent damage that they might cause to the resultant performance and suitability of affected waste packages. Understanding, therefore, how these grouting materials are affected by exposure to temperatures and conditions mimicking such a situation provide significant insight into their potential resilience.

Quantifying the impact of variations in hydration state upon engineering performance will be achieved via the following objectives:

1. Identify suitable treatment and exposure conditions to mimic or simulate fire scenarios and/or other deleterious environments.

2. Preparing and aging samples to ensure a range of different sample compositions are analysed at a variety of hydration states and following a range of varying exposure conditions.
  3. Application of a range of suitable testing methods to quantify damage and hence, potential resilience to fire scenarios or other damage which may occur in service.
- 3. The overarching industrial aim of the project is to understand how changes to composition impact upon hydration and performance with the key goal of ensuring a continuity of supply in an attempt to futureproof this treatment technology.**

The significant changes that have occurred within the UK over recent years in the cement industry and the iron industry highlight the importance of understanding and quantifying the effects of changes in supply and hence composition. The change in supply of clinker for the production of grouting materials that occurred during this project highlights the challenges faced by the industry and the need for a deep and thorough understanding of the potential ramifications that supply changes may have upon grout hydration, microstructural development and, ultimately, waste package performance.

The changes occurring in the UK iron industry over recent years have been well publicised. One fallout of plant closures and uncertainties on the future of the remaining, aging, blast furnaces is the impact that this has on the already volatile supply of slag. A better understanding of how changes impact hydration and performance is essential in ensuring that supply of materials that produce consistent, high quality and suitable cementitious grouts is maintained.

In order to clearly elucidate the impact of compositional changes, the project needed to fulfil a number of specific objectives:

1. Analysis of mix designs reflecting a range of compositions, including legacy, current and potential future specifications was essential. It was crucial too that the compositional limits set out in the slightly outdated industrial documentation was challenged, in an effort to broaden the potential compositions of future powder supply.
2. Aims 1 and 2 needed to be clearly met in order to allow for a thorough understanding of the impacts of legacy and potential future changes to supply. Techniques to quantify hydration and microstructural development should be relevant and suitable for the materials studied.

## 2. Literature review

The following review has been split into three distinct sections. First, it will provide an overview of the current knowledge and understanding of cementitious materials based on OPC and significantly those containing slag; secondly, it will discuss the use of these materials for the treatment of intermediate level nuclear waste (ILW) and finally it will probe the microstructural development of such systems and consider their durability and hence suitability for such an application.

### 2.1 Cement chemistry

Portland Cement (PC) and materials based on it are by far the most commonly used construction material in the world (Purnell and Black, 2012). Their flexibility and versatility mean that they are often suitable, and in many instances preferable, for a wide range of alternative applications; from medicine (dental and skeletal) to art (sculpture) and, as in the focus of the materials in this study, for the treatment of hazardous waste streams.

Cement as defined by the British Standards Institute (BSI, 2011) is '[a] material...that has hydraulic properties, when mixed with water it sets and hardens by means of hydration. After hardening it retains both its strength and its stability even when placed under water.'

#### 2.1.1 Ordinary Portland cement (OPC)

Portland Cement (or the slight variant, CEMI) is the most abundantly produced and consumed cementitious material, both within the UK and internationally; it far outstrips alternative cements in construction applications and is also the most commonly utilised 'cement' for nuclear waste conditioning. It is formed through the calcination of limestone with an aluminosilicate source (generally a clay) within a kiln at roughly 1450°C. The resultant material, clinker, is mixed with around 5% gypsum (Bye, 1999) and ground to a fine powder to produce PC.

Within the nuclear industry, this material is referred to as 'OPC'; and whilst this terminology is technically something of a misnomer, it allows for the nuclear specific variant of the material to be differentiated from Portland cement materials that are used within the construction trade. The slight nuances and variations in chemical and physical composition would likely have no discernible impact upon performance in construction applications; they do, however, have significant ramifications when applied as encapsulants for nuclear waste streams. Further, these disparities have a large bearing on the supply of materials owing to the potential interactions that could occur between certain additions and some waste species.

The process of pre-grinding the raw materials, heating to a specified temperature and for a pre-determined time and subsequently grinding the resultant clinker is generally kept constant within a facility. However, since the supply of raw materials varies slightly and since kilns and operating parameters will also be inconsistent across facilities, it is necessary to have national standards to ensure that all cements meet desired specifications in terms of composition and hence performance. To this end, the associated British Standard (BSI, 2011) provides specification limits for OPC in the UK which define envelopes of conformity in terms of both chemical composition and physical properties.

To clarify, OPC in this context refers to the material used in the preparation of grouts for nuclear waste encapsulation, which differ slightly from CEMI used in construction. The key differences in preparation are the omission of minor additional constituents (MACs) and a lower limestone addition to the ground clinker, as well as the absence of organic grinding aids in the granulation process.

#### *2.1.1.1 Composition*

Ground clinker, which accounts for roughly 95% of OPC is comprised primarily of 4 principal crystalline phases (defined in cement chemistry nomenclature as);  $C_3S$  (alite),  $C_2S$  (belite),  $C_3A$  (tricalcium aluminate) and  $C_4AF$  (tetracalcium aluminoferrite) (Taylor, 1997). The remainder is generally made up of impurities containing Al, Fe, Mg, Na, sulphates, phosphates and CaO (Bye, 1999).

When mixed with water the phases present within the cement powder hydrate; that is to say they react with the hydrogen ions present to form solid hydrate products (namely C-S-H, CH and other iron containing materials). This dynamic process is complex, with the rate and, hence, degree of hydration dependent upon a large number of factors. This

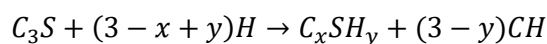
complexity is further exacerbated in the presence of aggregates; however, since the systems investigated in the present study are pastes, the following provides an insight into the process in the absence of fine or coarse aggregate.

Hydration is a dissolution-precipitation process, heterogeneous in nature as it involves anhydrous, hydrated and liquid phases. It follows therefore that for hydration to proceed the solubility of potential hydration products must be lower than the anhydrous phases (Scrivener and Nonat, 2011). The hydration of these 4 principle phases occurs concurrently but at considerably differing rates; there is almost certainly some interaction between the hydrating phases, however for clarity it is most suitable to discuss their hydration independent of one another.

#### 2.1.1.1.1 Tricalcium silicate

Tricalcium silicate ( $C_3S$ ), commonly referred to as alite in its impure form, is the most abundant phase within an anhydrous cement, typically accounting for 50-70% by weight (Taylor, 1997). Its hydration is the most rapid of the 4 principal phases and as such it provides much of the early strength development.

The reaction of  $C_3S$  with water results in the formation of calcium silicate hydrate (C-S-H) [where the dashes denote the fact that there are compositional variations in the C-S-H gel] as well as the formation of portlandite (CH), as denoted in Equation 1 –



*Equation 1*

Where 'x' represents the Ca/Si ratio, which for a pure OPC system is accepted to be in the region of 1.75 (Richardson, 2008). 'y' represents the water content, and is thought to be equal to 4 in saturated conditions, but is sensitive to changes in humidity and liable to dehydration (Bye, 1999).

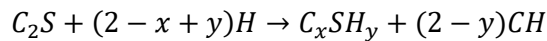
C-S-H is a poorly crystalline 'gel' with a range of compositions; providing much of the strength of the hydrated cement paste. Its structure is such that other elements may be incorporated into it, particularly aluminium (Richardson et al., 1993).

Intermixed within the C-S-H gel is the crystalline hydration product portlandite (CH) which, as the second most abundant phase within a hydrated OPC paste, accounts for roughly 25% of the hydrated mass (Glasser, 2001). It is the portlandite that contributes

significantly to the internal pH of the cement matrix; the presence of portlandite is also important for the hydration of slag (as occurs within grouts used for ILW treatment) as discussed in more detail in Section 2.1.2.

#### 2.1.1.1.2 Dicalcium silicate

Belite, the impure form of dicalcium silicate ( $C_2S$ ) is the second most abundant phase within an OPC powder, typically representing between 15 and 30% of the anhydrous material. Belite hydrates much more slowly than alite and as such contributes little to early age strength development (Taylor, 1997). Belite is generally present within OPC as the  $\beta$ - $C_2S$  polymorph; its reaction with water results in the formation of the same hydration products as  $C_3S$ , but with reduced portlandite production, as outlined in Equation 2 -

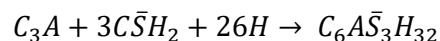


*Equation 2*

#### 2.1.1.1.3 Tricalcium aluminate

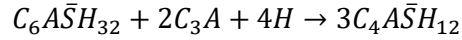
$C_3A$  will react rapidly with water to form the hexagonal calcium aluminate hydrates,  $C_4AH_{13}$  and  $C_2AH_8$  (Brown et al., 1986) and may result in a flash set of the hydrating cement; to counteract this, a sulphate source (gypsum) is intermixed with the cement clinker during manufacture to delay hydration and allow for mixing, transport and placing of the wet grout, mortar or concrete prior to hardening. In the context of nuclear waste treatment this is yet more critical, since it is imperative that the grout maintains its fluidity for a sufficiently long time to allow pumping and placement in a manner that results in the production of an acceptable waste package.

This introduction of gypsum into the system results in the formation of an AFt phase, ettringite, via the following reaction –



*Equation 3*

When the gypsum has all been consumed in the formation of ettringite the availability of sulphates in solution is diminished; below a certain sulphate concentration ettringite becomes unstable and continued hydration of  $C_3A$  results in the formation of an AFm phase (monosulphoaluminate hydrate) (Bensted and Barnes, 2002) as illustrated –



Equation 4

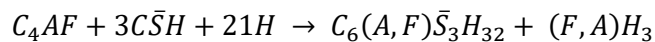
Within a typical CEMI system, the presence of limestone can lead to the formation of both hemi- and monocarboaluminates.

#### 2.1.1.1.4 Calcium aluminoferrite

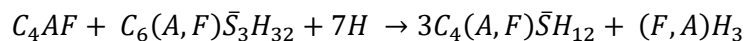
The ferrite phase within cement is generally referred to as  $C_4AF$ ; in reality the phase exists over a range of compositions, with the general formula  $C_2F_{(2-x)}A_xO_{10}$  where  $x$  lies in the range 0 to 1.4, with  $C_4AF$  representing a value of  $x = 1$ . The ferrite phase may be considered as a solid solution between  $C_2F$  and a hypothetical  $C_2A$ . The reactivity of the ferrite phase is diminished with increasing iron content (as  $x$  decreases). For simplification (and as  $x$  is generally very close to 1 in most common cements) the ferrite phase is commonly explained with reference to  $C_4AF$ .

Hydration of  $C_4AF$  is very similar to that of  $C_3A$ , especially in the presence of gypsum. AFt is produced along with an iron rich gel, later converting to AFm. General assumptions suggest that  $C_4AF$  is less reactive than  $C_3A$  (Bensted and Barnes, 2002) and that during hydration there is a competition for gypsum. Jawed *et al.* (1976) found that the conversion from ettringite to AFm was accelerated in the presence of  $C_3A$ , suggesting that  $C_3A$  is more efficient at competing for sulphate ions.

A convenient way to represent the reactions of the ferrite phase is –



And –



Where (A,F) indicated aluminium with variable substitution of iron, and (F,A) indicates iron with variable substitution of aluminium. The (F,A) $H_3$  is an amorphous phase that forms in small amounts to maintain the correct reaction stoichiometry. Because of the substituted iron, the main reaction products are not pure ettringite and

monosulfoaluminate, although they have the same crystal structure. Instead, cement chemists have given them the names AFt and AFm, respectively, where the m indicates monosulfate (one sulfate ion) and the t indicates trisulfate. In a portland cement paste where the  $C_3A$  and  $C_4AF$  are intimately mixed together, it can be safely assumed that the aluminum-bearing reaction products are never completely free of iron, and so the terms AFm and AFt are more correct.

### 2.1.1.2 Hydration

Having an understanding of the hydration of OPC, and blends based upon it, is fundamentally important for all its potential applications. Research attempting to fully understand and quantify the kinetic mechanisms of cement hydration has been ongoing for decades and whilst great progress has been made and potential mechanisms suggested, no definitive conclusions have been drawn (Bullard et al., 2011, Gartner et al., 2002). Scrivener *et al.* (2015a) recently detailed much of the recent progress that has been made in understanding hydration, drawing upon the most significant contributions made in the efforts towards elucidation of the mechanism controlling hydration kinetics.

As discussed, upon contact with water the 4 principal phases present within anhydrous cement begin to hydrate. This hydration is exothermic and reference to a plot of heat liberation with respect to time (as obtained via the application of an isothermal conduction calorimeter) is a simple and common means of displaying and discussing kinetics, see Figure 2-1.

In this schematic, the rapid dissolution phase and the induction (or dormant) period are both represented as stage I. The dissolution of  $C_3S$ ,  $C_4A$  and calcium sulphate occurs almost instantaneously, resulting in significant heat release. Following dissolution of the surface ions of the phases present, a period of low activity begins. Numerous hypotheses as to the cause of this induction period have been proposed; the most salient of which are explained and discussed by Juilland (2009) and Gartner *et al.* (2002).

Recent investigations by Juilland *et al.* (2010) strongly suggest that the mechanism controlling this period of little activity, denoted as stage I in Figure 2-1 (and subsequent acceleration period, stage II) may be explained via a dissolution theory based upon research conducted in the field of geochemistry. The mechanism suggests that

dissolution is initially dominated by the formation of etch pits on the surfaces of cement grains, later becoming limited to step retreat from such pits

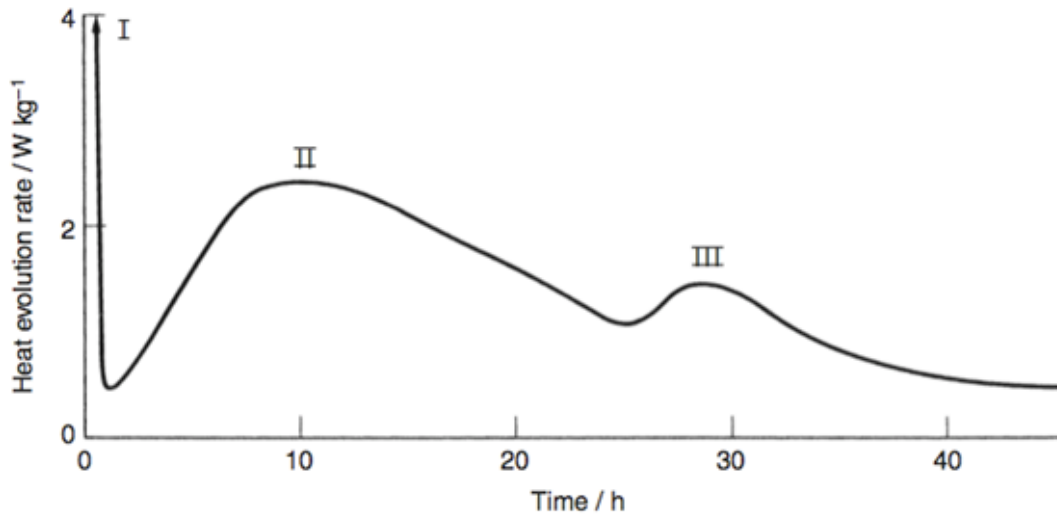


Figure 2-1: Heat evolution curve of a typical modern portland cement [From (Bye, 1999)]

The presence of this induction period is essential for civil engineering applications and is crucial in the case of encapsulation of nuclear waste streams; the remote operation of the infilling process necessitates strict controls on the flow properties and setting time of grouting materials. Whilst it is true that grouts for ILW encapsulation contain high levels of replacement by slag, it is the hydration of the OPC within the systems (and in particular the alite) that controls the setting characteristics and is significant in affecting rheological properties in general.

Stage II is the main heat evolution peak and is a result of the formation and growth of C-S-H and Portlandite. As discussed above, the 'trigger' leading to the acceleration of these reactions is still a controversial and unresolved issue. From the numerous proposed theories, Bullard and Flatt (2010) have suggested that there are two mechanisms which appear most likely; the 'geochemical' approach as discussed by Juilland *et al.* or the presence of an inhibiting layer.

Often observed in heat evolution curves, and exaggerated as stage III in Figure 2-1, is the presence of a small 'hump' on the deceleration shoulder of the main heat evolution peak (stage II). This increase in heat release is a result of C<sub>3</sub>A hydration following depletion of sulphate ions in solution and results in the formation of AFt.

Beyond this initial period of rapid reaction, hydration occurs at an ever diminishing rate. Hydration beyond 24 hours for an OPC is typically referred to as 'later age'; it is at this time that inner-product C-S-H is formed within the shells of the original cement grains. Any AFt formed during stage III will transform into AFm as it reacts with any remaining C<sub>3</sub>A. Continued hydration results in densification of outer product C-S-H and a refinement of the pore structure.

It is often erroneously suggested that OPC hydration is all but complete after 1 year. The work of Taylor *et al.* (2007) has shown significant differences in the microstructure and morphology of outer product C-S-H in pastes at 20 years compared to at 14 months. The work of Taylor *et al.* (2007) elucidated the continued hydration of neat OPC systems, with further investigation into composite cement systems (Taylor et al., 2010) highlighting significant micro- and nano-structural changes occurring between 1 and 20 years.

### 2.1.2 Composite cements

Composite cements are a combination of OPC and at least one supplementary cementitious material (SCM). Almost all commonly available cements in the UK are now composites, a result of the continued drive for reduced embodied carbon and increased usage of industrial by-products. These substitute materials require no pre-clinkering and as such help in offsetting the unavoidable energy usage and anthropogenic CO<sub>2</sub> emissions associated with the production of OPC.

The use of SCMs is beneficial for a number of construction challenges and particular environments. Within the area of nuclear waste treatment they may provide or induce a number of advantageous attributes and characteristics. The impact of particular SCMs (in particular blastfurnace slag) upon both the physical and chemical properties of a grouting material help to enhance performance in both a wet state, prior to setting; and in the hardened, hydrated encapsulated waste package.

A plethora of SCMs are commercially available internationally and cover a wide range of compositions (Figure 2-2). Availability of specific SCMs is highly variable and geographically sensitive (given the low financial value of the large majority). The most abundant SCMs, slag and pulverised fuel ash (PFA), are generally readily available; their supply is, however, dependent upon the primary processes from which they arise (the production of pig iron for steel manufacture, and the burning of coal for energy production, respectively).

Within the UK, the grouts used for the treatment of (some) low- and (the large majority of) intermediate level waste (LLW and ILW) are produced from a combination of OPC and slag. Since slag has a close chemical composition to OPC; much more so than fly ash or natural pozzolans, (see Figure 2-2) it is possible to replace a high portion of the powder fraction in this way. There are a number of reasons as to why this is advantageous, many of which will be covered in Section 2.1.2.1.

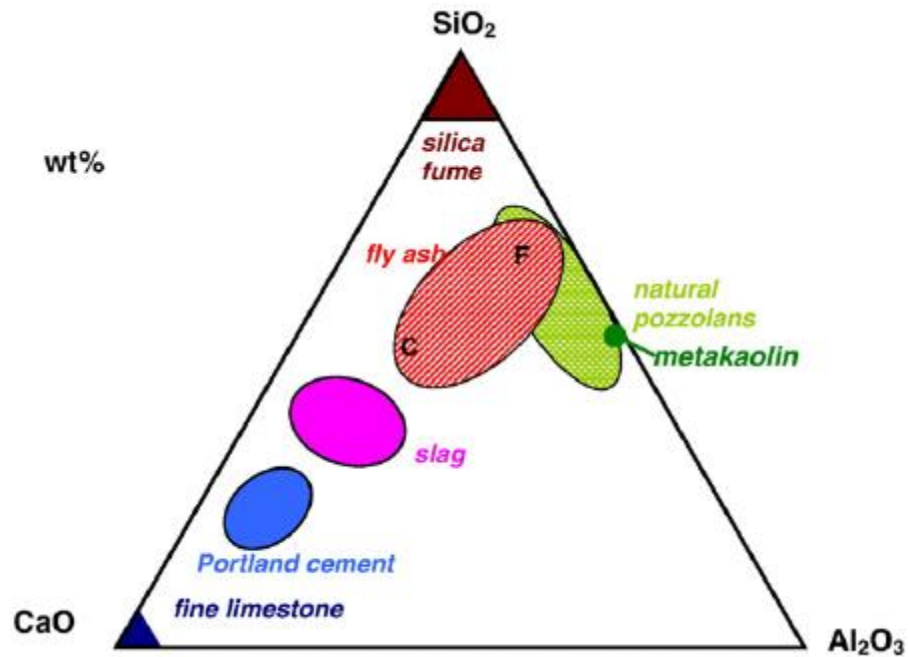


Figure 2-2:  $\text{CaO-Al}_2\text{O}_3\text{-SiO}_2$  ternary diagram of cementitious materials (Lothenbach et al., 2011)

#### 2.1.2.1 Blastfurnace slag (BFS)

Slag is an industrial by-product formed within a blast-furnace during the production of pig iron. For each tonne of iron yielded, roughly 300 kg of slag is produced (Neville, 1997). International pig iron production for 2015 was 1.18 billion tonnes (U S Geological Survey, 2016); suggesting the potential for the production of roughly 350 million tonnes of slag annually.

The process of producing pig iron involves combining virgin iron ore, which is high in iron oxides and contains some impurities in the form of silica and alumina; with a fuel source and reducing agent, coke, and a fluxing agent, which is typically a mixture of limestone and dolomite.

UK pig iron production was relatively conservative at around 9 million tonnes for 2015 and is only set to reduce further in the coming years due to closure of a number of blast-furnaces. This comes as a result of a changing economic climate as prices of steel continue to drop due to over-production in the Chinese market (BBC, 2015) and a general oversaturation of the market that shows no sign of abating.

At temperatures approaching  $1500^\circ\text{C}$  within the kiln, the mixture is molten; the iron ore is reduced to iron and the impurities combine with the flux to form the molten slag. Due

to the disparity in density, the slag rises to the top of the blast-furnace from where it is removed before being quenched rapidly via spraying with high pressure water. The result is an amorphous granulated material with a glass content typically in excess of 90% (Moranville-Regourd, 1998).

Not all slag is quenched to form an amorphous hydraulic material; in many cases it is allowed to cool naturally, since this is a cheaper and simpler alternative for many steel producers. The resultant material is not suitable as an SCM but is often used as a lightweight aggregate. Whilst not all slag is ultimately utilised within cementitious materials, it is still the most abundantly available SCM both in the UK and globally.

In the UK, BFS must conform to specifications set out in the associated British Standard, BS EN 197-1 (BSI, 2011); the most pertinent of which are:

- $\frac{(CaO+MgO)}{SiO_2} \geq 1$
- More than  $\frac{2}{3}$  (by mass) of the slag must be amorphous and exhibit hydraulic properties upon activation
- The CaO, SiO<sub>2</sub> and MgO content combined should exceed  $\frac{2}{3}$  (by mass) of the slag.

Further factors, including physical properties such as particle size distribution and specific surface area play an important role in governing both rheological properties and characteristics of the hardened hydrated cementitious matrix. BS EN 197-1 does, however, not include limits for these parameters.

#### 2.1.2.1.1 Composition and impact upon hydration

The chemical composition of the resultant slag can vary over a relatively wide range (Figure 2-2) due to disparities in ore sources, flux composition, coke consumption, furnace design and type of iron being smelted. Slag is a glassy material, comprised largely of CaO, SiO<sub>2</sub>, Al<sub>2</sub>O<sub>3</sub> and MgO; often with small quantities of SO<sub>3</sub>, Fe<sub>2</sub>O<sub>3</sub> and MnO.

Literature suggests, (Taylor, 1997, Lang, 2002) that whilst there may exist large compositional variability on an international level, the disparity in chemistry of slags produced in the UK generally tend to fall within a smaller envelope, see Table 2-1.

Table 2-1: Typical ranges of slag composition (%), modified from Lang (2002)

Oxide phase	UK (%)	USA (%)
CaO	39.9-40.5	29-42
SiO <sub>2</sub>	35.2-37	32-40
Al <sub>2</sub> O <sub>3</sub>	11-13.1	7-17
MgO	8.3-8.8	8-19
S	0.9-1.1	0.7-2.2
Na <sub>2</sub> O+K <sub>2</sub> O	0.5-0.7	-
Mn	0.28-0.35	0.2-1

XRF data providing the oxide composition of the slag powders, as well as the OPC powders, used within this study are given in Table 3-1. From comparing the composition of the materials in the present study with the typical figures of Lang (2002) it is possible to notice that there appears to be something of a trend towards a slightly higher CaO content with Al<sub>2</sub>O<sub>3</sub> contents being in decline.

Section 2.1.1.2 provides a detailed explanation of hydration of OPC as a pure system. Within a blended material the hydration of OPC and slag occur concurrently but at varying rates. Since slag is latently hydraulic, it will react with water and hydrate, eventually, leading the grout to set and begin to harden. In practice, this process is far too slow to be feasible for any construction application; it is therefore essential to activate slag hydration within an alkaline medium. This may be achieved via the route of geopolymerisation (Duxson et al., 2006, Provis and Van Deventer, 2009, Van Deventer et al., 2012) or more commonly, as in the materials investigated in the present study, through blending with OPC.

Understanding and quantifying hydration of composite systems is challenging due to the fact that both the OPC and the slag (and/or other SCM) hydrate concomitantly and impact upon the hydration of one another. The presence of an SCM within a composite cement is known to accelerate the hydration of the OPC through what is known as the *filler effect* (Berodier and Scrivener, 2014, Berodier, 2015, Ogawa et al., 1980). This effect is thought to be due to a combination of factors; namely that the SCM increases shearing through reducing the inter-particle distance and hence decrease the diffusion path of chemical species (Berodier and Scrivener, 2014): and a *dilution effect* (Scrivener et al., 2015b) whereby the water: OPC ratio is increased (significantly in composites

such as those within the present study, which incorporate high levels of replacement by slag), resulting in relatively more space within the hydrating matrix into which the OPC hydrates may grow (Berodier and Scrivener, 2015). A further aspect of the *filler effect* which is only really significant when using much finer SCMs (such as silica fume) is the provision of extra nucleation sites to promote early hydration (Rossen, 2014, Korpa et al., 2008).

The work of Berodier (2015) not only highlighted the enhanced early to mid-age hydration (first 28 days) of OPC in the presence of an SCM (Scrivener et al., 2015b); it also elucidated the absence of hydration of the SCM itself (both slag and PFA) within the first 24 hours (2015). This lack of early hydration is likely due largely to the comparatively lower reactivity of the slag in comparison to OPC. Furthermore, the conditions within the hydrating matrix during these early stages are not optimal for slag hydration, since a more alkaline environment is required to promote and accelerate this reaction. This increase in alkalinity occurs as a result of dissolution of alkaline species from the OPC and the formation of CH from OPC hydration. The presence of CH is further beneficial as it is destabilised and 'consumed' via the hydration of the slag (Lothenbach et al., 2011). This effect is more pronounced at higher levels of replacement, as is the case within the present study. Moreover, slag loading has an impact upon the rate and degree of reaction, with slightly more slag having been found to react in a given time at lower replacement levels (Taylor et al., 2010, Whittaker, 2014).

Given the comparatively higher  $\text{Al}_2\text{O}_3$  content, and lower CaO content of slag in relation to OPC it is not surprising that composite cements display a lower Ca/Si ratio in the C-S-H than neat Portland cement pastes (Chen and Brouwers, 2006). This is coupled with an increase in the Al/Ca ratio, with both ratios following a linear trend with increasing slag content within the matrix (Richardson, 2000).

In addition to the changes induced upon the C-S-H within the hydrated paste, there are a number of other modifications to the phase assemblages and hydrates that are formed through replacing a fraction of the OPC with slag. Much work in the field of thermodynamic modelling has been performed in this regard (Whittaker et al., 2014, Lothenbach et al., 2012, De Weerd et al., 2011, Ben Haha et al., 2012); and the most effective way to represent the (predicted) changes induced through increasing slag loading is to plot composition against slag content, see Figure 2-3 (Lothenbach et al., 2011).

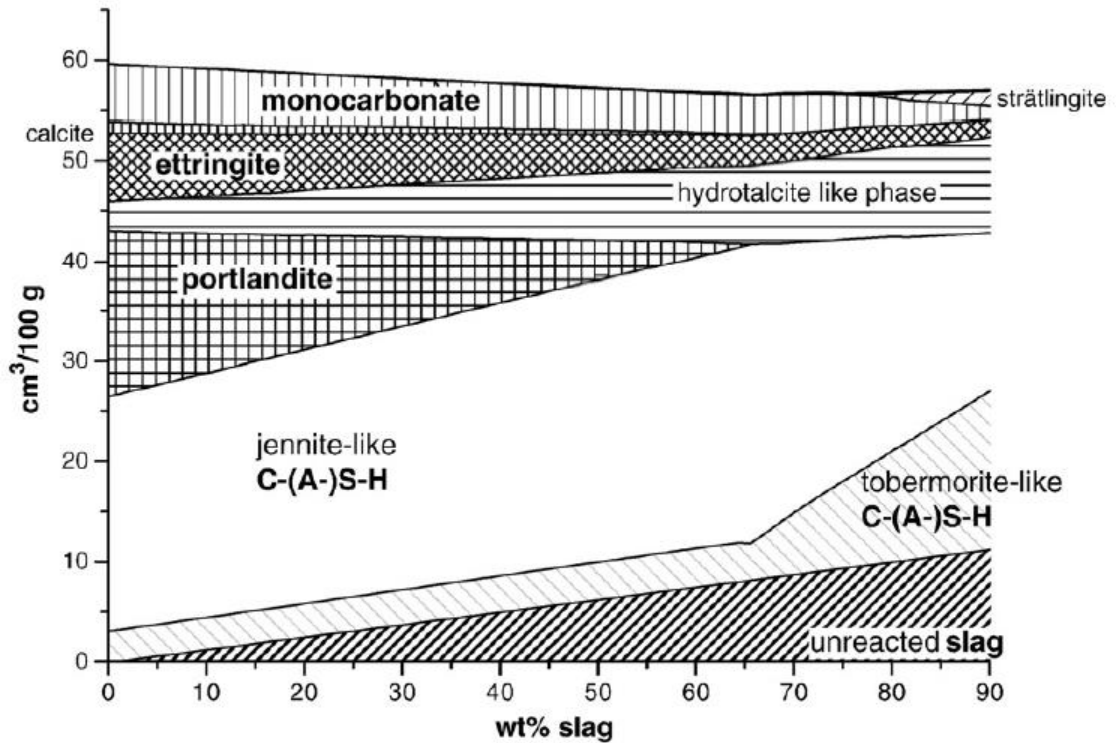


Figure 2-3: Modelled changes in hydrates formed within an OPC: slag blended system, with materials of typical composition and assuming 75% hydration of the slag component (Lothenbach et al., 2011).

These predicted changes to composition are largely in agreement with observed experimental results (Pane and Hansen, 2005, Escalante et al., 2001, Codina et al., 2008). The increased Al content of the composite cement brought about by an increasing slag content is incorporated into the main binding phase, C-(A-)S-H as well as hydrotalcite.

Given the amorphous nature of these hydrated phases it is very difficult to fully quantify their exact chemistry and composition. As a result, there remain gaps in knowledge, despite over half a century of research (Myers, 2015).

The chemical changes induced through replacement by slag are clearly illustrated in Figure 2-3; the ramifications of which should be clearly understood and planned for in the preparation of waste packages, as well as more generally in other applications. Coupled with these changes to the internal chemistry and phase assemblage are the physical changes that occur within the hydrating grout matrix.

Richardson and Groves (1992) identified changes in the morphology of the C-S-H as a result of replacement by slag; showing that the outer product (OP) C-S-H tends from a fibrillar to a 'foil-like' morphology as slag loading is increased. One benefit of this shift in

microstructural development is a more finely distributed porosity as coarse capillary pores are filled with hydrates, reducing interconnectivity and likely contributing to reduced rates of diffusion of ionic species (Page et al., 1981).

## **2.2 Treatment and disposal technologies for nuclear waste**

Within the UK, government policy for the final disposal of higher activity wastes is within a deep geological facility (NDA, 2010b) wherein there is the potential for retrievability (DECC, 2011). In the interim, until a suitable site is identified, licenced and constructed; wastes are to be pre-conditioned and maintained in safe and secure storage.

There exists a wide range of waste streams within the UK, all requiring disposal (with many requiring pre-conditioning, pre-treatment or encapsulation). Given the large disparity in compositions, volumes and activity levels, it is necessary to define a number of classifications of waste in order to begin to identify the most suitable and effective route to treatment for each waste stream.

A long and varied history of nuclear power in the UK carries with it a great deal of research and development, industrial changes, various reactor designs and an internationally significant reprocessing programme. One by-product of this development, in particular the reprocessing of spent fuel, has been the production of a large volume of highly variable waste streams.

This variability in waste composition has necessitated the development and implementation of a wide range of treatment and encapsulation technologies. It has been suggested that the only way to tackle the range and scope of waste streams is through the application of a 'toolbox' of different treatment options and encapsulant formulations (Milestone et al., 2006).

### **2.2.1 Classification of wastes and preferred routes to treatment**

The 2013 UK Radioactive Waste Inventory (NDA, 2013a) provides an overview of the scope of the challenge faced in dealing with the current stockpile, and future arisings, of radioactive waste. The report gives a breakdown of the different waste classifications and the preferred routes to treatment for each, with reference to the waste hierarchy and a brief description of the different treatment technologies currently being utilised for a wide range of waste streams.

### *2.2.1.1 Low level waste (LLW)*

The vast majority of waste covered within the UK inventory falls into the category of LLW (93.6% by volume); and of this, the bulk is classified as very low level waste (VLLW) (63.2% of total waste volume). This bulk waste accounts for less than 0.0001% of the total activity of all wastes covered within the inventory (NDA, 2013c).

LLW is defined as 'having a radioactive content not exceeding 4 GBq (gigabecquerels) per tonne of alpha ( $\alpha$ ), or 12 GBq per tonne of beta ( $\beta$ ) / gamma ( $\gamma$ )' (NDA, 2010a). Waste streams falling into this category are managed by the low level waste repository (LLWR) near to Drigg in Cumbria, on behalf of the NDA, and by Dounreay Site Restoration Ltd. (DSRL) at the LLW vaults adjacent to the Dounreay site in the Scottish Highlands.

A range of management options are implemented, mandated by a waste hierarchy (prevent > minimise > re-use > recycle > dispose) and include a number of intelligent solutions to reduce waste volume, including super-compaction and incineration of suitable waste streams. Certain high volume waste streams, consisting largely of slightly contaminated rubble, are, wherever possible, routed to permitted landfill sites rather than disposed of at the LLWR site (NDA, 2013a).

### *2.2.1.2 Intermediate level waste (ILW)*

ILW is defined as 'exceeding the upper boundaries of LLW, but not requiring heating to be taken into account in the design of storage or disposal facilities' (NDA, 2010a) and accounts for 6.4% by volume of all wastes covered by the Radioactive Waste Inventory (roughly 290,000 m<sup>3</sup>). ILW accounts for roughly 5% of the total activity of all waste (NDA, 2013c).

Conditioning of ILW represents the greatest challenge in preparing the waste stockpile for storage and final placement within a geological facility, due largely to the extent of variability in the waste streams covered within this classification, see Figure 2-4.

The preferred route to treatment for the large majority of wastes covered within this classification is encapsulation within a cementitious matrix (accounting for 83% of all ILW conditioned to date (NDA, 2013b). this technique is applicable to a wide range of waste compositions due to its versatility, the ease with which composition may be

augmented to suit any particular waste stream and the reliability with which the process can be performed (Utton and Godfrey, 2010).

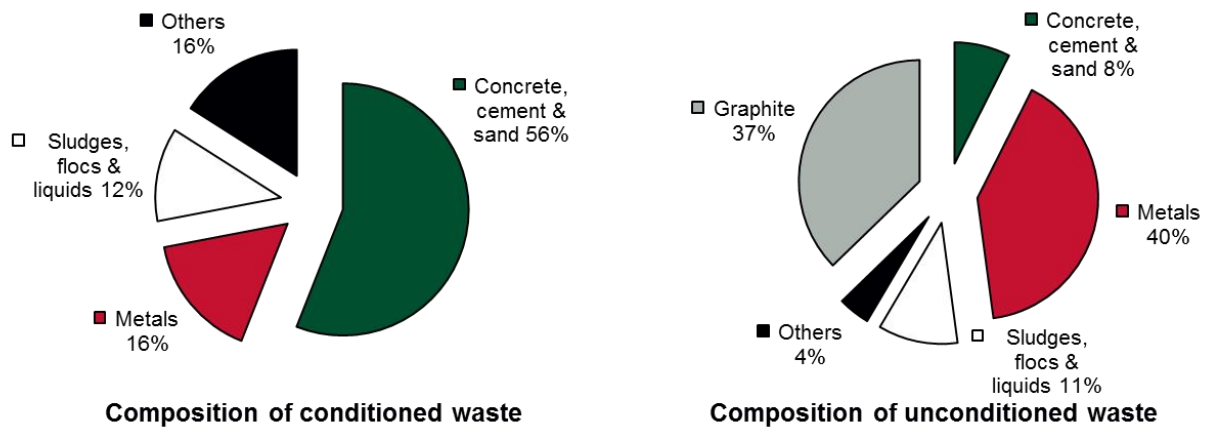


Figure 2-4: Composition of treated and untreated ILW streams within the UK waste inventory, modified from (NDA, 2013b)

A further advantage of the application of these particular cementitious grouts is their expedient rheological, and in particular their flow, properties; which are maintained for a sufficiently long and reliable period of time (with a minimum flow value as determined via an industrially accepted test required to be achieved 2.5 hours after mixing) (Miller, 2000). The resultant ability to pump the grout over long distances ensures that there is minimal contact between operatives and waste packages, negating many potential health and safety hazards posed by this potentially hazardous process.

Limits on setting time (4-18 hours) (Miller, 2000) ensure that grout integrity is maintained, avoiding segregation or the formation of 'bleed water' on the top of a waste package, which would constitute a secondary waste stream.

ILW is conditioned at a number of sites across the UK, including five plants at Sellafield site, one each at Dounreay and Harwell, and three at Trawsfynydd. All but one of these plants encapsulate waste with a cementitious grout (the exception being the resin solidification plant at Trawsfynydd which, until recent completion of all treatment at the site, used a polymer formulation to treat ion exchange materials).

Of the nine remaining active plants, six condition wastes within 500 litre stainless steel drums (as illustrated in Figure 2-5), with waste at Trawsfynydd's two remaining plants treated in 3m<sup>3</sup> drums and large items at Sellafield immobilised within large concrete boxes.

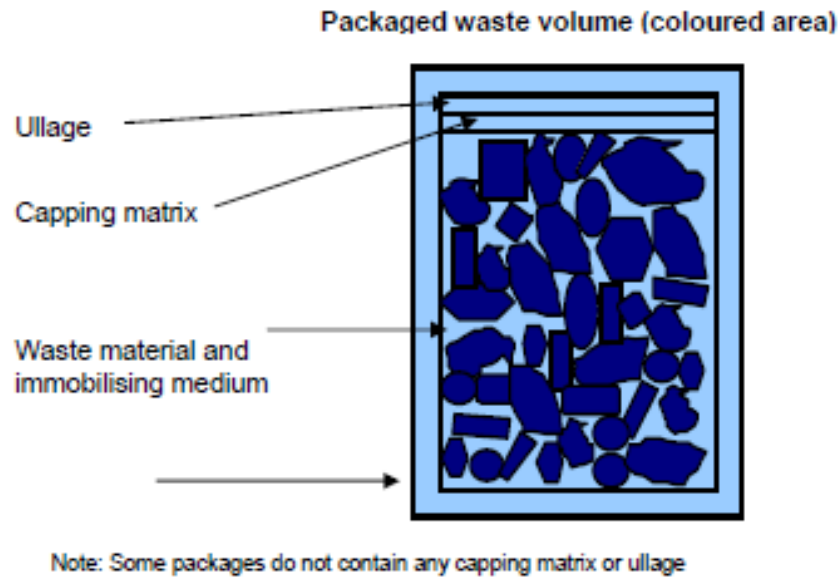


*Figure 2-5: Schematic of a generic conditioned ILW waste package within a 500L stainless steel drum (NDA, 2013d).*

In order to ensure consistency and conformity across all conditioned waste packages a standard procedure is applied. Firstly, the drum is fitted with a down pipe through which the grout will be introduced. The waste materials are then added, the volume of which is highly dependent upon the nature of the waste, but will typically be in the region of 20-50% of the total conditioned volume (NDA, 2010a). A mesh cover is then fixed above the waste materials to minimise movement prior to placement of the encapsulating grout, whilst allowing space for a capping matrix to be later added and in certain instances an ullage space (Figure 2-5).

The grout, which is normally a mixture of OPC and slag at a ratio of 1:3, but may be up to 1:9, is prepared. In certain cases, but much less frequently, grouts may be prepared with PFA rather than slag. The fluid grout is pumped to the waste filled drum and enters via the down pipe, thus minimising the potential for air to get trapped within the packaged waste matrix and maximising the contact between waste and grout.

This protocol was developed by British Nuclear Fuels Ltd. (BNFL), who identified 9 criteria which must be satisfied by these grouting systems and processes, as summarised below –

- Adequate flow characteristics to penetrate the wastes and infill void space.
- Ability to be pumped over extended periods without suffering segregation.
- Remain workable for a minimum of 2.5 hours.

- Achieve 'set' within 24 hours and gain sufficient strength to allow transport at this time.
- The peak temperature within a 500L drum should not exceed 100°C.
- The temperature profile across a 500L drum should not exceed 30°C.
- There should not be visible bleed water on the surface of the grout at 24 hours.
- The grout should be chemically compatible with the waste and the container material.
- Any materials used should not prejudice any of the options for eventual disposal.

There are, understandably, tight limits on the composition of the materials used in the preparation of these grouting materials. These limits are, in fact, one of the key drivers behind the need for the research included within the current study. The combination of the minimal control that the nuclear industry has over the production and specification of the materials used for the production of these grouts, coupled with compositional limits both in terms of chemistry and physical properties, has resulted in a number of supply issues both historically and in the current climate.

Whilst the process of treatment is well defined, a thorough understanding of the implications of changes to supply must be determined; further, new and developing techniques must be implemented to gain significant additional insight into the hydration of these grouts; to understand their engineering performance and resilience to deleterious environments. It is also essential that any potential threats to future supply are identified, with suitable mitigating options fully addressed and opportunities for improvements adequately explored. This underpinning in understanding coupled with efforts to futureproof supply are more important than ever given the current industrial uncertainties and significant changes taking place within the UK cement and steel industries.

### *2.2.1.3 High level waste (HLW)*

HLW is produced as a result of reprocessing of spent nuclear fuel and is initially in the form of concentrated nitric acid. HLW accounts for 0.02% by mass of the UK nuclear waste inventory (NDA, 2013a) but contains roughly 95% of the total activity (NDA, 2013c) and as a result generates significant heat. This heat must be taken into consideration for both the encapsulation technology applied, storage in the interim and design and implementation of a final disposal method (NDA, 2015).

The concentrated solution is mixed with crushed borosilicate glass and heated in a furnace to form a molten product. This vitrified material is then poured into 150 litre stainless steel canisters which are fitted with welded lids (NDA, 2016b) before being placed into air-cooled storage vessels where they are to remain for at least 50 years to allow for significant radioactive decay to occur, and hence less heat producing waste packages.

Once a GDF has been constructed and is ready to receive both ILW and HLW, these canisters will be placed inside two further containers before being transported to the final disposal facility.

## **2.2.2 Cementitious systems for ILW encapsulation**

As discussed in Section 2.2.1.2 the main route to treatment for ILW streams is encapsulation within a cement-based matrix. Historic research has provided a wealth of underpinning knowledge which suggests the suitability of cementitious materials for such an application (Atkins and Glasser, 1992, Glasser, 2001, Glasser, 1992, Wilding, 1992, Ghattas et al., 1992, Faucon et al., 1998, Palmer and Fairhall, 1992, Gougar et al., 1996, Glasser and Atkins, 1994).

The grouts generally used to encapsulate ILW here in the UK are a blend of OPC with slag, usually at a OPC: slag of 1:3, but occasionally with a ratio as high as 1:9 depending upon waste stream and waste package size, amongst other factors. As discussed in detail in Section 2.1.2.1, this significant replacement by slag provides a number of advantageous properties, both rheologically to the 'wet' grout and physically and chemically to the hardened grout matrix.

In order to achieve these beneficial properties, it has historically been necessary to prepare grouts for ILW encapsulation with a coarser slag fraction than would typically be used in a construction application. This has the effect of ensuring good rheological properties (i.e. good flow whilst ensuring no segregation or bleeding) whilst also allowing for a low water/binder ratio (w/b) to be achieved (typically 0.35, but possibly  $\pm 0.02$  of this, depending on the waste stream being treated).

In more recent years, and as a result of continued significant issues with supply, the slag component changed to a blended material (with bimodal particle size distribution, see Figure 3-2 S1<sub>f</sub> and S1<sub>c</sub>), whereby a slag with physical properties that would typically be seen in construction applications, has been blended at a ratio of 65:35 with a much

coarser material. This blending has had the effect of maintaining the rheological properties of the grouts without necessitating an increase in water content. Until now, no study into the impact that this shift in composition has upon hydration and engineering performance has been made.

Understanding and quantifying the reactions and interactions occurring between these complex and dynamic composite systems and waste species incorporated into them is challenging. This difficulty is compounded further by the hazardous nature of active wastes, which has had a significant impact upon the number of laboratory-based experiments incorporating any of these radioactive materials. The lack of cross-disciplinary knowledge and experience with such problems, applications and techniques means that there exists something of a paucity of overarching relevant literature. Valuable data on certain specific species-waste interactions have been contributed to by research in the fields of toxic and hazardous waste stabilisation/solidification.

The uniqueness of the chemical environment within a hydrating composite cement system means that whilst some data exists, the complete picture of performance with regards all potential radioactive waste species interactions remains unclear. As Glasser (2011) puts it 'we are as yet some way from having a complete quantitative understanding of the various mechanisms involved.'

#### *2.2.2.1 Grout/waste interactions*

A combination of chemical and physical interactions between grouting matrix and encapsulated waste contribute, amongst a range of other factors, towards the immobilisation potential of a treated waste package. There are a number of factors which contribute towards these 'chemical interactions', which will become the dominating factors in mitigating or minimising release of waste species as time progresses (Glasser, 1992) and degradation of conditioned, stored waste packages inevitably proceeds.

Table 2-2 provides an overview of the main mechanisms by which radioactive species are immobilised, or have significantly reduced solubility and/or mobility within a cemented waste package. Examples are provided for each of the mechanisms, however owing to the complexity of the vast majority of ILW streams, the presence of a range of radioactive species will undoubtedly result in a combination of all mechanisms occurring concurrently at different rates and to various extents within any one treated waste drum. For the purpose of clarity, a brief explanation is provided for each individual mechanism in Section 2.2.2.2.

Table 2-2: Reactions between cementitious grout and radwaste species, from (Glasser, 2011).

Binding mechanism	Characteristic features and comments
Sorption	Characteristically encountered at low species concentration but with low capacity. High surface area C-S-H is the main source of sorption for cesium
Structural substitution (radwaste substitution competitive for sites)	Crystalline components of cement offer potential anion and cation sites for uptake of radioactive species, e.g. chlorides in AFm, nickel in hydrotalcite-like phase, etc.
Characteristic phase formation (radwaste species essential)	Ca-U-OH is the ideal 'characteristic' phase for uranium and, similarly, CaSn(OH) <sub>6</sub> for tin
Oxy/hydroxyl precipitates	Often metastable and short-lived, e.g. Cr(OH) <sub>3</sub> . Difficult to identify on account of low crystallinity
Mixed mechanisms	Combinations of the above, often concentration-dependent

The chemical immobilisation potential of cementitious grouts shows a large variation across different waste species dependent on electronic configuration; where generally speaking, multivalent cations are more readily incorporated than monovalent cations, with anionic species showing a high degree of variability. This disparity in performance is further complicated by both speciation and oxidation state, which may have additional ramifications upon the mobility of a specific element within a conditioned waste package.

Continuous progress is being made in furthering knowledge and understanding of sorption processes and other binding mechanisms within cementitious materials. This advancement is reflected in the numerous journal papers published on the subject and the subsequent review articles collating the state of knowledge at the time of publication (Bradbury and Van Loon, 1997, Wieland et al., 2003, Evans, 2008).

For a thorough understanding of the current state of knowledge and progress on the subject, the publications of *Glasser* cited herein and the most recent review article of *Evans* (2008) provide an excellent starting point.

### 2.2.2.2 Binding of waste species

Sorption is the overarching term for a number of processes occurring within a conditioned waste package, including absorption, physical adsorption and chemical adsorption. Additionally, physical adsorption may be further sub-divided into surface complexation, ion exchange and 'other mechanisms', namely formation of solid-solutions and coprecipitation (Evans, 2008).

The source of much of the sorption potential of the hydrated cement paste is the high volume of C-S-H within the system, due to its amorphous nanoporous structure and very high effective surface area. Whilst the structure of C-S-H is not known for certain, it is believed to consist of very small 'gel' platelets (10-20nm) (Glasser, 2011); this composition lends itself well to a range of non-specific mechanisms of incorporation.

Of the crystalline phases formed upon hydration of OPC or composites thereof, Portlandite does not provide scope for sorption or incorporation chemically. The high pH buffering capacity it provides does, however, promote other mechanisms of immobilisation. Research suggests that AFm, AFt, hydrotalcite and hydrogarnet (when present within a hydrated system) provide potential 'sorbing' surfaces for dissolved radionuclides (Wieland et al., 2003, Ochs et al., 2015). *Glasser* (2011) defines this interaction as a structural substitution, distinct from the sorptive interaction occurring between the C-S-H and radionuclides in solution.

Cationic species may also bind through precipitation as either an amorphous oxide or hydroxide (Hf and Th for example) but are predicted to be thermodynamically unstable. Precipitation may occur as a result of reaction with one or more of the constituent phases of the cementing grout, it is predicted that these precipitates are metastable and are likely to react further either to form crystalline phases or to substitute into crystalline hydrates (AFm, and possibly AFt). In all instances, the precipitation and stability of the phases formed are dependent upon a number of factors, including, but not limited to; temperature, concentration and cement (and SCM/additive) composition.

### *2.2.2.3 Deterioration considerations of cementitious matrices in GDF service environments*

Cementitious grouts are currently used to condition much of the UK ILW inventory as a means of providing a primary barrier to release of radioactive species. It is envisaged that much of the infrastructure of the final geological disposal facility (GDF) will also be constructed from OPC based materials and sealed/infilled with similar materials (IAEA, 2009, Crossland and Vines, 2001).

With cementitious materials playing such an integral role in both the treatment of ILW and storage/disposal of ILW and HLW, it is imperative that there exists a clear and thorough appreciation of the long-term performance of waste packages, and the deep geological facility in which they're stored.

There exists very little research investigating samples at very late age. The rapid evolution and constant changes in the composition of both clinker and SCMs makes the task of undertaking analysis on mature, well developed grouts, mortars and concretes yet more difficult. Quantifying and understanding performance within realistic service environments provides a further challenge. Two approaches are often applied in scenarios where it is not possible to feasibly determine long-term performance; accelerated testing and modelling.

Accelerated testing by means of exposure to elevated levels of deleterious species (CO<sub>2</sub>, sulphates, chloride environments etc.) is a popular technique for gaining significant insight into potential performance within service scenarios (Papadakis, 2000, Roy et al., 1999, De Ceukelaire and Van Nieuwenburg, 1993). Many tests have made use of electrical potential or electrochemical methods to enhance or accelerate deterioration (Saito and Deguchi, 2000, Saito et al., 1992, Sugiyama et al., 2010b) with varying degrees of success.

Modelling of hydration, deterioration and transport properties provides a powerful tool in understanding performance, but it is imperative that models are based upon, and validated by, experimental results with rigorous testing conducted. Modelling accounts for a large portion of research into cementitious materials and is becoming an increasingly powerful tool, with improving computing power leading to great progress (Kamali et al., 2003, Yang et al., 2015).

A thorough understanding of performance and deterioration within a GDF over very long timescales is highly challenging and multi-faceted. Reference to findings from both accelerated testing and modelling provide useful insights into predicted performance. It

should, however, be borne in mind that there are a number of drawbacks with each approach.

## **2.3 Microstructural development and durability considerations**

Hydration, microstructure and durability are intimately linked. A clear understanding of these relationships is crucial in determining the suitability of conditioned wastes for their intended disposal scenario. Whilst it is clear that internal chemistry becomes the key governing factor at very late ages, a strong appreciation of microstructural development and the impact that it has on durability is vital in ensuring waste package integrity for the envisaged extended storage scenarios, and to ensure resilience during transport and the early stages following placement within a GDF.

It is intended for a GDF to be constructed, filled and closed; with inbuilt retrievability but essentially the intention of never disturbing nor interacting with the wastes again. It is essential, therefore, that a high degree of confidence is developed in the long-term performance of both the waste packages and the repository as a whole.

Since it is not practical nor feasible to conduct field trials of any meaningful length of time, in relation to the intended design life of a GDF; a thorough understanding of the development of the cementitious grouting materials, on a microscopic scale, is required to give insight into predicted long-term performance.

### **2.3.1 Techniques to probe microstructure in two and three-dimensions**

Elucidation of the microstructural development of cementitious materials has been a topic of scientific interest for a number of years, made ever more pertinent by the key role it plays in determining permeability and hence durability of cement-based structures and/or waste forms. There exists a wealth of techniques which have been applied in efforts to shed light on the pore spaces of hydrated cement pastes, grouts, mortars and concretes with varying degrees of success.

With all techniques there are advantages and limitations; some of these shortcomings relate to the extrapolation from two dimensions to three; a large majority of techniques require sample pre-treatment which is likely to introduce errors or have an adverse effect upon the fragile hydrates and microstructural features of a specimen and further techniques have limits to resolution which restrict their applicability.

It is particularly challenging to provide insight into the features and characteristics of a complete pore network since the length scales of all pores within a hydrating

cementitious material cover several orders of magnitude, from  $< 1\text{ nm}$  to  $> 1\text{ mm}$  (Stauffer and Aharony, 1994). Accurately identifying very small pores becomes increasingly challenging as the limits of resolution of each technique are reached, confidently defining pore space from solid material too becomes more and more difficult at very low length scales.

The following represent the most commonly applied and emerging techniques for this specific purpose; a clear understanding of the strengths and weaknesses of each allows for the selection of the most appropriate method for a given application. Clearly, as is the case in many previous studies, a combination of the following techniques is required to give sufficient and meaningful details of the microstructural development of a sample or group of samples.

It should be noted here that the first two techniques discussed below have not been applied within this study. It was felt that an understanding of each, including their strengths and weaknesses, previous applications and links to other techniques, provides an essential starting point for appreciating the current landscape and the ways in which probing and understanding microstructural development may be advanced. Further, since both techniques have been historically fairly ubiquitous within this area of research, to omit them would be to overlook a great deal of underpinning fundamental research.

#### *2.3.1.1 Mercury intrusion porosimetry (MIP)*

Intrusion of mercury or other non-wetting materials, such as Woods' metal, is one of the most commonly applied techniques for investigating the pore network and pore size distributions of cementitious materials. First applied by Winslow and Diamond (1969), the method has been used extensively to elucidate the porosity of cementitious materials ever since (Abell et al., 1999, Winslow, 1984, Winslow et al., 1994). When applying this technique, mercury is able to intrude pores down to roughly 2 nm in diameter (Aligizaki, 2005) and up to a maximum diameter of around 100  $\mu\text{m}$ .

In recent years, application of MIP has diminished slightly since it was shown to be largely inappropriate for analysing cement-based systems by one of the original advocates for its use (Diamond, 2000). MIP is limited by a number of factors; firstly, it assumes a cylindrical pore geometry (Willis et al., 1998) and secondly it is affected by an 'ink-bottle effect' (Moro and Böhni, 2002) in which it may underestimate total pore volume by limitations associated to the entry throats of large pores. A further issue with

MIP is the necessity for samples to be preconditioned prior to analysis and the subsequent errors that both drying technique and applied parameters may have upon results (Gallé, 2001).

MIP has been used to analyse cementitious grouts as used for ILW encapsulation in a number of previous studies (Collier et al., 2008, Collier et al., 2009b, Gorce and Milestone, 2007) with varying success. As a supplementary technique it is able to provide a range of interesting results, such as providing an accurate insight into the pore-size distribution within samples when applying the pressurization-depressurization cycling method (Zhou et al., 2010) which has been shown to give results in line with other applied test methods (Kaufmann et al., 2009).

#### *2.3.1.2 Nitrogen or water sorption (BET method)*

A further technique which has been used extensively to probe the pore structures within cementitious materials is that of sorption with one of two common adsorbates (nitrogen and water vapour), based upon the BET method (Brunauer et al., 1938). Again, there exists a great deal of controversy surrounding the application of this technique (Rarick et al., 1995) for the purpose of analysing pore structures within cement-based materials (Juenger and Jennings, 2001).

The BET method is capable of providing data on pores in the region of 0.3-300 nm (Zhou et al., 2010) and information on the specific surface area of hydrates within a system. Previous investigations have shown that adsorption of water vapour gives consistently higher values of porosity than does N<sub>2</sub> (Odler, 2003); a full understanding of the causes of this are as yet still unclear. Some researchers suggest that since H<sub>2</sub>O molecules are smaller than N<sub>2</sub> molecules, they are able to access smaller pore openings (Brunauer et al., 1967); however there is also the belief that water vapour may be interacting with the C-S-H of the hydrated sample (Juenger and Jennings, 2001).

As with MIP, samples must be pre-conditioned before they can be analysed via the BET method. Similarly, the drying method employed has been shown to have a significant impact upon the calculated properties (Snoeck et al., 2014, Zhang and Scherer, 2011) and as such it is very difficult to compare results across different studies unless the exact same drying technique and protocol has been employed.

### 2.3.1.3 Scanning electron microscopy (SEM)

SEM is one of the most versatile techniques for the analysis of cementitious materials and is most often performed in backscattered mode (SEM-BSE) on flat polished samples (Scrivener, 2004). High magnification, monochromatic images can be obtained of either topological features (in secondary electron mode); or more commonly, to provide information on composition (Goldstein et al., 2012). Compositional information can then be coupled with energy dispersive x-ray (EDX) data to determine degree and rate of hydration of different phases present within samples.

The method has the benefit of allowing for reproducible results to be obtained and for representative areas of samples to be analysed; however, the necessity of sample pre-drying and the limitations of observing samples in only two dimensions must not be overlooked.

It is generally agreed (Collier et al., 2008, Hearn and Hooton, 1992, Scrivener et al., 2016) that solvent replacement represents the least damaging option for water removal for samples prepared for SEM-BSE and the other techniques discussed here; however other techniques may also be suitable in certain cases.

The issue of extrapolation from two to three dimensions, as is the case for this technique is best explained with reference to the following figure (Scrivener, 2004). Where –

- a.) It is very unlikely that the analysed section will pass through the centre of a particle or pore, exaggerating hydrate phases in relation to anhydrous material.
- b.) The calculated pore size distribution will be underestimated since this 2D representation will be skewed towards smaller sections of larger pores.
- c.) It is not possible to determine interconnectivity of pores and pore networks, since pores which are in fact connected may appear not to be when viewed in two dimensions.

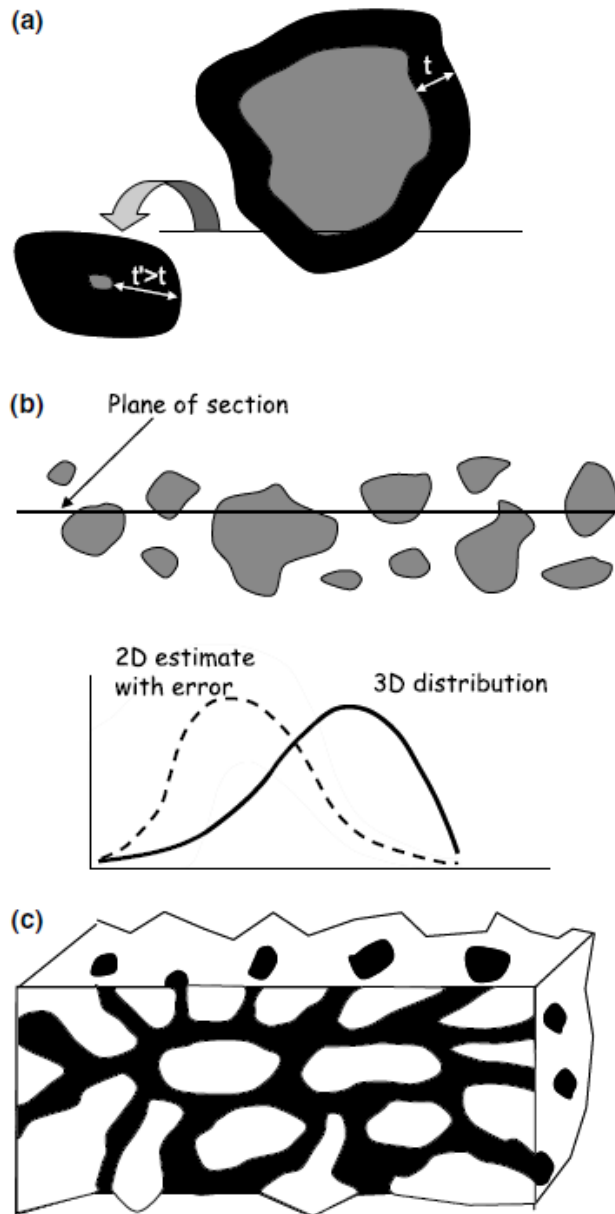


*Figure 2-6: Limitations of extrapolation from two to three dimensions with respect to feature sizes and interconnectivity (Scrivener, 2004)*

Further to gaining insight into porosity and microstructural development, SEM-BSE coupled with EDX analysis may be used to determine degree of hydration of OPC and SCMs within composite cement systems (Scrivener et al., 2015b) as discussed in more detail in Section 3.3.7.

#### 2.3.1.4 X-ray micro-computed tomography (X- $\mu$ CT)

More recently, the use of X- $\mu$ CT has gained significant popularity as a viable technique for probing the microstructural development of cement-based materials (Maire and Withers, 2014). Perhaps one of the earliest examples of the application of X- $\mu$ CT for analysis of microstructural development of hydrating cementitious materials is in the work of Helfen et al. (2005). Whilst there are clearly limitations to the technique of X- $\mu$ CT, it is the only method included herein where sample preparation is not required and non-destructive analysis is performed, thus providing the scope for the same sample to be analysed multiple times to follow continued hydration and development of the internal microstructure.

The vast majority of early X- $\mu$ CT analysis was performed at specialist synchrotron facilities (Gallucci et al., 2007, Beckmann et al., 2007, Promentilla et al., 2008, Promentilla et al., 2009, Sugiyama et al., 2010b); however, more recently with continued developments and improvements, lab-scale equipment is becoming increasingly popular and is able to offer a much simpler and cost effective alternative (Bossa et al., 2015, Zhang et al., 2012) capable of achieving sub-micron resolution in certain cases.

Development of subsequent post-processing analysis tools and programs has allowed for quantifiable results to be obtained relating to the inter-connectivity and tortuosity of pore networks within analysed samples (Nakashima and Watanabe, 2002, Watanabe and Nakashima, 2002, Nakashima et al., 2004, Nakashima and Kamiya, 2007, Nakashima et al., 2008).

Clearly there are a number of limitations to the application of X- $\mu$ CT, as is the case for all techniques. A key limitation with current lab-based systems relates to resolution, which is generally a factor of sample size, with typical maximum resolution roughly in the region of sample size/4000 (e.g. a resolution of roughly 2.5  $\mu$ m could be expected for a sample of diameter 10mm when using a lab-based machine).

A further challenge when analysing samples via X- $\mu$ CT is the difficulty surrounding thresholding and segmentation (Provis et al., 2012, Promentilla et al., 2007, Promentilla et al., 2008). Accurately identifying which areas within a sample, or more commonly a smaller representative region of interest, represent pore space and which are associated with solids (both anhydrous material and hydration products) can be very difficult given the resolution limits of most CT systems in relation to the size of the features within a hydrating cement-based matrix.

### 2.3.2 Techniques to follow degree of hydration of SCMs

It is essential to understand the extent of reaction of the SCM within a composite cement irrespective of application. A confident assessment of performance within a given service environment and accurate lifetime predictions are impossible without a thorough understanding of reaction and hydration; all of which becomes more important in the case of grouting matrices for nuclear wastes given both the potential hazard posed and the timescales involved.

Accurately determining the rate and degree of reaction/hydration of SCMs is challenging for a number of reasons. Firstly, there is the interaction between the SCM and the ground clinker component, the so called 'filler effect' which was discussed in more detail in Section 2.1.2 (Berodier and Scrivener, 2014). Secondly, the amorphous nature of most SCMs make them very difficult to quantify via classical techniques, XRD for example. Finally, reaction of SCMs can vary greatly from composite cement systems to geopolymer or alkali activated systems, meaning that simplification or comparisons are not possible.

The recent paper of Scrivener et al. (2015b) provides an excellent overview of the key direct and indirect techniques which may be applied to measure or follow SCM hydration. In the interest of brevity and pertinence, the following literature review will focus upon the application of techniques for following the hydration of slag within composite cement systems. For a broader introduction to the different methods available for a range of SCMs, the aforementioned paper is highly recommended.

#### 2.3.2.1 Direct methods

There exist four methods which may be applied to directly determine degree of SCM hydration; selective dissolution, BSE image analysis, XRD coupled with Rietveld analysis or the PONKCS method and NMR. Of the four, only one has been applied within the work presented here.

Application of selective dissolution (EDTA method) was considered but later dismissed, owing to the number of inherent flaws, uncertainties and the necessity of 'corrections' to obtain accurate results. The work of Kocaba (2010) highlighted the difficulties with this technique, and whilst it has been used for a large number of historic studies (Luke and

Glasser, 1987, Goguel, 1995, Lumley et al., 1996) it has been shown to be inferior to the other methods available.

Application of BSE image analysis has become an increasingly popular technique over recent years (Kocaba, 2010, Feng et al., 2004, Kolani et al., 2012, Utton, 2006, Gruyaert, 2011, Whittaker, 2014), especially with the improvements that have been made in the quality and speed of EDX mapping potential. This technique has been applied within the present study, with more information of the acquisition of images and elemental maps, as well as analysis, provided in Section 3.3.7.

Analysis of XRD patterns with the application of the partial or no known crystal structure (PONKCS) method has been utilised recently with slag blended cement systems (Snellings et al., 2014b). Results in this study were of good accuracy, however the technique is complex and specialist owing to complete overlap of the broad 'humps' produced as a result of diffuse scattering caused by the anhydrous slag and the C-S-H phase.

The final direct technique which may be applied in determining SCM degree of hydration is solid-state nuclear magnetic resonance (NMR) (Skibsted et al., 2007). This technique appears to give results which are consistent with other, indirect, approaches however it is relatively challenging when dealing with slag since there may be overlap of peaks with clinker phases (Scrivener et al., 2015b). Since access to NMR facilities was not as readily available as that of high quality SEM, it was not utilised in the present study.

#### *2.3.2.2 Indirect methods*

Determining rate and degree of hydration of an SCM within a composite cement system via any of the available indirect methods requires inference based upon hypotheses. It is therefore essential that these hypotheses, as well as the method itself, are as accurate and as true as possible. It is also crucial to have an understanding and appreciation of the interactions between the SCM and the clinker phases during hydration; including acceleration of reaction of the clinker phases due to 'filler effect' and changes to the composition of the C-S-H as a result of replacement. Accuracy in assumed composition of hydrates, in particular C-S-H, is essential since any errors will be magnified at high levels of replacement and at higher degrees of SCM hydration.

Two methods, chemical shrinkage and calorimetry, can be seen to lie within a grey area somewhere between direct and indirect. The methodologies for each are described in detail in Sections 3.3.2 and 3.3.3 respectively and have both been successfully applied

in previous studies (Kocaba, 2010, Kocaba et al., 2012, Whittaker, 2014, Berodier, 2015). To ensure accuracy with each technique it is essential that a suitable inert filler is used – typically quartz of a matching particle size distribution (PSD); thus guaranteeing that hydration due to filler effect is precisely accounted for.

Further challenges of the calorimetry approach are related to the very low heat evolution of samples at later ages; in order to mitigate against these potential errors, it is essential that suitable and accurate reference samples are used and that the machine is precisely calibrated and has a stable baseline. Since there appears to be no definitive enthalpy value for slag, nor an agreed upon method to calculate it (Scrivener et al., 2015b), as a result it is necessary to corroborate results with those obtained via a direct method (usually SEM image analysis). An additional consideration is the disparity in the effects of kinetics on the aluminate phase, since there is often a disparity in the interaction of slag with this phase in relation to quartz.

The work of Whittaker (2014) suggested that this reaction and the associated ‘hump’ from this interaction has no impact upon the validity of results at later age. This has been corroborated in an unpublished study carried out by Nanocem as part of an internal project (Myers et al., 2011).

Chemical shrinkage, as determined via dilatometry has been applied to cementitious systems for many years, almost exclusively based on the methodology developed by Geiker (1983). In recent years, technological advancements have allowed for accurate and stable results to be easily and consistently obtained (Costoya, 2008, Kocaba, 2010, Whittaker, 2014, Berodier, 2015). As with all techniques, there are a number of potential pitfalls which must be overcome, with precision and care required in sample preparation. Maintaining sample size and sample dimensions, as well as avoiding leakage within prepared samples is essential in ensuring accuracy; as is ensuring temperature stability within the system, with this factor becoming more pronounced with increasing levels of replacement by slag.

Preliminary testing of this technique, coupled with replicating previous testing showed the repeatability of the method. Whilst there are uncertainties with the specific volumes and stoichiometry of many of the hydrates present within the systems, particularly C-S-H (Scrivener et al., 2015b); this method is an accurate and inexpensive way of following hydration.

Two further methods using results from thermogravimetric analysis may be applied to provide an estimate of degree of SCM reaction; measurement of bound water content or Portlandite content. The bound water method is widely used to provide insight into

degree of hydration within plain Portland cement paste samples. The suitability of this technique is significantly reduced within composite systems owing to the increased complexity of the systems and the inability to separate the water bound due to the hydration of the clinker component and the contribution of bound water due to hydration of the SCM component. Whilst this technique is unsuitable for providing quantitative results, it is a very rapid and simple method of comparing hydration in a qualitative manner, to highlight the presence or otherwise of continued hydration, especially at later age.

Reference to portlandite content, which can be determined via thermal analysis, is often used as a comparative method to follow continued hydration of SCMs, based on the work of Pane and Hansen (2005). There are issues associated with this technique, including those surrounding the filler effect, the induced changes to C-S-H composition associated with replacement and the potential formation of other hydrates, such as hemiacarbonate or strätlingite. Nevertheless, this technique provides a very simple comparison across samples, so long as its limitations are well understood and accounted for.

## 2.4 Previous studies involving grouts for ILW encapsulation

Research into grouting formulations and specifications began in earnest in the mid-1980s after the official decision had been made to proceed with cementation as the primary route to treatment of intermediate level waste streams (Elsden, 1984). Industrially, much research and development was conducted internally, primarily at the Sellafield site, with very little published in the public domain.

The small number of book sections (Heafield and Fairhall, 1987), journal papers (Fairhall and Palmer, 1987) and, no-longer classified, industrial documents (Fairhall et al., 1985) show that the current specification does not deviate significantly from these originally developed formulations, nor have the specification limits on the chemical and physical composition of the clinker and slag components of the grouting materials changed over this time.

The one significant change relates to the inclusion of a fraction of a much coarser material, Calumite (constituting 35% of the slag fraction) into the current and legacy specification. This change was implemented when it was no longer possible to obtain slag that met the original specification, a result of plant closures and issues with continuity of supply.

A very interesting paper published more recently (Angus et al., 2010), provides some insight into the supply challenges that have been faced in the decades since the grouting specifications were developed; and the ways in which they have historically been addressed. Of note is that the issues discussed (namely supply of slag) have caused continuing and increasing problems in the years following this publication. Both slag and clinker supply have been changed in previous years and there are further concerns surrounding future slag supply given the volatility and uncertainty in the national and global markets.

Research into cementation of ILW is relatively disjointed; owing to a number of factors, including the numerous changes that have occurred within the nuclear industry over the years and the sensitivity of the research matter. In order to present some of the key underpinning and most relevant papers in the field they have been split into three sub-categories –

- Work published directly from industry
  - This section provides insight into the decisions and developments that led to the development and introduction of grouting as the primary method of conditioning for ILW.

- Publications from Glasser and Atkins
  - Reference to papers published over the past 30 years which primarily dealt with outlining the key areas of research and development breakthroughs and requirements.
- Research from the Immobilisation Science Laboratory (ISL) at Sheffield University
  - The group at the ISL has been actively involved in researching cementitious grouts for ILW treatment for over 15 years; this section gives a brief introduction to the work that has been conducted and the aspects of application that have been investigated.

#### **2.4.1 Published works from the nuclear industry**

The work of Elsdon (1984) serves very well to set the scene at the onset of the drive to condition all legacy waste in the UK and to develop methods to deal with all newly arising materials from reprocessing and decommissioning operations. The paper provides a brief overview of the objectives of conditioning and an introduction to the range of waste streams requiring treatment.

At the time of publication there were already two small treatment facilities in operation within the UK, with others in operation internationally. Official specifications had not at that point been developed but it was clear that treatment within a cementitious grout was the preferred route to conditioning.

Subsequent publications from Fairhall and Palmer (1985, 1987, 1992) showed clear development of the formulations and procedures implemented in the treatment of ILW. During the years 1984 to 1992 there was significant investment in R&D and construction, with the building of 3 large ILW encapsulation facilities at Sellafield site (Palmer and Fairhall, 1992). Over this period, British Nuclear Fuels Ltd. (BNFL) had developed a 'cement specification for ILW immobilisation' (Fairhall et al., 1985), which has had a number of addendum issues in the years since; the standard specifications and conformity limits have remained very much the same throughout this time (except for some very slight relaxations in chemical compositional limits much later).

Wilding (1992) provided a thorough overview of the vision towards waste treatment and gave a relatively in-depth overview of grout specifications and some of the key engineering considerations which led to the development of the specification. Within this

study there was clear reference to the risk posed by fire scenarios, highlighting the significance of better understanding of the effects of this, amongst other transport and handling considerations.

#### **2.4.2 The works of Glasser and Atkins**

Glasser and Atkins have played a pivotal role during this period of research and development. Their research represents a large volume of highly significant underpinning knowledge covering a wide range of scientific and engineering problems relating to the challenges surrounding treatment of ILW. Some of this work covered applications of modelling, but the most significant contributions relate to periodic overviews of the landscape, challenges and progress within the field.

Very early work during this period (Glasser et al., 1986, Atkins and Glasser, 1992, Atkins et al., 1992) laid the foundations for modelling of cement/waste interactions and paved the way for further, more powerful, research in this field. Clearly the computational power used at that time was poor by today's standards but the model was based on sound chemistry and therefore relatively powerful and insightful.

Glasser was involved in research alongside the UK nuclear industry for a great number of years; but as has been the case historically, there has been very little published literature relative to the volume of research conducted. The large majority of publications from Glasser and Atkins relate to broad overviews of the current state of the art and specific challenges and issues faced by the technology.

These publications span more than two decades, with the first (Atkins and Glasser, 1992) providing a thorough introduction to the engineering challenges relating to rheological properties of grout formulations, heat evolution considerations and resilience to service environments. Since this initial publication a number of subsequent journal papers have been published (1994, 1997, 2001, 2011).

The most recent in this series of reviews of research and development provides a thorough overview on the current trends and challenges in continued research. The report focuses on considerations for modelling, binding mechanisms, impact of pH, impact of heat of hydration, redox potential and non-Portland cement based systems (Glasser, 2013).

This represents the most exhaustive report into the current state of knowledge and research challenges faced as a whole in the future of treatment, storage and disposal of ILW within cementitious grouts.

### **2.4.3 Research from the University of Sheffield**

The Immobilisation Science Laboratory (ISL) at the University of Sheffield has been actively involved in research surrounding the application of cementitious materials for the treatment of nuclear waste for a number of years; over that time the group has published a considerable volume of research. Industrial involvement has ensured that a wide scope of the engineering challenges has been investigated, with the incorporation of a wide range of materials and mix designs.

Much of the early studies at Sheffield were conducted by Hill and Sharp, with preliminary investigations into phase assemblage (2002) and the effect of elevated temperatures (2002, 2003). The work of Hill then went on to focus on the encapsulation potential of different grouting formulations with respect to a number of radioactive analogues (2003, 2005).

A number of other projects within the ISL continued on from this; extending investigations in a number of directions. The works of Utton (2003, 2006, 2008, 2010, 2011) probed the impact of temperature on grouts at high levels of replacement by slag and also the immobilisation potential of barium containing waste streams.

The works of Collier (2004, 2006, 2006, 2009a, 2009b, 2010, 2010, 2011) focused largely on the treatment of a particular iron containing flocculant waste stream with later works investigating the treatment of magnesium containing wastes and investigation into activated cementing formulations. The research of Setiadi (2006b, 2006a) focused on the interactions between metals and composite cements, in particular aluminium and magnesium.

Further research conducted by Gorce (2006, 2007) probed the microstructural development of slag composite cements at 75% replacement. The key findings surrounded the reduction in the prevalence of capillary pores, relative to plain Portland cement samples, but an increase in the volume of gel pores. Borges (2008, 2010, 2012) studied the impact of deterioration on grouting matrices via the application of accelerated carbonation and cyclic wetting/drying; aiming to gain a greater

understanding of the potential long-term behaviour and performance of a range of grouting formulations based on Portland cement and blended with either slag or PFA.

In recent years, there has been a trend towards the study of novel formulations which are not based on Portland cement. The need for a range of different grouting formulations in order to deal with the wide variety of waste streams was highlighted by Milestone et al. (2006); the group at the ISL has played an active role in expanding knowledge into a variety of different potential grouting matrices. Recent projects have focused on magnesia based systems (Walling et al., 2015) blended magnesium potassium phosphate cements (Gardner et al., 2015) and  $\text{Ba}(\text{OH})_2$  blended systems (Mobasher, 2015) to address some very specific engineering challenges.

## 2.5 Summary

The hydration of neat Portland cements is now relatively well understood and the picture for composite cements incorporating high levels of replacement by slag is becoming ever clearer with continued breakthroughs in analysis techniques and the publication of academically rigorous research.

A thorough understanding of the interaction of cementitious materials with encapsulated nuclear wastes, however, still requires a great deal of further investigation. Whilst a number of studies have been conducted, both industrially and academically, the disconnect between research means that a number of key questions remain unanswered.

This field of study is hugely varied and a significant volume of research will be required in order to have a clear picture of the interactions occurring between waste and encapsulant. Factors such as temperature, surrounding strata, pH and ageing/degradation also play key roles in the design of both treatment technologies and the selection of suitable engineering barriers to mitigate the risk posed to the public.

Within the UK there is a significant issue with regards the supply of cementitious materials that meet the tight specification limits set out for encapsulants used in the treatment of ILW. These limits are based upon legacy research which identified chemical and physical compositional envelopes which result in grouts that meet a number of rheological requirements and do not result in significant heat evolution as a result of hydration. Whilst these factors are all significant in terms of logistics and avoidance of

heat-induced cracking, there has been no consideration of long-term performance, grout hydration and compatibility with specific waste species/streams.

Quantifying hydration and engineering performance as a function of composition is crucial in gaining significant insight into suitability of current, legacy and future grout specifications and in ensuring that the risk posed to the public is minimal in the final design and implementation of a GDF.

## **3. Materials and methods**

Chapter 3 provides details on the materials and experimental techniques used within this study. Information is provided on sample preparation as well as details of the range of techniques used to subsequently quantify the hydration, microstructure and composition of the various grout formulations.

Wherever possible, testing was conducted by the author at the University of Leeds; however, in the very few instances where access to equipment or facilities meant that this was not possible, credit has been given to the instrument operator responsible for acquisition.

### **3.1 Characterisation of Raw Materials**

The materials studied throughout this project were obtained from a number of sources. It was therefore necessary to fully characterise them prior to the commencement of experimental investigation. A number of the materials were comminuted at the University of Leeds using a planetary mill, it was therefore essential that the physical properties of all anhydrous powders was well characterised to ensure consistency and conformity. In order to achieve this, a number of techniques were applied, and where possible compared with supplied data or otherwise repeated elsewhere to check equipment calibrations and avoid the potential for erroneous results due to, for example, operator error.

#### **3.1.1 XRF**

XRF analysis (Philips PW2440 sequential X-ray fluorescence spectrometer) was carried out at Sheffield Hallam University on all of the anhydrous powders. Certain materials, including the two OPC powders and Scunthorpe slag (S1f), were provided along with their chemical composition, these powders were reanalysed to ensure consistency and accuracy.

#### **3.1.2 Determination of Particle Size Distribution (PSD)**

Particle size distribution was determined via laser granulometry (Malvern Mastersizer 2000E) using isopropanol as the dispersant and a rotating paddle (3000 rpm) to disperse and disagglomerate the particles prior to measurement (in addition to stirring by hand for 2 minutes prior to placing samples into the machine). Obscuration was maintained at 8-10% with 10 measurements taken per sample and an acquisition time of 10 seconds and a pause time of 5 seconds between repeat measurements; parameters were informed by previous studies (Arvaniti et al., 2014b) and maintained across all materials for consistency.

Materials received from Hanson, via>NNL, were first analysed to ensure that the laser diffractometer was properly calibrated and results were in agreement with those provided by the supplier, whilst also ensuring that the materials were consistent and well

homogenised across sample tubs. Materials which were comminuted at the University of Leeds were analysed using the same technique and operating parameters.

In order to determine the appropriate operating parameters to obtain suitably graded material for this application as defined industrially (BNFL, 2000) it was necessary to determine suitable residence times within the planetary mill used for comminution (Glen Creston GyRo mill) to achieve comparable PSD across a range of materials. After suitable parameters had been determined a number of samples were analysed to ensure consistency and conformity.

In order to ensure suitably graded material (see Figure 3-2) it was necessary to first sieve the raw slag to ensure that material of similar fineness was pulverised, producing a consistent PSD profile. There was some concern that this sieving may result in fractions with varied composition, however subsequent XRF analysis showed negligible disparity in chemical composition.

### **3.1.3 Methods to determine density**

The density of anhydrous powders was determined at the University of Leeds using an Ultracycrometer 1000 (Quantachrome instruments) and verified by Hanson using a Quantachrome MUP-6DC machine. Results were in agreement within a range of  $\pm 0.5\%$  and are given in Table 3-3.

### **3.1.4 Methods to determine Specific Surface Area (SSA)**

Accurately determining specific surface area of OPC, slag and quartz powders can be relatively complex given their irregular shapes, varied PSD profiles and differences in density and refractive indices (Arvaniti et al., 2014a). The issue arises as a result of simplifications and/or assumptions made by the respective techniques, the most common being that of modelling particles as spheres.

One method applied to determine the specific surface area of materials was Blaine fineness (ASTM C204-96a). The technique is based on the principle of determining air flow through a compacted bed of powder of known porosity (generally 0.5 where possible). The time taken for a fixed volume of air to pass through a bed (12.7 mm in

diameter and 15 mm in depth) is used to determine specific surface area ( $S_w$ ) via application of the following equation –

$$S_w = K\sqrt{t}$$

*Equation 5*

Where  $t$  is time and  $K$  is the apparatus constant, determined via analysis of the equipment calibration cement produced and distributed by the National Institute of Standards and Technology (NIST), Washington, USA. (Hewlett, 2003). During this experiment the pressure steadily decreases as air flows through the specimen.

The method has been used extensively within the cement industry for many years to ensure and maintain conformity, however it is open to potential operator error and has been shown to provide less accurate results when used to analyse coarser materials (with respect to standard specifications for cementitious powders) (Costoya, 2008).

Further determination of SSA was performed by Paul Rounce (Hanson cement group, Scunthorpe); applying the Lea and Nurse method. This technique is similar to that of the Blaine method, however a larger sample is analysed, with slightly different parameters, significantly the pressure remains constant and after passing through the sample the air continues through a length of capillary tubing. The method is based on the Carman-Kozeny equation –

$$S_w = \frac{N}{\rho(1 - \varepsilon)} \sqrt{\frac{\varepsilon^3 A \Delta p}{\eta Q L}}$$

*Equation 6*

Where –

$A$ ,  $L$  and  $\varepsilon$  are the cement bed cross-sectional area, thickness and porosity;

$\eta$  is the Stokes viscosity of air and  $Q$  is the rate of flow of air;

$\rho$  is the powder density;

$\Delta p$  is the drop in pressure across the compacted bed, and

$N$  is a dimensionless constant which is dependent upon the units chosen.

The apparatus is fitted with two manometers which measure the pressure drop across the cement bed ( $h_1$ ) and the pressure drop across the capillary ( $h_2$ ), with the second manometer acting as a flowmeter (Hewlett, 2003). Specific surface area can then be deduced from these manometer readings via the following equation –

$$S_w = \frac{K}{\rho} \sqrt{\frac{h_1}{h_2}}$$

*Equation 7*

Where, as with the Blaine method, K is an apparatus constant.

### 3.2 Materials

Whilst very similar in composition to 'standard' construction cement and slag powders, the materials used within the study (and hence for the treatment of ILW) have been prepared without the addition of minor additional constituents (MACs) and ground in the absence of organic grinding aids. These omissions are significant for two reasons. Firstly, their inclusion could potentially result in adverse reactions or complexations when mixed with waste streams, rendering them unsuitable as waste packages.

The second reason as to why these compositional nuances are significant is how they impact upon supply. The use of MACs and grinding aids are ubiquitous in the preparation of clinker to form OPC and slag for construction purposes as both help to reduce the embodied carbon of the materials through improving grinding efficiency and powder processing or reducing the clinker content of the OPC (and its associated embodied carbon, both anthropogenic and created through production). Within standard applications, the inclusion of a small amount of limestone, as a MAC, also accelerates some of the hydration reactions whilst also providing nucleation sites to further enhance early age hydration.

Given that the construction trade accounts for well over 99% of all OPC and slag used both nationally and globally it is very difficult to source materials which are not prepared in this manner. This presents the nuclear industry with a potential continuity of supply issue and is one of the key drivers behind this project.

Table 3-1: Chemical composition of as received materials determined via XRF

Oxide (%)	C1	C2	S1 <sub>f</sub>	S1 <sub>d</sub> /S3 <sub>c</sub>	S2 <sub>d</sub> /S2 <sub>f</sub>
<b>CaO</b>	65.4	64.6	39.8	40.5	43.2
<b>SiO<sub>2</sub></b>	21.1	20.3	37.2	36.0	36.1
<b>Al<sub>2</sub>O<sub>3</sub></b>	4.5	5.2	10.8	11.8	10.8
<b>TiO<sub>2</sub></b>	0.4	0.3	0.7	0.9	0.7
<b>MnO</b>	0.1	0.04	0.4	0.4	0.4
<b>Fe<sub>2</sub>O<sub>3</sub></b>	2.8	2.6	0.4	0.25	0.5
<b>MgO</b>	1.0	2.4	7.9	7.9	3.7
<b>K<sub>2</sub>O</b>	0.7	0.8	0.6	0.6	0.9
<b>Na<sub>2</sub>O</b>	0.3	0.4	0.2	0.3	0.16
<b>SO<sub>3</sub></b>	3.4	2.8	1.7	0.6	0.6
<b>Basicity ratios</b>					
<b>C/S</b>			1.07	1.13	1.20
<b>(C+Mg)/S</b>			1.28	1.34	1.3
<b>(C+Mg+Al)/S</b>			1.57	1.67	1.60

Table 3-2: Clinker phases as determined via Bogue analysis

	C1	C2
<b>C<sub>3</sub>S</b>	54.7	58.9
<b>C<sub>2</sub>S</b>	18.2	13.8
<b>C<sub>3</sub>A</b>	7.5	6.5
<b>C<sub>4</sub>AF</b>	9.0	15.4

Table 3-3: Physical properties of anhydrous materials at time of mixing

Material	d <sub>0.1</sub> (µm)	d <sub>0.5</sub> (µm)	d <sub>0.9</sub> (µm)	SSA (m <sup>2</sup> /Kg)	Density (g/cm <sup>3</sup> )
<b>C1</b>	3	17.5	50	325	3.16
<b>C2</b>	2.7	15.5	50	384	3.15
<b>S1<sub>c</sub></b> <b>(Calumite)</b>	85	350	800		2.80
<b>S1<sub>f</sub></b>	1.5	7.3	24	526	2.95
<b>S2<sub>c</sub></b>	4.1	40.5	145	262	2.91
<b>S2<sub>f</sub></b>	2.2	17	58	365	2.90
<b>S3<sub>c</sub></b>	3.9	36	135	294	2.91

The chemical compositions and physical properties of the as received and ground materials are given in Tables 3.1, 3.2 and 3.3. The margin of error of the techniques employed to determine these values are largely inferred, partly through the rounding up of results (to 1 decimal place in the case of the XRF values given in Table 3.1, and likewise for the Bogue values in Table 3.2).

Values for PSD, as shown in Table 3.3 are believed to be accurate within an error of 2-3%, in line with the work of (Arvaniti et al., 2014b) with analysis performed under consistent operating parameters.

### 3.2.1 Ordinary Portland Cement (OPC)

The two cements used in this project were supplied by Hanson cement via NNL and represent the current and legacy specification powders (C1, from Ketton, is the current specification powder; C2, from Ribblesdale, is the legacy material which was used to produce grouting material until early 2015). At the onset of the project the supply of OPC powder was in the process of switching, the result being that there was both industrial and academic interest in understanding the impact of this upon hydration and resultant microstructural development and performance of grouting matrices.

The chemical and physical composition of each is provided in Table 3-1 and Table 3-3. Chemically there was little difference between the two OPC powders, with the most significant factors in this regard being the slightly higher MgO content of the 'legacy' OPC powder, C2.

The physical composition of both powders, as determined via laser granulometry, pycnometry and application of the Lea and Nurse method (Sections 3.1.2, 3.1.3 and 3.1.4) are provided in Table 3-3. C2 contained a higher fraction of finer material, the result being a specific surface area 20% higher than observed for C1.

Figure 3-1 shows the particle size distribution (PSD) of the two OPC powders, the presence of a higher fraction of fine material in C2 is the reason behind the relatively higher specific surface area. Had these powders been produced under typical processing conditions (with grinding aids and MACs), they would be classed as CEM1 42.5N cements.

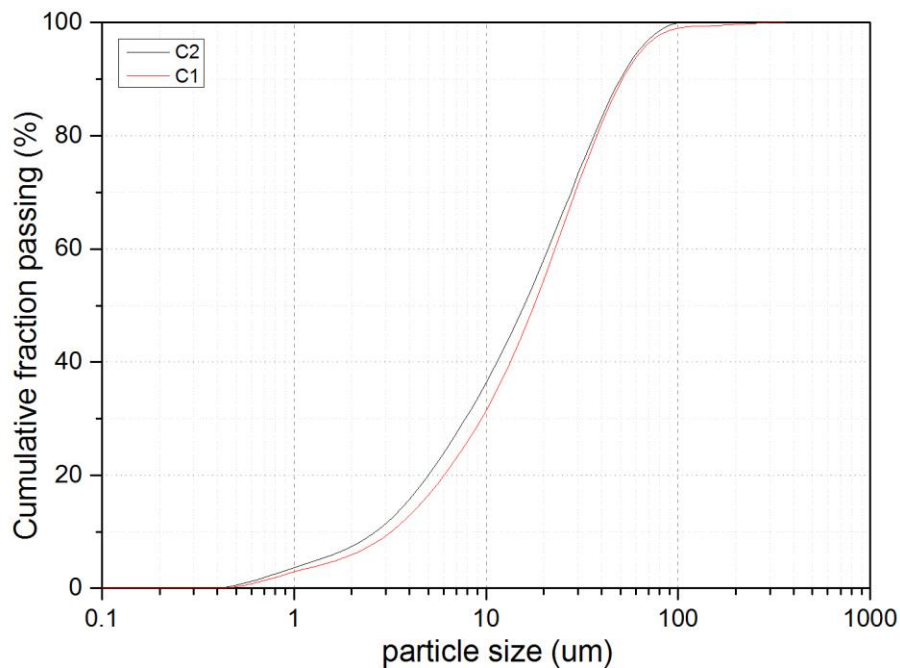


*Figure 3-1: Particle size distribution of cements*

### 3.2.2 Blastfurnace Slag (slag)

The three slag powders used throughout the project were sourced from either Hanson cement (via NNL) or from Redcar blast furnace (slag 2). S1<sub>f</sub> and S1<sub>c</sub> (Calumite) were

received prepared and pre-ground (in the case of S1<sub>f</sub>) by Hanson. Calumite, which is generally used in the production of glass, has a much coarser PSD than the other slags investigated within this study and is incorporated into the current (C1S1) and legacy (C2S1) grout formulations to offset the fineness of the S1<sub>f</sub> slag that is now used (at a ratio of 65:35 S1<sub>f</sub>: Calumite). This inclusion ensures conformity with limits for rheology, flow, setting time and avoidance of the formation of bleed water.

Table 3-4: Legend of mix designs of powder compositions studied

Mix	Powder composition	Context
<b>C1S1</b>	OPC 1 - Ketton, BFS - 65% Scunthorpe fine, 35% very coarse Calumite	Current specification grout for ILW encapsulation
<b>C2S1</b>	OPC 2 - Ribblesdale, BFS - 65% Scunthorpe fine, 35% very coarse Calumite	Legacy specification, used up until very recently when supply of OPC had to be change
<b>C1S2c</b>	OPC 1 - Ketton, BFS - Teesport coarse grind	Potential replacement formulation identified which is at the 'coarse limit' for BFS composition as defined by BNFL
<b>C1S2f</b>	OPC 1 - Ketton, BFS - Teesport fine grind	Potential replacement formulation identified which is at the 'fine limit' for BFS composition as defined by BNFL
<b>C2S2c</b>	OPC 2 - Ribblesdale, BFS - Teesport coarse grind	Prepared to provide a direct comparison with C1S2c (as C1S1 and C2S1), to allow for quantification of composition of OPC on hydration and performance
<b>C1S3c</b>	OPC 1 - Ketton, BFS - Calumite coarse grind (matching PSD to Teesport coarse)	Very coarse Calumite material was ground to matching PSD of S2c to allow for direct comparison and quantification of impact of changes to chemical composition whilst maintaining physical properties

Historically, slag complied with a specification (BNFL, 2000) in which there were relatively tight limits on fineness (270-310 m<sup>2</sup>/kg as determined via Blaine permeability method). Due to issues with material supply it was necessary to go outside of this specification, since the historic limits define a slag much coarser than those which are typically used in the construction industry (who essentially dictate grinding of slag, being by far the main consumer).

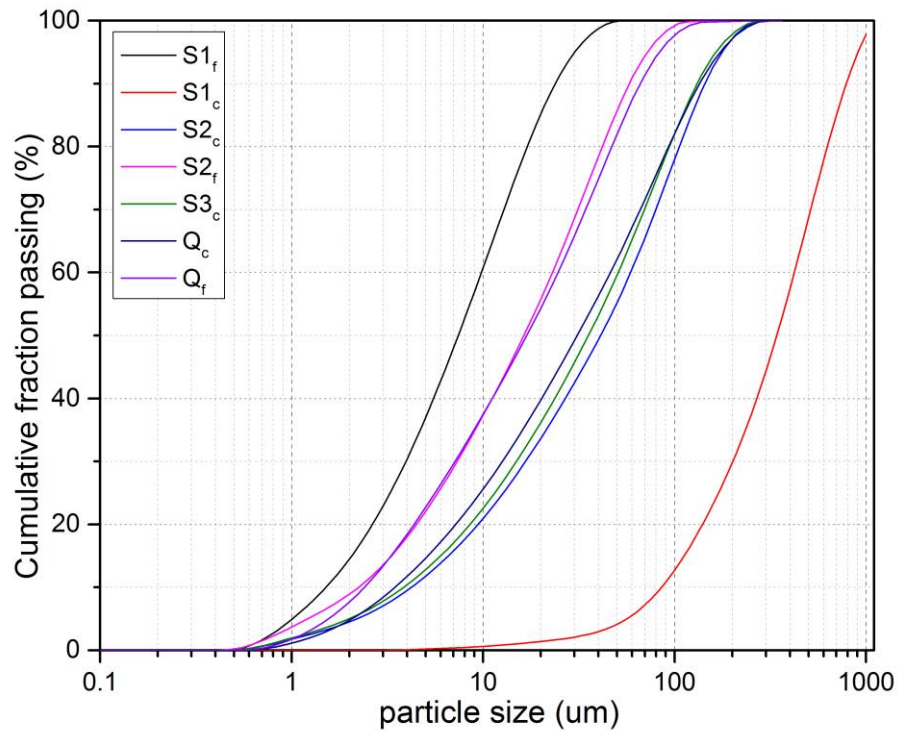


Figure 3-2: Particle size distribution of slag powders and quartz

S2 was received in its raw form from Redcar steelworks; it was first oven dried at 105°C overnight to remove any moisture and reduce agglomeration. Once dry, the slag was sieved into 3 fractions (>64µm, 64µm-600µm and >600µm) before grinding; this provided powders of tighter particle size distributions and was necessary in order to ensure that ground materials had a standard resultant PSD following grinding (see Figure 3-2). Material graded below 64µm was ground to produce S2f and material between 64 µm and 600µm was ground to produce S2c

Grinding was performed using a Glen Cresson planetary mill; slag was ground in batches of 150g ± 0.1g, with a 'trial and error' approach taken to determine the optimum residence time to achieve a material of suitable PSD and SSA for both a 'fine' and 'coarse' fraction. Laser granulometry (Section 3.1.2) was performed on ground materials in order to calculate optimum residence times within the grinding mill. Subsequently, large volumes of materials (in the order of 10s of KGs) were ground for each fraction and homogenised within tubs which were sealed until material was required for testing.

In order to achieve materials of similar physical properties (S2, S3 and quartz, to be used as an inert filler in certain techniques) it was decided that the PSD as determined

via laser diffraction would be used to inform consistency, given its comparatively improved suitability to these materials in relation to other potential analysis methods (Arvaniti et al., 2014b) and the speed and consistency with which it can be performed.

### **3.3 Experimental Techniques**

#### **3.3.1 Mix Designs and Sample Preparation**

All testing was conducted on paste samples since this is the grouting material that is used for the treatment of ILW (and some LLW) in the UK. Mixes were prepared in line with the specification for grouting materials as outlined in legacy BNFL technical specifications (BNFL, 2000) in so far as powder ratios were maintained, water binder ratio (w/b) and chemical compositions fell within specification. The only deviation from these limits was in the PSD of the powders (in particular S2<sub>c</sub> and S2<sub>f</sub>) as this was one of the key parameters of investigation given its bearing upon performance and the historical compoment that it has had upon powder supply. All samples were prepared at a w/b of 0.35.

#### **3.3.2 Dilatometry**

##### *3.3.2.1 Principle of chemical shrinkage*

It has long been observed that the volume of hydrated cementitious materials is lower than the combined volume of the constituent materials prior to the onset of hydration (Powers, 1935), with the first reported measurements made by Le Chatelier (1905). This phenomenon is a result of water having a lower specific volume when bound to a solid than when free as a liquid. It provides a simple and accurate means for following the rate of hydration of cementitious materials and offers the possibility of isolating the rates of hydration of distinct phases through replacement with inert filler material.

A number of different techniques have been applied over the years to follow chemical shrinkage, including gravimetry in which the change in specific gravity is measured, via pycnometry in which the change in weight is determined, or as in this study, via

dilatometry. The method protocol was first developed by Geiker (1983) with a number of more recent studies making use of technological advancements (Geiker, 2016) to increase accuracy and allow for continuous measurement to be made (Costoya, 2008, Kocaba, 2010, Whittaker, 2014, Berodier, 2015).

### *3.3.2.2 Sample preparation and experimental setup*

Mixes were prepared by first combining 100g of the powder fraction (OPC and slag, or OPC and quartz) and mixing vigorously by hand, shaking for 5 minutes in a sealed container. 50g of material was weighed out and combined with 17.5g of deionised water (w/b 0.35) and mixed by hand for 2 minutes. The resultant paste was weighed into 3 plastic beakers (34mm internal diameter),  $15 \pm 0.01$ g of paste per sample. Each sample was tapped firmly against a hard surface so as to remove any entrapped air, water was added to the top of the samples very carefully to avoid disturbance and to ensure that no interference was made with the sample. Each beaker was subsequently sealed with a rubber bung through which a 1ml pipette was placed, with the water from the beaker filling the pipette in the process. A small amount of water was removed from each pipette and the samples were sealed with a few drops of paraffin oil dyed with 1-(methylamino) anthraquinone; this served two purposes, first it blocked the interface between the water and air, creating a seal and stopping evaporation and secondly it provided an easily distinguishable tracer by which shrinkage could be measured.

Samples were placed into a water bath in a lab maintained at  $20^{\circ}\text{C} \pm 0.5^{\circ}$  with the pipettes held in place in a specially designed rig. A webcam connected to a PC was placed in front of the samples and used a macro to record images at a 5 minute timestep for the duration of the experiment. Images were processed using Axiovision software to extract data on the water level within the capillaries and hence, knowing the internal diameter of the capillary, the total shrinkage of each sample was determined.

### 3.3.3 Isothermal Conduction Calorimetry (ICC)

#### 3.3.3.1 Principle of isothermal conduction calorimetry

Due to the exothermic nature of cement (and composite cement) hydration it is possible to monitor and precisely assess hydration kinetics in real time without the need for samples to be altered in any way. Modern calorimeters employ a twin channel setup in order for materials to be analysed with respect to a reference sample, this ensures that any 'noise' or 'drift' to the signal, caused by external factors within the laboratory, is accounted for and does not negatively impact upon the accuracy of results, allowing for repeatability and reproducibility across research institutes (Wadsö and Arndt, 2016). In order for a reference material to be representative it must have comparable thermal properties as well as being physically similar (Wadsö, 2010); this investigation, in line with previous studies has employed quartz as a reference material as well as for use as an inert filler to isolate the hydration of the distinct anhydrous materials present within the grouting matrices (Whittaker et al., 2014, Kocaba et al., 2012).

#### 3.3.3.2 Sample preparation and experimental setup

Heat liberation of the grouting matrices, along with pastes prepared with the slag fraction replaced by inert quartz of matching PSD (see Figure 3-2), was measured using a Tam Air parallel 8-channel calorimeter. 100g of anhydrous material was combined as described in Section 3.3.2; of this, 6.67g  $\pm$ 0.001g was weighed into a 20ml plastic ampoule. 2.33ml  $\pm$ 0.001ml of water was added and the paste was combined using an orbital shaker set to speed 5 for 2 minutes. Selection of a standard sample size, as well as a consistent and precise sample preparation regimen has been shown to be essential in ensuring accurate and comparable results (Wadsö, 2010, Kocaba, 2010), the parameters employed within this study were in line with the standard operating procedures used within the civil engineering department at the University of Leeds, as developed previously (Whittaker, 2014).

Owing to the relatively long duration of testing via ICC (the reasoning for which is discussed further in Section 3.3.3.3) is it imperative that the specific heat capacities of the samples and references are equal. Since the specific heat capacities of each of the constituent materials is known, water – 4.18 J/(g.K) (Holman, 1981), cement - 0.75

J/(g.K) (based on measurements for C<sub>3</sub>S and C<sub>2</sub>S from (Todd, 1951)) and quartz 0.8 J/(g.K) and it is known from the simple law of mixtures (De Schutter and Taerwe, 1995) that –

$$C_p^{(fresh\ paste)} = M_f^{water} \cdot C_p^{water} + M_f^{cement} \cdot C_p^{cement}$$

*Equation 8*

Where-

$M_f^{water}$  – mass fraction of water in paste;

$M_f^{cement}$  – mass fraction of cement;

$C_p^{water}$  – specific heat of water;

$C_p^{cement}$  – specific heat of cement.

In each reference channel was placed a quartz and water reference sample (7.1 g and 2.33 ml respectively), these references served as analogues and allowed for the resolving of temperature artefacts, since the specific heat capacity of each sample and reference is equal to 1.64 J/(g.K) (Bentz, 2007).

### *3.3.3.3 Isolation of heat liberated due to slag hydration*

Through replacing the slag fraction of each individual mix with inert quartz of matching PSD it was possible to isolate the heat liberation as a result of slag hydration. This replacement accounted for the 'filler effect' (Berodier and Scrivener, 2014, Lothenbach et al., 2011, Gutteridge and Dalziel, 1990) caused by replacement within composite cements whereby there was a dilution as the water to cement ratio (w/c) was enhanced whilst the w/b remained constant, thereby providing a larger volume into which hydrate phases could grow. Filler effect also accounts for (although to a much lesser degree) the provision of nucleation sites on which the cement grains may hydrate.

It was the difference in heat between the standard, slag containing mix and this quartz replacement paste that was the heat evolved as a result of slag hydration. In order for these results to be accurate it was imperative that the PSD of the quartz was equal to that of the slag (see Figure 3-1) and that the specific heat capacities of the sample and reference were equal and consistent across all samples. Since the testing extended for 28 days, after which time the exothermic reaction was highly diminished it was

imperative that accuracy was maintained to avoid signal drift or erroneous introduction of background noise artefacts.

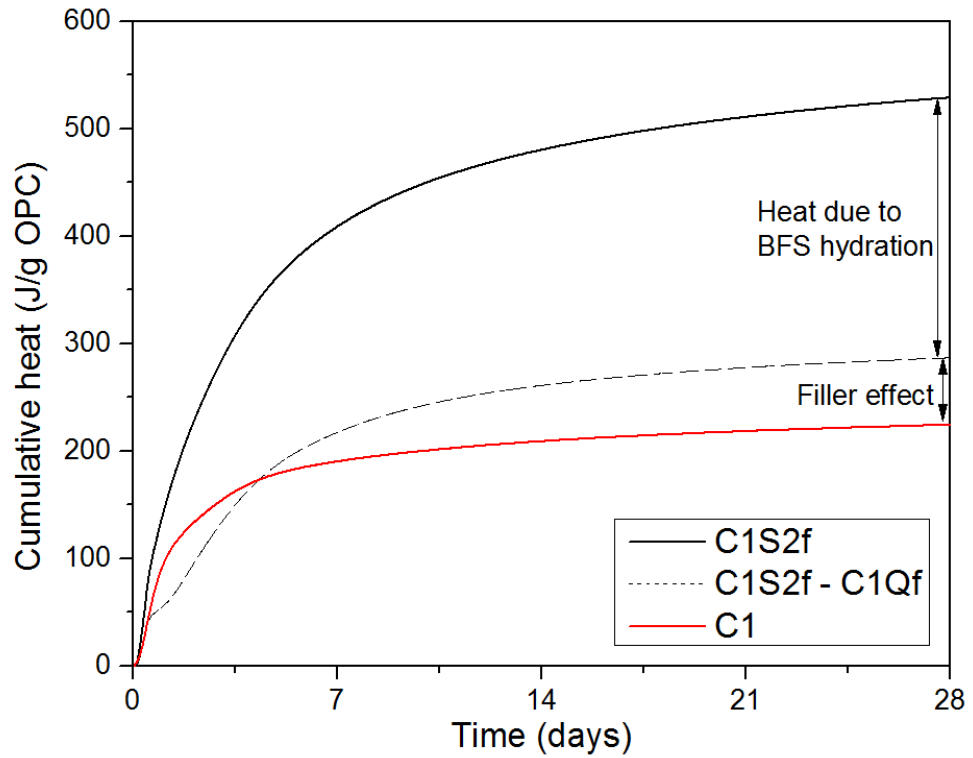


Figure 3-3: Segmentation of heat of hydration from reaction of slag

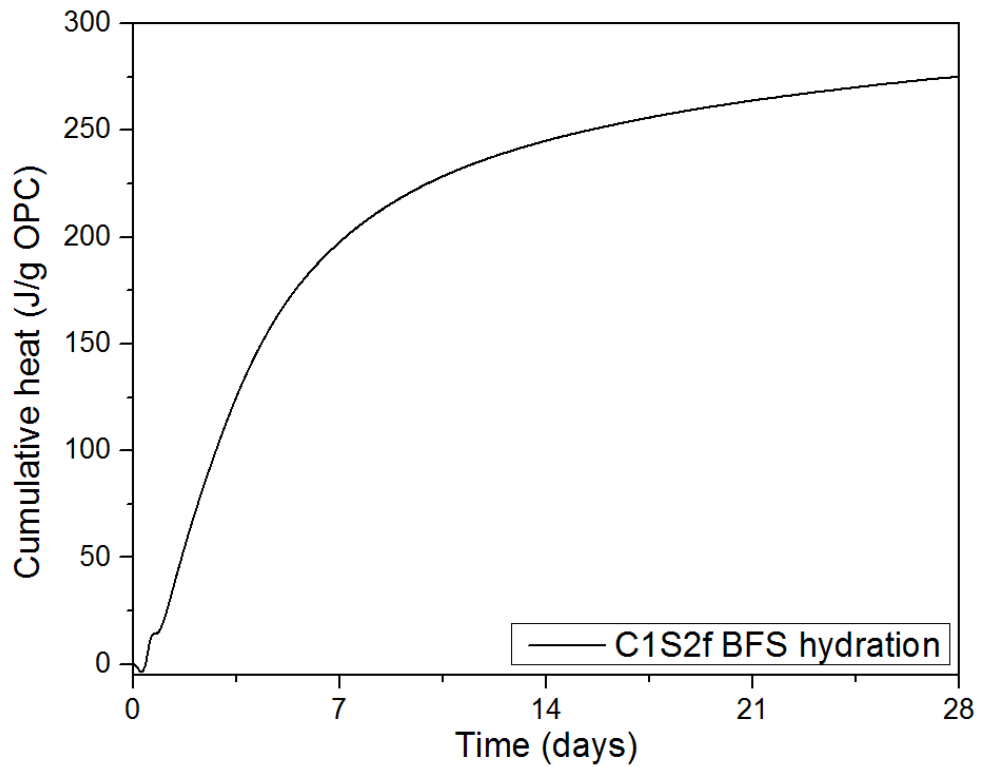


Figure 3-4: Heat released due to slag hydration in the system C1S2f

In some cases, at early age a slight negative result was observed (see Figure 3-4). Similar occurrences have been noted in previous studies (Whittaker, 2014) in which the disparity was attributed to formation of different hydrates in the quartz replacement system.

### 3.3.4 Drying of samples for secondary analysis techniques

For a number of techniques, as described in Sections 3.3.5, 3.3.6, 3.3.7, 3.3.9 and 3.3.10 it was necessary to first dry samples to arrest hydration and render them suitable for analysis, whilst taking care to minimise the impact upon the microstructure and chemical composition of each sample. A number of studies have previously been conducted to assess the impact of a range of drying techniques (Collier et al., 2008, Gallé, 2001, Zhang and Glasser, 2000, Snoeck et al., 2014, Korpa and Trettin, 2006) with the consensus being that solvent replacement appears to be the least detrimental to the microstructure of the sample (Collier et al., 2008, Day and Marsh, 1988, Hearn and Hooton, 1992). Where feasible, this approach was taken within the current study. The most suitable methods for hydration stopping, as determined by (Zhang and Scherer, 2011) are shown in Table 3-5 and form the basis for the selection of drying methodology applied throughout this study.

*Table 3-5: Selection of techniques for arresting hydration (Zhang and Scherer, 2011)*

To preserve microstructure:	solvent-replacement > vacuum-drying > F-drying > oven-drying
To preserve composition:	F-drying > oven-drying > solvent-replacement
To save time/ for large samples:	oven-drying > F-drying > solvent-replacement

Samples prepared for TGA, XRD and SEM were dried via solvent replacement using isopropyl alcohol (IPA). Sections (10mm diameter and 2mm thick) were cut from samples which had been prepared as described in Section 3.3.2.2.

To arrest hydration, the 2 mm thick sections were placed in IPA at a liquid: solid ratios of 200:1 in glass beakers. Samples were placed onto small mesh stands to accelerate exchange of the unbound water with the IPA. After 7 days, samples were removed and placed in a desiccator over silica gel under a negative pressure; the system was pumped but with a slight 'leak' in the system to provide a flow of air to accelerate the evaporation process.

For larger samples, as required in Sections 3.3.9 and 3.3.10 a different method was employed to arrest hydration. Samples for permeability and sorptivity testing were cylindrical, having a diameter of 27 mm and a height of 40 mm  $\pm$  2 mm; as such it would have been impractical to attempt to arrest hydration via solvent exchange. A thorough review of the available literature suggested that the most suitable method was oven drying but at a temperature which would minimise the detrimental effects of the technique (Collier et al., 2008, Zhang and Scherer, 2011).

Given that the samples had previously been conditioned to 28 and 180 days respectively it was deemed that the time taken to render them fully dry, whilst not ideal, was acceptable since it was the only way to guarantee that significant damage to the microstructure was not caused.

Freeze-drying or oven drying at 105°C was deemed too aggressive and likely to cause unacceptable microstructural damage, whilst solvent exchange, F-drying or vacuum drying posed logistical issues and more complex time dependent issues.

### **3.3.5 Thermogravimetric Analysis (TGA/DTA)**

#### *3.3.5.1 Principle of thermogravimetric analysis*

Through heating a known mass of material at a constant rate and measuring the dynamic weight loss as a function of temperature it is possible to determine the composition of a number of distinct phases, including the mass loss due to the dehydration of bound water, the dehydroxylation of calcium hydroxide and the decarbonation of calcium carbonate (Bhatty, 1986).

Since the range of decomposition temperatures of the different phases present within the samples are known, and results for both the thermogravimetry (TGA) and its derivative (DTA) have been collected, it was possible to determine the mass contents of each phase within each system and how this varied with respect to time. Previous

studies have used these results to obtain degree of hydration of the cementitious matrix (Pane and Hansen, 2005).

Figure 3-5 shows an example of the TGA, DTA and  $\delta$ DTA curves for a grouting material hydrated to 28 days; the water bearing phases, including C-S-H, ettringite and AFm, decompose first with the decomposition of C-S-H extending from the test onset at 40°C up to 415°C. Ettringite decomposition occurs in the region 100-150°C with AFm phases decomposing at a range of temperatures within this region. CH will dehydrate in the region 420-550°C, and depending on the sample this decomposition may be complete below this upper limit, as is the case in the sample shown in Figure 3-5. Any mass loss observed from 600°C will be due to decarbonation of calcite, with any phase transformations being highlighted by peaks in the DTA and  $\delta$ DTA curves but having no attributable mass loss.

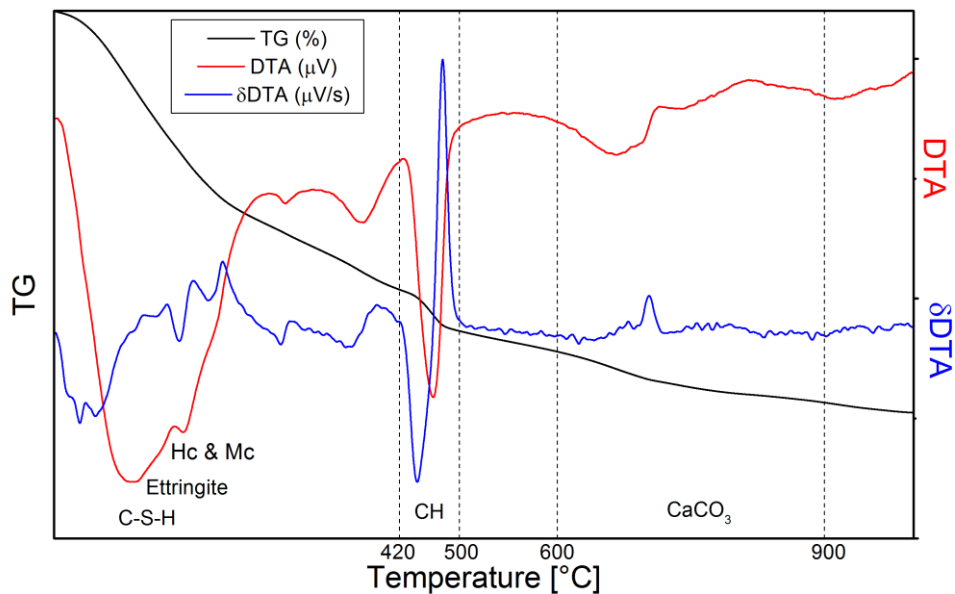


Figure 3-5: TGA, DTA and  $\delta$ DTA for C1S2c system hydrated for 28 days

The accuracy and resolution of results obtained via this method are highly dependent upon a number of factors; including sample size, heating ramp rate and crucible type; it is essential that all of these variables remains constant throughout testing to ensure that results are consistent and accurate.

### 3.3.5.2 *Sample preparation and experimental setup*

Samples were prepared as outlined in Section 3.3.4 with hydration arrested via solvent replacement. Once dried samples were crushed in a pestle and mortar to a fine powder and weighed into 50 ml alumina crucibles, 50mg  $\pm$  2mg of material was used for each sample at each testing age. Samples were analysed using a Mettler Toledo TGA/DSC1 at a temperature range of 40-1000°C and a ramp rate of 10°C/min under a nitrogen atmosphere, operating at a flow rate of 50 ml/min.

### 3.3.5.3 *Determination of composition*

Due to the overlapping of decomposition curves it is challenging to determine exactly the mass loss as a result of the dehydration or decarbonation of Portlandite (CH) or calcite (if it is indeed present within the sample). There are two methods which may be employed to determine the weight loss and hence the quantity of each phase within the sample.

The first method, referred to as the derivative method, makes use of the 2<sup>nd</sup> derivative,  $\delta$ DTA, to accurately identify the temperature range in which dehydroxylation of portlandite occurs (Monteagudo et al., 2014, Bhatt, 1986), it is possible to use this information to identify the points at which the reaction starts since the sensitivity of the machine is very high. The method is very basic in that one simply must measure the total mass at both points and determine the difference in mass before and after the decomposition. The continued dehydration of other phases during this period means that the results obtained via the derivative method are not completely accurate.

The second, and most commonly applied approach is the tangent method. From the onset and end points at which the decomposition is identified (via the aid of the DTA and  $\delta$ DTA curves) a tangent is plotted from the TGA curve. A line is drawn through the midpoint of these two tangents and the difference between the two intersects is taken as the mass loss due to dehydroxylation of portlandite (see Figure 3-6).

With the application of the tangent method there is inevitably an inherent margin of error. In a previous study, Kocaba (2010) found that results would typically deviate by around 8-10%, owing to both variations in samples and determination of CH via the application of the method described. Nevertheless, the method has been found to yield reproducible results free from significant operator error, within the ranges discussed.

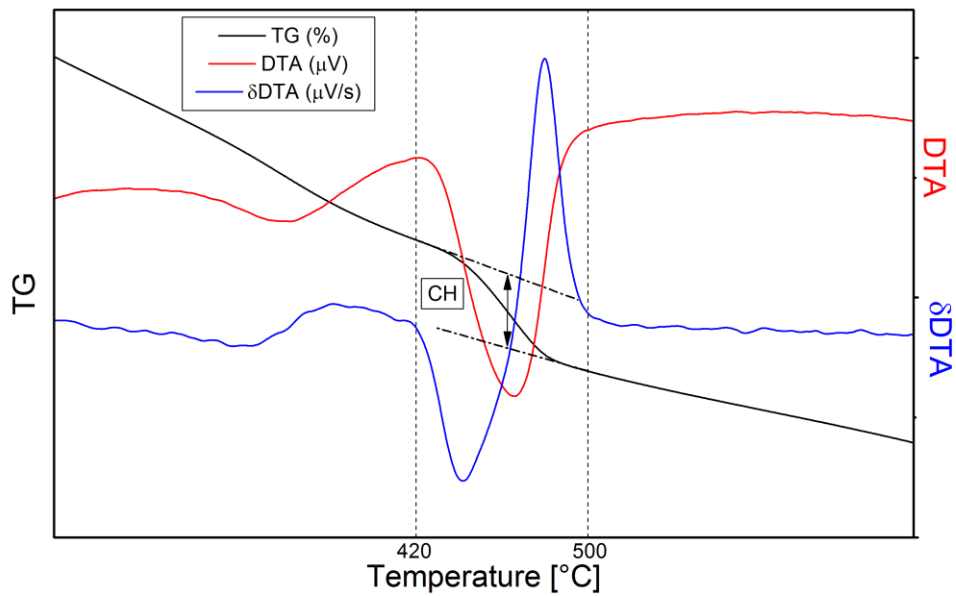


Figure 3-6: Determination of CH content from tangent method

#### 3.3.5.4 Determination of bound water content

The chemically bound water within each sample gives an indication towards continued hydration and can be used as a quick and simple means of identifying continued hydration as a function of time. As samples were pre-dried via solvent exchange, the mass loss as a result of bound water ( $W_n$ ) can be taken as that occurring between 50 and 550°C, the point at which all water bearing phases are considered to be fully dehydrated, where bound water is calculated by:

$$W_n = \left( \frac{W_{50} - W_{550}}{W_{550}} \right) \times 100$$

Where:

$W_{50}$  – mass loss at 50°C

$W_{550}$  – mass loss at 500°C

### 3.3.6 X-ray Diffraction (XRD)

#### 3.3.6.1 Principle of X-ray diffraction

X-ray diffraction allows for the identification and compositional determination of any crystalline phases present within a material. Since crystals are regular in structure, their elastic scattering of incident X-ray photons over a range of incident angles can be used to identify their unique composition through the application of Bragg's law –

$$n\lambda = 2d\sin\theta$$

*Equation 9*

Where –

$n$  is an integer value, known as the order of reflection

$\lambda$  is the wavelength of the X-ray beam

$D$  is the inter-planar spacing of and crystalline phases within the sample; and

$\theta$  is the angle of incidence of the X-ray beam, relative to the sample.

By bombarding a sample with a focused beam of X-rays and collecting those which have been elastically scattered and passed through a receiving slit and collimator it is possible to determine the composition of the crystal structure which has interacted with the incident X-rays, since each crystalline compound has a unique planar spacing.

A large mass of the hydration products, as well as most of the phases present within the anhydrous slags, are amorphous or poorly crystalline with no well-defined peaks. These amorphous phases appear as broad humps within the resultant XRD pattern. In recent decades, the application of Rietveld refinement (Rietveld, 1969) has become increasingly prevalent (Scrivener et al., 2004, Le Saoût et al., 2011, Snellings et al., 2014a) as a means of quantifying phase composition and determining contents of amorphous phases within these complex hydrating materials.

More recently, a number of studies have applied the Partial Or No Known Crystal Structure (PONKCS) method (Scarlett and Madsen, 2006) to quantify hydration in blended cements (Snellings et al., 2014b) as well as in alkali activated systems (Williams et al., 2011) and hydrating alite pastes (Bergold et al., 2013). The technique is based on Rietveld refinement but is enhanced slightly by making use of the fact that the humps of amorphous phases are unique (Juenger and Siddique, 2015), negating the application of a manual background fit and improving accuracy.

Whilst these techniques and methods show great promise, they have not been applied herein since this was considered outside of the scope of the present study. XRD analysis has been performed in this instance for the identification of the presence of crystalline phases, chiefly CH and the various AFt and AFm phases.

#### *3.3.6.2 Sample preparation and experimental setup*

Samples were prepared as outlined in Section 3.3.4; hydrated to pre-determined ages before being hydration stopped through immersion in IPA. After suitable drying, samples were ground to a very fine powder and backloaded into 16mm sample holders with the aid of a frosted glass slide; this ensured a well compacted sample bed whilst avoiding preferential orientation.

Analysis was performed using a Bruker D2 phaser desktop machine equipped with  $\text{CuK}\alpha$  X-ray source and LYNXEYE detector operating at a voltage of 40 kV and current of 40 mA. XRD patterns were acquired in the range  $7-70^\circ 2\theta$  at a step size of  $0.034^\circ$  with a complete analysis taking 93 minutes per sample. During analysis samples were rotated around the vertical goniometer axis to improve particle statistics.

### **3.3.7 Scanning Electron Microscopy (SEM)**

#### *3.3.7.1 Principle of scanning electron microscopy*

SEM is one of the most common methods employed in the analysis and investigation of cementitious materials. The microscope fires a focused beam of electrons onto the surface of a sample (usually in a raster scan pattern) and is able to extract information on the properties and composition through the detection of a number of resultant signals which are produced. Secondary electrons, which are emitted from the sample when atoms within it are excited by the electron beam, allow for a topographic image of a specimen to be created. Whilst this mode is the most commonly used with scanning electron microscopes it is not pertinent to the current study.

Backscattered electrons, which are reflected back off the surface of a sample via elastic scattering, allow for an understanding of the composition and discrimination between the phases present within a sample. The rate at which electrons are backscattered from

a sample is highly dependent upon the electron density of the atom which has interacted with the electron beam. From this information a grey-scale image of the sample surface is produced in which heavier materials appear lighter, less dense elements appear darker and pores appear black.

Through analysis of flat, polished sections it is possible to accurately analyse a range of samples with consistent brightness and contrast and subsequently determine the quantities of the phases present (Scrivener, 2004, Snellings et al., 2014b). Since the technique is based on analysing a 3-D sample from a 2-D surface it relies upon the principles of stereography and is limited in that it is unable to provide accurate information on the true shape, size and morphology of particles.

Figure 3-7 shows a typical micrograph at 800x magnification, in this case of the C1S2c system (with 25% OPC and 75% slag) hydrated for 28 days. The associated grey level histogram is also shown and annotated to show the peak positions of the different anhydrous and hydrated phases present. The threshold for arbitrary determination of porosity, as suggested in (Scrivener et al., 1987) and the associated work of (Patel et al., 1988) is also illustrated.

As is clearly evident from the histogram shown in Figure 3-7 there is significant overlap in the peaks associated with Portlandite (CH) and anhydrous slag, since their mean atomic densities are comparable. In order to accurately isolate the anhydrous slag fraction and hence determine slag hydration, it was necessary to subsequently collect magnesium EDX maps for each micrograph. From XRF analysis it is apparent that Mg content is higher in the slag fraction than within the OPC in each system; and due to the low solubility of Mg it remains within the boundary of the initial, anhydrous slag grain boundary.

Generally, analysis in backscattered mode on flat polished samples will remove any topographical effects. However, within some of the samples analysed herein some slight discrepancies have been noted. Within the C1S1 and C2S1 samples, the very large Calumite grains appear to have caused preferential polishing, since these phases are much harder than the surrounding hydrates (see Figure 4-7).

Analysis of flat polished sections via BSE-IA is generally accepted to produce accurate and repeatable results. However, given the limitations in resolution (particularly in relation to other indirect methods, such as dilatometry, see Figure 4-19) it has often been shown that results obtained at early age result in an overestimation in degree of slag hydration (Kocaba, 2010, Whittaker, 2014) since the very small anhydrous slag grains cannot be detected at the typical magnification used within the technique.

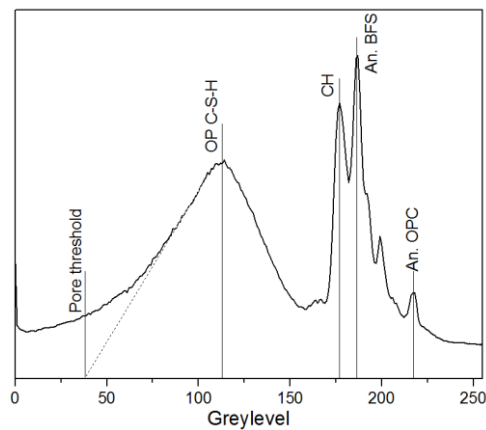
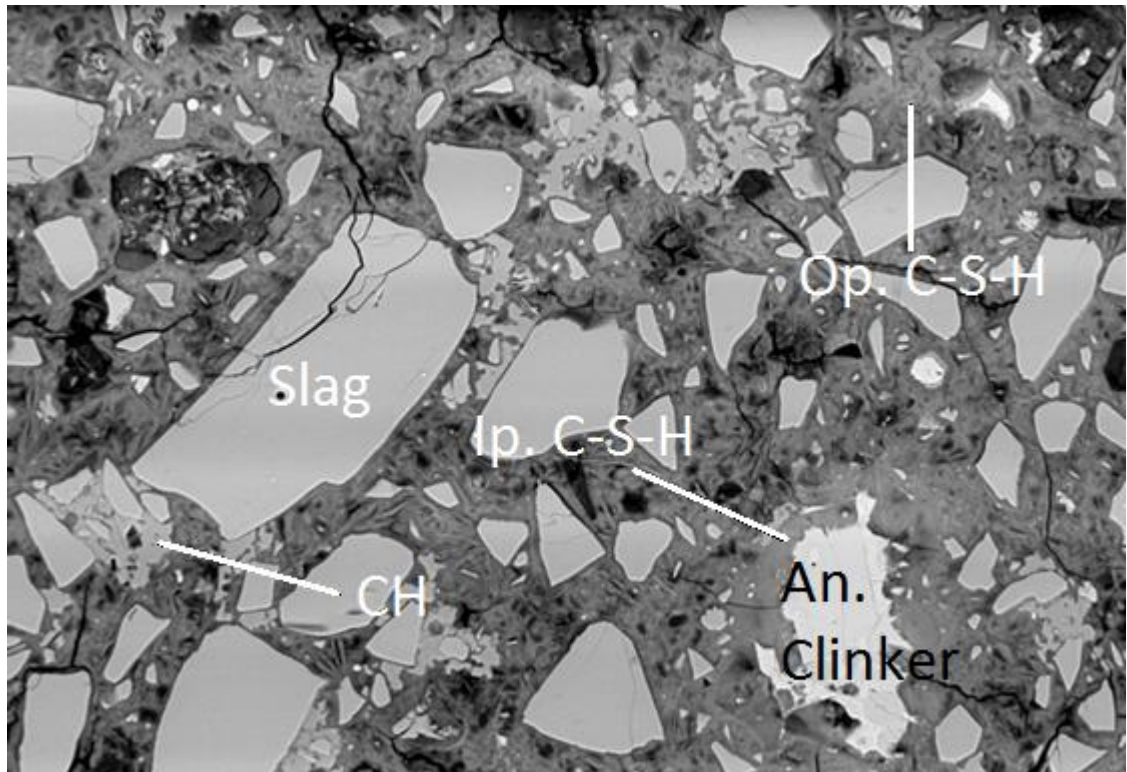


Figure 3-7: SEM micrograph of C1S2c system at 28 days with corresponding grey level histogram

### 3.3.7.2 Determining degree of hydration of slag

Figure 3-8 shows a segmented micrograph, which has been achieved via some slight image processing (smoothing and applying a median filter) followed by thresholding, overlaying the Mg map at a relatively low opacity and performing a further thresholding to isolate the anhydrous slag.

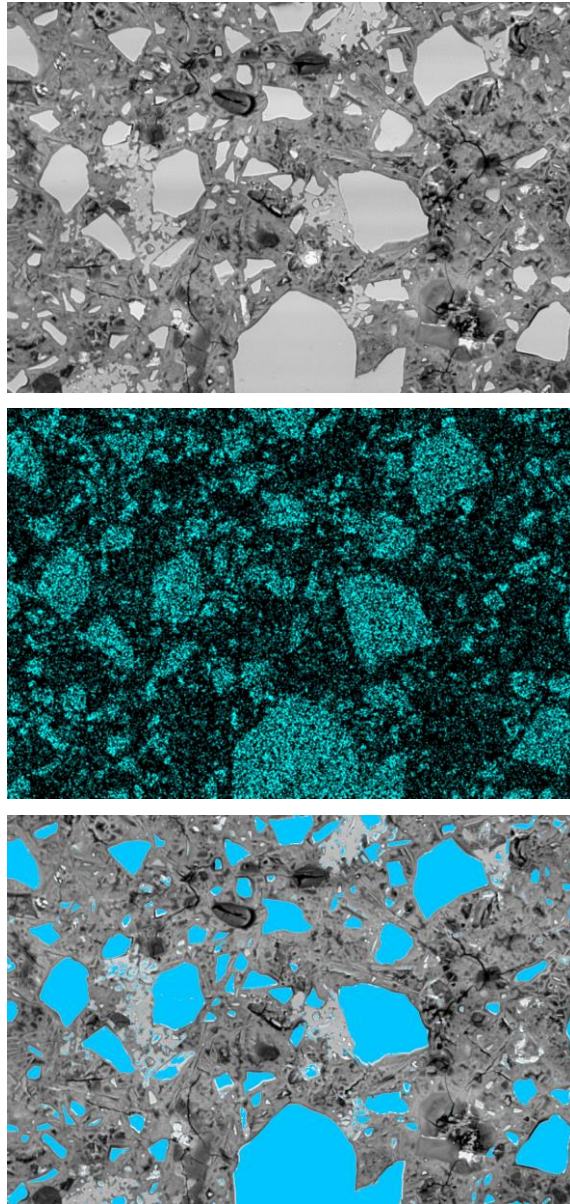


Figure 3-8: (a) C1S2c system hydrated for 28 days, (b). Associated Mg map and (c). anhydrous slag fraction isolated

Given the heterogeneous nature of these samples and determination of degree of hydration from a 2-D surface it is necessary to repeat this process over a number of images. A preliminary study within this project, supplemented by significant investigation in the work of (Whittaker, 2014) showed that at a magnification of 800x, 50 images is sufficient to provide accurate and repeatable results. Independent analysis of a data set in which both the author and *Whittaker* processed a set of 50 images the results were in agreement within an error of 0.2%, suggesting that the only factors that may affect accuracy are the settings applied when collecting images and EDX maps.

Processing the images as described above, using ImageJ 1.50g software, results in the creation of a binary image in which only the anhydrous slag is selected. From this it is possible to determine the degree of slag hydration through the application of the following equation (Kocaba, 2010) –

$$DoH_{BFS} = \frac{Vf_{An.BFS}(t_0) - Vf_{An.BFS}(t)}{Vf_{An.BFS}(t_0)}$$

*Equation 10*

Where –

$Vf_{An.BFS}(t_0)$  – Initial volume fraction of slag;

$Vf_{An.BFS}(t)$  – Volume fraction of slag at time t.

### *3.3.7.3 Sample preparation and experimental setup*

Samples were first cut and hydration stopped as outlined in Section 3.3.4 before being encapsulated in resin, ground with fine SiC paper (600-2500 grit) to expose the sample surface and polished with diamond paste to a fineness of 0.25  $\mu\text{m}$ . Samples were then mounted and splutter coated with carbon (10 nm in thickness).

Samples were analysed at a range of ages for 2 to 365 days using a Carl Zeiss EVO MA15 machine equipped with Oxford instruments AZtec Energy EDX system with 80mm SDD detector. Images were acquired at 800x magnification at a working distance of 8.5mm and an accelerating voltage of 15 keV. EDX maps for Mg were collected with a count rate of 30,000+ cps with an acquisition time of 100 seconds. Subsequent image analysis was performed using ImageJ software as outlined above.

## **3.3.8 X-ray micro-Computational Tomography (X- $\mu$ CT)**

### *3.3.8.1 Principle of X- $\mu$ CT.*

For a thorough introduction to computational tomography and its application to materials science the works of both Stock and Banhart provide a great starting point (Stock, 2008b, Banhart, 2008).

Materials such as cementitious grouts and concrete may be imaged via X- $\mu$ CT owing to the disparity in density of the different phases present, be they water or air filled pores, hydration products or anhydrous material. These differences in density affect the way in which the incident x-rays interact with the material and ultimately, their attenuation. The mass attenuation coefficient of each distinct phase present within a material is a strong function of its atomic number and of the x-ray wavelength and as such it is possible to image the internal structure of such materials in a non-destructive manner and, as in this study, without any pre-treatment prior to analysis.

Analysis and imaging of materials via X- $\mu$ CT is capable of achieving sub-micron resolution in certain applications and particularly when using synchrotron radiation with its high intensity x-rays and very high flux (Provis et al., 2012, Promentilla et al., 2009). The achievable image resolution is, however, a function of sample size as well as the interplay of contrast sensitivity and spatial resolution achievable within the sample (Stock, 2008a). Within a desktop based system, as was applied in the current study, a feasible resolution in the region of 'sample size/4000' is reasonable, i.e. for the 5mm samples studied a voxel size of just over 1.25  $\mu$ m.

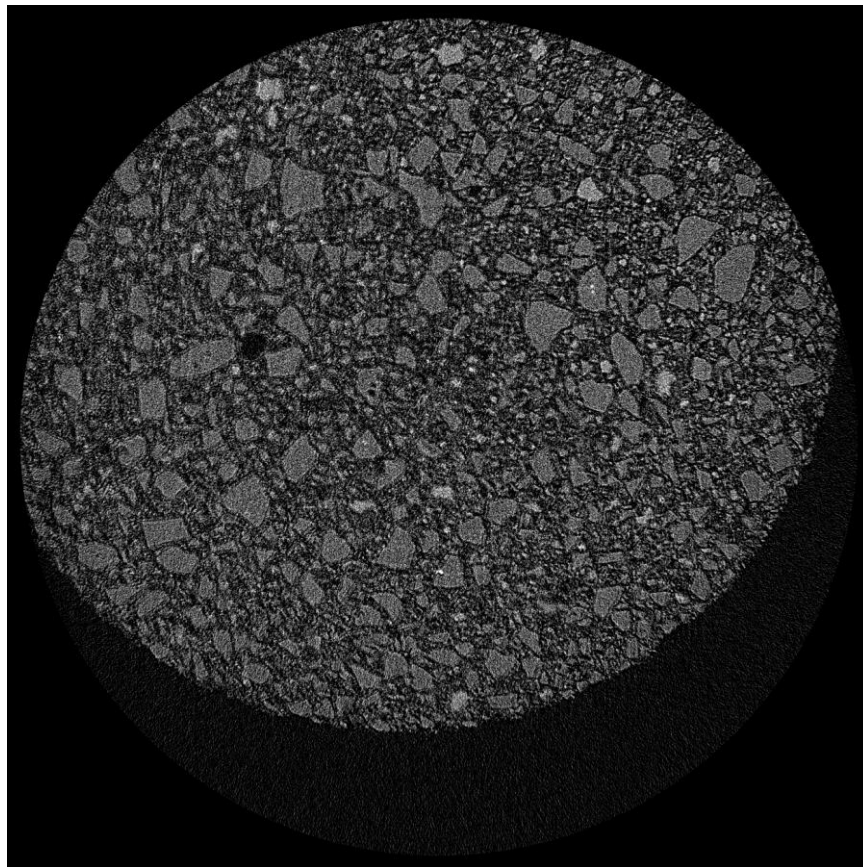


*Figure 3-9: Example reconstructed slice through X-ray  $\mu$ CT scan. Sample shown is C1S2c following heat-treatment to 800°C at 7 days*

### 3.3.8.2 *Sample preparation and experimental setup*

Samples were mixed by hand for 5 minutes and subsequently injected with a syringe into thin cylindrical quartz glass capillaries (5mm internal diameter, 10 $\mu$ m wall thickness); the benefits of this preparation protocol were demonstrated previously (Gallucci et al., 2007) and include a reduction in absorption effects and crucially this preparation method negates the requirement for samples to be pre-conditioned, be that fracturing of a larger sample to produce a suitably sized section for analysis or hydration stopping by means of solvent replacement, oven-drying, freeze-drying or other methods; all of which may have deleterious effects upon the microstructure.

Samples were sealed and stored at 20°C for 7 or 28 days prior to testing. A number of samples were conditioned to 28 days before being heated in a furnace to either 400°C or 800°C. This heating regime was in line with industrial testing methods (NDA, 2010c) and through mimicking these conditions it is possible to quantify the changes induced upon the pore structure, quantifying the resilience or otherwise of waste packages in such scenarios. Samples were placed in the furnace and heated to the desired temperature, where they were held for 30 minutes before being allowed to cool in air to room temperature.

Imaging was performed at NNL's Central Lab, Sellafield, using a Bruker Skyscan 1172 equipped with an 11Mp CCD camera and coupled scintillator with a maximum resolution of 0.5 $\mu$ m. Images were acquired at a step size of 0.15° (1200 steps in a 180° scan) with an exposure time of 8.3s per step, for a total scan time of 2 hours 46 minutes per sample. Resolution was limited by sample size and the object to source distance, with voxel sizes ranging from 1.24 to 1.62 $\mu$ m<sup>3</sup>, actual figures for each sample are given in Table 3-6.

Table 3-6: Details of samples analysed via X-ray  $\mu$ CT

Mix	Age	Heat treated?	Temperature (°C)	voxel size ( $\mu\text{m}^3$ )
C1S1	7	x		1.28
	28	x		1.59
	28	✓	400	1.35
	28	✓	800	1.24
C2S1	7	x		1.35
	28	x		1.62
C1S2c	7	x		1.35
	28	x		1.57
	28	✓	800	1.57
C1S2f	7	x		1.42
	28	x		1.28
C1S2c	7	x		0.54
	7	✓	200	0.54
	7	✓	800	0.54
	28	x		0.53
	60	x		0.53
C1S2f	7	x		0.53
	7	✓	200	0.54
	7	✓	800	0.53
	28	x		0.53
	60	x		0.53

Images were reconstructed using freely available dedicated Bruker software; NRecon. This was implemented to correct misalignment, reduce ring artefacts and correct against beam hardening, whilst allowing for brightness and contrast to be enhanced to improve subsequent segmentation. NRecon produces reconstructed slices which must then be converted into .bmp format so that they may be opened in DigiUtility; to this end, freely available IrfanView software was implemented.

### 3.3.7.3 Selection of a volume of interest (VOI) and porosity segmentation

DigiUtility, developed by Structure Vision Ltd. was used to build VOIs from the reconstructed slices. A VOI is a segmented cubic volume of the total sample and provides a representative region of the sample to be analysed whilst ensuring that data processing remains possible with the memory limitations of the machine used for analysis (a dual-core desktop PC with 8GB RAM and a 3.2GHz processor).

It is essential that the selection of each VOI is large enough to avoid the potential of errors or inaccurate results brought about by finite size error (Garboczi and Bentz, 2001). Previous studies (Provis et al., 2012) suggest that a VOI representing  $100\mu\text{m}^3$  or greater than 3-5 times the size of the largest distinct feature of the sample is sufficient, however this assertion is highly dependent upon the composition of the sample and it is prudent and often essential to err on the side of caution and select a larger VOI to minimise uncertainty. In many previous studies it has been observed that VOIs in the region of  $250^3 - 500^3$  are common (i.e. a cubic volume of edge length 250 pixels, for example) (Nakashima and Kamiya, 2007, Nakashima and Nakano, 2012, Nakashima et al., 2004, Altendorf, 2011, Bentz et al., 2000), particularly when subsequent random walk simulation is performed. In certain instances, VOIs may be outside of this range, for example (Lu et al., 2006) studied  $200^3$  volumes and (Darma et al., 2013) investigated volumes of  $600^3$ ; in the case of the former this ensured that only the bulk matrix was imaged and large aggregates were avoided, and in the latter this allowed for the large features of interest (cracks in this study) within the samples to be suitably investigated and the avoidance of finite size error.

A preliminary study was necessary to determine a suitable VOI size for each of the mixes. Due to time constraints only 4 of the project mixes were studied, each at 7 and 28 days, and with a number of heat-treated samples included (11 samples in total) for the complete list of samples studied via X- $\mu$ CT see Table 3-6.

For mixes C1S2c and C1S2f, in which both the OPC and slag were of a relatively typical PSD, with  $d_{0.5}$  values in the range  $16-41\mu\text{m}$ , a VOI of  $400^3$  was more than adequate to avoid any errors associated with finite size; the largest distinct features were roughly  $1/100^{\text{th}}$  of the total volume.

With the C1S1 and C2S1 mixes both containing Calumite (S1<sub>c</sub>) it was necessary to determine the suitability of  $400^3$  VOIs, since the Calumite grains are of considerable size ( $d_{0.5} - 350\mu\text{m}$  as determined via laser diffractometry). In order to ensure that results are representative it has been necessary to increase VOI size to  $600^3$ . In order to ensure

that these VOIs were representative, a larger VOI was first constructed for each sample at sizes ranging from 1000x1000x600 to 1800x1800x600 (limited by cracking and surface effects present within certain samples). These large VOIs were segmented to determine the complete porosity for each sample, avoiding finite size error and local effects. Once porosity values had been calculated, VOIs ( $600^3$  voxels) which were deemed to be representative of each sample were created; limiting to this value ensured consistency and allowed for subsequent tortuosity measurements to be made via random walk simulation whilst avoiding issues associated with computational processing power, maintaining a cubic VOI also ensured that errors due to any anisotropic effects were minimised.

This process of VOI selection often required some degree of trial and error to ensure that the selected volume both contained a typical volume of Calumite as found within the sample as a whole and had a porosity equal or very close to that of the large VOIs created in the previous step.

Selection of a threshold value for each sample in order to define porosity is a fundamentally important step and previous studies (Provis et al., 2012) have shown that a slight change in segmentation point from the corresponding grey-level histogram can have a significant impact upon calculated porosity and yet further influence on the subsequently determined tortuosity.

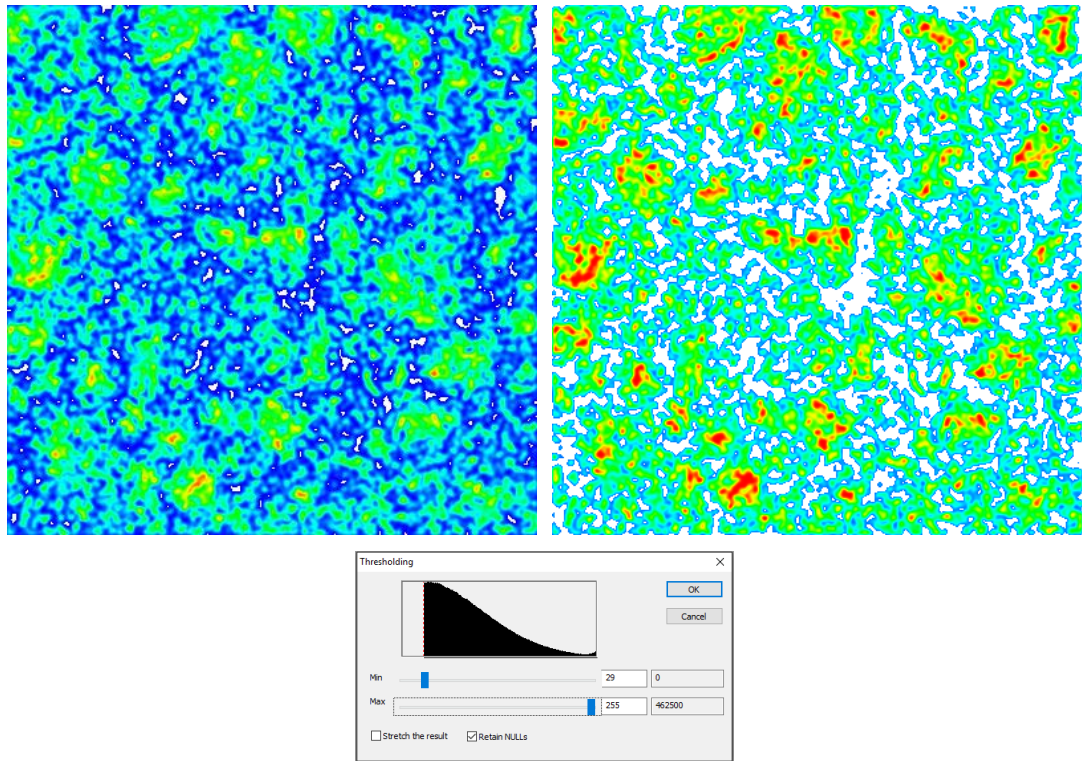


*Figure 3-10: segmentation of VOI to yield porosity - (left). Section through untreated VOI (right). Same section of VOI following thresholding and (bottom). Corresponding histogram with threshold point highlighted.*

Owing to the composition of the materials investigated in this study it was not possible to easily define a transition point, as is possible with other porous materials including sedimentary rocks (Nakashima et al., 2004, Nakashima et al., 2008) or igneous rock samples (Ikeda et al., 2000); nor was it feasible to accurately identify a mid-point in peaks between porosity and hydration products (as well as anhydrous material) as has been reported in studies investigating pure cement pastes (i.e. no replacement by slag or other SCM) (Gallucci et al., 2007, Bossa et al., 2015).

From Figure 3-10 it is noticeable that there is no separation in peaks between pore space and solid phases. This was the case in a number of previous studies of cement pastes (Promentilla et al., 2009, Sugiyama et al., 2010b), composite cements containing PFA (Promentilla and Sugiyama, 2010) and alkali activated binders (Provis et al., 2012). In each of these cases, and similarly in this study, it is necessary to use a global thresholding technique, aided by a visual inspection. Selecting the threshold point half-way up the shoulder of the peak in grey scale gives a good starting point; aiding this with a comparison to the corresponding slices under investigation and modifying the selection as appropriate to provide the most realistic representation of the sample in line with our understanding of the microstructure of these systems.

### 3.3.8.3 Determination of tortuosity from random-walk simulations

Each VOI was subsequently subjected to random-walk simulations to provide a quantifiable comparison of the inter-connectivity and tortuosity of the internal pore network. In-house software, DigiUtility (Structure Vision Ltd.), developed by Dr. Xiaodong Jia was used to perform this task with codes based on those developed by Nakashima (Nakashima and Watanabe, 2002, Nakashima and Kamiya, 2007) which have been implemented in a number of subsequent studies (Promentilla et al., 2009, Provis et al., 2012, Sugiyama et al., 2010b, Promentilla et al., 2008, Darma et al., 2013, Promentilla et al., 2016).

For a thorough understanding of the development of the technique and the programs, one should consult the most authoritative paper on the subject prepared by (Nakashima and Kamiya, 2007) and for a more in depth understanding of the principles of percolation theory, the work of (Stauffer and Aharony, 1994) is recommended.

The main points to note when conducting a random walk simulation are:

- each random walk is a discrete lattice walk in a simple cubic lattice
- Each walker is seeded at random anywhere within the pore space.
- For each timestep ( $\tau$ ) the walker will attempt to move to a face adjacent voxel, if the voxel corresponds to pore space the move is made, if it is solid the walker remains in its initial voxel but 1 timestep is recorded.
- Only face adjacent moves are possible, edge connected and vortex connected voxels are not considered.
- If the walker reaches the edge of the VOI, a mirrored boundary condition, as represented in Figure 3-11 will be observed.
- Random walks should be of significant length ( $\tau \geq 100,000$ ) to ensure that they are well above the limit at which restricted diffusion begins.
- A sufficient number of random walks ( $\geq 2000$ ) should be performed in order to ensure that a representative value for tortuosity is obtained.

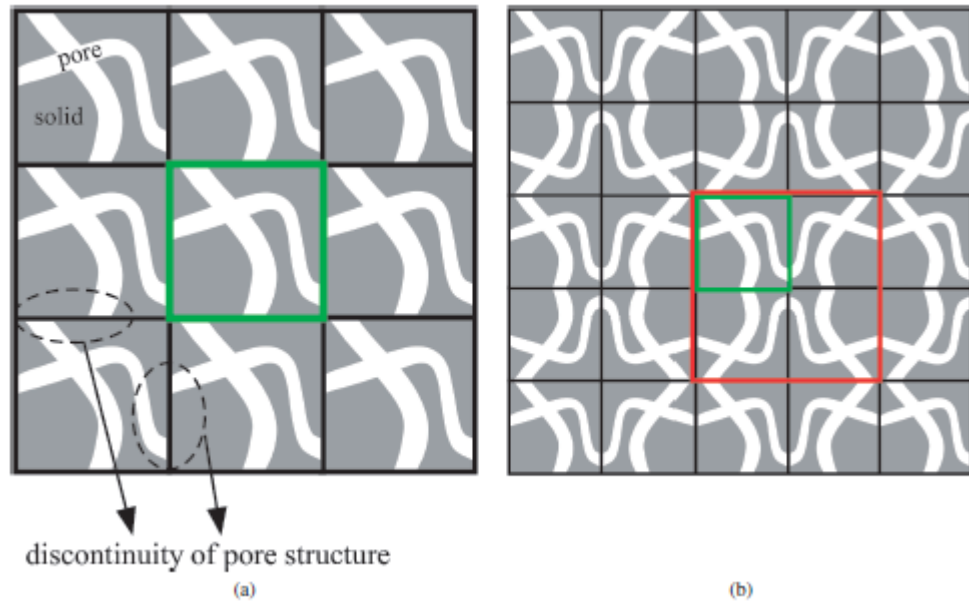


Figure 3-11: simplified representation of the mirror boundary condition employed. (a). A simple periodic boundary condition (b). a mirrored boundary condition yielding a continuous percolated pore network to ensure accurate estimation of tortuosity (Nakashima and Kamiya, 2007).

Simulations were performed with 6000 random walkers per sample, each moving for 400,000 timesteps ( $\tau$ ). Preliminary simulations were performed over a range of values from 2000 to 10000 walkers and with  $\tau$  values from 200,000 – 2,000,000 in order to determine the minimum cut-off point for which a representative tortuosity value would be obtained (in order to minimise computation time. Very similar results to those obtained by Provis et al. (2012) were observed. It was thus determined that maintaining matching values, which corresponded to significantly above the ‘cut-off’ value was suitable, whilst not significantly increasing computation time nor risking system crashes through overloading.

VOIs of  $400^3$  or  $600^3$  (for Calumite containing mixes, C1S1 and C2S1) were found to be representative, as discussed above. Attempts to increase the size further and conduct random walk simulations was not possible due to processing power limits. However, every effort was made to ensure that VOIs were representative of the whole bulk matrix.

Tortuosity ( $T$ ) is defined as the mean square ratio of diffusive displacement within the porous media as a function of diffusive displacement in free space, where –

$$T = \frac{D_0}{D_{(t)}} = \frac{a^2}{\frac{d\langle r(t)^2 \rangle}{d\tau}}$$

As  $t$  and  $\tau \rightarrow \infty$

Where –

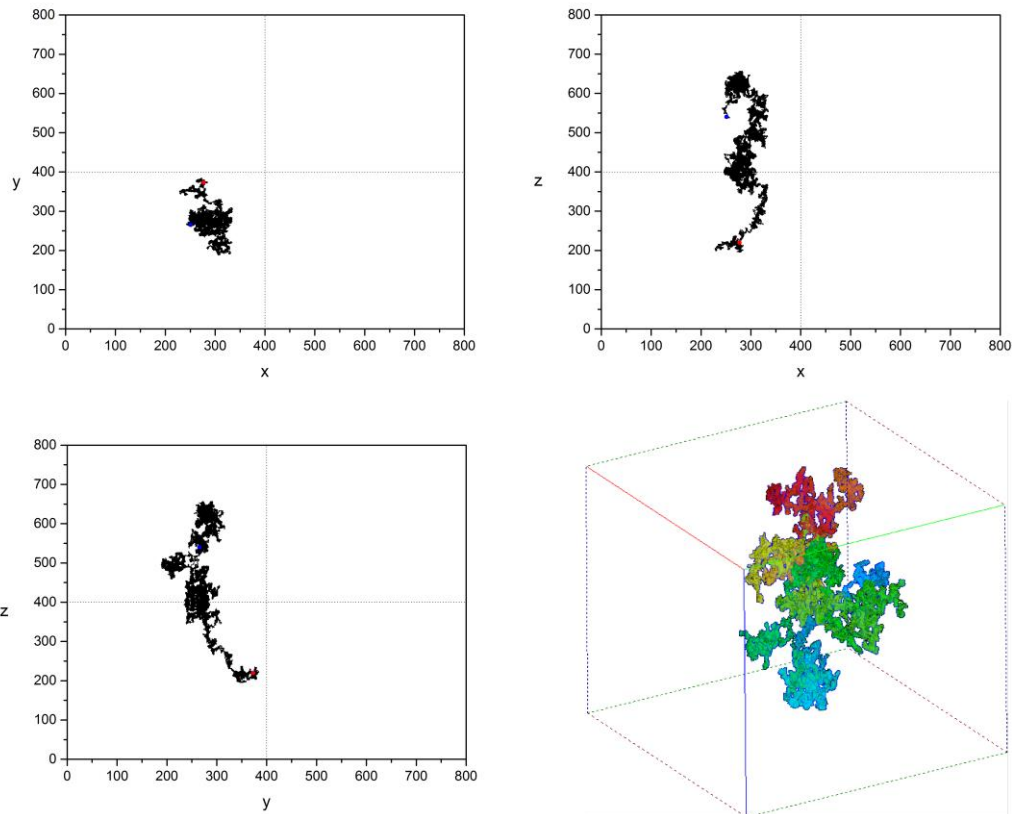
$D_0$  is the diffusion coefficient of the walker in free space without solids (e.g.,  $H_2O$  self-diffusivity in bulk water).

$D(t)$  is the diffusion coefficient of the walker within the porous media at time  $t$ .

$a$  is the lattice constant of the simple cubic lattice (i.e., the dimension of a cubic CT voxel);

$\tau$  is the dimensionless integer time.

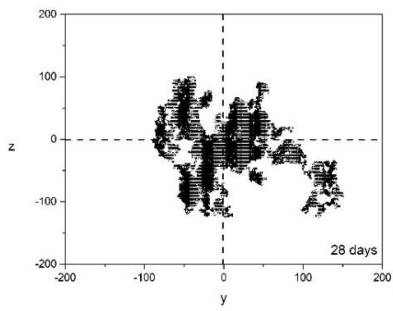
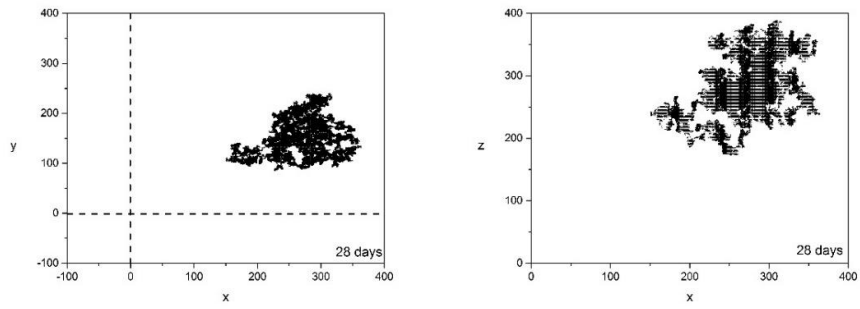
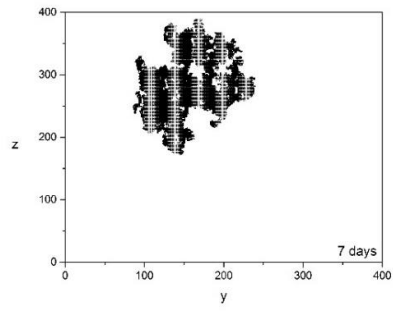
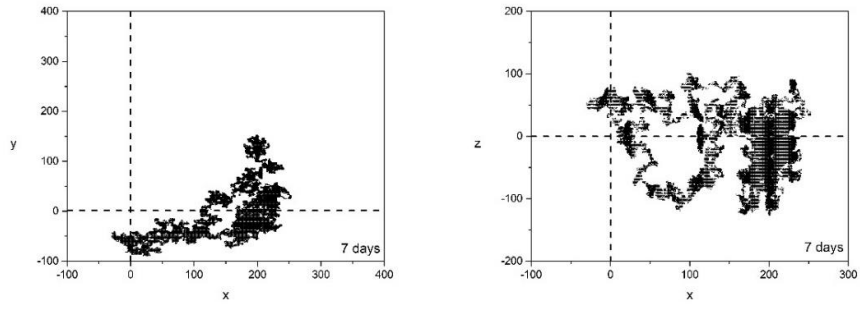
With a suitably high value for  $\tau$  and a large number of random walks performed per sample, it is possible to determine a geometrically meaningful tortuosity value for each sample VOI. Each corresponding tortuosity value is intimately linked to the restricted diffusion characteristics of the sample; through ensuring that the VOI analysed for a given sample is representative of the bulk matrix it is possible to elucidate the interconnectivity of the pore network within a grout.



*Figure 3-12: Example trajectory (400,000 timesteps) in 3 orthogonal planes of random walker in segmented pore space within C1S2c system at 28 days*

Figure 3-12 shows the route taken by an example random walker in free space within the pore network of a segmented VOI. This process is repeated 6000 times per sample and the raw data is analysed to determine statistically meaningful results for each sample. As the figure shows, the random walker in this instance passed through the edge of the segmented VOI and observed the mirror boundary condition (Figure 3-11), visible in the top right and bottom left images of the figure.

Figure 3-13 gives examples of random walkers for a variety of samples at a range of ages and with or without heat-treatment. Whilst it is not possible to make clear comparisons across the samples from these isolated examples, it is interesting to note that there appears to be a reduction in pore connectivity as a function of time (from 7 to 28 days) and then a significant increase in connectivity, and an associated reduction in tortuosity, as a result of heating to 800°C



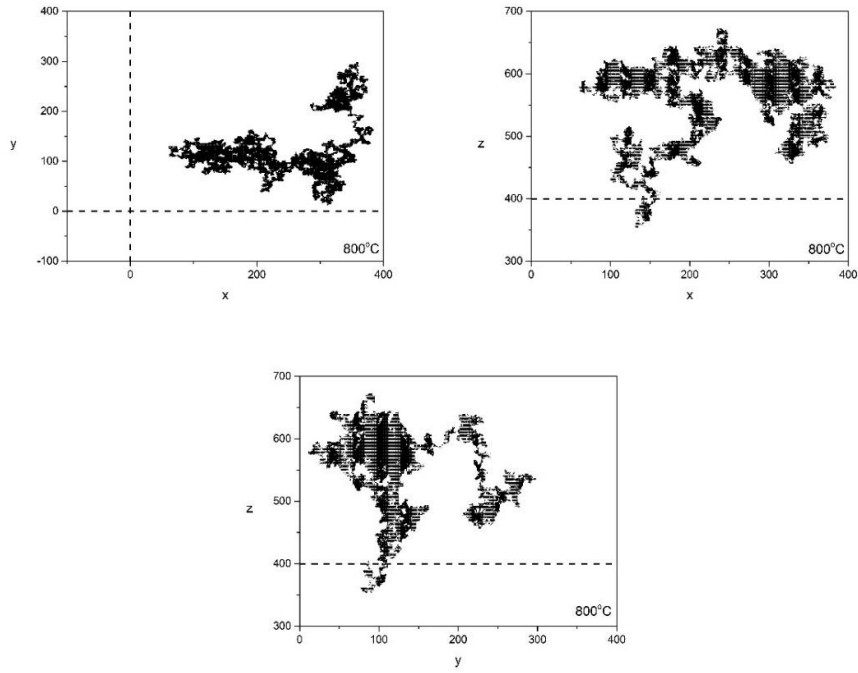


*Figure 3-13: Trajectories of walkers within the digitized pore networks of segmented VOIs in 3 dimensions, representing the C1S1 system at 7 days, 28 days and at 28 days following heat-treatment to  $800^{\circ}\text{C}$*

### **3.3.9 Gas Permeability (Leeds cell)**

#### *3.3.9.1 Principle of measuring gas permeability*

The permeability of a waste package is a significant parameter to be considered since it will directly impact the rate at which non-chemically bound waste species are able to migrate into the biosphere. There exist a large number of experimental devices which have been developed in order to determine the steady state gas (and liquid) permeability within cementitious materials by means of application of a constant pressure through a sample mounted within a tri-axial pressure cell with unidirectional flow (Cabrera and Lynsdale, 1988, Loosveldt et al., 2002, Dinku and Reinhardt, 1997, Poon et al., 1986, Hearn and Mills, 1991).

Gas permeability is often used as a qualitative indicator towards durability and service life predictions, since permeability plays a significant role in governing the rate at which aggressive or deleterious species may enter the material. Similarly, the permeability will play a significant role in controlling the rate at which unbound waste species (as could be present within the materials investigated herein, in practice) are able to migrate into the surrounding area. Since pH is also a key factor affecting radionuclide solubility and mobility, it is also important that the rate of carbonation is as low as possible. As carbonation is driven by the gas diffusivity of the material, this test may also be seen as a qualitative comparative measure of carbonation resistance potential.

#### *3.3.9.2 Sample preparation and experimental setup*

Cylindrical samples ( $27.5 \pm 0.25$  mm in diameter and  $35 \pm 3$  mm in height) were cast in triplicate in individual plastic containers and stored in sealed conditions at 20°C and 98% RH for 28 days. Samples were oven dried at 50°C, until constant weight, as outlined in Section 3.3.4 and the top and bottom surfaces were removed with coarse SiC paper to expose the internal pore structure. Removal of the outer surface ensured consistency across samples and avoided any surface effects impacting upon the accuracy of measurements.

A number of samples were heat-treated prior to analysis to assess their resilience to a potential fire, or similar catastrophic event within a deep geological facility. Samples

were heated to temperatures of 200, 400 and 800°C with residence times of 30 minutes. All samples were subsequently oven-dried to constant weight as outlined above.

Analysis was performed using the Leeds cell gas permeameter; samples were weighed and measured using digital Vernier Callipers before being placed into the Leeds Cell (Figure 3-14). The sample (S) is placed into the rubber holder (A), which is then enclosed within the plastic sleeve (B); this is then placed into the analysis cell with the metal O-ring (C) placed on top before the system is sealed with the cell lid [fitted with a pressure gauge] (D) and closed to be air tight.

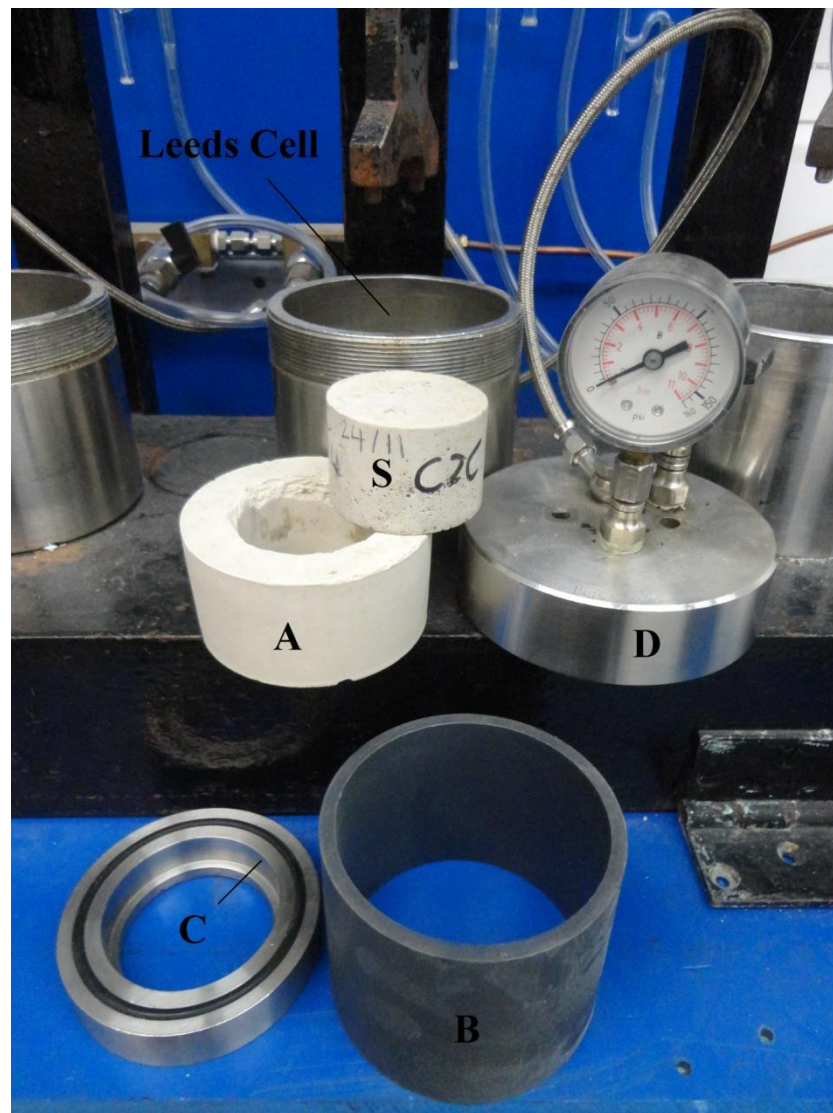


*Figure 3-14: Components of the Leeds cell*

Gas (in the case of this study,  $N_2$ ) is then forced through the sample at a known, constant pressure (between 1 and 4 bar). Time is allowed for the sample to equilibrate and reach a steady rate of gas flow through the sample (this generally takes roughly 15 minutes).

With the aid of a bubble flow meter, the time taken for a known volume of N<sub>2</sub> to pass through the sample is recorded and the intrinsic permeability is determined via the application of the following modified D'Arcy equation –

$$K = \frac{2P_{out} vL\eta}{A(P_{in}^2 - P_{out}^2)}$$

*Equation 11*

Where –

P<sub>out</sub> is the pressure at which the flow rate is measured (atmospheric, 1.01325 Bar)

v is the flow rate, measured in cm<sup>3</sup>/s

L is the length of the specimen, in meters

η is the viscosity of N<sub>2</sub> at ambient temperature (1.756 x10<sup>-6</sup> at 22°C, the lab temperature)

A is the cross-sectional area of the specimen in m<sup>2</sup>

P<sub>in</sub> is the inlet pressure (bar).

### *3.3.9.3 Determination of intrinsic permeability*

Samples were analysed in triplicate to ensure that a representative result was obtained for each mix design. It was known prior to testing that cracking within samples has a significant impact upon the obtained permeability measurement and in some cases resulted in samples too damaged to accurately or reasonably determine a result. Within the present study it was not possible to test samples which had been subjected to heat-treatment up to 800°C as cracking was so severe that it was not possible to measure flow, even at the lowest operating pressures of the equipment.

Testing of three samples per mix design ensured that any samples which had suffered from cracking or damage during drying could easily be identified and these results omitted. This was necessary during preliminary testing; however, omission of outlying results was not required for the samples included in the current study. Some shrinkage cracking was observed within certain samples; this will be discussed in more detail in the results section.

In order to determine a true value for the intrinsic permeability of samples, the average flow rate and hence permeability at 3 applied pressures was determined for each

sample. Figure 3-14 shows the determination of the intrinsic permeability, a line of best fit is applied to the values obtained and the calculated value for intrinsic permeability is the intercept point of the line extending through the Y-axis (where applied pressure = 0).

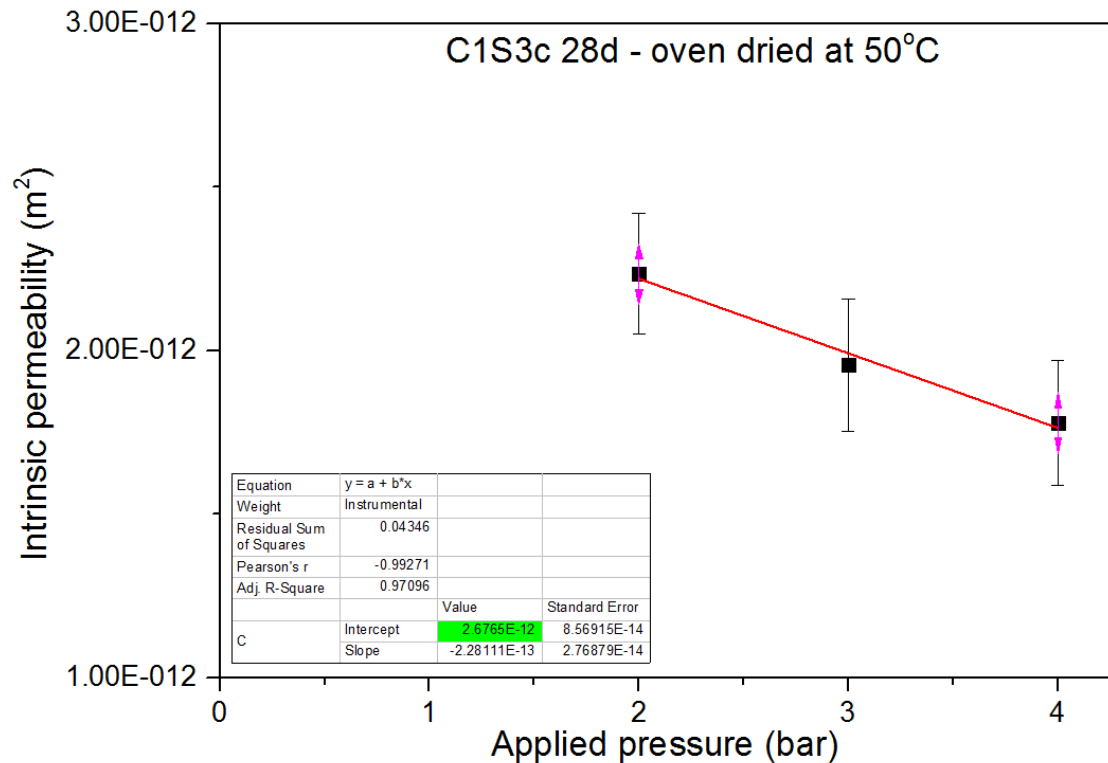


Figure 3-15: Determination of intrinsic permeability for sample C1S3c hydrated for 28 days and hydration stopped via oven drying at 50°C

### 3.3.10 Sorptivity

#### 3.3.10.1 Principle of sorptivity testing

The determination of sorptivity of a cementitious material is a relatively quick and simple procedure. The experimental procedure applied in the current study, as within many in the relevant literature (Hall, 1989, Lockington et al., 1999, Tasdemir, 2003, Wong et al., 2009, Güneyisi and Mermerdaş, 2007) provides high quality, repeatable and reproducible results via application of a very simple test (Hall, 1989).

Sorptivity is known to be strongly influenced via a number of compositional parameters, including water content, binder type, curing period, pre-conditioning method and the

presence or otherwise of aggregates (Wong et al., 2009). Since the samples within the present study have equal water content, curing period and have all been prepared, stored and pre-conditioned simultaneously, under the same conditions; it is assumed that all variations in performance are a result of microstructural differences brought about by disparities in mix designs and anhydrous powder composition.

In order to obtain quantifiable and meaningful results it is necessary to first completely remove all unbound water from each sample, thus ensuring that the initial saturation conditions are equal. As discussed by (Hall, 1989), samples that have varying initial degrees of saturation will exhibit inconsistent rates of absorption and there will not be a linear relation between mass change and  $T^{1/2}$ , as is observed in a large majority of inorganic building materials, and likewise those included in the present study.

### 3.3.10.2 Sample preparation and experimental setup

The same samples as had been used for permeability testing were used to determine sorptivity. The lower 15-20mm of the sides of each sample was carefully coated in a layer of petroleum jelly, taking care as to not contaminate the bottom surface of the cylinder. Once coated, the samples were weighed using a set of Ohaus Precision Standard scales (accuracy  $\pm 0.01\text{g}$ ).

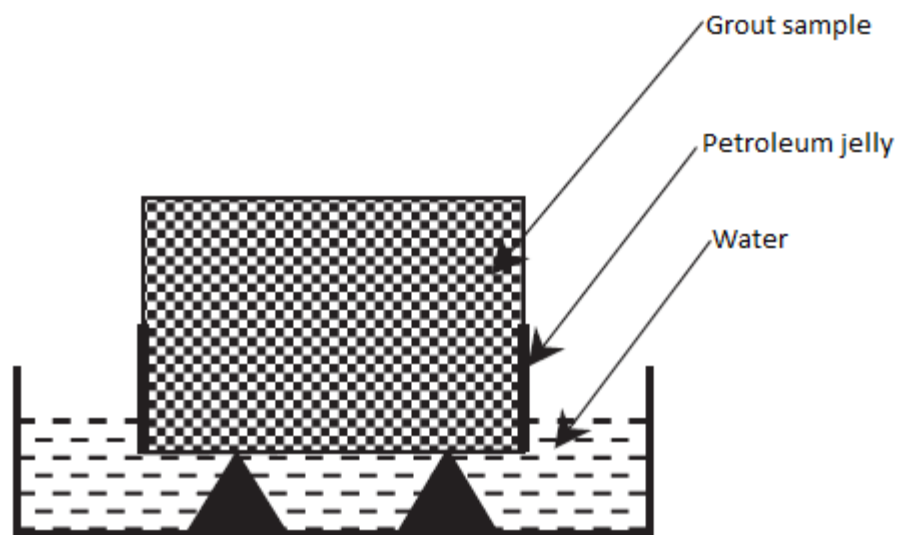


Figure 3-16: experimental setup for sorptivity testing, modified from (Tasdemir, 2003)

Samples were placed on top of small mesh stands within a pan containing potable water, maintained at 5mm above the base of the sample, as illustrated in Figure 3-16. Mass change was recorded as a function of the square root of time ( $T^{1/2}$ ) and the sorptivity coefficient for each mix was calculated via the application of the following equation –

$$\frac{Q}{A} = k\sqrt{T} + c$$

*Equation 12*

Where –

Q is the volume of water adsorbed ( $\text{cm}^3$ )

A is the cross-sectional area of specimen in contact with the water ( $\text{cm}^2$ )

T is the time (minutes)

k is the sorptivity coefficient ( $\text{cm}/\text{min}^{1/2}$ ); and

c is an arbitrary constant, a result of filling of open surface pores at the onset of the experiment

k is determined through plotting  $\frac{Q}{A}$  against  $\sqrt{T}$ ; where k is the slope of the linear relationship.

### **3.4 Summary**

The techniques applied within the present study represent the most effective means of assessing and following hydration and microstructural development of composite cement systems. This is the most rigorous investigation into cementitious materials that are used in the treatment of nuclear waste in the UK and how their hydration and subsequent performance are impacted by changes in powder composition.

Applying such a suite of techniques has allowed for the ramifications of changes to supply to be thoroughly investigated, with the impacts of changes to the chemistry and particle size distributions (PSD) of the different cementitious powders compared and contrasted.

This study represents the first time in which X-ray  $\mu\text{CT}$  has been applied to probe the microstructural development of cementitious grouts for nuclear waste treatment, and with very high resolution, on untreated samples. Further, investigation into heat-treated

samples has shown the resilience, or otherwise, of these grouting formulations of various compositions.

Subsequent analysis of results from X-ray  $\mu$ CT in which a recurring Monte Carlo simulation was performed to investigate the interconnectivity of the percolating pore networks of the various systems, has allowed for these results to be quantified into statistically meaningful values.

Gaining insight into the engineering performance of grouting materials is crucial in order to provide a baseline from which long-term in service performance can be accurately and confidently predicted and planned for. Clearly, there are limitations to the degree to which these results remain relevant and pertinent; however, critically evaluating permeability and sorptivity (following exposure to temperatures as would be experienced within a fire scenario) provides significant insight into performance of the various grout compositions studied.

The key objective of the testing procedures employed within the present study was to gain significant insight into the relationship –

**Composition → hydration → microstructure → performance**

Whereby the techniques should provide the greatest possible insight into the impacts that changes to composition have upon hydration and microstructural development; and ultimately what this means for subsequent performance.

# **4. Hydration, microstructural development and engineering performance of cementitious grouts for ILW encapsulation**

Hydration of both OPC and SCMs such as slag may be determined via a number of direct and indirect methods. Following hydration of the clinker component and the slag within these systems both present their own challenges. Through applying a range of techniques, it has been possible to assess the impact of changes to the chemical and physical composition of the anhydrous materials upon the rate and degree of their hydration.

## **4.1 Early age grout hydration**

### **4.1.1 Bound water and portlandite content determined via thermogravimetric analysis (TGA)**

Determination of the bound water content of a grout is a quick and simple method for identifying continued hydration. In neat Portland cements the technique generally provides consistently good results (Pane and Hansen, 2005) but the complexities induced by the blending of OPC with SCMs make the technique less useful for composite cements (Scrivener et al., 2015b, Massazza, 1998). Nevertheless, provided that suitable sample preparation has been performed and consistent parameters are applied, results will provide some insight towards hydration.

Gruyaert (2011) applied a modified version of the equation proposed by Pane and Hansen (2005) in an attempt to provide an estimate towards weighted degree of hydration from bound water content. The results of Gruyaert (2011) proved inconclusive but did appear to give a quick and simple indication towards continued hydration. The findings of Darquennes et al. (2013) seemed to contradict the findings of other studies in suggesting that higher levels of replacement by slag accelerate slag hydration.

Analysis of bound water, therefore, provides a quick and simple representation of continued hydration but is limited in providing any more insightful information.

Figure 4-1 shows the increase in bound water content with time as hydration proceeded within the investigated mixes. Hydration within these samples proceeded more slowly than would be observed in a typical grout for construction purposes given the high level of replacement by slag. Further, hydration is likely to be even more retarded, especially at early age, in relation to more standard composite cement blends. This is due to the higher PSD and hence lower SSA of the clinker component, but more significantly the slag fraction within these grouts. Similar results were obtained by Whittaker (2014) and Gruyaert (2011) in slag composites with high levels of replacement by slag.

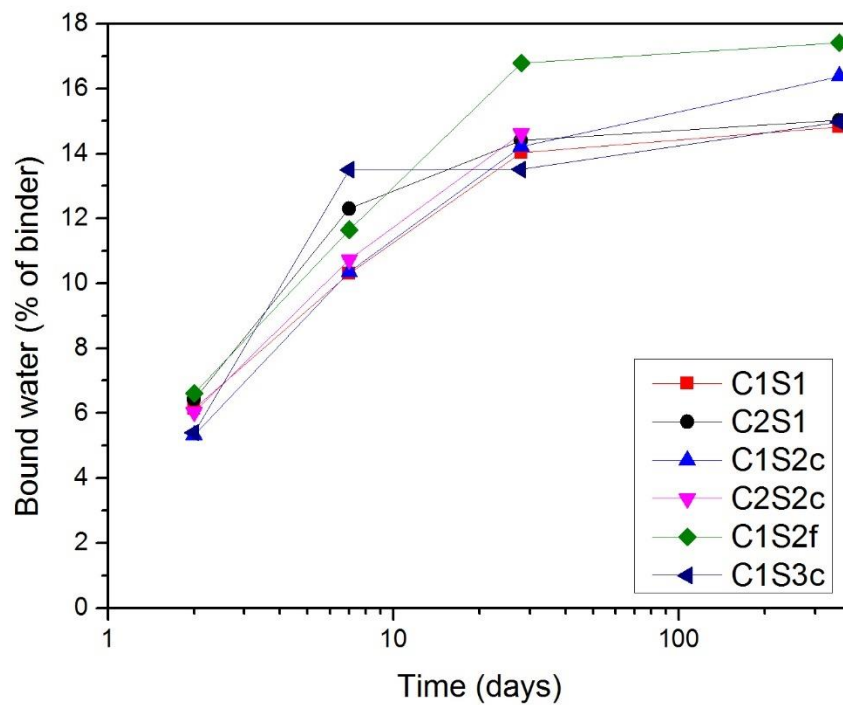


Figure 4-1: Bound water content as a function of time

A gradual increase in bound water content was observed for all samples as hydration proceeded; this increase in bound water slows with time as rate of hydration decreased. This retardation from 28 to 365 days was most marked in the C1S1 and C2S1 samples, likely due to the lower later age hydration of the slag within each mix. The presence of the much larger Calumite grains (accounting for 35%wt of the slag in both mixes) served to reduce total slag hydration without significantly affecting early age hydration; in both

instances, the hydration of the much finer S1f was likely accelerated due to both its increase in specific surface area and the availability of a comparatively higher volume of water to drive the hydration reaction.

The one slightly surprising finding relates to the early age results for the C1S2f samples. These sample are shown via other methods to hydrate to a much higher degree within the first 7 days. However, bound water contents at these ages were similar to the other systems. At later ages, bound water contents were higher than for all other samples but the disparity was not as high as might be expected when considering the variation in degree of hydration.

Portlandite contents, as determined via the tangent method, are shown in Figure 4-2. Results are comparable to those obtained by Borges et al. (2010) at the same slag loading and prepared with materials of very similar chemical and physical composition. Portlandite content was much lower than in pure OPC systems (Taylor et al., 1985a) but also lower than determined in composite cements with lower levels of replacement by BFS (Monteagudo et al., 2014, Taylor et al., 1985b, Whittaker et al., 2014).

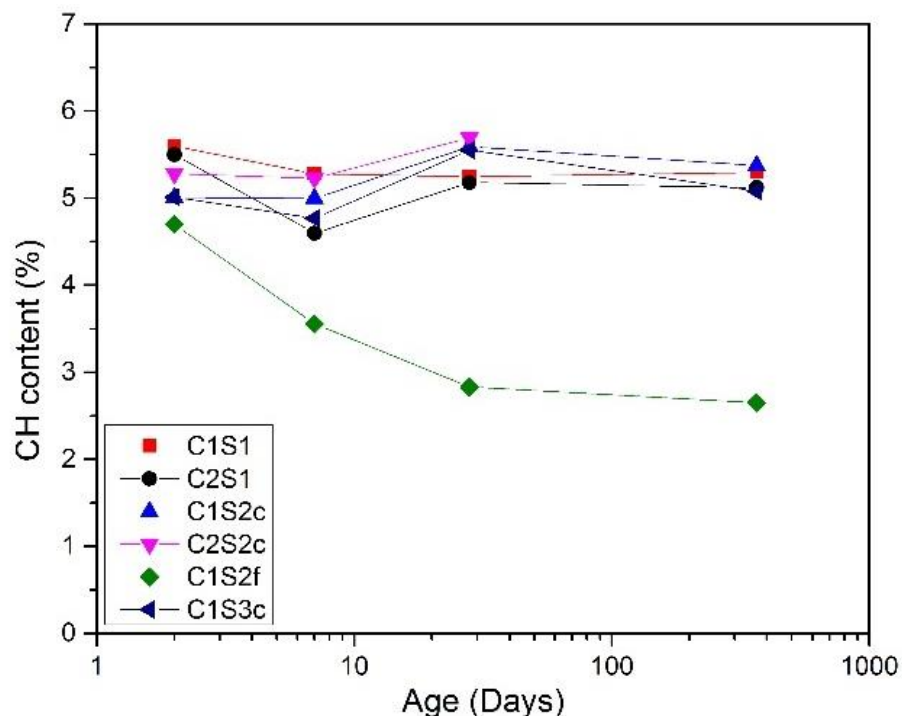


Figure 4-2: CH content as a function of time, determined via TGA

Figure 4-2 shows a comparatively lower portlandite content within the C1S2f system, which was expected since the finer slag was expected to hydrate to a higher degree. Within this mix, the CH content decreased with time, contrary to the results for all other mix designs. This reduction in CH content suggests a higher rate of later age slag

hydration in which some of the CH present within the hydrating matrix is consumed in the formation of secondary C-S-H. A consistent portlandite content with time was observed with all other mixes, in agreement with a large number of previous studies with a wide range of level of replacement by BFS (Harrisson et al., 1986, Taylor et al., 1985b, Whittaker et al., 2014, Hinrichs and Odler, 1989).

The presence of portlandite within grouts at high levels of replacement is not in agreement with predictions made by thermodynamic models (Atkins et al., 1990, Lothenbach et al., 2011, Chen, 2006). Within these models the degree of slag reaction was assumed (Chen and Lothenbach assumed 70% and 75% hydration respectively); with these levels of hydration not reached at higher levels of replacement, as within this study. A further factor which is believed to contribute to the presence of residual portlandite, even at later age is the lack of available space into which hydrates can grow (Berodier and Scrivener, 2015, Berodier, 2015). This pore filling clearly has a significant impact, leading to a significant retardation in later age slag hydration which is exacerbated within this study since the w/b ratio (0.35) was much lower than in many previous studies and significantly lower than would be typical in construction applications.

The presence of some Portlandite within these grouting materials is generally seen to be advantageous since it will maintain the high internal pH of the waste package and reduce the solubility of a number of radioactive species.

#### **4.1.2 Determination of degree of hydration and microstructural development from BSE-IA**

Whilst samples younger than 2 days were not analysed in the present study (Figure 4-3), results at this age were similar to those obtained in previous investigations (Kocaba et al., 2012), with around 50% of clinker having hydrated. This is not surprising since in both this study and the work of Kocaba (2010) the filler effect was significant, leading to enhanced clinker hydration (Berodier and Scrivener, 2014). The effect of shear from the slag within each system coupled with a dilution effect appear to be the key factors in accelerating early age clinker hydration.

Samples analysed via BSE-IA were 10mm in diameter and 2mm thick; and prepared as outlined in Section 3.3.7.3. The total area analysed per sample was equal to

approximately 2.4 x 1.8 mm given the magnification of 800x and the grid analysis technique, covering 7x7 images (plus 1).

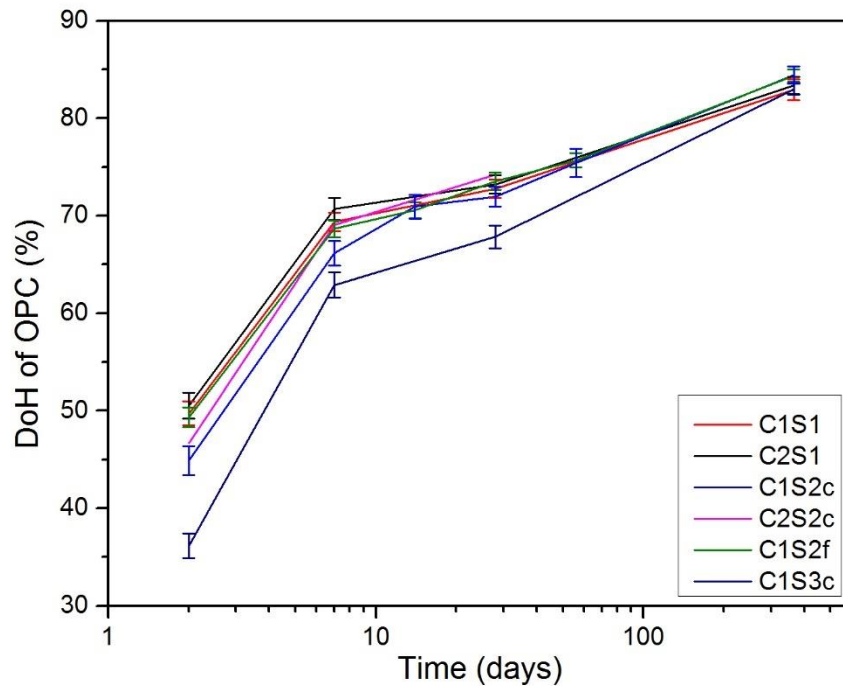


Figure 4-3: Evolution of clinker hydration from BSE-IA

At lower levels of replacement (40%), Berodier and Scrivener (2014) determined that the specific surface area of the SCM or filler (inert quartz) was significant in the degree to which clinker hydration was enhanced. Similar results may also be extracted from the work of Kocaba (2010) and appear consistent irrespective of clinker source. It is also highly probable that the disparity in alkali content in the slags within the aforementioned study may have an impact and contribute to the disparity in clinker hydration at early age within that study.

Within the present study, at higher levels of replacement by slag (75%) there was not the same incongruence as a result of the SSA of the slag. It is proposed that since the level of replacement in this study was very high, clinker hydration was restricted more by physical factors including dissolution rate, availability of space and the surface to volume ratio of the clinker itself; the result being that there was no discernible difference between results other than for the C1S3c system. The lower rate of clinker hydration at early age within the C1S3c system (Figure 4-3) may have been a result of a lower alkali content of the slag fraction within this grout. At 365 days the level of clinker hydration was comparable across all mix designs and was similar, although perhaps slightly lower,

than results obtained in previous studies with higher w/b ratios and/or lower slag loading (Whittaker et al., 2014, Kocaba et al., 2012) and slightly lower than in blends prepared with a higher level of slag replacement (Utton, 2006).

The degree of hydration (DoH) of the slag fraction within each grout was determined at a range of ages from 2 to 365 days via BSE-IA. Owing to the high level of slag replacement, low early strength development and complications surrounding hydration stopping; 2 days was determined to be the lowest achievable age at which to prepare, mount and analyse samples.

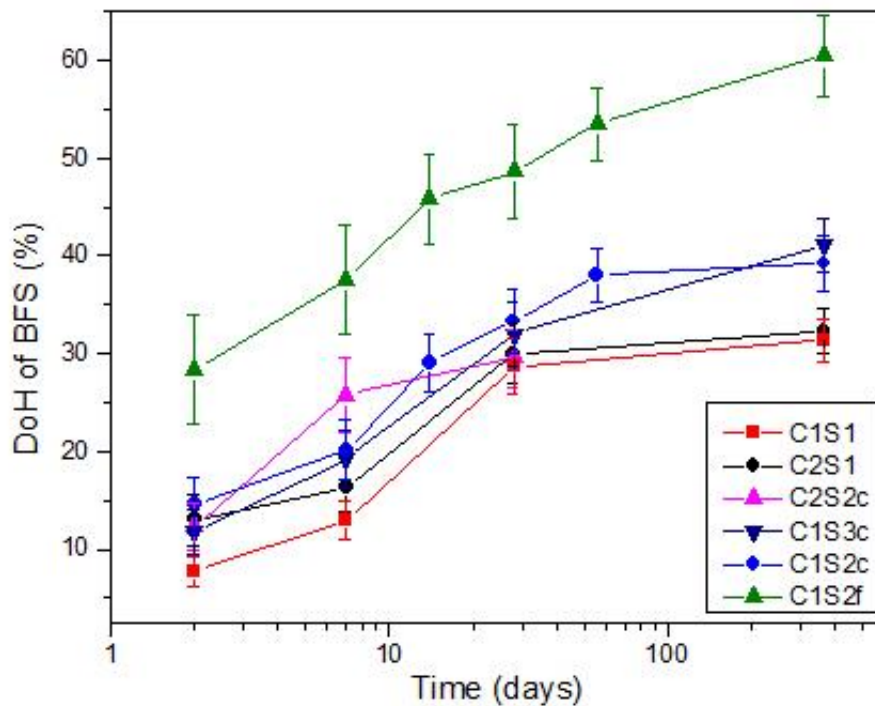


Figure 4-4: Evolution of slag hydration with time from BSE-IA

Slag hydration was typically very low at early age due to the relative coarseness of the slag fraction (in all but the C1S2f mix) and the high slag loading of the mixes. Hydration proceeded gradually at early age but continued hydration began to diminish with time, a result of a combination of factors but largely governed by the availability of pore space to accommodate hydration products (Berodier and Scrivener, 2015). This reduction in later age hydration appeared less prevalent in the C1S2f system, which is surprising since this grout showed the highest degree of slag hydration at all ages.

The chemical composition of the slag fractions appeared not to have a significant impact upon rate and degree of hydration, with all other factors remaining constant, (compare

C1S2c and C1S3c). Similar rates and overall degrees of hydration were observed, despite the disparities in both C/S ratio and alkali content, with S2c having preferable values to S3c for both (C/S of 1.20 compared to 1.125 and combined alkali content of 0.77 compared to 0.61 %  $\text{Na}_2\text{O}_{\text{equivalent}}$ ) both early and later age degree of hydration agreed within the margin of error of the technique.

The chemical composition and physical properties of the clinker component appeared not to have a dramatic impact upon slag hydration, with the results for C1S1 and C2S1 being very similar at all ages. This also applies for the C1S2c and C2S2c samples, with minimal differences observed up to 28 days

The key factor in controlling the rate and degree of slag hydration within the present study was the fineness of the slag fraction (Tan et al., 2014). The mix containing the finer slag (C1S2f) showed a comparatively much higher early age hydration with the disparity in relation to the other mixes remaining almost constant with time.

The slag fraction accounted for by the much coarser Calumite grains in the C1S1 and C2S1 samples became increasingly significant with time as much of the finer slag reached its hydration limit and no Calumite hydration was observed. The dilution effect caused by the presence of Calumite at early age appeared to promote and accelerate the early age hydration of the remainder of the slag fraction within these grouts with the later age and overall degree of slag hydration suffering as a result. If degree of hydration of the Calumite is assumed to be 0%, the degree of hydration of the 'non-Calumite' slag within the C1S1 and C2S1 systems would be comparable to that of the slag in the C1S2f system.

These results are generally in good agreement with those obtained in other investigations in which high levels (>65%) of replacement by slag have been studied, especially those in which the same technique has been applied with the same level of rigour (Whittaker, 2014, Utton, 2006). In all instances, there existed a large volume of unreacted slag after 1 year of hydration, with predictions based on modelling, and observations of much older samples (Taylor et al., 2010) suggesting that much of the slag present within systems such as these will remain anhydrous indefinitely.

Table 4-1: Rate of slag hydration (% of 28 day hydration)

Time (days)	C1S2c	C1S2f	C1S1	C2S1	C2S2c	C1S3c
2	43.6	58.3	27.0	43.4	32.4	36.6
7	60.5	77.2	45.3	54.4	53.2	59.9
14	87.2	94.2				
28	100	100	100	100	100	100
56	114.2	110.0				
365	123.3	124.3	109.4	107.8		122.2

Table 4-1 shows the degree of slag hydration relative to 28 days for all mix designs. What is clearly apparent is the high early age hydration of the fine S<sub>2f</sub> slag within the C1S2<sub>f</sub> system, relative to the coarser slag within all of the other mix designs investigated. The current and legacy grout formulations (C1S1 and C2S1) show comparatively slow hydration at very early age, and relatively low later age hydration (beyond 28 days). This reduced rate of hydration is due largely to the presence of the unreactive Calumite grains, which account for 35% of the slag fraction within these mixes.

Determination of hydration of distinct clinker and slag phases, as well as measurement of 'coarse porosity' (discussed later) via the application of image analysis was a time consuming and labour intensive exercise. The results are, however, accurate and repeatable, providing significant insight into the continued hydration of composite cementitious materials.

Comparing the results of the present study with those of previous investigations (Figure 4-5) a number of observations become clear. It is important to first note the differences between the mix designs since they ultimately have an impact; in the work of both Whittaker (2014) and Kocaba (2010), all mixes were prepared with a w/b of 0.5, significantly higher than the 0.35 within this study. The slag powders were generally finer than the majority of those investigated here, and in most cases the grouts were prepared with lower levels of replacement by slag (40%). All of these factors would be expected to reduce overall degree of hydration. Previous studies suggest that rate of slag hydration appears not to have an impact on the rate of its hydration (Hinrichs and Odler, 1989, Chen, 2006, Gruyaert et al., 2010) but clearly, there will be a marked reduction in total hydration.

Nevertheless, some interesting trends hold true. At 40% replacement, Kocaba suggested that slag fineness is a significant factor, particularly at early age. Further, Kocaba's results match very closely those of the present study when comparing the 'coarser' slags, until medium/late age at which point the impact of the disparity in w/b became increasingly significant and the availability of pore space for continued hydration became the dominant factor.

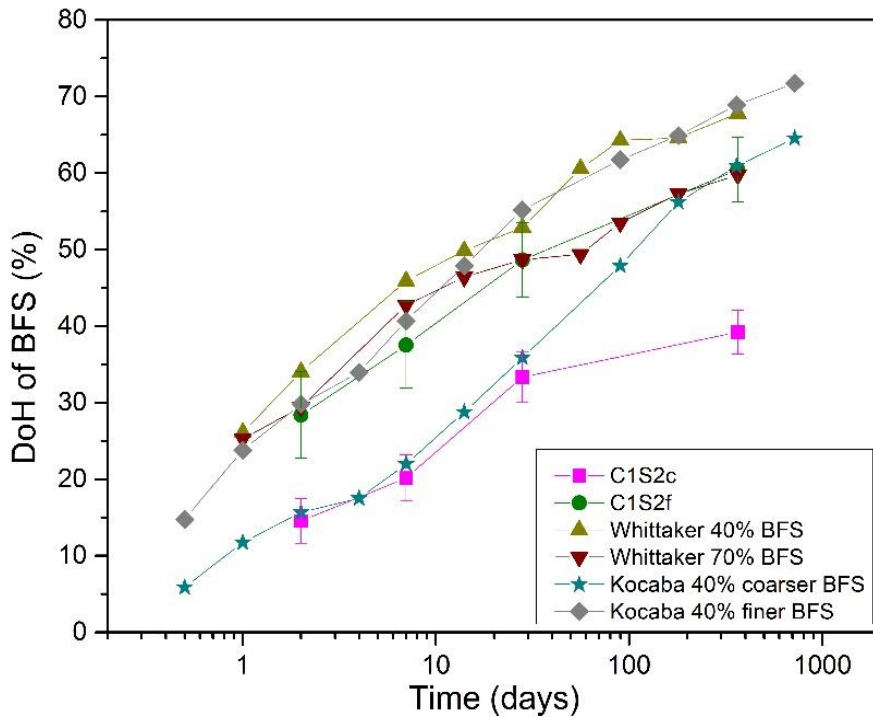


Figure 4-5: Evolution of slag hydration of selected mixes from BSE-IA compared to the results of Whittaker (2014) and Kocaba (2010)

The work of Whittaker provided similar results, slag loading did not appear to have a great impact upon rate of hydration at early age (Hinrichs and Odler, 1989), however there was a divergence between the 40% and 70% slag blends after 14 days.

Clearly there are a number of factors which control degree of slag hydration; however, the results presented in Figure 4-5 strongly suggest that fineness is the dominant factor in controlling hydration of slag (Escalante et al., 2001). This is particularly visible at early

age and also at later age if other significant factors (slag loading and w/b) remain constant.

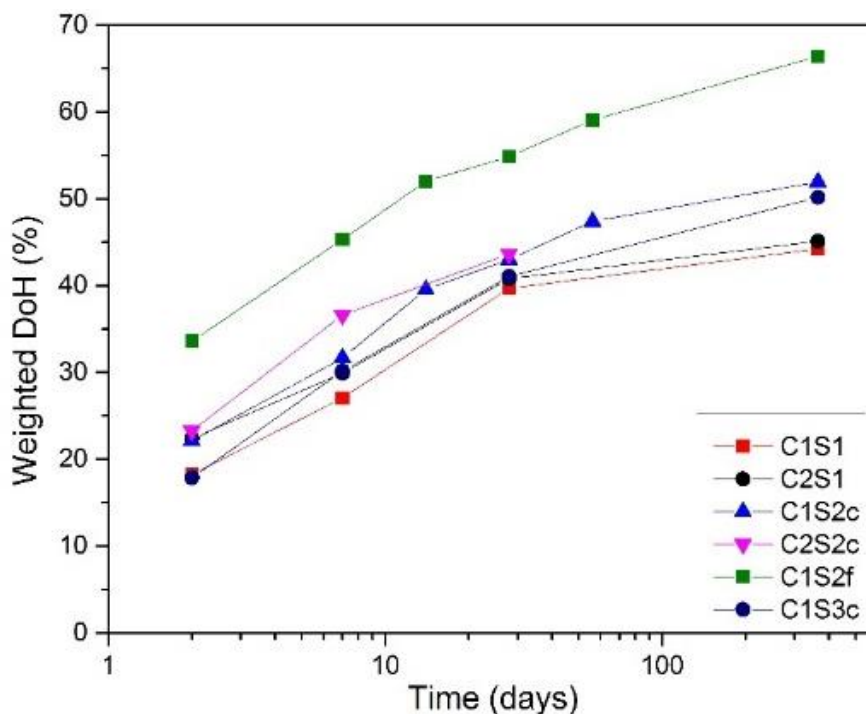


Figure 4-6: Weighted degree of hydration of all blends as a function of time

The term weighted degree of hydration relates to the estimated 'total' hydration of each grout at each time of testing. It is the combination of the hydration of the clinker phases (accounting for 25% of the weighted value) and the hydration of the slag phases (accounting for 75% of the weighted value) to give a relatively precise estimate of total hydration. There is clearly an associated error for these values, but since they are based on calculations rather than analysis of a number of samples, error bars have not been added.

Figure 4-6 highlights that weighted DoH is largely governed by slag hydration, since it accounts for 75% of material in each mix and since clinker hydration is very similar across all mix designs (Gruyaert, 2011, Utton, 2006). Clearly, slag fineness is the most significant factor in both rate and degree of grout hydration.

It also appears, although not conclusively, that clinker type appears to have a small influence upon weighted DoH; this may, however, just be coincidence since the

difference is within the margin of error of the technique, especially since results have been combined.

The continued hydration of each mix, as plotted in the figures above, is clearly visible through observation of corresponding micrographs.

Figure 4-7 shows the hydration within the C1S1 system from 2 to 365 days, with clear pore filling occurring as a result of continued clinker and, later, slag hydration. There remained a high volume of anhydrous material even after 1 year, most notably the large Calumite grains show no visible signs of hydration. A considerable degree of slag hydration appeared to have occurred between 7 and 28 days, consistent with the results plotted in Figure 4-4.

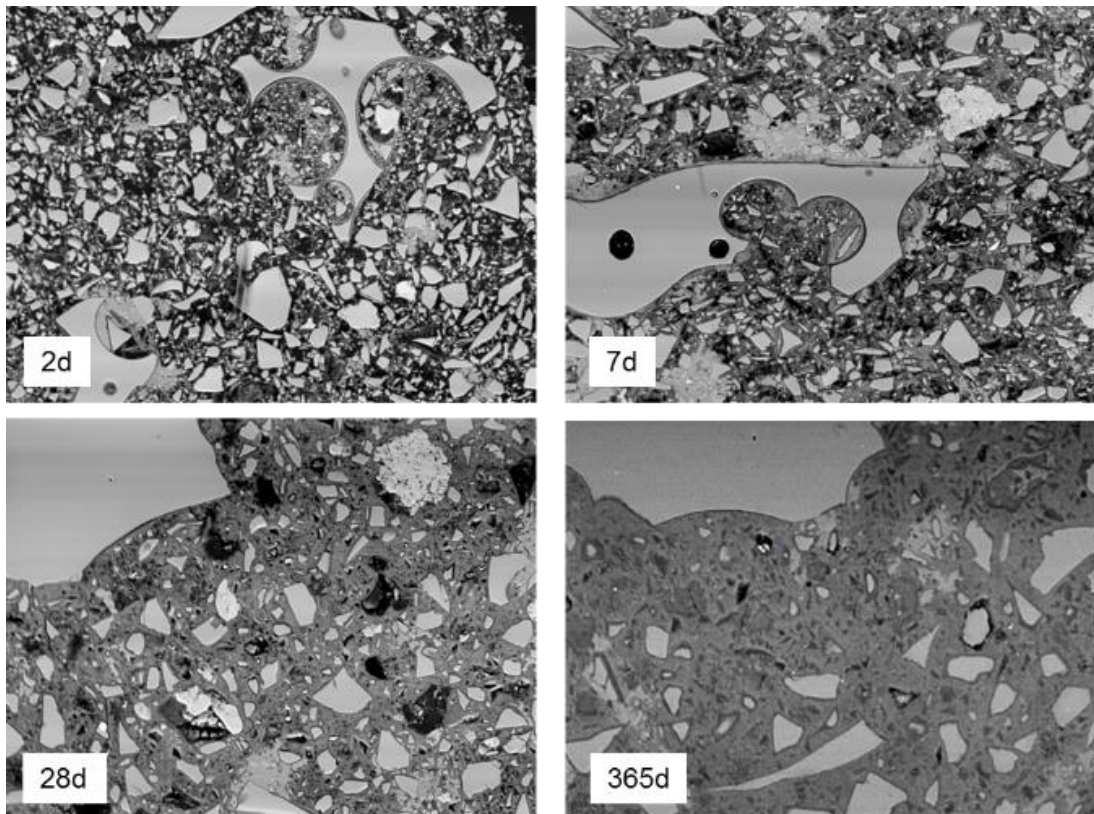


Figure 4-7: Microstructural development of C1S1 system at ages 2-365 days imaged at 800x magnification

The apparent lack of hydration of Calumite might best be explained by the comparatively low specific surface area of these large grains relative to that of both the clinker and the

much finer slag within both the C1S1 and C2S1 grout formulations. Clearly, given the chemical composition of the materials, the clinker phases hydrate most rapidly. Following this, the conditions within the hydrating matrix are preferable for slag hydration (with CH presence elevating pH), at which point the fine slag begins to hydrate, filling much of the capillary porosity. Hydration of the large Calumite grains is hindered both by the reduction in surrounding capillary porosity and the reduced availability of unbound water with which to react coupled with the reduced CH content and pH due to hydration of the much finer slag fraction.

Similar results to those for C1S1 can be seen for the C1S2c system, as shown in Figure 4-8. Again, slag hydration was low at early age with large volumes of both pore space and anhydrous material visible at 2 days and 7 days. As with the results for C1S1, a clear filling of pores can be observed between 7 and 28 days. A significant volume of anhydrous material remained at 365 days with clinker phases and areas of CH still visible.

Many of the larger sized slag particles showed limited hydration, but hydration rims are visible, unlike the significantly larger Calumite grains present within the C1S1 and C2S1 systems. Likewise, the slag grains here seemed well bound within the hydration products of the cementitious matrix, with results suggesting that this is not always the case for the larger grains in these other mix designs.

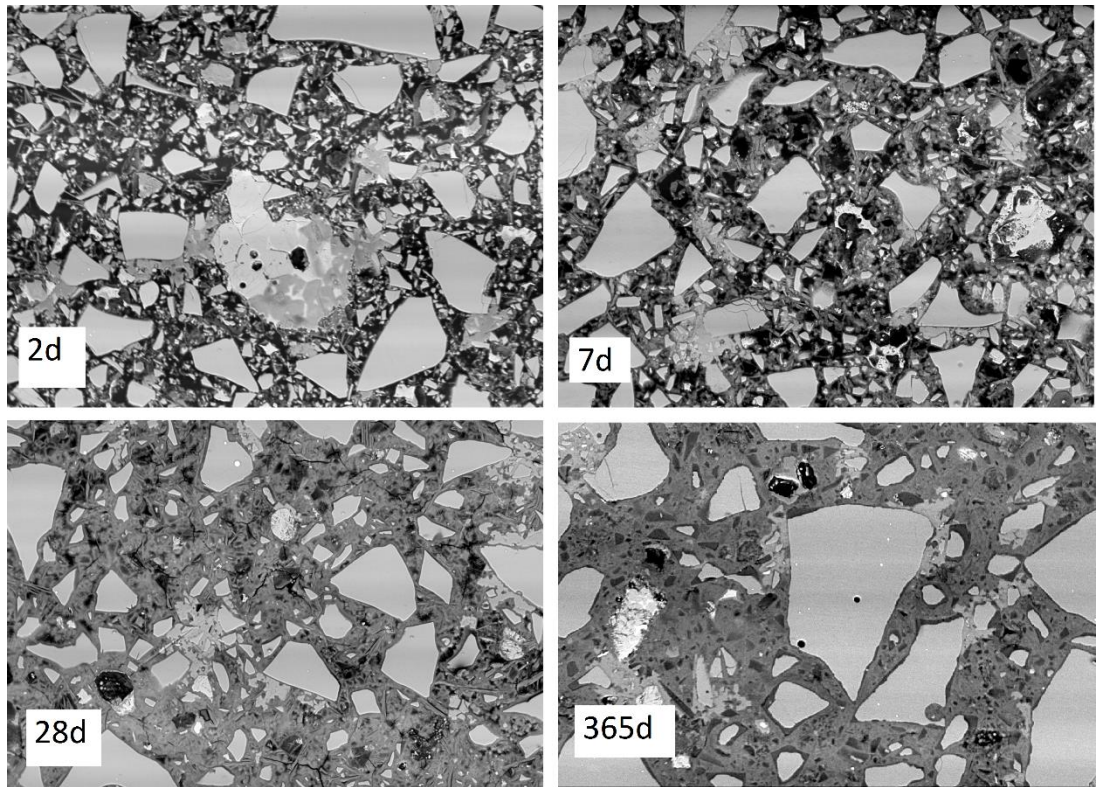


Figure 4-8: Microstructural development of C1S2c system at ages 2-365 days imaged at 800x magnification

Micrographs for the C1S2f system are shown in Figure 4-9; slag hydration at early age has proceeded much more rapidly than for all of the other systems studied and this has resulted in a considerable reduction in observable, or coarse, porosity at 2 and 7 days. Where coarse porosity is anything over  $0.3\mu\text{m}$  since this is the resolution limit of this technique at these operating parameters (analysing samples at 800x mag. with a resolution of 2048x1624 pixels) allows for identification of features with a minimum size of 2x2 pixels, or around  $0.3\mu\text{m}$ .

Hydration between 7 and 28 days continued at a comparable rate to the other samples shown above, with porosity continuing to decrease as new hydrates filled larger capillary pores. Slag hydration proceeded at an ever decreasing rate up to 365 days, at which point the observable porosity (hereafter referred to as 'coarse porosity') appeared to be all but filled with hydrates. A small quantity of anhydrous clinker as well as CH remained visible.

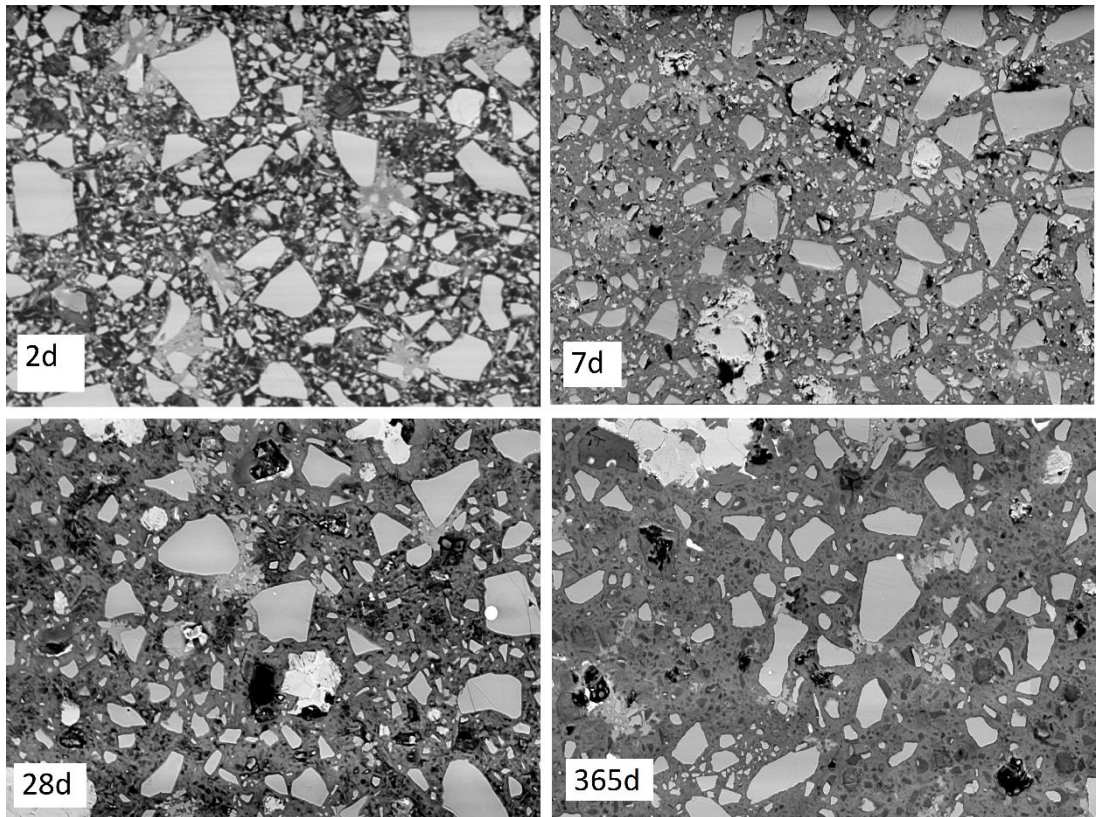


Figure 4-9: Microstructural development of C1S2f system at ages 2-365 days imaged at 800x magnification

These findings are in agreement with those observed via thermogravimetric analysis where a gradual increase in bound water content was found. Results at 28 days were largely in agreement, suggesting that determination of bound water may potentially be suitable as an initial qualitative measure of weighted DoH (if samples are prepared with a matching w/b and slag loading), but that detailed or quantitative results are not possible.

The mix design C1S2f was the only to experience a drop in CH content with time, suggesting possible consumption at higher levels of slag hydration but still far from complete CH consumption even at these relatively high levels of replacement by slag.

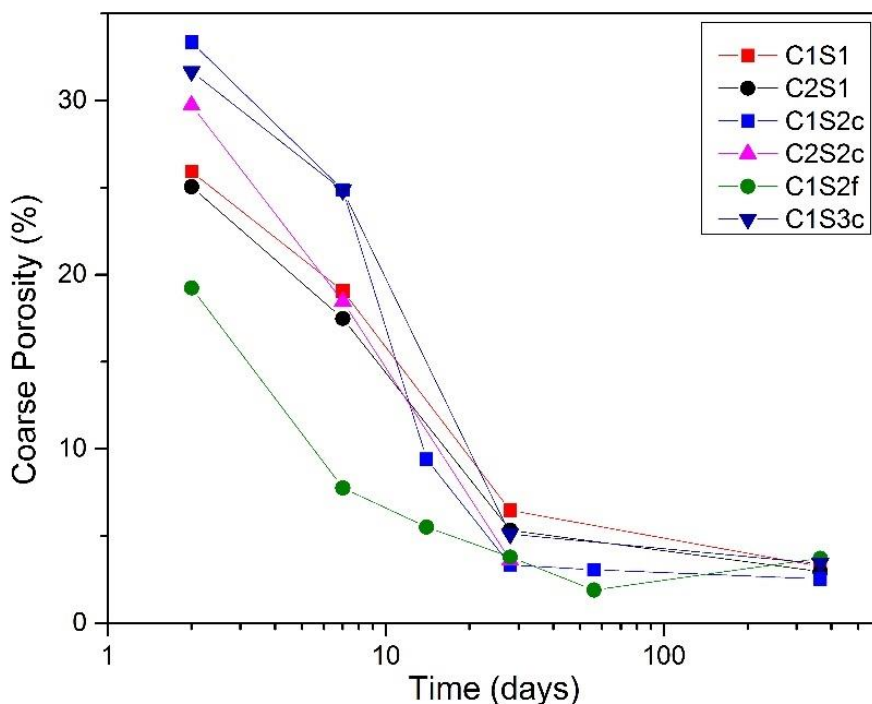


Figure 4-10: Coarse porosity as a function of time, determined via BSE-IA

At early age, the C1S2f system showed the lowest coarse porosity (Figure 4-10), owing to the higher weighted degree of hydration (Figure 4-6). At 2 days, the C1S1 and C2S1 systems showed the 2<sup>nd</sup> and 3<sup>rd</sup> lowest porosity values despite a comparatively lower degree of hydration of slag (Figure 4-4). The presence of the much larger Calumite grains, which appear to be unreactive, serve merely to fill space within the hydrating matrix; as a result of their presence, coarse porosity is lower at a comparable weighted degree of hydration (Figure 4-6) and is comparable to all other formulations studied at 365 days, despite a lower weighted hydration degree.

Porosity of these grouting materials is a very significant factor, since porosity essentially governs permeability and the rate at which deleterious species may enter the waste packages, or the rate at which mobile species are able to leach out into the surrounding biosphere. A reduction in coarse porosity has clear ramifications upon the rate at which leaching will occur but also will affect the rate at which waste packages will begin to degrade after significantly long periods of time within a GDF setting.

Comparison of the C1S2c and C1S3c systems indicates that chemical composition of the slag fraction has little impact, with similar degrees of slag hydration and weighted DoH at all ages; resulting in similar calculated values for coarse porosity.

Clinker composition appeared significant at early age (compare C1S2c and C2S2c), with the mix containing the finer clinker (C2) displaying a slightly higher weighted DoH and a corresponding lower coarse porosity (

Figure 4-10). This trend continued with the C1S1 and C2S1 samples but the disparity at early age was less significant, possibly a result of the presence of the larger Calumite grains.

Coarse porosity values obtained within this study were much higher at early age than in a number of previous studies using the same technique (Whittaker, 2014, Ogirigbo, 2016). This is a result of a lower overall degree of hydration, caused by the comparatively high level of replacement by slag (Gruyaert, 2011, Lumley et al., 1996). These comparatively high results are despite the lower w/b used for the mixes studied here. Following continued hydration at later ages values are in line with those found in other studies (Whittaker, 2014, Kocaba, 2010), where continued slag hydration is serving to fill much of the coarser pore space (Berodier and Scrivener, 2015).

### 4.1.3 Following early age hydration by means of chemical shrinkage (dilatometry) and isothermal conduction calorimetry

#### 4.1.3.1 Dilatometry

Figure 4-11 shows the total mean chemical shrinkage of each mix (from results obtained in triplicate). Continued hydration occurred for all mix designs, but at varying rates. Clinker source appeared to have an impact at early age, with the C2 containing mixes initially experiencing higher rates of shrinkage. These observations were consistent with results from BSE-IA; suggesting that the finer clinker hydrated more rapidly and enhanced conditions for early age slag hydration. However, this enhanced rate of hydration was not maintained. In both cases, comparable rates of hydration were reached at around 9 and 14 days respectively when comparing C1S1 with C2S1 and C1S2c with C2S2c.

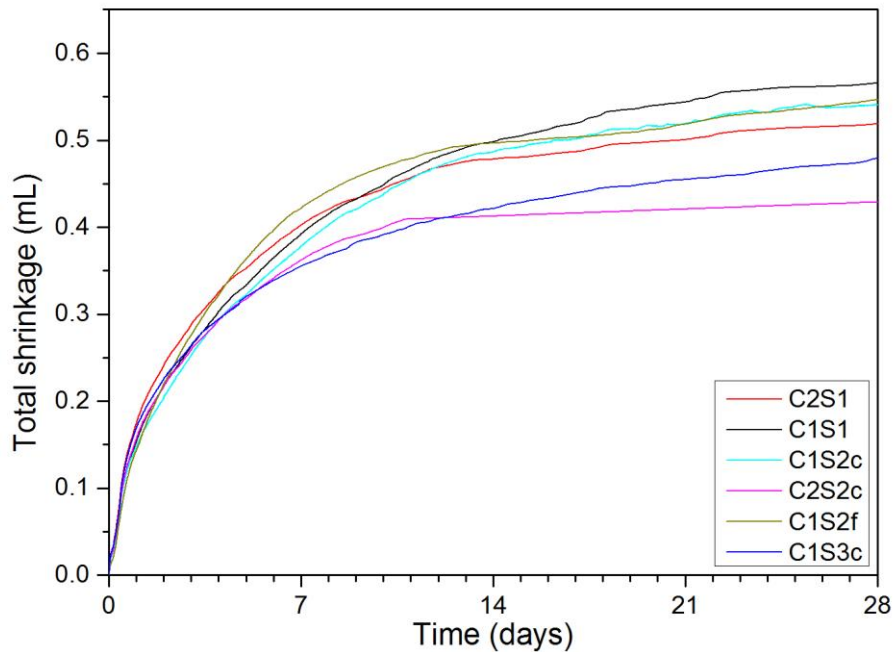


Figure 4-11: Evolution of chemical shrinkage for all project mixes up to 28 days

For each mix design, a comparable set of samples was prepared with inert quartz of matching particle size distribution replacing the slag fraction. The corresponding curve for each 'filler' system was subtracted from the original in order to isolate the contribution of the slag fraction towards shrinkage; results are plotted in Figure 4-11. Testing was repeated several times for a number of samples with consistent results obtained throughout. Deviation between results across each run was very low, standard error bars would not be visible were they to be added to the associated figures.

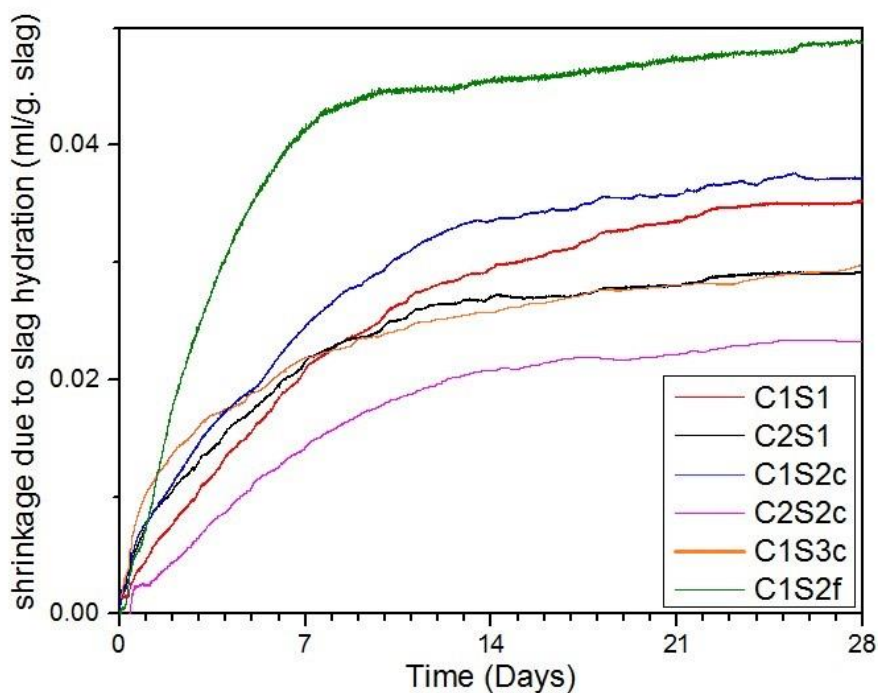


Figure 4-12: Isolated shrinkage as a result of slag hydration for all mix designs

As can be seen in Figure 4-12, there existed a degree of variability across mix designs. In order to account for this discrepancy, chemical shrinkage and ICC data were calibrated against degrees of slag hydration from BSE-IA to produce calibration values, as shown in Table 4-2 and Table 4-3 respectively. Whilst it is not possible to use the chemical shrinkage method independently to determine slag hydration, when coupled with a suitable accurate direct method, such as image analysis at later age, it provides very accurate in line results at early age and up to 28 days (Berodier, 2015).

Analysis was repeated up to 56 days in the case of the C1S2c and C1S2f mix designs. In both instances, samples continued to shrink beyond 28 days but at an ever decreasing rate, bringing into question the validity of the measurements at later age and the suitability of the technique beyond this initial period.

Figure 4-13 shows the average results from this 56-day run, with results also plotted for the corresponding quartz replacement mixes. Within these mixes, the slag fraction is of the same source and hence of matching composition, with the only variable being the fineness and hence specific surface area. It can be seen that this change in physical composition has a significant impact upon hydration and, hence, chemical shrinkage. At this high level of replacement, it would appear that the fineness of the SCM or filler has negligible impact upon the rate of clinker hydration, as highlighted by the similarity in results for the two quartz replacement samples plotted in Figure 4-13. Clearly, slag fineness is highly significant for its own hydration (Tan et al., 2014), but the filler effect due to increased provision of nucleation sites has minimal impact on clinker hydration at these high levels of replacement.

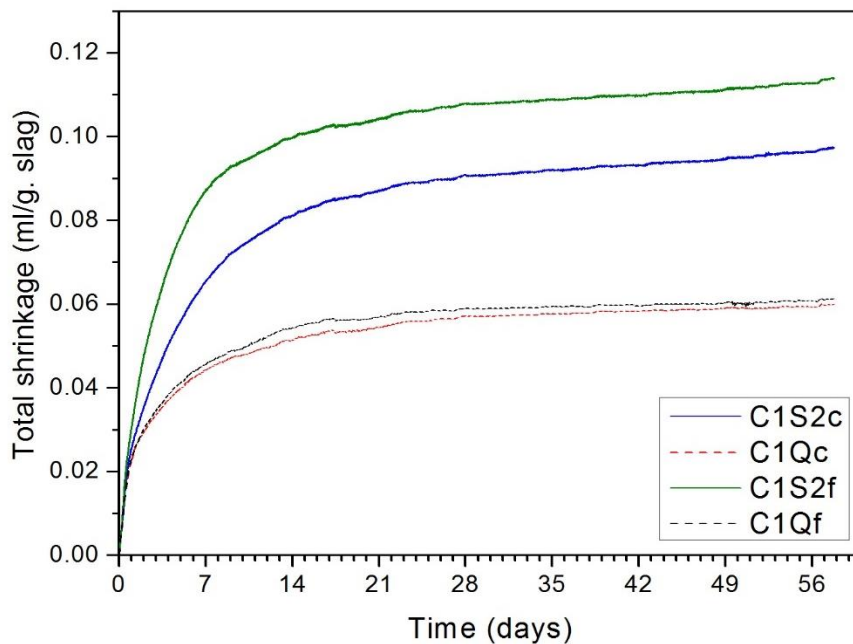


Figure 4-13: Evolution of chemical shrinkage for C1S2c and C1S2f and associated quartz blends over 56 days

Figure 4-14 gives the isolated shrinkage as a result of slag hydration for the C1S2c, C1S2f and C1S3c systems over 28 days. Comparing the C1S2c and C1S2f systems, it is clear that slag fineness plays a significant role in early age hydration, with a substantial difference in results over the first 7 days following casting. From this point onwards,

hydration of the two mixes proceeded at a very similar rate, very much in agreement with results obtained via BSE-IA over the period 7-56 days (Figure 4-4).

Comparing C1S2c with C1S3c there was a degree of disparity, particularly at early age but in general the results appear close, suggesting that whilst slag chemistry undoubtedly had some impact upon hydration, fineness played a more crucial role.

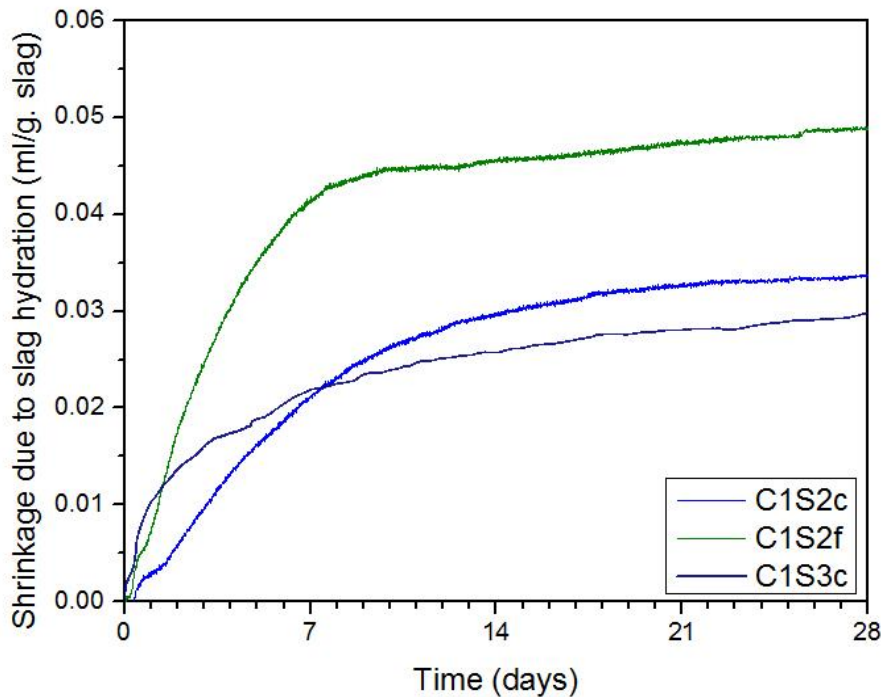


Figure 4-14: Chemical shrinkage as a function of slag chemistry and fineness

#### 4.1.3.2 Isothermal conduction calorimetry

Heat of hydration is a significant factor when designing grouting matrices for the treatment of ILW. Since waste packages are typically large (500L drums or 3m<sup>3</sup> boxes) and require a significant volume of encapsulating grout, it is important to understand the heat evolution profiles, since a very large exotherm could potentially lead to thermal cracking in the centre of a conditioned waste package. The grouts studied here are well below the specification limits for peak or cumulative heat evolution and therefore there would be no chance of thermal cracking occurring if they were to be utilised. Note that the highest peak heat of the mixes investigated was shown by the current, C1S1 (Figure 4-15) and legacy, C2S1 (Figure 4-16) formulations; with these results being consistent with those obtained industrially (Carruthers and Collier, 2013).

Figure 4-15 shows the heat flow of all mix designs prepared with clinker C1 over the 3 days following casting. It is apparent that slag fineness plays an important role in early age clinker hydration (Berodier and Scrivener, 2014), but beyond a few days the significance of slag (or other SCM) fineness becomes increasingly less significant. What is also apparent from the results here is that slag fineness not only governs the rate of clinker hydration to some degree, but increasing slag fineness has a coupled effect of increasing slag reactivity at early age through increasing surface to volume ratio and improving conditions within the hydrating matrix by accelerating clinker hydration.

Although not shown here, the rate of heat release for the C1S2f system remained higher than for the other mixes investigated for the first 6 days, after which the rate of heat release was comparable. This is in agreement with the results observed in both BSE-IA (Figure 4-4) and chemical shrinkage (Figure 4-13), in which the finer slag was observed to hydrate more rapidly at early age; beyond which, rates of hydration were similar across all mix designs.

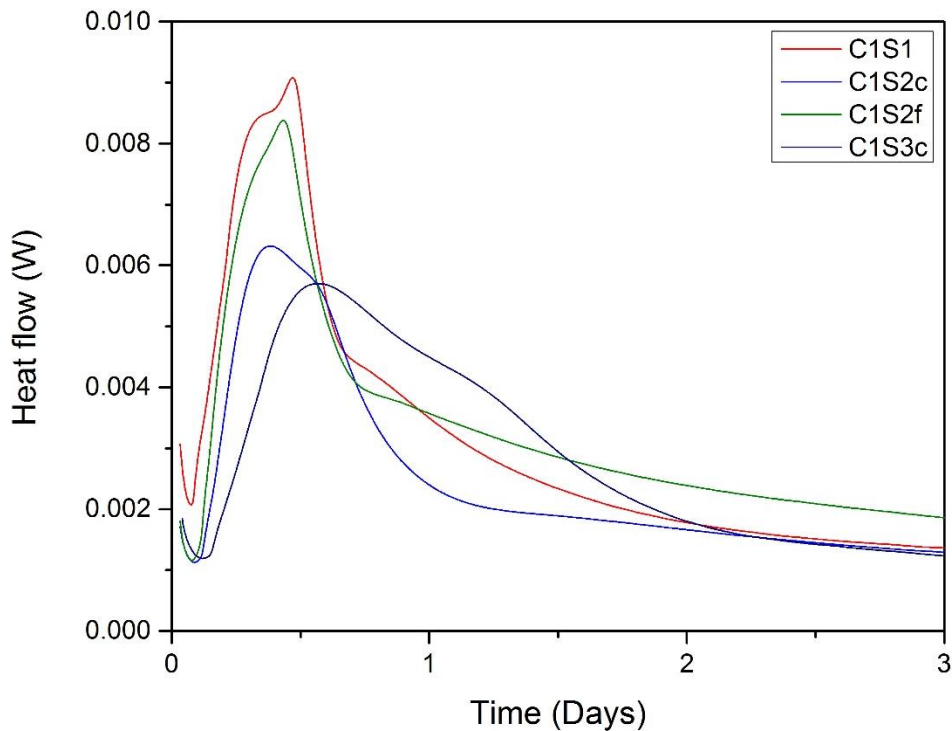


Figure 4-15: Heat evolution of C1 systems over 3 days

Figure 4-16 shows the results for the two systems based on clinker C2. These findings were very much in agreement with those observed above in Figure 4-15, whereby the finer slag fraction included in C1S1 and C2S1 promoted early age clinker hydration.

These effects were short-lived as dissolution continued and the filler effect due to nucleation was no longer significant and was superseded by the dilution effect (Berodier and Scrivener, 2014).

Through comparing the early age hydration of the C1S2c (Figure 4-15) and C2S2c (

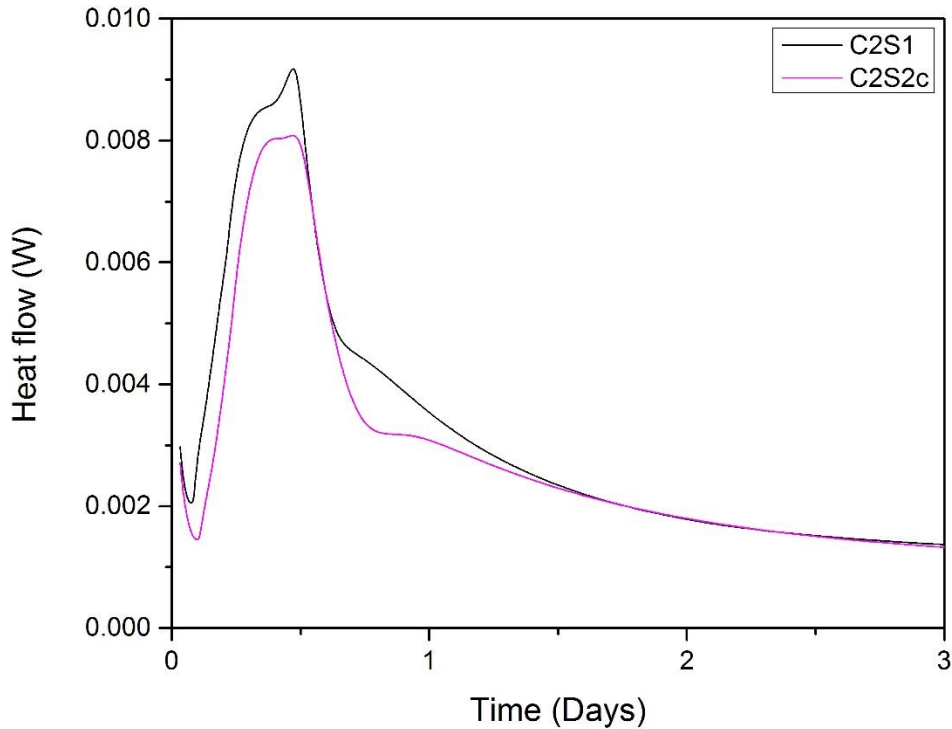


Figure 4-16) systems, it is clear that clinker fineness was highly significant in determining its early age hydration; peak 1 was much more pronounced for the C2S2c system and showed a much slower deceleration than C1S2c. At 2 days, all but the C1S2f system displayed comparable levels of heat of hydration, suggesting that beyond this point, slag fineness is the key parameter in determining continued hydration rate of the grouting systems.

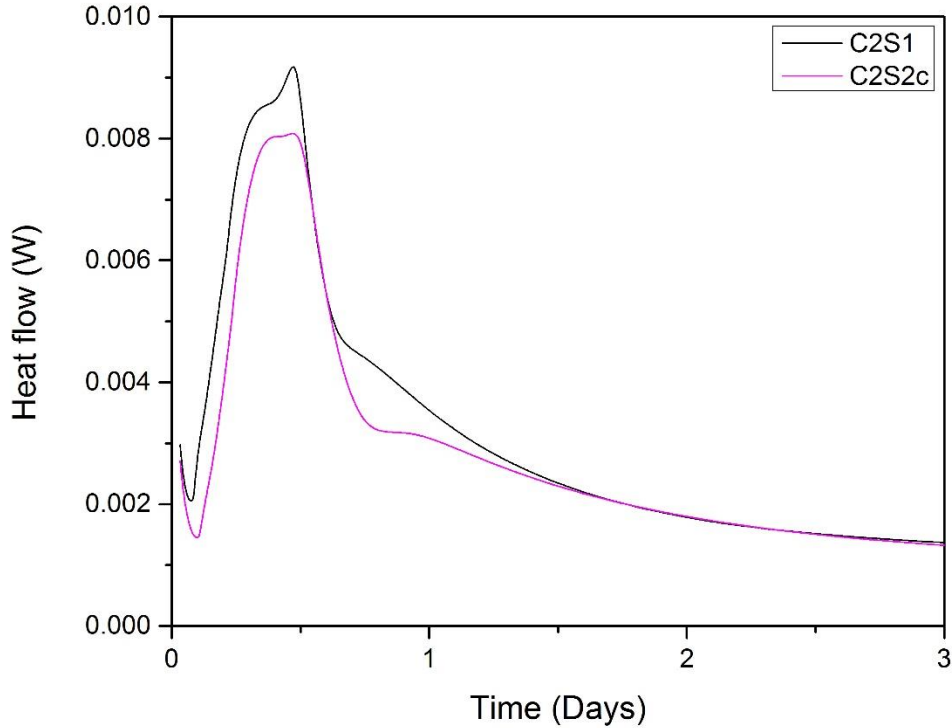


Figure 4-16: Heat evolution of C2 systems over 3 days

Heat due to slag hydration has been isolated (Figure 4-17) in the same way as described for chemical shrinkage; samples were prepared with quartz of matching PSD replacing the slag fraction. Since the exact enthalpy of each slag was not known, and there were a number of additional factors to consider, it is not a direct measure of hydration. Corroboration with a direct method was required; in this instance BSE-IA (Figure 4-20 and Table 4-3) to determine a calibration factor for each mix design.

The finest slag, S2f, liberated the greatest heat of all the investigated mixes; which was not surprising and is in agreement with results from BSE-IA (Figure 4-4). The slightly anomalous result here pertains to slag S3c, within the C1S3c system. It may be that additional interactions were occurring within this grout formulation that cannot be accurately quantified via this technique. Later comparison will show that these results showed the weakest correlation to BSE-IA, with a significantly different calibration factor to the other mixes studied herein.

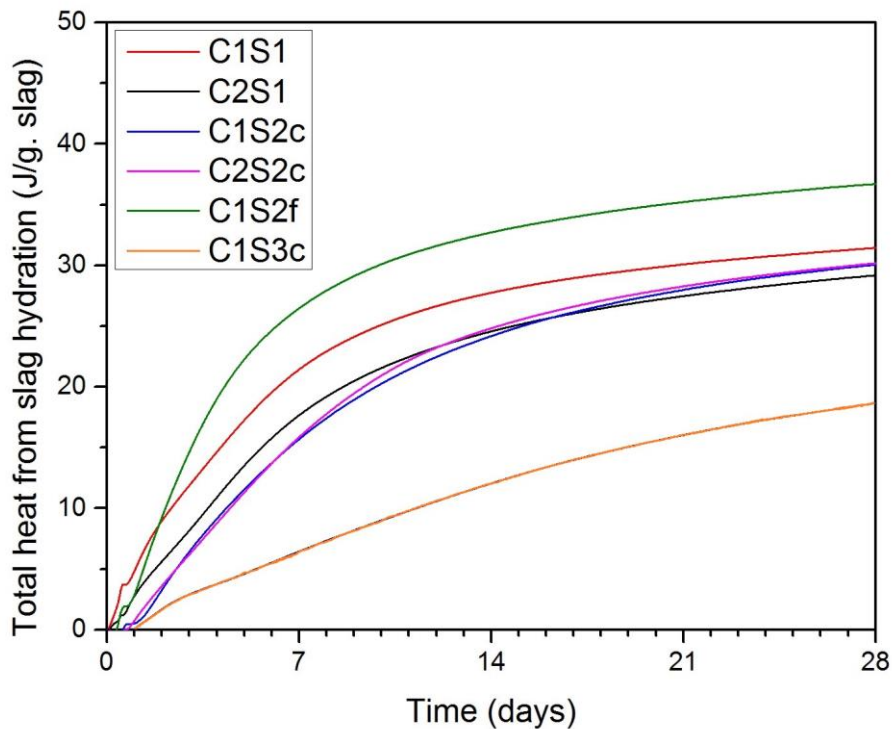


Figure 4-17: Isolated heat due to slag hydration within all grouts

Testing of the C1S3c system was repeated on numerous occasions with repeats performed across a range of channels within the TamAir system; all results were in agreement, suggesting that other, at present unexplained, interactions were occurring between the slag and clinker phases within this grout. If we compare the degree of slag hydration from BSE-IA (Figure 4-4) and ICC (Figure 4-14) it was slightly lower than the comparable C1S2c system, but not to such an extent that would explain this disparity in heat evolution.

#### 1.1.4 Corroboration of methods to determine hydration kinetics

Both chemical shrinkage and ICC provide a powerful means of following early age hydration, but these indirect methods cannot independently quantify isolated slag hydration within a cementitious material. As such it is necessary to corroborate each with a suitable direct method (in this instance, BSE-IA).

#### 4.1.4.1 Chemical shrinkage coupled with BSE-IA

Calibration factors, using the results for each sample at 28 days are shown in Table 4-2. These factors have been calculated as a means of following and assessing hydration of the different samples and highlight the variability across mix designs – indicating that there is not a simple and universal relationship between rate of shrinkage and degree of slag hydration. Similar results contrasting heat of hydration with degree of slag hydration are shown later.

There is no strong relationship between calibration factors and other mineralogical or physical properties within the results shown here. However, all calibration factors were in agreement to within a factor of 2. The highest calibration factor value obtained, for the C1S1 system; and the lowest value for the C1S2f system, represent the mixes in which the lowest and highest degrees of slag hydration were calculated. It may be that a certain degree of shrinkage is experienced irrespective of slag hydration, which would account somewhat for the disparity in calculated calibration factors.

*Table 4-2: Calibration factors correlating chemical shrinkage with degree of hydration as determined via BSE-IA at 28 days*

<b>Sample</b>	<b>Degree of hydration from BSE-IA (%)</b>	<b>Chemical shrinkage (ml/g. slag)</b>	<b>Calibration factor (ml/g. slag, x10<sup>-3</sup>)</b>
<b>C2S1</b>	30.00	0.0293	0.9766
<b>C1S1</b>	28.64	0.0353	1.2312
<b>C1S2c</b>	33.34	0.0372	1.1150
<b>C2S2c</b>	29.56	0.0189	0.6381
<b>C1S2f</b>	48.64	0.0599	1.2322
<b>C1S3c</b>	32.11	0.0298	0.9289

The calibrated curves for all systems are shown in Figure 4-18; there is a strong correlation across all samples with good repeatability and very low standard deviation across samples tested via chemical shrinkage. These strong correlations across all

samples highlights the suitability of the chemical shrinkage technique even at these high levels of replacement by slag.

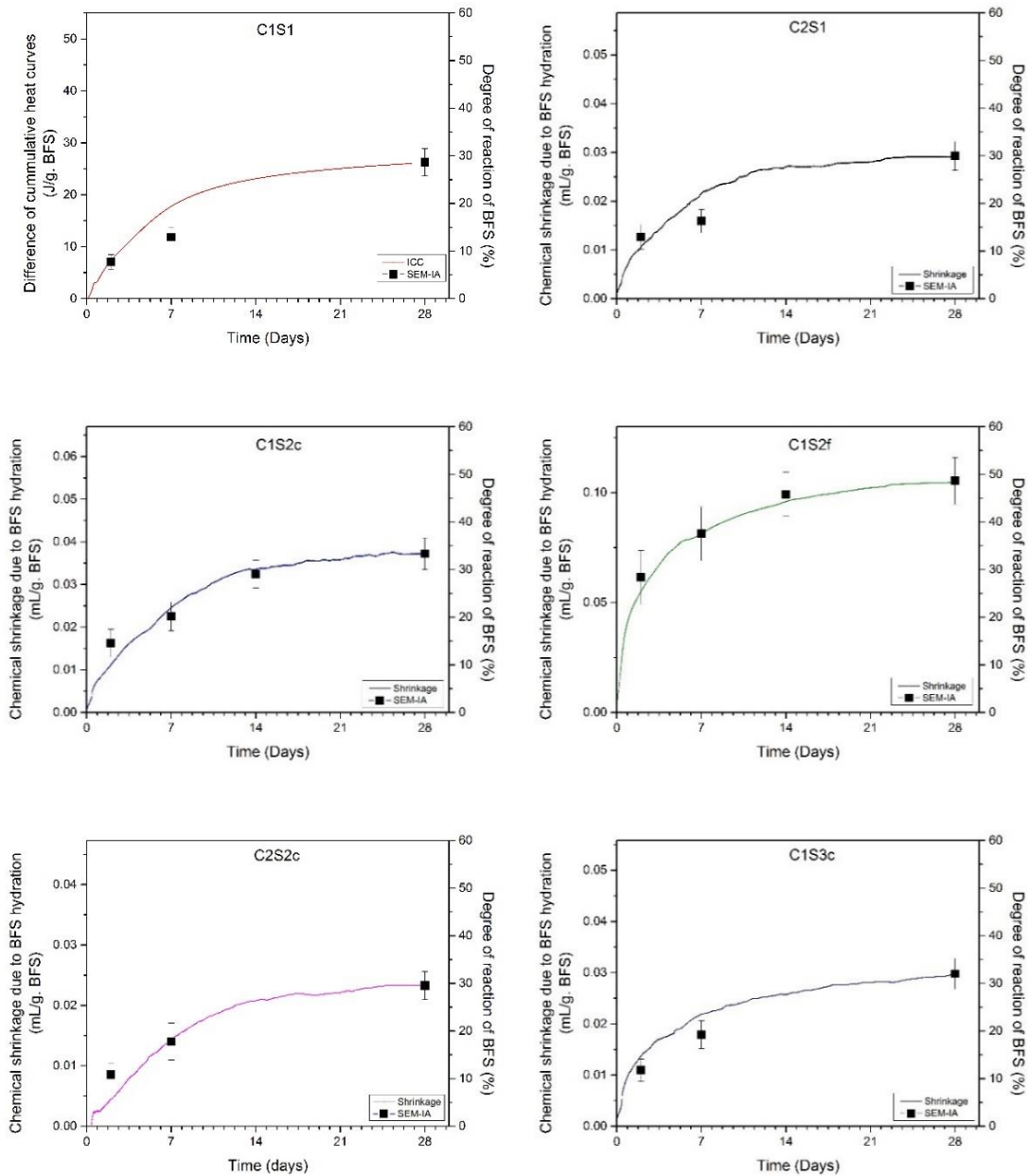


Figure 4-18: Chemical shrinkage calibrated with BSE-IA for all systems up to 28 days

Testing was extended to 56 days for the C1S2c and C1S2f samples, with calibrated results shown in Figure 4-19. Calibrating to 56 days appears to overestimate slag hydration at earlier ages in comparison to BSE-IA. Berodier (2015) suggests that the kinetics of later age hydration are controlled by the availability of space into which new hydrates may grow, this may explain the loss in accuracy of the technique at later age,

with the effects being more pronounced in the current study, owing to the lower w/b ratio of 0.35.

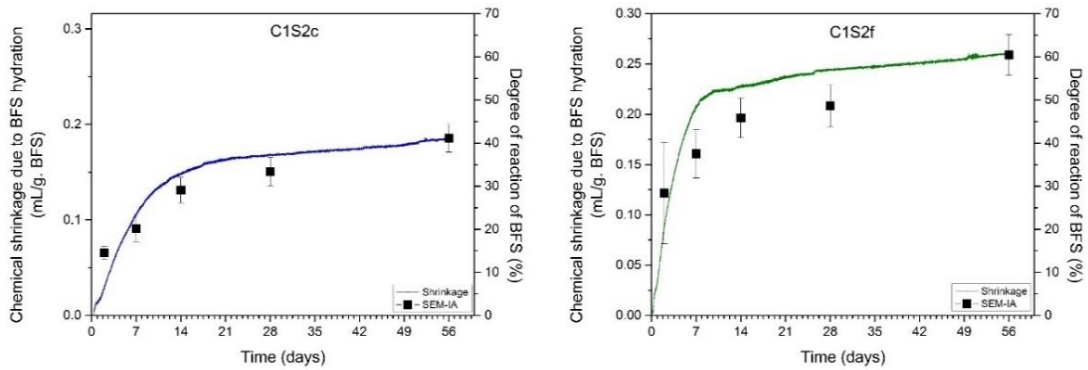


Figure 4-19: Chemical shrinkage due to slag hydration, calibrated with BSE-IA for C1S2c and C2S1f systems up to 56 days

#### 4.1.4.2 Isothermal conduction calorimetry coupled with BSE-IA

Calibration factors relating heat due to slag hydration with DoH as determined via BSE-IA are given in Table 4-3. Again, the outlier here was the C1S3c system with a noticeably lower calibration factor than all other grouts, the result being that early age slag hydration appears to be underestimated via calorimetry for this system, with very accurate results obtained in all other instances.

*Table 4-3: Calibration factors relating isolated heat release due to slag hydration with degree of hydration as determined via BSE-IA at 28 days*

<b>Sample</b>	<b>Degree of hydration from BSE-IA (%)</b>	<b>Heat due to slag hydration (J/g. slag)</b>	<b>Calibration factor (J/g. slag)</b>
<b>C2S1</b>	30.00	29.18	0.97
<b>C1S1</b>	28.64	24.45	0.85
<b>C1S2c</b>	33.34	31.45	0.94
<b>C2S2c</b>	29.56	30.05	1.02
<b>C1S2f</b>	48.64	30.17	0.62
<b>C1S3c</b>	32.11	9.51	0.30

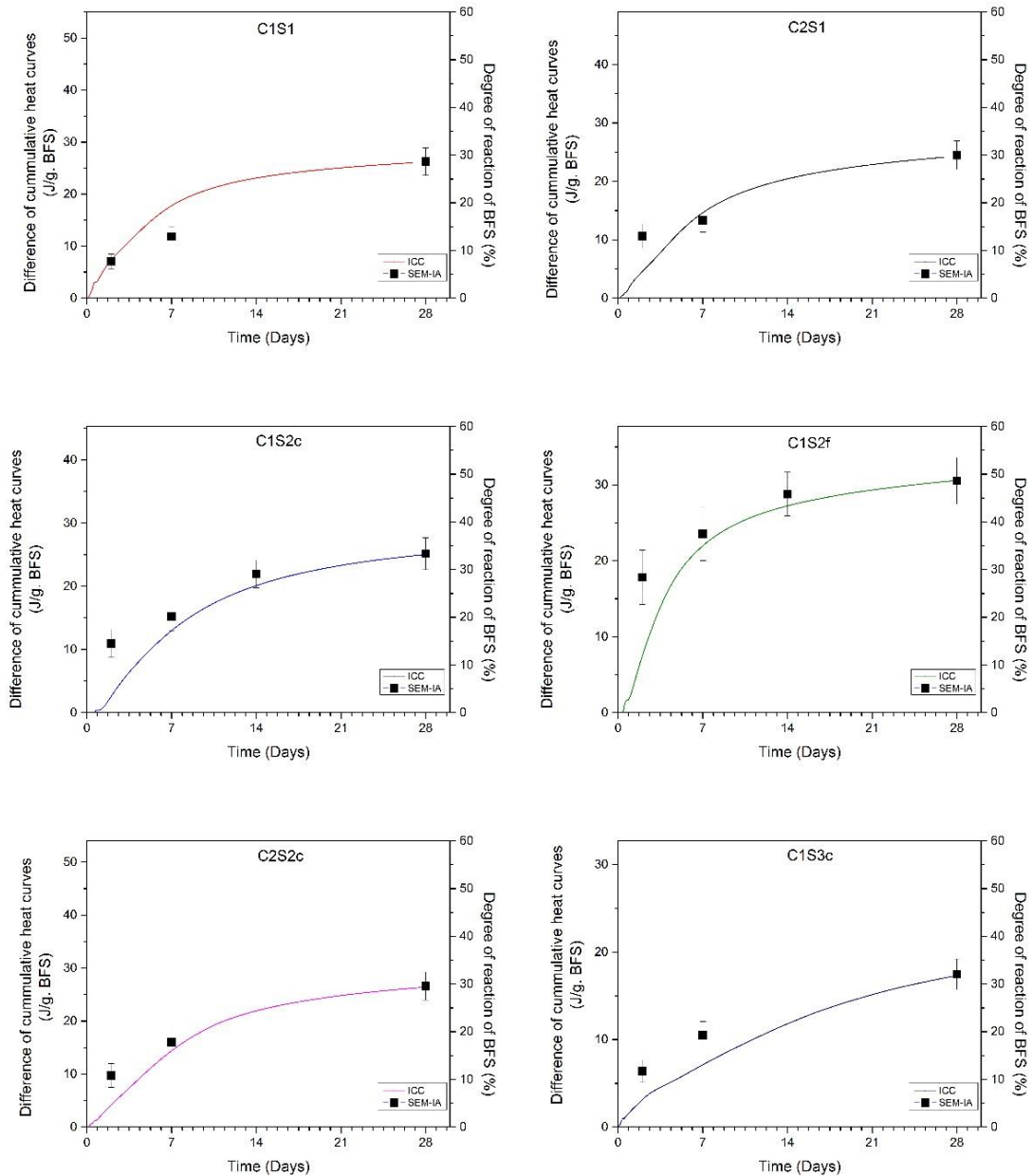


Figure 4-20: Heat evolution due to slag hydration, calibrated with BSE-IA for all systems up to 28 days

Calorimetry and chemical shrinkage typically follow the same trends (Figure 4-21). There is often a slight disparity at early age due to the 'relaxation' of samples analysed via chemical shrinkage, but otherwise results are in good agreement (Whittaker, 2014). The low heat of hydration of the C1S3c system has resulted in a divergence with the results for this grout.

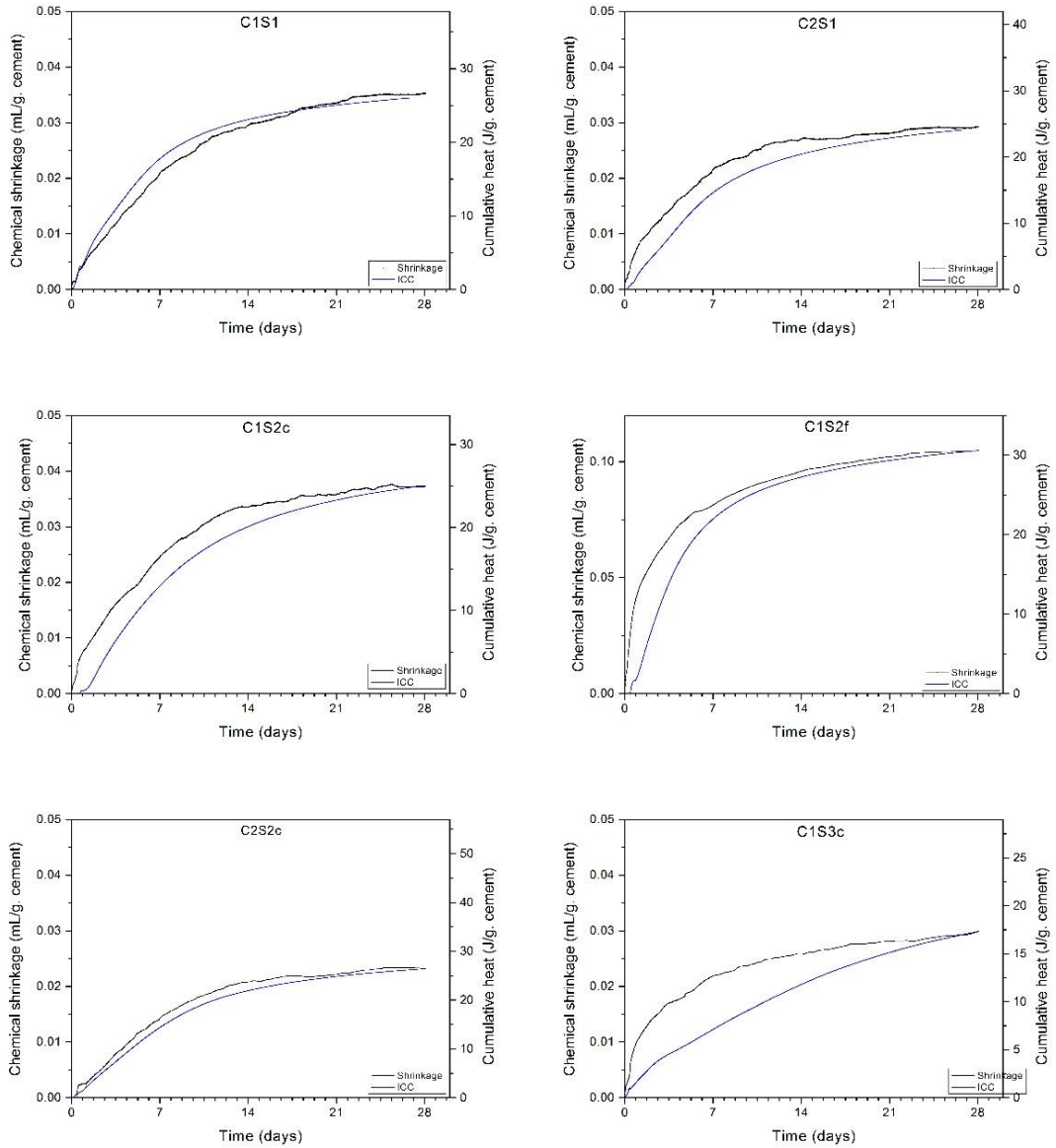


Figure 4-21: Correlation between calorimetry and chemical shrinkage for all mix designs

Results for the C1S2c system are poor, due to a high degree of disparity at early age; perhaps a result of negative results calculated for calorimetry (due to interaction between the clinker and quartz within the reference sample). If this negative section of the curve were to be omitted there would clearly be a much closer correlation throughout the duration of the experiments.

## 4.2 XRD analysis

XRD was used to identify the presence, and consumption, of clinker phases as a function of time for each mix design (Figure 4-22). The low relative clinker content of the mixes studied resulted in small peaks associated with anhydrous clinker phases even at very early age.

Given the equal level of replacement by slag in each system, it is not surprising that rates and degrees of consumption of clinker phases are comparable across samples. At 2 days, the peak associated with  $C_3A$  is still visible, although very small, for the curves associated with the C1S1, C2S2c and C1S3c samples. At 7 days  $C_3A$  is no longer present in any of the samples.

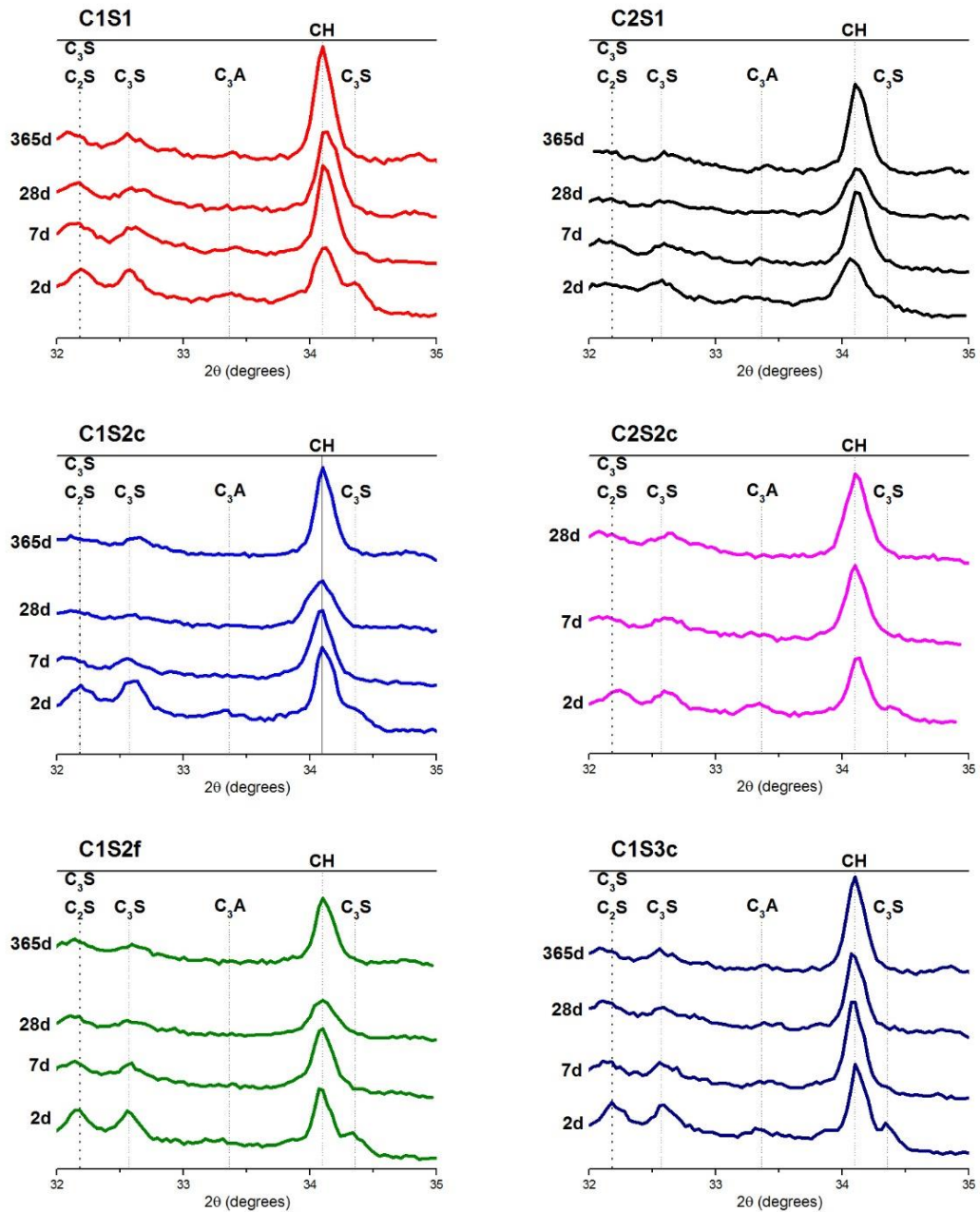


Figure 4-22: XRD patterns of all samples, showing hydration of the clinker phases from 2 to 365 days

Peaks associated with  $C_3S$  and  $C_2S$  become less pronounced with time for all samples, with very small reflections still visible at 365 days, in agreement with findings from BSE-IA.

The peak associated with portlandite (CH) highlights the hydration of  $C_3S$  and  $C_2S$ , with its presence at 365 days highlighting that it is not completely consumed through the hydration of the slag within each system. Its presence also suggests that availability of

CH is not the controlling factor in later age slag hydration, within the mix designs investigated within the present study. Within the C1S2f system, the peak for CH is less pronounced, a result of a larger degree of slag hydration compared to the other mix designs investigated, with the peak still clearly visible at 365 days (Richardson, 1999, Richardson and Groves, 1997).

Figure 4-23 shows the evolution of the AFt and AFm phases for each mix design over the period 2 to 365 days. Ettringite is present in all systems at 2 days but is only detected, and at a lower concentration, in the C2S1 and C1S3c systems at 7 days; it is no longer present within any of the samples beyond this point.

Hydrotalcite (Ht) appears most prevalent in the C1S2f system at 7 days, suggesting comparatively high levels of slag hydration at this age (Richardson et al., 2002, Lumley et al., 1996); in agreement with results above (Figure 4-4 and Figure 4-11). Ht is observed at later age in all samples (Codina et al., 2008, Glasser et al., 1999), with quantity increasing with continued slag hydration. Ht content at 365 days appears lower for the slag 2 containing blends, likely a result of the lower Mg content of the slag (Lothenbach et al., 2011, Taylor, 1997).

Hemicarboaluminate (Hc) was detected in small quantities at early age in some samples (C1S3c and C2S1 in particular) but was no longer visible in any samples at 365 days. Comparable aluminium contents of the slags within this study are likely the reason that there is little disparity in Hc content.

Monosulphoaluminate (Ms) is present in all samples at 7 days, produced through the reaction of the ettringite (formed at early age) with unreacted  $C_3S$  (Baquerizo et al., 2015). At 365 days, Ms is detected in all samples and appears to be most prominent in the slag 2 blended samples.

Overall, the AFt and AFm phases formed within all of the grouting formulations follow the same general trends (Escalante-Garcia and Sharp, 2004); the high level of replacement by slag in all blends and the relatively similar compositions has resulted in the production of much the same hydrates (Codina et al., 2008). The most significant difference appears to be the relatively lower Ht content in the slag 2 containing mixes, a result of the disparity in Mg content (Luke and Glasser, 1987).

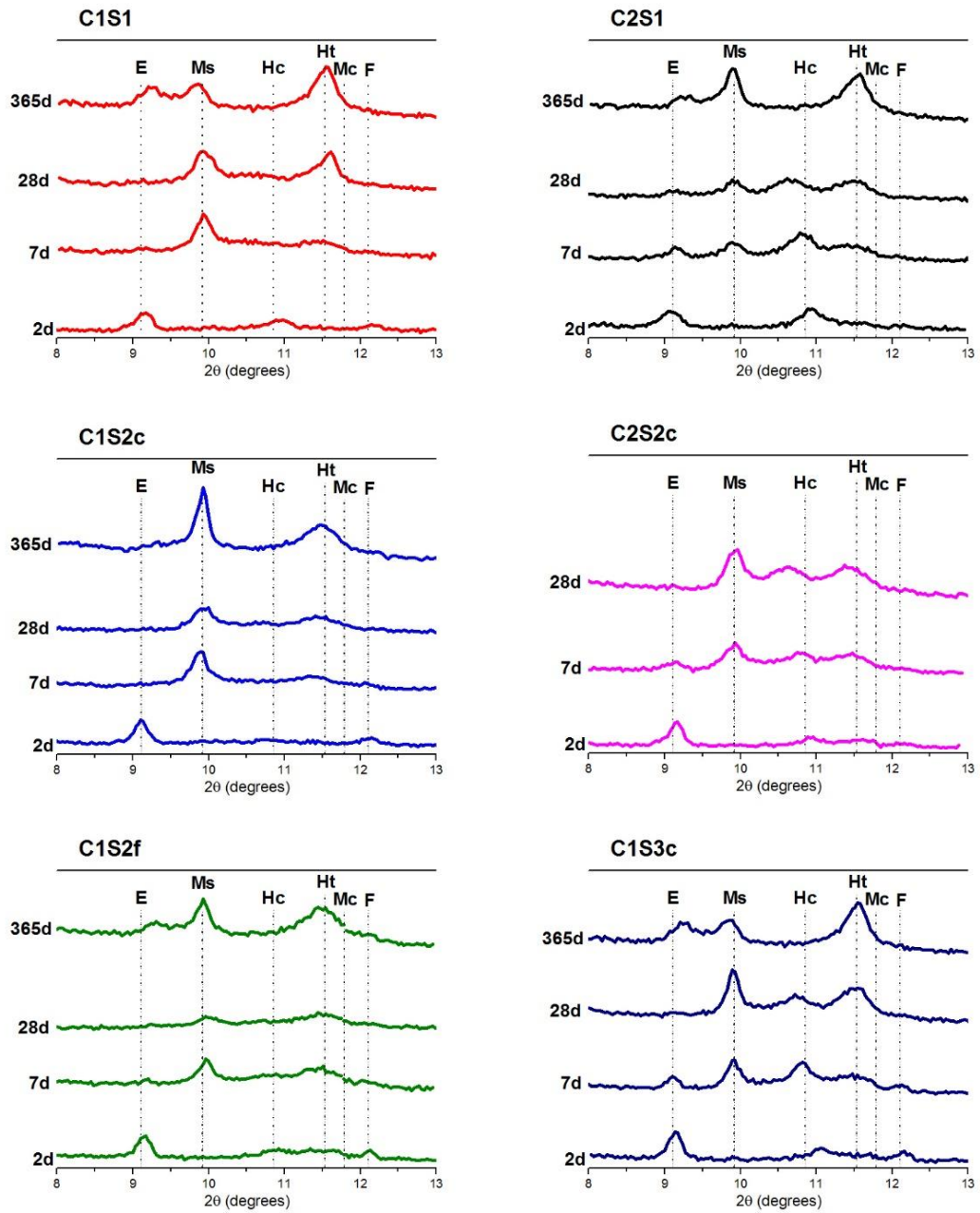


Figure 4-23: XRD patterns of all samples showing AFt and AFm phases

Where E - ettringite, Ms - calcium monosulphate, Hc – calcium hemicarboaluminate, Ht – hydrotalcite, Mc – calcium monocarboaluminate and F - ferrite

### 4.3 Assessing impact of hydration on microstructural development and transport properties

The permeability of a waste package is ultimately the key parameter which will define its long term performance. Permeability is intimately linked to porosity and will govern the rate at which waste species are able to leach from a conditioned waste package and also the rate at which deleterious species are able to enter and disrupt the internal microstructure.

#### 4.3.1 Intrinsic gas permeability

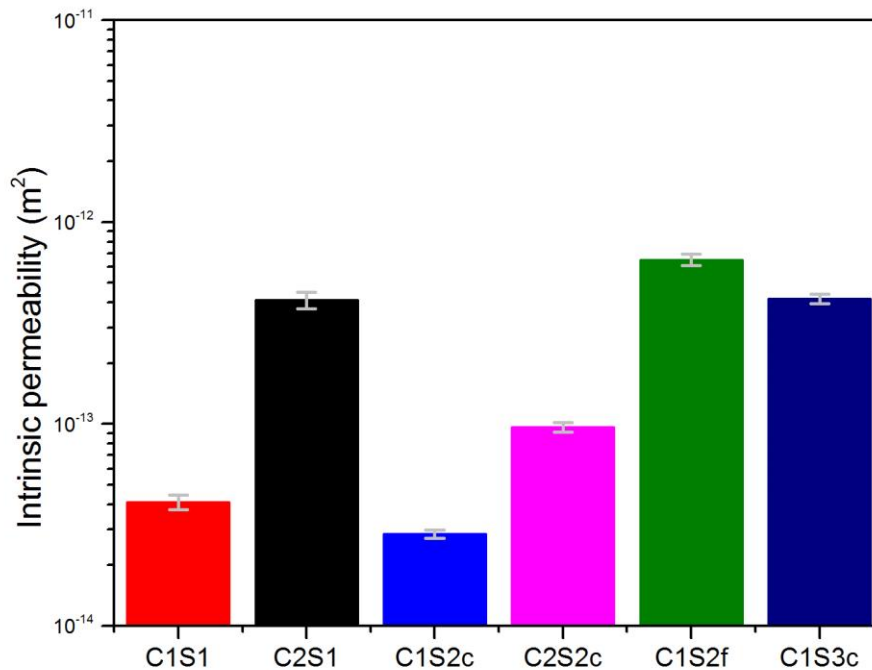


Figure 4-24: Intrinsic permeability of samples at 28 days, which have not been dried nor exposed to elevated temperatures

Accurately measuring and assessing permeability of cementitious matrices is a challenging process. Ensuring that samples are tested under consistent conditions and obtaining results which are indicative of actual performance can be very challenging. The results presented in Figure 4-24 were obtained from samples which received no

pre-conditioning (that is they were not dried, heated or stored in a low relative humidity environment prior to testing); the results here therefore represent the theoretical actual intrinsic permeability of the grouting matrices at 28 days hydration.

The results here (Figure 4-24) do not tend to fit with what might be expected, given the degrees of hydration (Figure 4-6) of the distinct grouting formulations and the resultant calculated coarse porosity values (Figure 4-10). One trend which may be observed is the apparent impact of clinker type, where mix designs prepared with C1 outperform those prepared with C2, with the C1S2c and C1S1 grouts performing best of all the mixes within the project.

The most surprising result relates to the C1S2f mix design, which showed the highest degree of hydration at all ages and the lowest coarse porosity values at all ages but exhibited the highest permeability of all mix designs. In fact, the result for C1S2f is more than an order of magnitude higher than the comparable C1S2c formulation. It may be that the testing method, in which N<sub>2</sub> gas is forced through the samples at up to 4 bar of pressure, has caused internal damage to these samples, moreso than for all other samples analysed.

#### **4.3.2 X-ray micro-computed tomography and random walk simulation**

X-ray  $\mu$ CT was performed on two separate occasions at NNL Central Laboratory using a Bruker Skyscan 1172 machine. Two different sample sizes were used (5mm and 2.5mm diameter), resulting in a disparity in achievable resolution (see Table 3-5 for a complete list of samples and associated resolution). This discrepancy in resolution had an impact upon the subsequent calculated pore-connectivity and tortuosity values; it has therefore been necessary to take care in comparing and contrasting results in a consistent and meaningful manner.

Figure 4-25 shows complete renderings of both the C1S2c and C2S1 samples at 28 days. These images give a really good visual indication as to the scale difference between the standard 'coarse' and 'fine' slag particles and the Calumite grains that are present in the C1S1 and C2S1 mix designs.

From these, and other complete renderings, smaller more computationally manageable volumes of interest (VOI) have been created for all of the samples analysed (Nakashima and Watanabe, 2002, Provis et al., 2012, Promentilla et al., 2016).

Figure 4-26 shows corresponding cross-sections of the 400 pixel<sup>3</sup> VOIs (with pixels of side length 1.57 and 1.62  $\mu\text{m}$ , respectively) corresponding to the samples shown in Figure 4-25, where the heat-scale is related to the relative density (white represents pore space and density increases from blue through green and yellow to red). The segmented porosity for the C1S2c sample is found to be slightly lower than that of the C2S1 sample, likely a result of the higher weighted DoH at this age (Figure 4-6) as hydrates are formed and fill some of the larger pore volumes (Richardson et al., 1989).

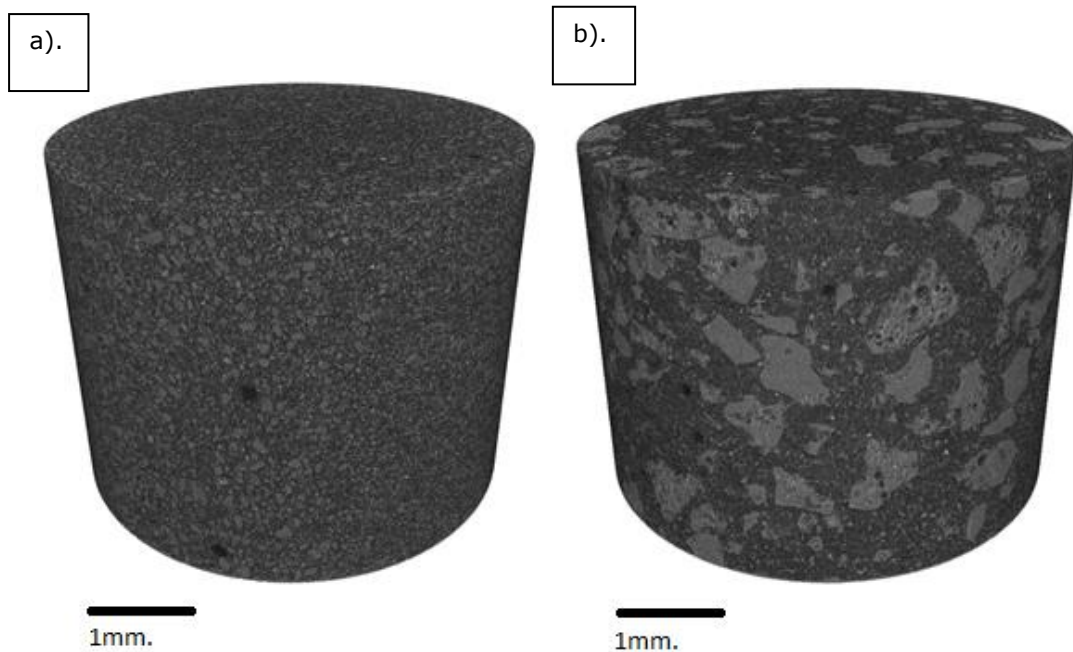


Figure 4-25: 3D rendering of 28 day aged samples from X-ray CT. a). C1S2c and b). C2S1

What can also be discerned from these cross-sections is the disparity in particle size between the Calumite and 'coarse' S2c slags, and the comparatively high anhydrous content of the C2S1 sample at 28 days (represented by larger red areas in Figure 4-26).

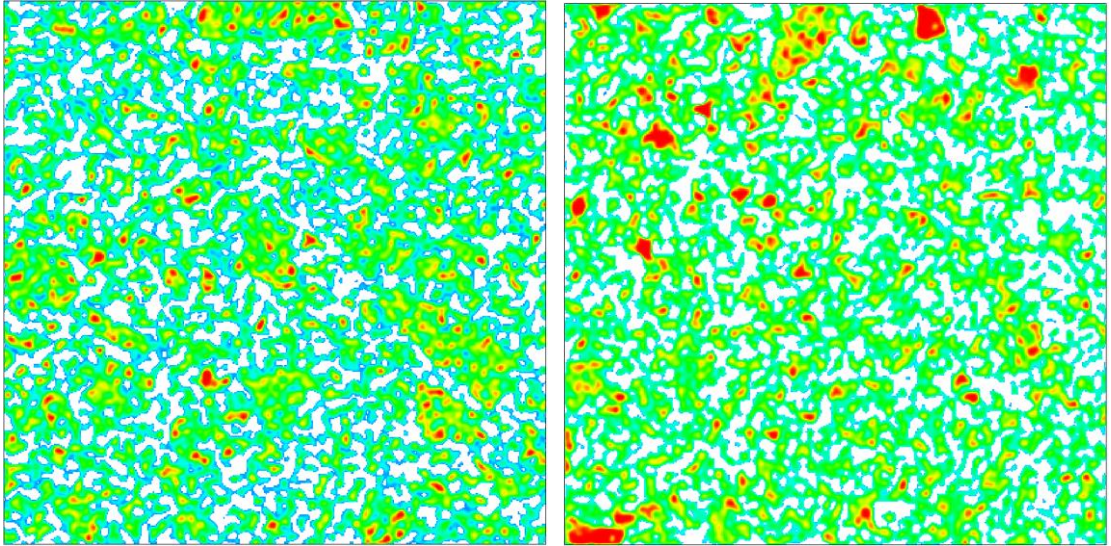


Figure 4-26: Cross-section through VOI of C1S2c and C2S1 samples at 28 days

Whilst resolution had very little impact in determined segmented porosity there was a clear impact upon pore connectivity and calculated tortuosity (Figure 4-27). Through increasing resolution smaller features were discernible, including small 'pore throats' which are not detected at a higher voxel size. Figure 4-28 shows representative cross sections of the C1S2c system at 0.53 and 1.57 $\mu\text{m}$  respectively; since both VOIs are 400 pixels<sup>3</sup> the areas represented here are not equal and particles may appear larger in the figure to the left.

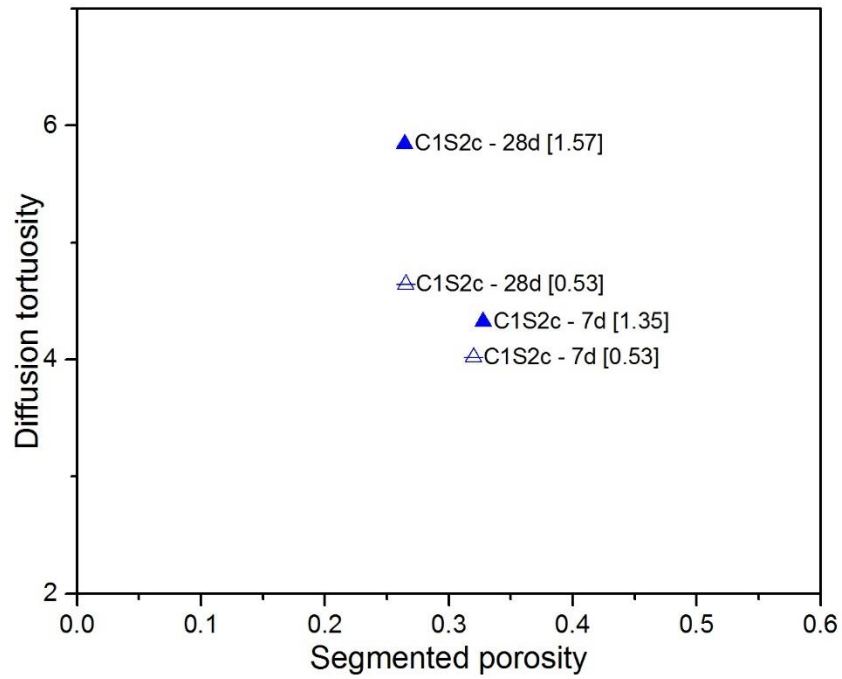


Figure 4-27: Impact of X-ray CT resolution on determined diffusion tortuosity

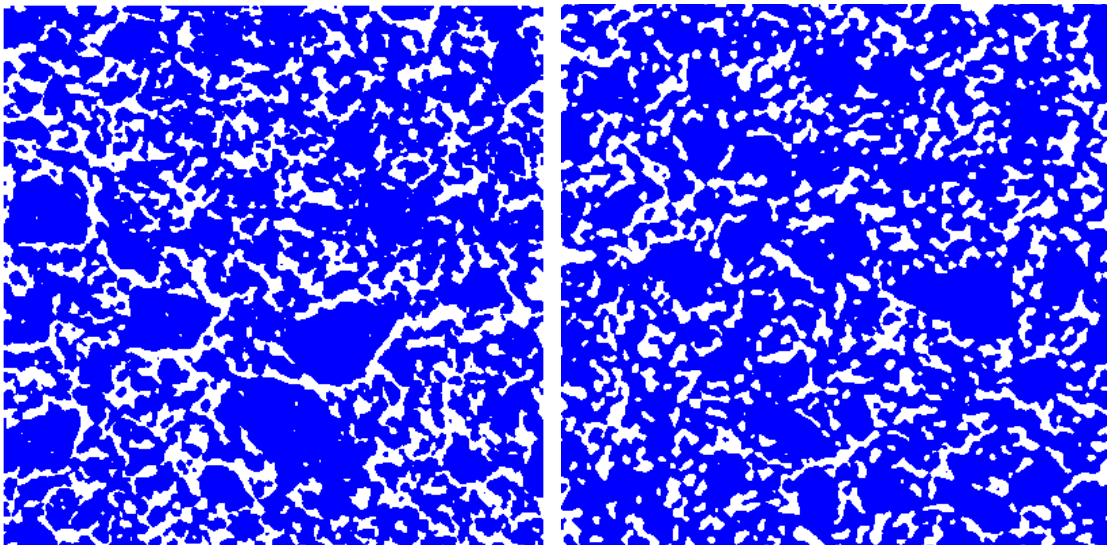


Figure 4-28: Cross-sections highlighting porosity in C1S2c system at high-resolution (left) and lower-resolution (right)

Further analysis confirms this assertion; determination of the total number of pores of 1000 voxels or larger in each VOI is given in Table 4-4. Increased resolution reduces the number of smaller isolated pores with the overall effect being a slight increase in the

total volume of the largest percolating pore and a reduction in the calculated diffusion tortuosity despite a very similar segmented porosity value. Gallucci et al. (2007) made similar observations when modifying the resolution within their study, a reduction in diffusion tortuosity would be expected had a similar random walk simulation analysis been performed.

The impact of resolution should always be borne in mind when applying this technique but does not counteract the significant insight that can be provided, particularly when scans of comparable resolution are compared and contrasted (Promentilla et al., 2009, Sugiyama et al., 2010a).

Clearly, there is a significant fraction of pores present within these systems that fall outside of the resolution limits of the X-ray  $\mu$ CT technique. Whilst these smaller capillary pores and gel pores are significant in the overall performance of the grouting materials they play a minimal role in determining permeability (Promentilla et al., 2009) and hence the potential leaching performance of a conditioned waste package.

*Table 4-4: Impact of resolution on pore connectivity and subsequent determined tortuosity*

Age (days)	Pixel resolution ( $\mu\text{m}$ )	Number of distinct pores over 1000 voxels	Volume (voxels <sup>3</sup> ) of largest percolating pore	Tortuosity value from random walk simulation
7	1.35	60	20820063	4.323
	0.53	12	20629659	4.017
28	1.57	41	16792390	5.844
	0.53	3	16724072	4.641

Figure 4-29 shows the impact of continued hydration upon segmented porosity and hence determined diffusion tortuosity of the percolating pore space of all samples analysed during the first set (1.2-1.6 $\mu\text{m}$ ). In the case of all formulations, porosity has

reduced as a function of time and continued hydration, resulting in a more tortuous microstructure.

This increase in tortuosity is most apparent in the C1S2c formulation (

Figure 4-29); in which significant hydration occurred between 7 and 28 days (Figure 4-4), resulting in significant pore filling. Beyond this point there was further hydration of the clinker and slag fractions with porosity reducing yet further up to 60 days (Figure 4-30).

Both C1S1 and C2S1 samples exhibited a higher tortuosity than C1S2c at 7 days, this is despite a lower calculated degree of hydration. Further, at a comparable porosity (see C1S1 - 7d and C1S2c – 7d) the C1S1 sample displays a higher diffusion tortuosity value. It is apparent that the large Calumite grains present with the C1S1 and C2S1 samples have an impact upon the interconnectivity of the pore space, serving to increase tortuosity at a given segmented porosity.

The relatively small increase in segmented porosity, and hence diffusion tortuosity for the C1S2f formulation may be explained by a relatively lower relative rate of hydration (see Table 4-1, where 77% of 28 day slag hydration is shown to occur within the first 7 days, compared to values of 60% or lower for all other mix designs).

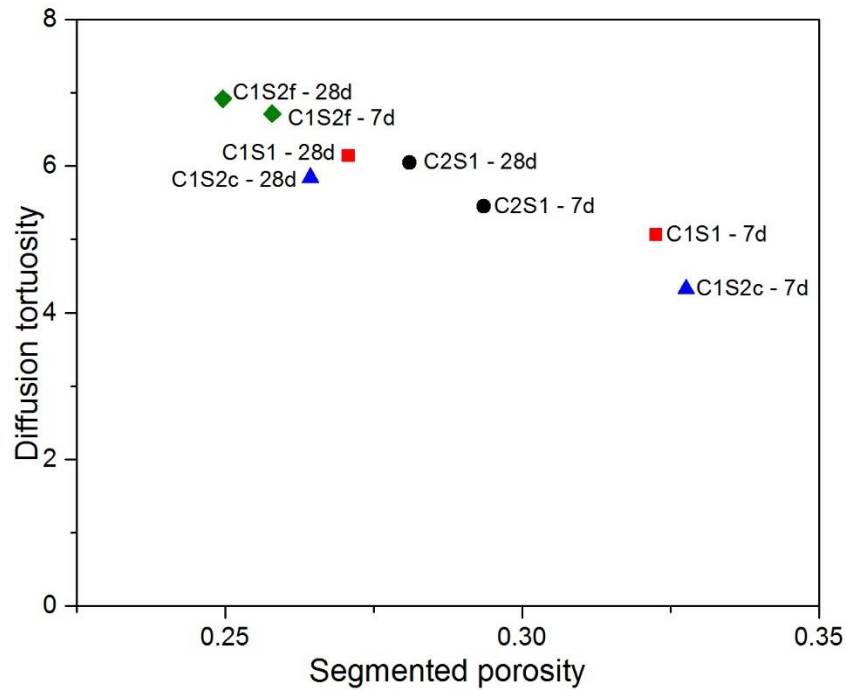


Figure 4-29: Diffusion tortuosity as a function of segmented porosity for all non-heat-treated samples analysed during first run (1.2-1.6 $\mu$ m)

For the C2S1 samples analysed, there is again a relatively low reduction in segmented porosity, this is despite a considerable degree of slag hydration over the same period (Table 4-1). Nevertheless, a statistically significant increase in diffusion tortuosity is observed, comparable to that seen for the C1S1 mix design.

The impact of slag fineness is highly evident here; the C1S2f formulation displayed by far the lowest porosity and highest tortuosity at 7 days. By 60 days a very dense microstructure had formed, resulting in a very low porosity value and a corresponding high diffusion tortuosity.

Continued hydration had a similar impact upon the C1S2c system; from 28 to 60 days there was a slight reduction in segmented porosity and a significant increase in the associated diffusion tortuosity.

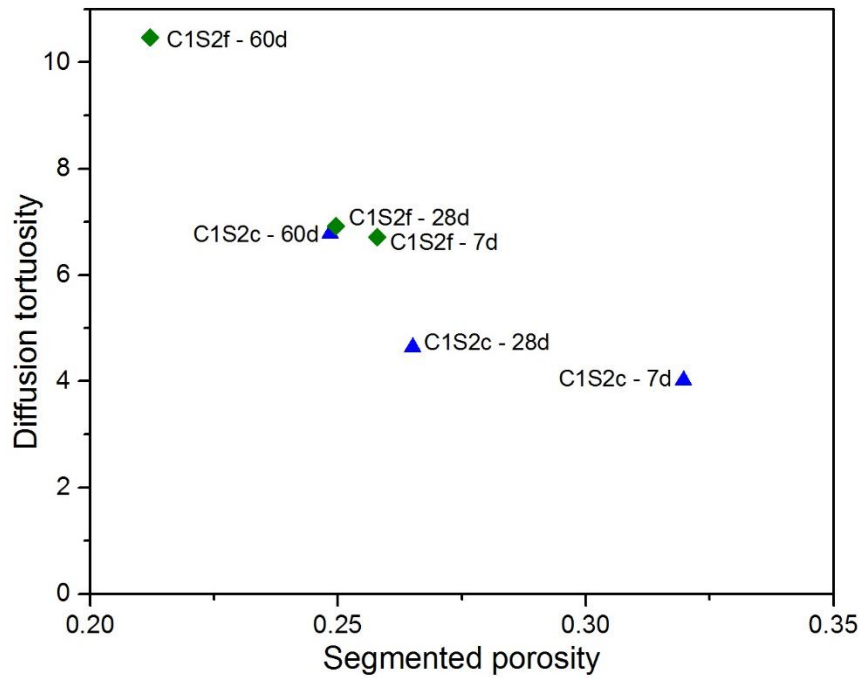


Figure 4-30: Diffusion tortuosity as a function of segmented porosity for C1S2c and C1S2f systems at 7, 28 and 60 days (second run at  $0.53\mu\text{m}$ ).

The results shown in Figure 4-30 appear to follow the same trend as those found in the work of Provis et al. (2012), with tortuosity varying inversely with porosity across the samples analysed. This trend would be expected to agree with the result of Bentz and Garboczi (1991) in which a percolation threshold, occurring at a porosity value of 0.18, would be found, and results being asymptotic at a tortuosity value of 1.

The results plotted in Figure 4-30 tend to suggest that there may be two separate trends for the two mix designs analysed; however, extrapolating from 3 data points could prove troublesome and it may be that whilst the segmented porosity values obtained for C1S2f – 7d and C1S2c – 28d are similar, it seems likely that within the VOIs analysed, the interconnectivity of the segmented pore space may have caused the apparent variation in calculated diffusion tortuosity.

This pore filling due to continued hydration is clearly evident from cross-sectional images of the reconstructed VOIs (Figure 4-31), where the pores become finer and appear less interconnected when viewed in 2 dimensions. This continuation of hydration reduced overall porosity and, significantly the volume of the largest percolating pore, from 20.6 million pixels<sup>3</sup> at 7 days to 13.0 million pixels<sup>3</sup> at 60 days within the C1S2c samples (Table 4-4).

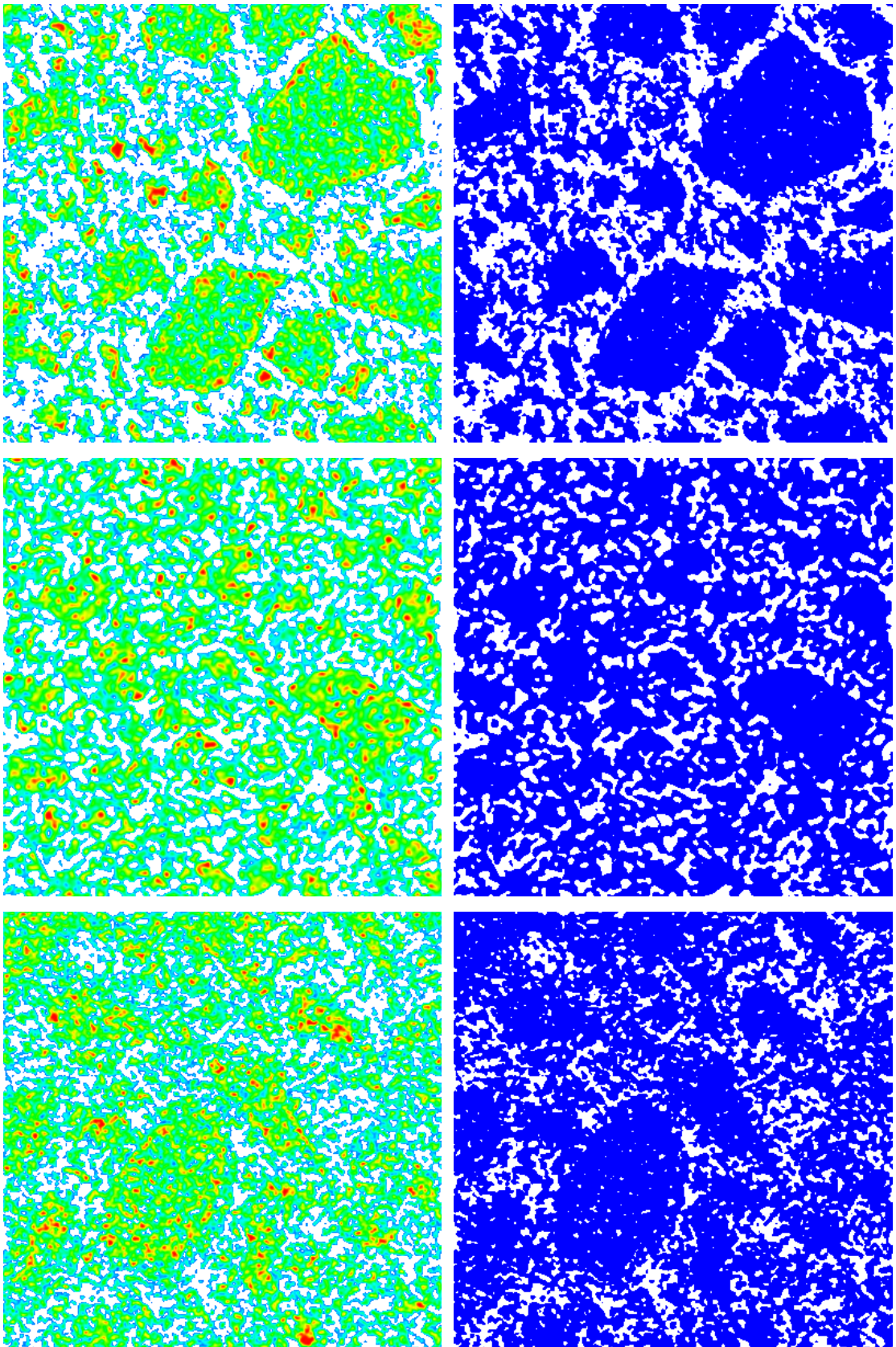


Figure 4-31: Evolution of microstructure and porosity of C1S2c grout at 7 days (top), 28 days (middle) and 60 days (bottom) at a resolution of  $0.53\mu\text{m}$

#### 4.4 Summary

1. Slag hydration is highly dependent upon fineness of grinding. Both rate and degree of hydration are impacted by fineness to a greater degree than chemical composition within the ranges studied herein.
2. Clinker hydration kinetics appear to be unaffected by either fineness or chemical composition within the mix designs investigated. At such high levels of replacement, it appears that dilution effects contribute to a consistent rate of clinker hydration. As with previous studies, even at high levels of replacement by slag, anhydrous clinker still remained after 1-year hydration.
3. At 75% replacement by slag, consumption of CH was not complete; levels lower than found in standard neat Portland cements were observed, but even at late age CH was observed in all samples. Within the C1S2f system, which was found to show the highest level of slag hydration, a lower CH content was recorded, suggesting partial, but not complete consumption.
4. When comparing slag hydration from BSE-IA with previous studies it appears that slag loading does not affect rate of hydration at early age, but that beyond 28 days, grouts prepared with higher slag contents experience a retardation in slag hydration.
5. The presence of large 'Calumite grains' within the C1S1 and C2S1 mix designs has had some interesting effects. These large slag grains appear to display none to very little hydration, even after 1 year; the result is a lower overall degree of slag hydration at later age. Interestingly though, comparable slag hydration (in relation to all but the C1S2f formulation) is observed up to 28 days, a further dilution effect must therefore be taking place within these grouts whereby the finer slag fraction hydrates more rapidly at early to medium age, slowing only at later age when presumably availability of pore space becomes a significant factor.
6. Chemical shrinkage via dilatometry and ICC remain suitable indirect methods to follow slag and clinker hydration independently even at these high levels of replacement. Within the present study, dilatometry was found to provide results which consistently agreed with those obtained via BSE-IA; the ease with which this technique can be applied and the minimization of potential external factors leading to errors in measurement make it a powerful and accessible method to follow and segment hydration in real time.
7. Ettringite is produced during early age hydration in all grouts but reacts with  $C_3S$  to form monosulphoaluminate within 7 days of casting. The significantly lower Mg

content of slag 2 has resulted in a small but noticeable difference in the formation of hydrotalcite within the C1S2c and C1S2f systems.

8. X-ray  $\mu$ CT provides a powerful emerging tool for the 3 dimensional investigation of cementitious materials without recourse to damaging preparation techniques. Application of subsequent analysis techniques such as recurring Monte Carlo methods, such as random walk simulations, allow for disparities, changes and microstructural developments to be compared and contrasted in quantifiably meaningful ways.

# **5. Impact of heat-treatment upon microstructure, phase assemblage and engineering performance of cementitious grouts for ILW encapsulation**

Exposure to high temperatures induced through potential fire scenarios represent one of the key concerns in the interim storage and final placement of treated waste packages. Quantifying the ways in which these exposure conditions might impact the composition, microstructure and hence performance of grouting materials is therefore of significant interest industrially as well as academically.

Testing in this regard was informed by industrial waste package accident performance testing protocols (NDA, 2010c) with matching exposure conditions. Samples used throughout this project are several orders of magnitude smaller than actual conditioned waste packages, however the reactions occurring and impact of exposure are of key significance in understanding the expected performance and potential resilience of treated waste streams.

## **5.1 Visual observations of heat-treated samples**

Cylindrical samples ( $27.5 \pm 0.25$  mm  $\phi$  and  $35 \pm 3$  mm in height) were heat-treated to 200, 400 and 800°C for 30 minutes. Images were captured following exposure to provide a visual reference and aid in assessing the resilience of each mix to such a scenario. Figure 5-1 shows the outer surface of the C1S1 and C1S2c samples before and after exposure to 800°C for 30 minutes.

The first observation to be made is the change of colour following heating, a result of the oxidation of the polysulphides present in the slag (Short et al., 2001). The next most obvious change is the significant cracking that has occurred, particularly in the C1S1 sample. Similar cracking was observed in the C2S1 sample, with cracks more consistent

with the C1S2c sample seen in all other mix designs. It is believed that this disparity in prevalence of cracks is a result of the large Calumite grains, as cracks appear to propagate around these large particles within the C1S1 and C2S1 grouts.

Whilst cracks were observed, to varying degrees, across all samples; there remained a degree of structural integrity even following heating to 800°C. This is consistent with a number of previous studies in which the inclusion of slag has been shown to reduce crack prevalence and improve resilience to fire scenarios (Wang, 2008, Mendes et al., 2012, Mendes et al., 2009) and subsequent compressive strength for both pastes and mortars (Delhomme et al., 2012).

Cracking was so severe in all samples heated to 800°C that it was not possible to perform subsequent permeability testing, as was planned and conducted for oven-dried samples and samples heated to 200 and 400°C respectively.

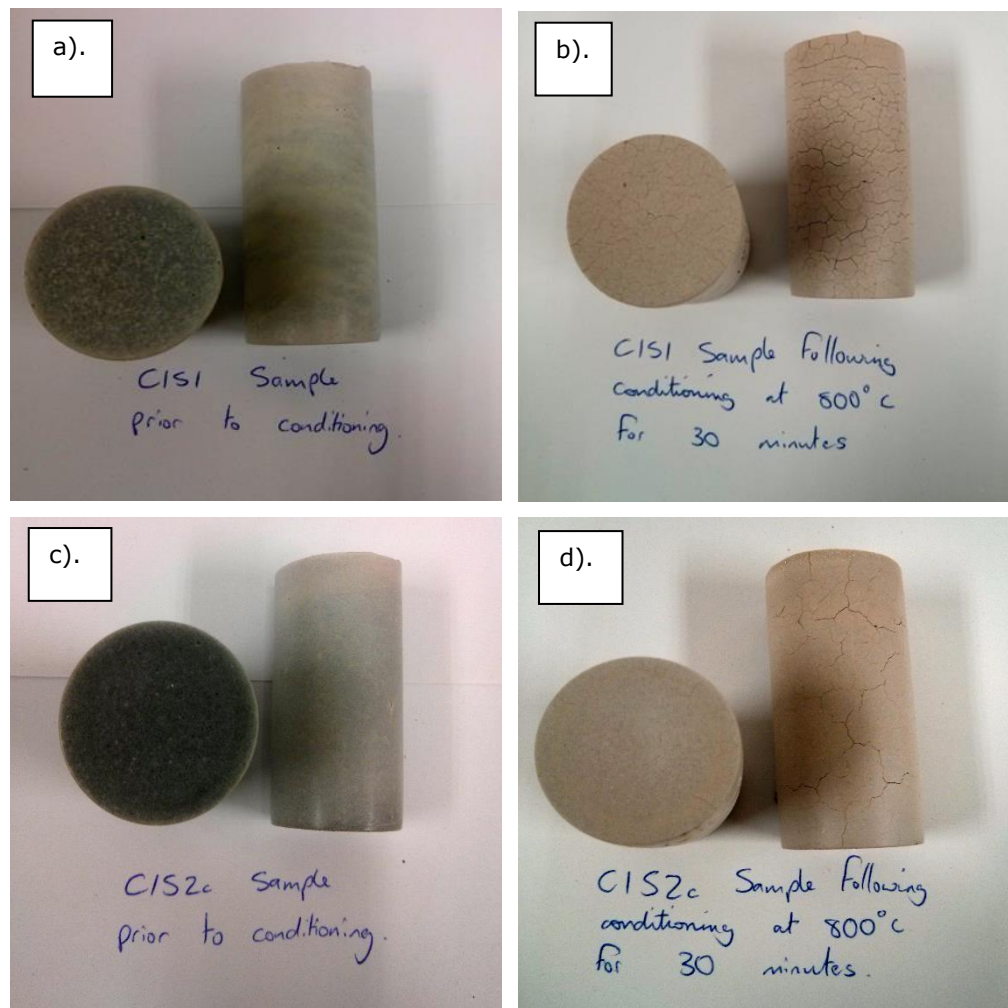


Figure 5-1: C1S1 and C1S2c samples before and after heat-treatment at 800°C

Micrographs of heat-treated samples were recorded at 800x magnification, in line with BSE-IA testing. Images for C1S1 and C1S2c samples after heating to 400 and 800°C are shown in Figure 5-2. Debonding of the large Calumite grains as a result of heating is apparent, with this becoming more pronounced with increased exposure temperature. The same observations were made for the C2S1 system with cracks appearing to propagate around the Calumite grains and extend into the bulk hydrates, with this becoming more pronounced with increasing temperature. Similar observations were made for mortar samples in the work of Fu et al. (2004), where tangential cracks were found to propagate around the coarser particles and subsequently through the hydrating matrix.

Heat-treatment had less of a pronounced effect upon the microstructure of the C1S2c system. Some loss of hydrates was experienced following heating to 400°C but there was very little visible cracking and anhydrous or partially hydrated slag grains remained well bound within the hydrates.

Following heating to 800°C cracking became much more pronounced with large gaps throughout the field of view shown in Figure 5-2D. The difference here with the corresponding micrograph for the C1S1 system is the way in which these cracks propagated through the sample.

Within the C1S2c system the path of least resistance through with the cracks proceeded was via the bulk hydrates, whereas the interfacial transition zone around the Calumite grains seemed to be the weakest point within the C1S1 and C2S1 systems. The lack of hydration of the Calumite grains may have been a contributing factor in this, after a year they showed no hydration, despite the latent hydraulic nature of these materials, and appeared to be less tightly bound within the largely hydrated bulk matrix than the anhydrous slag present within the other mix designs.

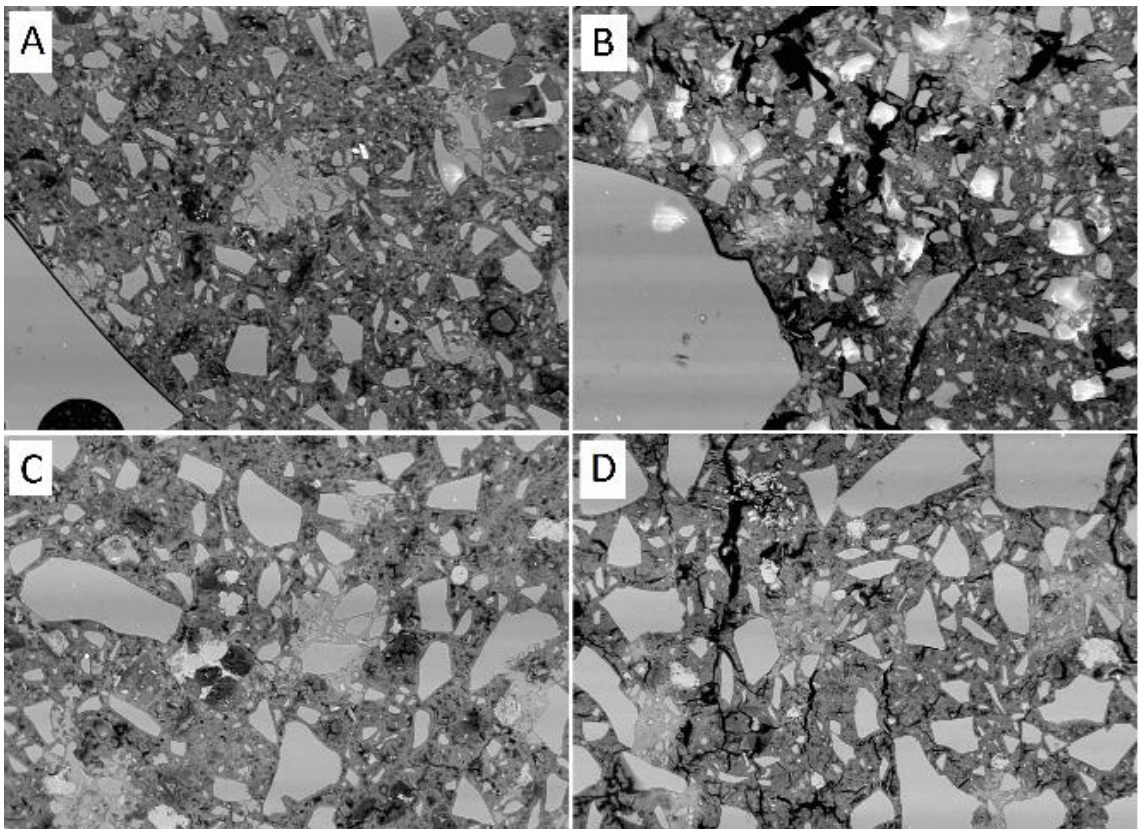


Figure 5-2: SEM micrographs of heat-treated samples at 800x magnification. A). C1S1 at 400°C. B). C1S1 at 800°C. C). C1S2c at 400°C & D). C1S2c at 800°C.

## 5.2 Physical properties of heat-treated samples

### 5.2.1 Intrinsic gas permeability

Permeability testing of heat-treated samples was conducted for all but those exposed to 800°C. The presence of cracks within those samples meant that even if testing were possible, meaningful results would not be obtained owing to the variability in resilience and the suitability of some samples to testing.

The resultant permeability of all treated and non-treated samples is given in Figure 5-3. There was a clear increase in permeability with exposure temperature, consistent across all mix designs but more pronounced in the case of certain mix designs. Oven drying at 50°C removes all of the unbound water from each sample, with the effect being that the determined permeability values fell within a smaller range than when samples had not been treated. The overall ranking of mix designs remained consistent following drying with the most notable increase observed for the C1S2f samples.

Drying to constant weight at 50°C typically resulted in a mass loss of 16-17% and took between 2 and 3 weeks for the samples analysed. In the case of the C1S2f samples, there was a slightly lower mass loss (14.4-14.6%) with a total drying time of just under 4 weeks, suggesting a more refined pore structure. This comparatively greater increase in permeability may have been a result of the prolonged exposure time and potential damage to some of the hydrates within the bulk of the samples, as this disparity was not evident following the higher exposure conditions (Figure 5-3).

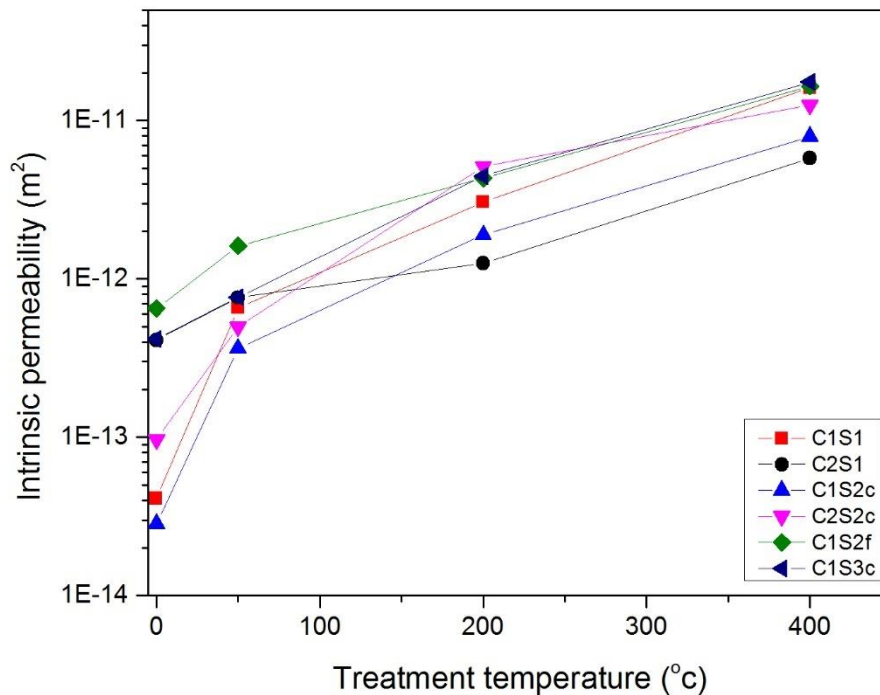


Figure 5-3: Intrinsic permeability of grout samples as a function of exposure conditions

Permeability increased following heating to 200°C as many of the hydrated phases within the samples became damaged. C-S-H at the outer edges of samples began to dehydrate leading to an increase in calculated permeability values. This increase in grout permeability continued following heating to 400°C with grouts all increasing in intrinsic permeability by around 4 - 5 times. The smallest relative increase was observed for the C2S2c system, in which permeability increased by an order of 2.45, followed by the C1S2f system, increasing by an order of 3.8; the highest relative increases were seen in the C1S1 and C2S1 systems, consistent with the relatively high rate of cracking observed via SEM (Figure 5-2).

The results obtained for the C1S2f system seemed to contradict the results from BSE-IA in which there was clearly a higher degree of grout hydration and a lower calculated coarse porosity, which would be expected to result in a lower intrinsic permeability. This not being the case could be a result of damage to the samples caused by the testing method, with these samples being more detrimentally affected than the others studied. The step increases in permeability from untreated to oven dried at 50°C to 200°C to 400°C were relatively low for the C1S2f system relative to the other grouts investigated,

suggesting that whilst permeability was greater than average, heating did not appear to damage the microstructure to the same degree as it did the other systems.

Permeability clearly increases as a function of mass loss, but the degree to which cracking is detrimental to grout permeability is orders of magnitude more significant. Results here are consistent with observations made in previous studies investigating the fire performance of cementitious materials with replacement by slag (Delhomme et al., 2012, Wang, 2008). Some microstructural damage is clearly caused at temperatures approaching 400°C with unbound water driven from the pore-network and dehydration or decomposition of much of the most abundant hydrate, C-S-H (Mendes et al., 2008, Handoo et al., 2002). Severe cracking, particularly in slag composite cements, occurs only beyond 400°C when CH decomposes (Peng and Huang, 2008) and when there is a more marked loss of material (in particular C-S-H) (Castellote et al., 2004)

Whilst the results obtained within the present study show that these small samples were highly susceptible to these elevated temperatures, the disparity in size between those studied here and actual full-scale waste packages raises some interesting points. There are clearly temperature profiles extending across the samples during exposure, with the centre of samples investigated here appearing not to reach the temperature of the surrounding atmosphere (later results show the presence of residual CH in the centre of samples heated to 800°C). Exposure to a high-temperature fire within a GDF setting would undoubtedly have detrimental effects upon conditioned waste packages, but the depth and degree to which these impacts would extend cannot accurately be determined.

### 5.2.2 Sorptivity

The sorptivity coefficients of all samples are given in Table 5-1, with a visual representation of increasing sorptivity as a function of exposure temperature given in Figure 5-4. Samples that were oven dried, without exposure to significant elevated temperatures showed results that might be expected; linking well to coarse porosity measurements (Figure 4-10) from BSE-IA, with the C1S2f grout displaying the lowest sorptivity value.

*Table 5-1: Sorptivity coefficients of oven-dried and heat-treated grout samples*

<b>Sample</b>	<b>Sorptivity coefficient, <math>k</math> (<math>m^3/m^2s^{1/2}</math>) <math>\times 10^{-6}</math></b>			
	<b>50°C</b>	<b>200°C</b>	<b>400°C</b>	<b>800°C</b>
<b>C1S1</b>	0.295	0.384	0.741	2.193
<b>C2S1</b>	0.311	0.342	0.552	1.322
<b>C1S2c</b>	0.368	0.358	0.493	1.879
<b>C2S2c</b>	0.403	0.422	0.569	2.061
<b>C1S2f</b>	0.210	0.571	0.921	2.975
<b>C1S3c</b>	0.442	0.529	0.674	1.510

Following heating to 200°C the performance of the majority of the mix designs is relatively unchanged. The key outlier to this trend is the C1S2f system, which saw its sorptivity coefficient almost triple, taking it from the best performing (following oven drying at 50°C) to the worst. The higher weighted degree of hydration may actually be detrimental when it comes to resilience to high temperatures, since there is a greater volume of hydrates which are highly susceptible to dehydration above relatively modest temperatures and significantly impacted as temperatures increase further towards those found within a fire scenario. The significant increase in sorptivity observed can almost certainly be attributed to capillary suction effects due to the significant loss of hydrates at the outer surface of these samples, relative to the other mix designs studied.

Heating to 400°C for 30 minutes resulted in a continuation of much the same trends, as the C1S2c, C2S2c and C1S3c systems observed small but not insignificant increases in sorptivity; as further C-S-H and other less abundant hydration products were damaged and dehydrated (Figure 3-5) (Alarcon-Ruiz et al., 2005). The C1S1 and C2S1 samples saw more noticeable increases in sorptivity, with 93 and 61% relative increases

compared to values after heating to 200°C. Similarly, the C1S2f sample showed a significant increase in sorptivity with a 61% increase on the value observed following heat-treatment at 200°C as yet more of the C-S-H is dehydrated through heating.

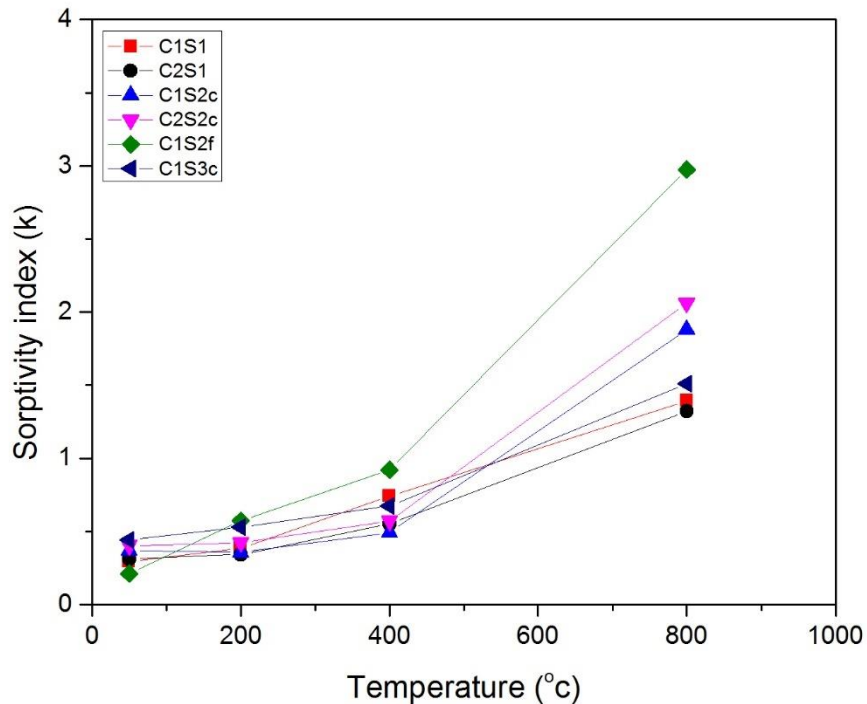


Figure 5-4: Sorptivity indices for all mixes following exposure to elevated temperatures

It may be that the cracking that is occurring in the C1S1 and C2S1 samples is allowing for damage to be caused to the internal microstructure more readily and for a larger volume of the hydrates within the samples to be damaged during the 30-minute heating period (see Figure 5-2A, where there is clear debonding of the calumite in the C1S1 system). For the C1S2f sample, whilst cracking appeared less prevalent, the total volume of hydrates present within the samples appeared to have an affect; with damage propagating from the outer surface and dehydrating much of the C-S-H and other hydrates as it did so.

Following heating to 800°C the trend in resultant sorptivity continued as samples experienced significant damage. The microstructure of the C1S2f system was most clearly affected, consistent with the results obtained following heating to 200 and 400°C, sorptivity increased more significantly than for all other mix designs as cracking led to further damage deeper into the samples.

Weighted degree of hydration (Figure 4-6) was clearly linked to sorptivity following heating, where presence of a higher volume of hydrates would prove detrimental in providing resilience to elevated temperatures as would be experienced during a fire scenario. There was a very strong correlation between overall degree of hydration at 28 days and sorptivity index (k) following heating to 800°C (Figure 5-4), likely due to the significant effects of such high temperature on the C-S-H present within each system. With increased level of hydration, a higher volume of C-S-H is formed, making a grout more susceptible to degradation of this phase.

The presence of the large Calumite grains within the C1S1 and C2S1 formulations has resulted in the lowest sorptivity values following heating to 800°C, having been higher than all other formulations (with the exception of C1S2f) following heating to 400°C. Whilst it appears that hydration products seem not to be as significantly impacted within these samples it is not possible to confidently compare the overall resultant performance of grouting formulations, especially since the C1S1 and C2S1 samples showed significantly more severe cracking following heating (Figure 5-1).

### **5.3 X-ray micro-computed tomography and random walk simulation**

A number of heat-treated samples were analysed via X-ray  $\mu$ CT during both sessions at NNL Central Laboratory. During the first visit some C1S1 and C1S2c samples which had been heat-treated were analysed (Figure 5-5). The disparity in size between samples heat-treated prior to X-ray  $\mu$ CT and those prepared for permeability and sorptivity testing was significant. The temperature profiles experienced across the larger samples meant that the core within each sample did not reach the temperature of the surrounding furnace; with the samples for X-ray  $\mu$ CT equilibrium was reached and more significant overall damage was experienced. Table 5-2 shows the associated mass losses for samples analysed via thermogravimetry and gives an insight into the damage caused within samples analysed via X-ray  $\mu$ CT and the slight disparity between mix designs.

*Table 5-2: Mass loss at target temperatures from samples analysed via TGA*

<b>Mix</b>	<b>Age (days)</b>	<b>Mass loss (%) to</b>		
		<b>200°C</b>	<b>400°C</b>	<b>800°C</b>
<b>C1S1</b>	2	2.93	4.18	7.10
	7	4.81	7.31	11.42
	28	6.07	10.00	14.20
<b>C2S1</b>	2	3.27	4.50	7.50
	7	6.51	9.20	12.74
	28	6.68	10.46	15.59
<b>C1S2c</b>	2	2.52	3.53	6.07
	7	4.64	7.22	11.37
	28	6.35	10.25	14.51
<b>C2S2c</b>	2	2.90	4.10	6.90
	7	4.85	7.59	11.32
	28	6.36	10.41	14.92
<b>C1S2f</b>	2	3.18	4.66	7.48
	7	5.51	8.44	12.43
	28	7.07	11.87	16.48
<b>C1S3c</b>	2	2.49	3.55	6.19
	7	4.53	7.14	10.32
	28	5.80	9.57	14.11

As discussed previously, one result of the presence of Calumite grains in the C1S1 and C2S1 systems was the degree to which they increase diffusion tortuosity for a given segmented porosity value through essentially forming small impermeable barriers within the samples (which more than offset the higher segmented porosity within the surrounding matrix); this, again, is further highlighted in Figure 5-5.

In line with results obtained via other techniques (Figure 5-3 and Figure 5-4), exposure to elevated temperatures resulted in microstructural damage, with deleterious ramifications for the resultant performance of grouting materials.

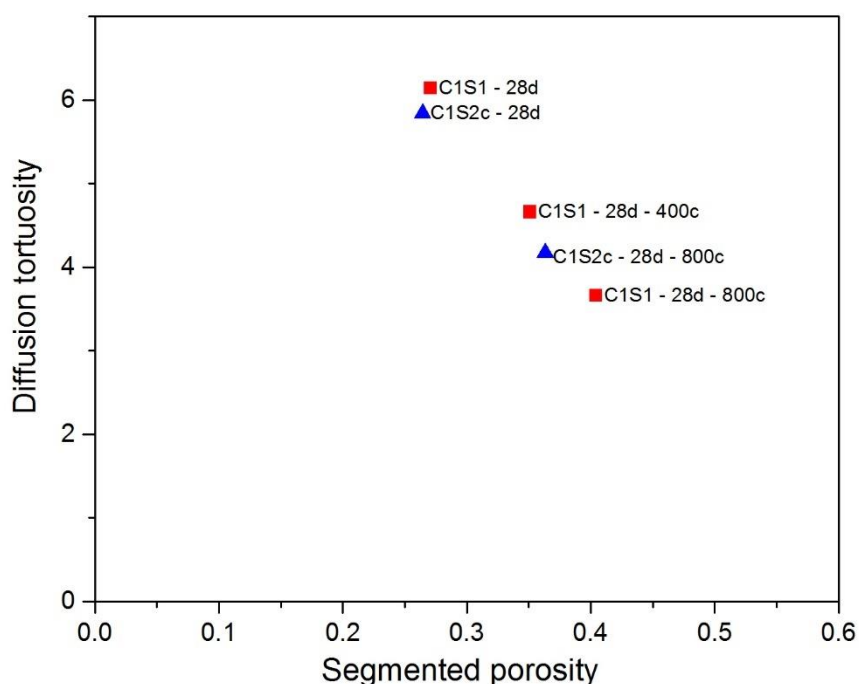


*Figure 5-5: diffusive tortuosity of C1S1 and C1S2c samples at 28 days with and without heat-treatment*

Heat-treatment had a much more evident detrimental impact upon the C1S1 sample in terms of induced damage leading to a reduction in diffusion tortuosity throughout its percolating pore space. The increase in porosity observed by the C1S1 sample is comparable with the damage caused to the C1S2c sample after heating to 800°C. as with the untreated samples, the presence of Calumite grains leads to a higher corresponding diffusion tortuosity value at a given segmented porosity. It may be that debonding of these large grains has begun as the hydrated phases in the surrounding matrix are dehydrated and damaged (reference to SEM images, Figure 5-2, would suggest that this was the case), but this is not yet manifesting in a significant reduction in corresponding diffusion tortuosity. Reference to Figure 5-6 (centre) shows localised debonding of the large Calumite grain within the VOI, this appears to be insignificant in relation to the diffusion effects of the percolating pore network.

Following heating to 800°C the C1S1 sample experiences a further loss in hydrates (as corroborated via TGA, in which the mass loss to 400°C was 9% and the mass loss to 800°C was 12.8%). This further loss of mass goes some way to explaining the disparity in subsequent diffusion tortuosity, but when compared to the mass loss for the C1S2c

sample does not provide a full explanation. Mass loss to 800°C for the C1S2c sample was 14.5%, consistent with the higher observed degree of grout hydration (Figure 4-6) and hence presence of a larger volume of hydrates. As might be expected, the increase is significant following such harsh conditions; the reduction in tortuosity in this case though can only be explained through a combination of this loss of mass coupled with significant debonding of the Calumite grains (Figure 5-2).

Figure 5-6 shows a representative cross-section of each of the samples, the bottom figure corresponding to the sample heated to 800°C is visibly different to those above it. The heating has caused significant damage to the hydrates within the bulk of the sample, causing a widening of the percolating pore space (clearly visible in the binary images to the right of Figure 5-6).

In practice this susceptibility to elevated temperatures could pose a significant risk to the suitability of waste package integrity. Whilst the possibility of such an event occurring is very low, the impact caused could have severe consequences. Previous studies in which similar samples were exposed to leaching (Promentilla et al., 2016, Sugiyama et al., 2010a) or freeze-thawing action (Promentilla and Sugiyama, 2010) showed similar results, with a significant increase in porosity and a corresponding reduction in diffusion tortuosity.

Clearly, deterioration of waste packages, be that via exposure to elevated temperatures, leaching or other external factors, poses a significant risk to the integrity and suitability of conditioned waste packages. Propagation of cracks through samples represents a significant factor in the rate at which continued damage may occur and the timescales that a waste package will remain functional within its final disposal scenario.

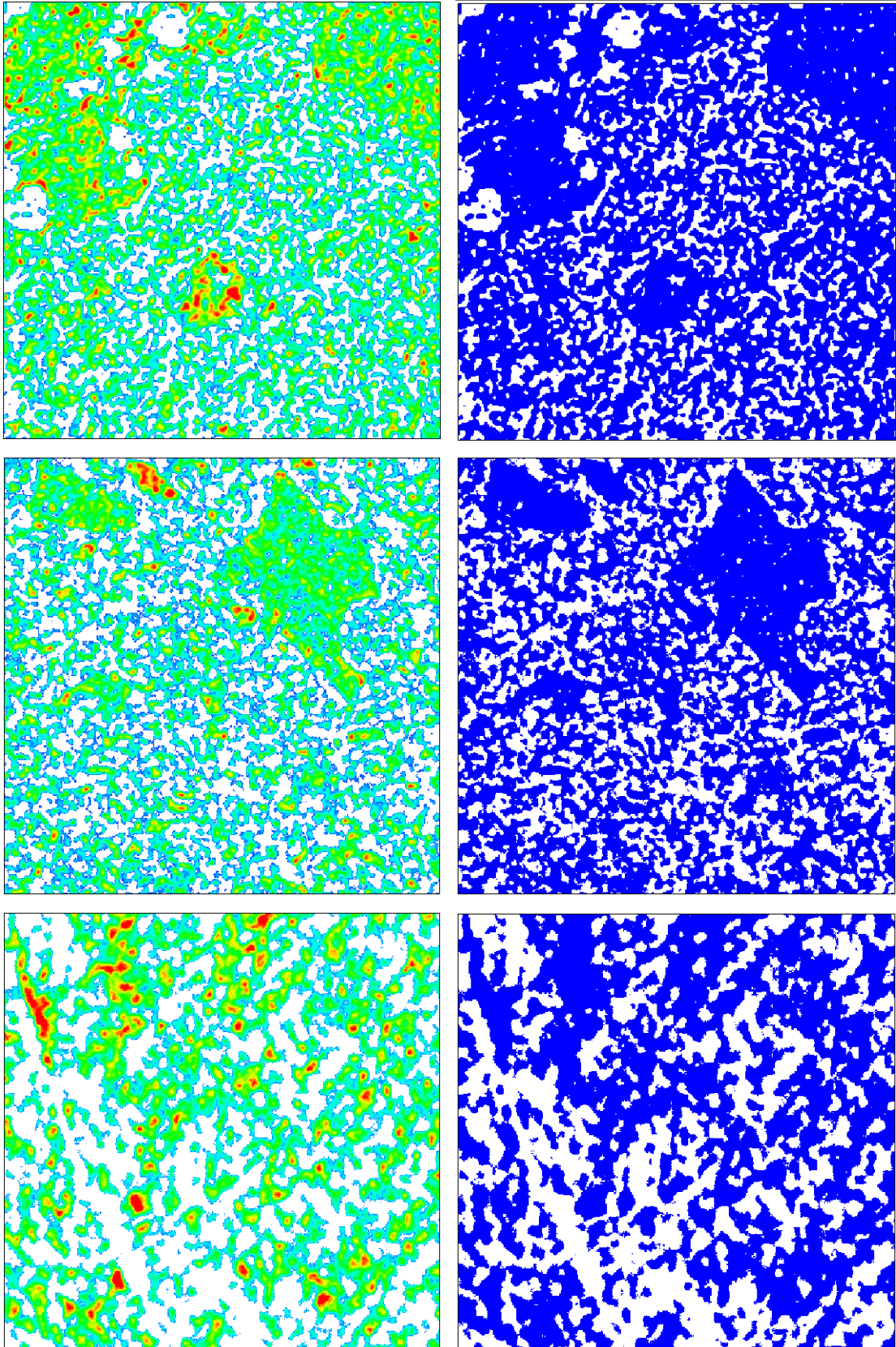


*Figure 5-6: Visual representation of damage induced through heating to C1S1 grouting formulation. Untreated grout at 28 days (top), heat-treated to 400°C (middle) and heat-treated to 800°C (bottom)*

The cross-sections to the left of Figure 5-6 show the relative density of the phases within the cross-section of the VOI, highlighting the significant loss of hydrate phases as a function of exposure temperature. The figures to the right show more clearly the resultant segmented porosity, the increasing width of pores and the damage caused to the internal microstructure of the samples due to exposure.

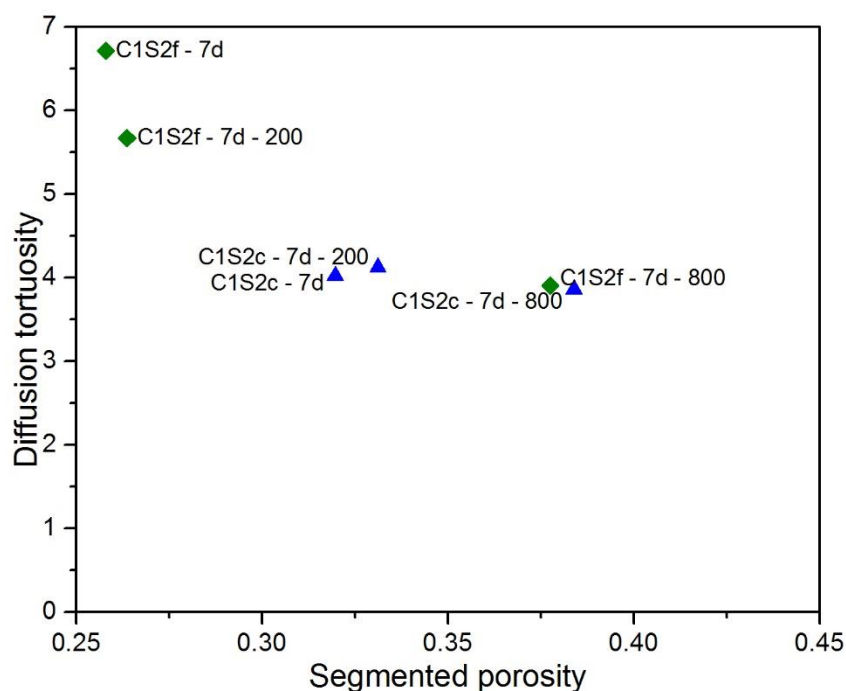


*Figure 5-7: Diffusive tortuosity of C1S2c and C1S2f samples at 7 days with and without heat-treatment*

During the second session of X-ray  $\mu$ CT analysis, smaller samples (2.5mm diameter, rather than 5mm) were analysed following heating to 200 or 800°C at 7 days. Since samples were smaller, younger and exposed to different conditions (with a resultant, and statistically significant increase in resolution) it has been necessary to separate analysis here into two distinct sections.

Figure 5-7 provides the result of random walk simulations carried out on the segmented VOIs created from the samples analysed during this session of analysis. As shown in Figure 4-30, there was a significant difference in the results for the untreated C1S2c and C1S2f samples; a result of the disparity in early age hydration leading to pore filling and a refining of the pore space to a higher degree within the C1S2f system.

As with the results obtained for untreated samples, those which have been exposed to elevated temperatures follow the same general trend as outlined in the work of Bentz and Garboczi (1991), with the asymptotic features described as in Figure 4-29 and Figure 4-30. Again, it is prudent not to draw separate trends for the two data sets, owing to the small number of data points within each, and the potential errors that exist within the technique.

The C1S2f system was much more susceptible to the more modest exposure condition (200°C) with a clear increase in the interconnectivity of the percolating pore space. This result is consistent with those obtained through permeability (Figure 5-3) and sorptivity (Figure 5-4) testing, in which the C1S2f grout formulation showed a significant reduction in performance, much more so than the C1S2c formulation, where the detrimental effects were much less apparent. This is consistent with results obtained through thermogravimetric analysis, in which mass loss to 200°C was noticeably higher for the C1S2f sample than for the C1S2c sample (5.8% compared to 4.9% respectively); indicative of the higher volume of hydrate phases within the sample.

The result obtained here for the C1S2c sample following exposure at 200°C is consistent with this assessment. An increase in porosity is observed, as has been seen for all other heat-treated samples; the difference here is that there is not the same associated drop in diffusion tortuosity. Figure 5-8 gives a 2 dimensional representation of the impact of this exposure upon the microstructure; there was quite clearly loss of hydrates leading to increased porosity.

This, seemingly, did not have any significant bearing upon calculated diffusion tortuosity. This result suggests that the microstructure within the grout prepared with the coarser slag (C1S2c) was more resilient to this deleterious heating and also that the anhydrous slag grains were well bound within the hydration products of the bulk matrix.

Following heating to 800°C both the C1S2c and C1S2f samples experienced similar damage with comparable resultant segmented porosity and tortuosity values calculated. Whilst it is not possible to directly compare the results here with those obtained at a lower resolution for the C1S1 system (Figure 5-5) the findings do appear to be relatively similar (if the disparity induced by resolution are also accounted for, see Figure 4-27).

TGA data showed a similar mass loss in the range 200-800°C for the C1S2f and C1S2c formulations (6.69% compared to 6.54%); with significant and comparable damage evidently caused to samples prepared for X-ray  $\mu$ CT (Figure 5-7)

It appears that anhydrous material remained undamaged in the C1S2c system (see Figure 5-8 bottom) but that much of the surrounding hydrates had been severely dehydrated; with the same being the case for the C1S2f sample (Figure 5-9).

There was undoubtedly significant damage caused to these samples through heating, which would be expected given the fragility of the hydrates and the size of the heated samples. Clearly, damage to full size waste packages would be less severe, especially at the centre of a large drum or box of conditioned waste, since a fire of relatively short duration would not raise the temperature across the entire package to such a degree (as is the case for the very small samples analysed via X-ray  $\mu$ CT).

As with the cross-sectional images for the C1S1 formulation (Figure 5-6), Figure 5-8 and Figure 5-9 show both the relative density (left) and the segmented pore network (in binary for ease of visualisation, to the right) of the untreated and exposed samples.

Whilst the cross-sectional images below show very representative areas within the VOIs of each sample, those above corresponding to the C1S1 sample may not always give a true indication of the size of the very large calumite grains. Owing to the size of these particles, the likelihood of bisecting through the centre of a grain is statistically highly unlikely [Figure 2-6 (Scrivener, 2004)]. Care has been taken to segment volumes within both the C1S1 and C2S1 samples which are representative of the samples as a whole, as discussed in Section 3.3.8.

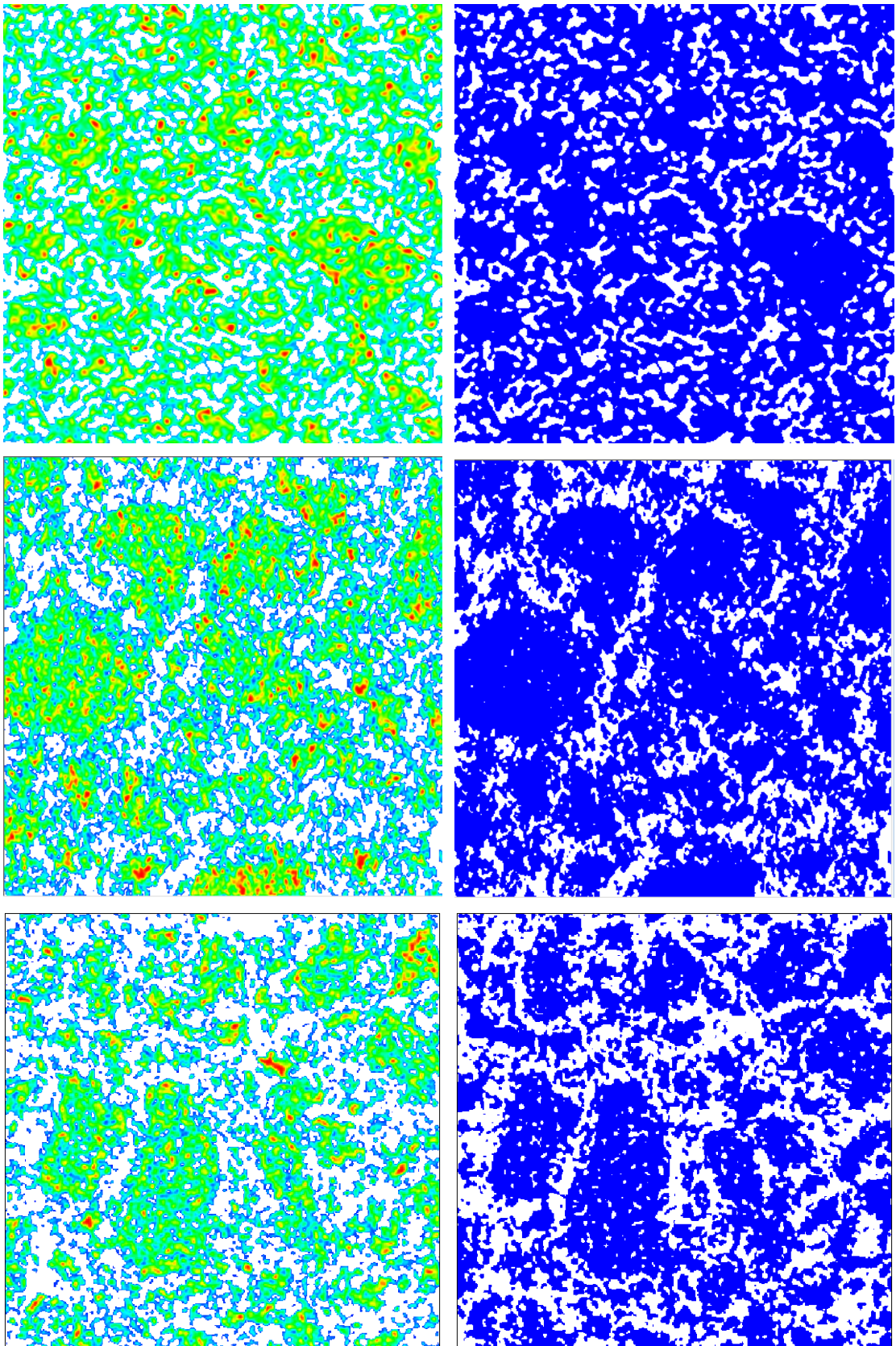
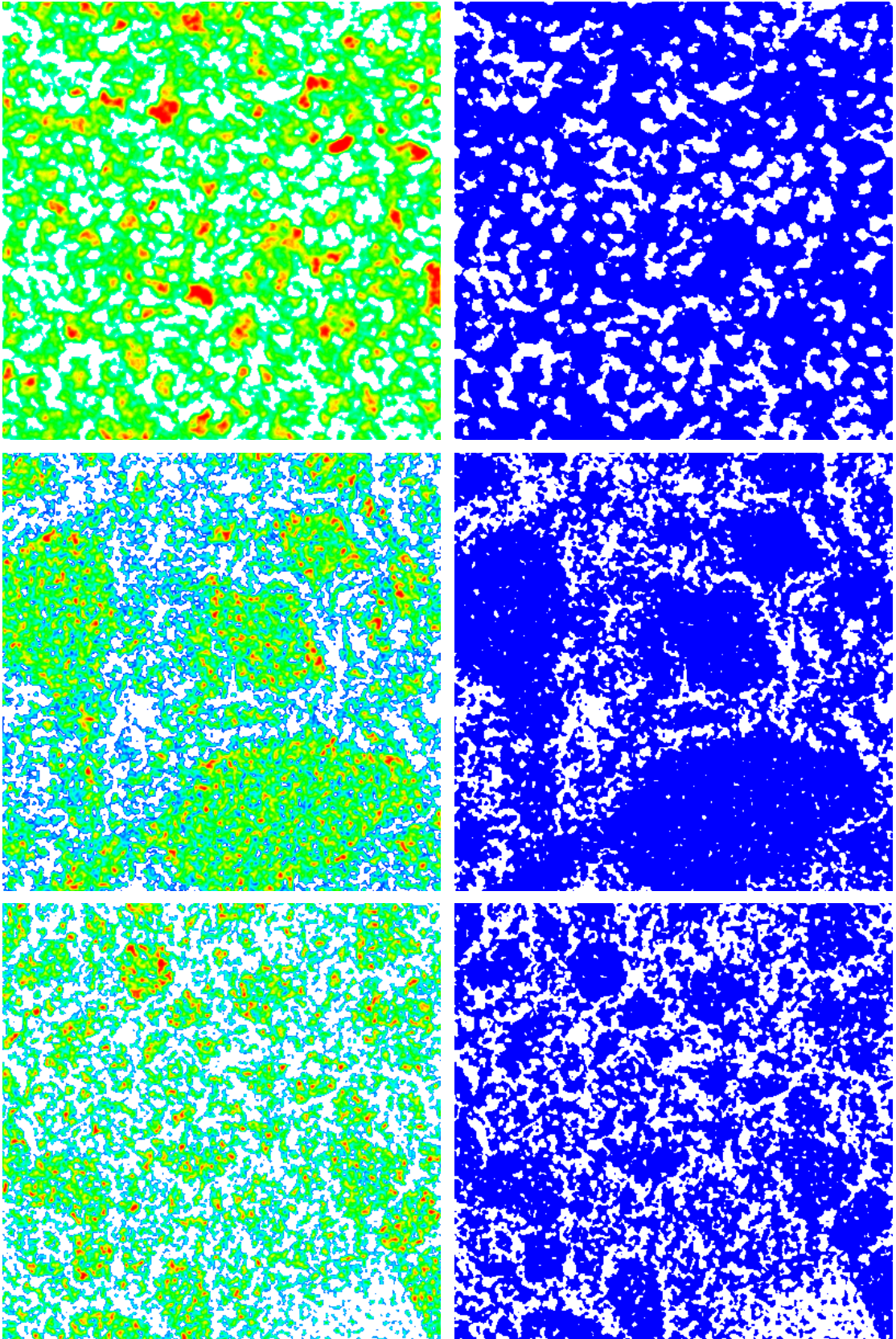


Figure 5-8: Visual representation of damage induced through heating to C1S2c grouting formulation. Untreated grout at 7 days (top), heat-treated to 200°C (middle) and heat-treated to 800°C (bottom)



*Figure 5-9: Visual representation of damage induced through heating to C1S2f grouting formulation. Untreated grout at 7 days (top), heat-treated to 200°C (middle) and heat-treated to 800°C (bottom)*

## 5.4 Phase assemblage following exposure to elevated temperatures

### 5.4.1 Portlandite content and mass loss determined via TGA

When samples were prepared for heat-treatment and subsequent permeability and sorptivity testing, an additional, identical, sample corresponding to each mix design was also prepared to allow for analysis via TGA and XRD. A central portion of each 27mm diameter by  $35 \pm 3$  mm sample was taken and prepared for analysis, as outlined in Section 3.3.4.

The determination of CH content provides some insight into both the degree of damage and the temperature profile within the samples and has previously been successfully applied to assess pure Portland cement concretes (Handoo et al., 2002). Within the present study, samples heated to 400°C showed no discernible loss of CH from the centre of the sample, consistent with what would be expected given the decomposition temperature of CH (Figure 3-5). The main observation to be made of samples heated to 400°C is the comparatively low CH content of the C1S2f grout and the comparatively high content within the C1S3c grout, likely a result of a disparity in slag hydration and the associated CH consumption (Taylor et al., 2010).

*Table 5-3: Mass loss at 550°C of samples from the centre of specimens previously heated to 800°C*

Sample	Mass loss to 550°C
C1S1	1.248
C2S1	1.040
C1S2c	0.854
C2S2c	1.138
C1S2f	2.068
C1S3c	1.798

Following heat-treatment at 800°C there was a loss of CH across all mix designs. This degree of CH loss varied and appeared to be affected by hydration and microstructural development of each individual grout formulation. For the C1S2f sample, 85% of the initial CH remained intact following heating, compared to 49-70% for all other samples,

suggesting that the finer microstructure and higher weighted degree of hydration had slowed the temperature rise at the centre of the sample and minimised damage away from the outer surface.

Complete loss of CH seems unlikely since it has been shown that dehydroxylation is reversible, with some rehydration occurring rapidly following cooling to ambient temperature (Alarcon-Ruiz et al., 2005). Since all samples were treated simultaneously this would be consistent across all mix designs and explains why residual CH content is higher than might otherwise be expected.

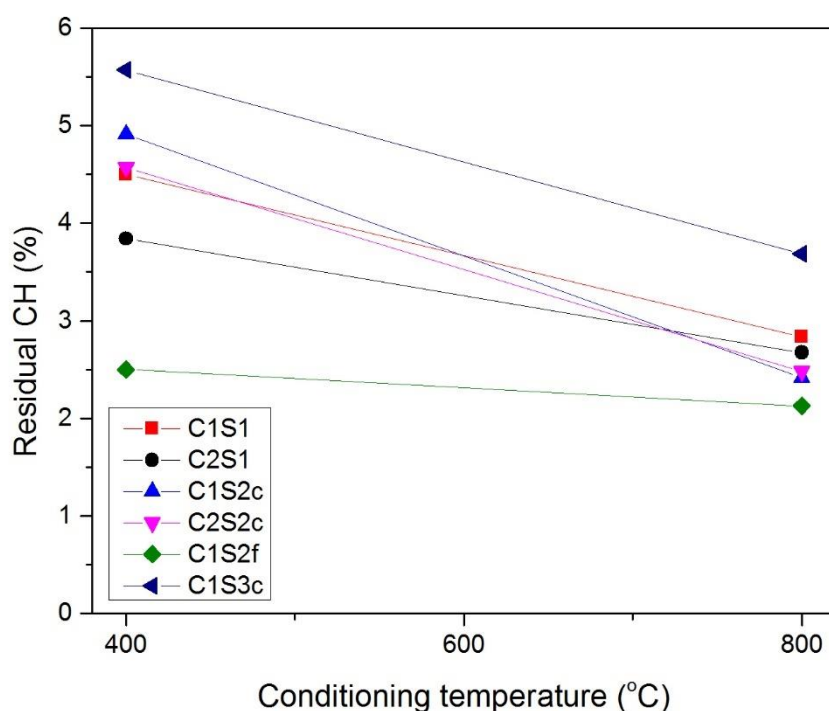


*Figure 5-10: CH content at centre of samples (27mm diameter) following heat-treatment*

The mass loss to 550°C of samples analysed via TGA (Table 5-3) is also interesting; the value for the C1S2f sample was higher than all others (only C1S3c showed a comparable loss in mass), suggesting that a greater volume of hydrates remained intact at the centre of this sample than in those of the other mix designs. The high mass loss for the C1S3c system could be partially explained by the comparatively high loss of CH, which would account for the relatively high associated value.

### 5.4.2 XRD analysis

In all instances, heating caused damage and decomposition of the crystalline phases in all samples. The peaks associated with CH are visible in the corresponding patterns for all samples up to 400°C but are significantly reduced after heating to 800°C, consistent with observations made in previous studies (Kim et al., 2013) and largely in agreement with observations made via TGA (Figure 5-10).

The monosulfate and hydrotalcite remained intact in all samples following heating to 200°C, but only remained visible following heating to 400°C in the C1S2f sample. Suggesting that the C1S2f specimen was the only one in which the temperature profile across the sample did not exceed those at which these phases decompose. For monosulfate, this decomposition takes place in the range 204-223°C (Singh et al., 1994), indicating that the central volume of the C1S2f sample was the only one not to reach this temperature when treated at 400°C.

Dehydration and dehydroxylation of hydrotalcite occurs beyond 100°C but, as with Portlandite, is a reversible process, with Ht identified in samples exposed to 300°C and subsequently stored in an ambient atmosphere (Rey et al., 1992). Presence of water has also been shown to facilitate reversibility following exposure to significantly higher temperatures.

Mass loss to 400°C during thermogravimetric analysis, at 28 days (Table 5-2), for the C1S2f sample was noticeably higher than for all other mix designs, indicative of the greater loss of hydrates due to thermal decomposition. It is therefore apparent that the thermal profile across the C1S2f grout samples progressed more slowly, a result of the more developed microstructure and filling of capillary porosity.

This reduction in the rate of temperature increase across the C1S2f sample in relation to all other mix designs is significant, and could prove highly important in the case of full-scale waste package exposure to similar conditions. The denser microstructure clearly had an influence on the temperature profile of the grouting material. Whilst sorptivity results (Figure 5-4) show a higher value for the C1S2f system, this is almost certainly a surface effect, and whilst significant in the case of the small samples within this study, in practice this formulation would undoubtedly prove to be more resilient in a fire scenario.

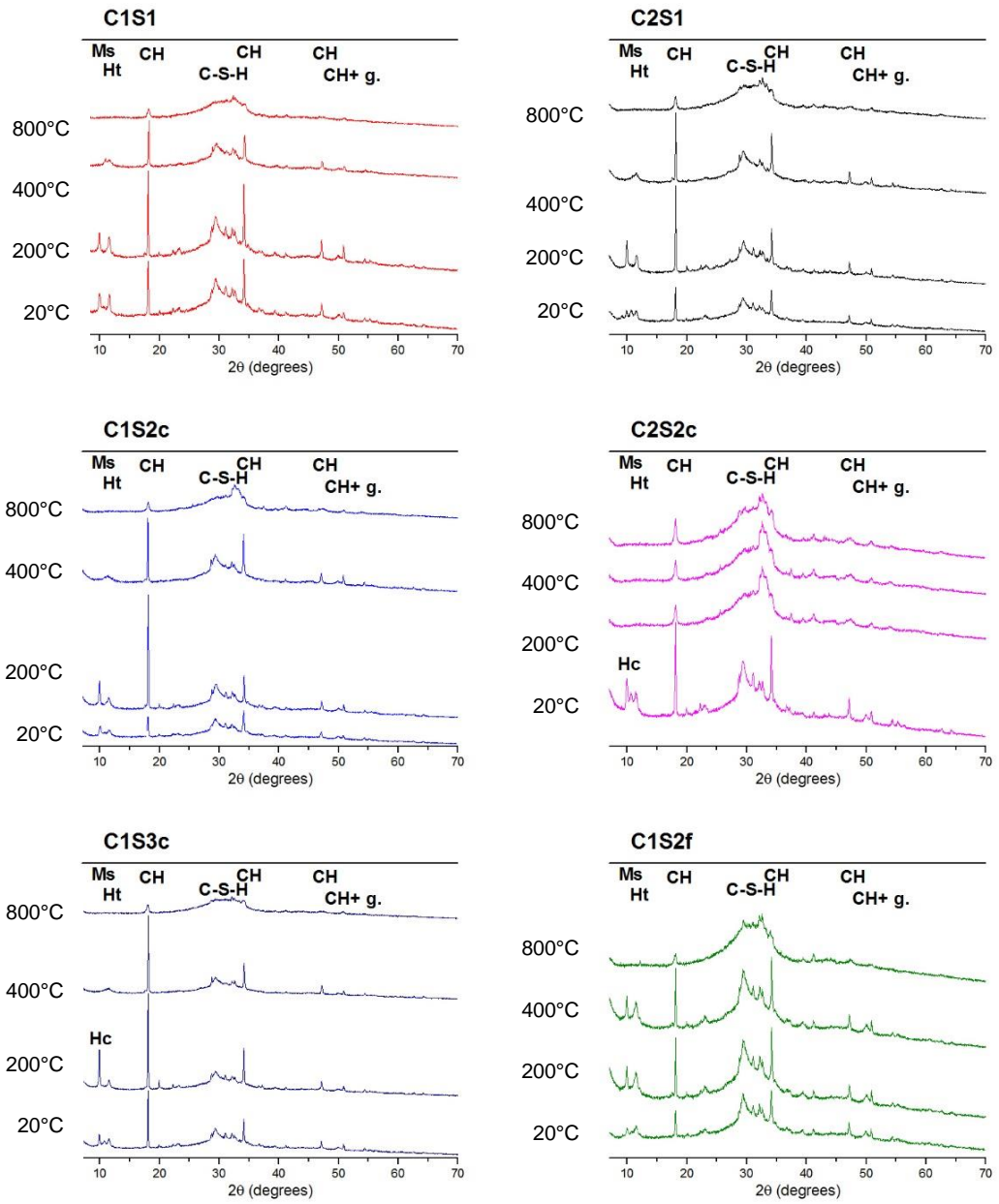


Figure 5-11: XRD patterns of heat-treated samples at 7-70° 2θ (Ms – monosulfate, Hc - hemicarboaluminate, Ht - hydrotalcite, g - gehlenite).

## 5.5 Summary

1. Severe damage and cracking within grouts for ILW encapsulation (at 75% replacement by slag) is not observed following heat-treatment at 200°C or 400°C. Grouts are, however, severely compromised when exposed to 800°C with significant cracks forming.

2. Presence of very large slag grains result in a grout that is more susceptible to elevated temperatures as cracks form and propagate through the interfacial zone at the grain boundary much more readily than in grouts prepared with a more typically graded slag.

3. Sorptivity testing provides interesting information as to the surface effects of heat-exposure and suggests that relatively high degree of grout hydration may in fact increase susceptibility to fire induced damage at the outermost edges of samples; or in practice, conditioned waste packages.

4. In severely fire damaged grouts there is very little correlation between sorptivity index and intrinsic gas permeability since the mechanisms controlling the two parameters differ. Micro- and macro-cracks induced through exposure to elevated temperatures govern the intrinsic permeability of a grouting matrix, whereas capillary suction and pore effects control the rate of sorptivity. Whilst both test methods provide valuable information as to the potential resilience of grouting formulations, significant insight into actual performance in field conditions would require a great deal more information.

5. The results obtained herein via X-ray  $\mu$ CT, coupled with random walk simulations provide a powerful means of understanding and quantifying the sub-micron-scale structure of hydrating cementitious materials; both untreated and following damage induced via heat exposure.

6. X-ray  $\mu$ CT shows very clearly the damage induced through heating and gives significant insight into the extensive damage that would be caused at the outer edges of conditioned waste packages in the event of a fire within a storage facility or GDF. Results show (Figure 5-6) the clear debonding of the Calumite grains as a result of exposure to elevated temperatures in the C1S1 system and a relatively higher degree of damage than experienced in the C1S2c and C1S2f systems, respectively.

7. The presence of crystalline materials (Ms and Ht) within the C1S2f samples following heat-treatment to 400°C indicates that the temperature at the core of these particular samples did not exceed the decomposition of these materials (between 204-223°C).

The same was not true of any other samples analysed and suggests that the finer microstructure of these samples, brought about by a higher relative degree of hydration, has an impact upon the rate of temperature change throughout the grouting material. This could clearly be significant in engineering practice; whilst the C1S2f formulation performs worst in many of the applied testing methods within the present study, the same would likely not be the case were full-scale waste packages to be analysed.

### **5.5.1 Industrial ramifications**

Whilst the samples analysed herein experienced significant damage as a result of exposure to elevated temperatures, the same would very likely not be the case for full scale waste packages, given the rate of temperature change through the grouting matrix. Nevertheless, there would clearly be negative impacts as a result of a fire scenario or other deleterious event occurring within a repository setting.

Incorporation of Calumite grains within grout formulations applied industrially has been the mainstay for a large number of years. Waste packages prepared with Calumite accounting for a significant portion of the grouting material will therefore make up a large percentage of waste packages conditioned to date. The results obtained herein show that there is a disconnect between the thermal properties of the Calumite and the surrounding hydrates within the grout, leading to thermal induced cracking. Whilst it is very unlikely that a fire event would occur within a GDF setting, the ramifications (relative to each individual waste package) must be thoroughly investigated and planned for.

Further study into the effects of a fire (or simulated fire scenario) on full scale waste packages would provide significant insight into the effects upon the structural integrity of resultant materials (and the resilience or otherwise of waste packages to these potential situations). X-ray  $\mu$ CT provides a powerful, high-resolution, non-destructive and relatively rapid means of assessing damage in 3-dimensions. Subsequent application of random walk simulation is computationally demanding but provides a quantitative means by which damage, and hence waste package integrity, may be assessed.

The results obtained within the present study show that application of a sacrificial layer, applied to the outer surface of conditioned waste packages would provide very good protection against fire induced damage. Within the sample mix designs analysed, exposure to set temperatures for 30 minutes did not result in these relatively small

(27mm diameter) samples reaching equilibrium; a relatively thin sacrificial layer would likely be sufficient to protect conditioned waste packages from damage.

# 6. Conclusions and further work

## Conclusions

This study was split into two distinct areas of investigation. The first of which investigated the impact that changes to the chemical and physical composition of the anhydrous constituent materials have on the hydration of grouts for ILW encapsulation. Understanding how changes induced either through alteration of supply, or introduced as a means of controlling rheological characteristics, affect hydration is key in gaining a more thorough understanding of microstructural development and ultimate performance.

This fundamental understanding of the intimate relationships of –

**Composition → hydration → microstructure → performance**

underpins the application of these materials to their intended purpose. Further, the results shown here confirm the suitability of particular techniques to follow slag and clinker hydration, whilst also illustrating some of the potential of other lesser applied techniques (in particular X-ray  $\mu$ CT).

The second aspect of this study was to provide insight into the impacts of elevated temperatures, as would be experienced in a fire exposure scenario. The chemical and physical effects of a range of exposure conditions were investigated and provide information as to the resilience of different grouting formulations to such potential deleterious environments.

## **Hydration, microstructural development and engineering performance**

### **Clinker composition and impact upon hydration**

At the high levels of replacement by slag found in grouts for ILW encapsulation, the resultant water/ cement ratio is very high. Consequently, there appears to be very little disparity in the rate of clinker hydration at all ages, for the two clinker compositions studied. Despite the variations in terms of both chemical composition (Tables 3-1 and 3-2) and physical properties (Table 3-3); the rate of clinker hydration within all grout formulations was relatively consistent across all mix designs, with the one slight outlier being the C1S3c grout at early age (Figure 4-3).

After 1 year of hydration, no disparity in clinker hydration was evident across all grout formulations. Results were comparable to those found in previous studies (Whittaker et al., 2014, Kocaba, 2010), suggesting that w/b plays no significant role in controlling clinker hydration in grouts with high levels of replacement by slag.

Any disparity in clinker hydration appeared to have minimal impact upon subsequent slag hydration. Overall degree of hydration of the grouting materials was largely controlled by the physical properties of the slag powders and the availability of pore space to accommodate new hydrates.

The variation in both physical properties and chemical composition of the clinker materials was somewhat significant (Tables 3-1, 3-2 and 3-3); however, both would be classed as CEM1 42.5N in standard construction applications. Use of a finer or more reactive clinker, more comparable to a CEM1 42.5R or 52.5 would clearly lead to more rapid hydration, with an associated increase in heat evolution at early age.

## **Slag fineness, chemical composition and subsequent hydration**

Slag fineness was found to have the most profound impact upon rate and degree of hydration, with there being very little discernible disparity between slags of differing composition (within the limits of composition of the slags analysed in the present study).

Comparing the hydration of the C1S2f and C1S2c systems, the rate of early age slag hydration was significantly impacted by fineness, with hydration occurring much more rapidly as a result of an increase in specific surface area. Indeed, the hydration of the fine slag in the C1S2f system was similar at 7 days to the slag in the C1S2c system after 56 days (Figure 4-4).

This relative disparity in degree of hydration is well illustrated in Figures 4-8 and 4-9. Where the C1S2f system showed a much lower porosity at early age (Figure 4-10) and a visibly much lower fraction of anhydrous slag.

Within both the current (C1S1) and legacy (C2S1) grout specifications the hydration of the slag fraction was similar to that of the grouts prepared with the 'coarse' slag fraction (C1S2c, C2S2c and C1S3c). At early age, the C1S1 and C2S1 formulations showed relatively low levels of slag hydration, likely a result of the presence of the large calumite grains (accounting for 35%wt. of the slag fraction). From 7 to 28 days both grouts displayed high levels of slag hydration, with further hydration beyond this point being much lower than all other mix designs investigated (Figure 4-4), owing primarily to the absence of hydration of the calumite grains.

Development of hydrates and phase assemblage within grouting formulations was relatively consistent, owing to the matching level of replacement by slag across all mix designs and the relatively low disparity in composition of the slags investigated (Table 3-1). Phase assemblages were as expected and consistent with previous studies (Borges et al., 2010, Whittaker et al., 2014).

## **Microstructural development as a function of time, slag fineness and weighted DoH**

Microstructural development was studied in 2 and 3 dimensions via SEM-BSE and X-ray  $\mu$ CT, respectively. In both instances, coarse porosity was shown to be a function of

hydration of the clinker and slag phases present within the grouting matrix. Within this, there is clearly an intimate relationship with time to allow for hydration to proceed; and fineness of slag, which was determined to have the most significant bearing on hydration.

Whilst SEM-BSE was able to clearly show this reduction in coarse porosity (Figure 4-10) in 2 dimensions, application of X-ray  $\mu$ CT was required to provide information on the impact that pore-filling had upon pore-connectivity. Since permeability is essentially governed by pore connectivity, understanding how this is impacted by hydration is highly significant.

X-ray  $\mu$ CT coupled with random walk simulations allowed for analysis of pore-connectivity and tortuosity as a function of time without recourse to damaging water-removal techniques. Results showed a clear relationship between hydration and subsequent porosity, which in turn controlled the interconnectivity of the percolating pore network. Further interesting observations were made possible by X-ray  $\mu$ CT and are discussed in more detail below.

### **Transport properties of grouting materials**

Determining accurate, reliable and representative results for transport properties of cementitious materials via the application of laboratory testing is a very challenging undertaking. The general need for samples to be pre-conditioned prior to analysis, in order to arrest hydration and render them in a state suitable for testing, introduces new variables which are highly challenging, and often impossible, to quantify. Nevertheless, this study aimed to apply some relatively common techniques to determine the disparity, if any, between the transport properties of the investigated grouts.

For samples which received no pre-treatment prior to analysis, results for intrinsic gas permeability showed one clear outlying result, with all other mix designs fitting with the expected trend. The samples which had been found to exhibit the highest weighted degree of hydration (C1S2f) displayed the highest corresponding permeability, whilst all other samples tending to perform largely as would be expected. The current hypothesis for this rather anomalous result is that the fragile hydrates present within the samples may be in some way damaged via the analysis technique (with this effect being exacerbated for the samples which displayed a higher degree of hydration).

Samples that were initially oven dried at 50°C displayed similar results, albeit with higher corresponding permeability values, suggesting that any damage caused through the applied drying technique was consistent across all grout formulations.

Results from sorptivity testing on oven-dried samples were more consistent with what would be expected, in relation to the results obtained for hydration and microstructural development. Sorptivity appeared to be intimately linked to porosity and driven by capillary suction, samples which were found to have the highest degree of hydration (and hence lowest capillary porosity) showed the lowest sorptivity values.

### **Application and suitability of X-ray $\mu$ CT and coupled random walk simulation**

X-ray  $\mu$ CT represents a powerful tool in gaining significant insight into the 3 dimensional microstructural development of cementitious materials, with respect to time, composition, hydration and as a result of exposure to deleterious environments. The potential to analyse samples without recourse to potentially damaging pre-conditioning allows for much more representative results to be obtained, and the non-damaging nature of analysis means that samples may be analysed at a range of times to follow hydration.

The application of X-ray  $\mu$ CT within the present study highlighted some interesting results and also allowed for some degree of quantification of the impact of resolution. The large calumite grains that were present within the C1S1 and C2S1 formulations were found to increase the diffusion tortuosity of the percolating pore space for a given porosity value. Whilst this impact was significant at early age (with samples analysed up to 28 days, and samples of other compositions at 60 days) it would be expected that continued hydration and pore filling, which appears more prevalent in the non-calumite containing grout formulations, would serve to significantly offset this effect.

Since the application of cementitious grouts for the treatment of ILW is a very long-term (essentially permanent) solution, continued hydration at very late age is highly significant. Whilst the limitations in time and access to facilities did not allow for very old samples to be analysed via X-ray  $\mu$ CT within the present study, it is expected that results would follow the same trends as observed via BSE-IA, with continued hydration leading to significant pore-filling and weighted degree of hydration (Figure 4-6) of the C1S1 and

C2S1 formulations slowing to a comparatively higher degree beyond the first few months.

Resolution is clearly a significant factor in identifying and segmenting the pores within a sample (Gallucci et al., 2007). Within the present study it has been possible to quantify this through the application of random walk simulations and pore analysis. Increasing resolution from 1.57 $\mu\text{m}$  to 0.53 $\mu\text{m}$  had an insignificant impact on segmented porosity; but, crucially, affected the measured interconnectivity of the pore network. The result of this increased resolution was to identify the very small pore throats that were lost at the lower resolution; consequentially, a lower diffusion tortuosity was determined.

## **Impact of heat-treatment**

### **Effect of exposure on phase assemblage**

From TGA it was evident that a greater volume of hydrates were formed in the C1S2f grout, relative to other formulations; for which comparable levels were observed up to and including 28 days. Mass loss beyond 400°C was significant and within larger samples led to significant cracking and damage to the internal microstructure.

Damage caused to samples exposed to elevated temperatures was somewhat incongruous and appeared to be a function of hydration and microstructural development. The presence of particular crystalline materials (namely monosulfate and hydrotalcite) following exposure to 400°C was only observed for the C1S2f formulation, indicating that different temperature profiles were experienced for different grout formulations. This reduced rate of temperature change within samples prepared with finer slag is of key significance with regards potential performance of waste packages in the event of a fire scenario within a storage or disposal facility.

## Engineering properties following exposure

Intrinsic gas permeability of heat-treated grouts did not provide significant insight into the effects of exposure, with samples exposed to the most severe conditions being unfit for testing. Application of sorptivity testing provided significant information as to the impact of exposure, but it was not possible to compare the results for grout formulations containing very large slag grains (C1S1 and C2S1) with more standard mix designs (C1S2c, C2S2c, C1S2f, C1S3c) since the presence of these large particles skewed the results.

The sorptivity index may be seen as an indicator towards the degree of damage experienced by a grouting material, particularly at the outer surface; where increased sorptivity was a function of coarse porosity, which in turn is governed by the overall degree of hydration of the material.

X-ray  $\mu$ CT provided significant insight into the damage caused within cementitious materials exposed to deleterious environments. Achieving meaningful and quantifiable results was something of a trade off since achievable resolution is a function of sample size (typically of the order sample size/4-5000). Since the samples analysed within the present study were significantly smaller than those tested via gas permeability and sorptivity (2.5mm, as opposed to 27mm), it is not possible to make direct correlations. The results obtained via X-ray  $\mu$ CT indicate the damage caused at the outer edges of the samples and provide significant insight into the effects of high temperatures and the resilience of particular mix designs.

Consistent with observations of samples prepared for permeability and sorptivity testing, cracking and sample fracture as a result of exposure to elevated temperatures was clearly visible in reconstructed VOIs from X-ray  $\mu$ CT (Figures 5-6, 5-8 and 5-9). Significant mass loss, particularly beyond 400°C was observed, in line with results obtained via TGA, and ultimately leading to significant crack formation and coarsening of pores within the bulk matrix.

When samples were exposed to temperatures of 800°C there was a slight disparity in subsequent segmented porosity and diffusion tortuosity values, with the calumite containing C1S1 formulation more negatively affected than the, more standard, C1S2c grout sample. It was clear that cracks were propagating around the large anhydrous slag grains and exacerbating the degree of damage experienced, and consequently the interconnectivity of the resultant pore space.

## **Overarching industrial conclusions**

### ***Context for legacy, current and future waste conditioning***

Research has shown (Taylor, 2010) that even at late age, there remains a large degree of anhydrous slag present within composite cement systems at high levels of replacement. This fact should always be borne in mind when considering conditioned waste packages as they remain in a continually changing state. This work has shown that hydration is affected as a result of the fineness of the different constituent phases present within the grouting matrix and that this has implications upon the microstructural development, which will ultimately affect engineering performance into the future.

An appreciation of how these changes will impact upon waste package integrity is crucial in order to ensure that the engineering barriers employed to mitigate risk to the public are sufficient in the design of storage and disposal facilities.

Legacy changes to powder supply and grout specifications and hence compositions have undoubtedly had impacts upon hydration and subsequent performance. Quantifying these impacts and ensuring that they do not result in unacceptable increased risk is essential for the long-term success of waste treatment.

Since the slag fraction accounts for (typically) 75% of the total powder fraction of the grouting materials, it plays the biggest role in controlling overall grout hydration; which in turn dictates microstructural development and the physical properties of a conditioned waste. Whilst a finer slag has clearly been shown to result in higher degrees of hydration and a resultant finer and more developed pore structure, application of a finer slag poses a number of logistical and engineering difficulties. Increasing powder fineness results in a more viscous 'stiffer' grout, at a set water to binder ratio, and increasing water content would lead to a higher total porosity within the conditioned waste (something which all concerned are very keen to avoid, since this will have a negative effect upon permeability and potential leaching rates of waste species).

Transitioning to the current (and most recent) specification incorporating Calumite was, at the time, an unavoidable decision, owing to the lack of availability of powder which conformed to the previous specification and an industrial refusal to increase the water content of the grouting materials. At the present stage, with hindsight and pragmatism, the author would suggest it prudent to revert back to a single powder of singular PSD (as opposed to the current bi-modal PSD that the blended slag fraction possesses). The present study has shown that not only does this avoidance of much larger grains result in an overall higher degree of grout hydration at later age, it also produces a grouting

material (and hence waste packages) which are more resilient to potential deleterious environments.

## Recommendations for further work

The use of cementitious grouts as conditioning matrices in the treatment of intermediate level nuclear waste is a highly complex challenge. The timescales involved, the variability in range of waste stream compositions and the large number of variables and assumptions that must be made when modelling and predicting performance mean that, on the whole, a vast volume of dedicated research is required.

This project has focused on the hydration and microstructural development of grouts and makes up just a small portion of this significant area of research. Further investigation in a number of areas would provide significant increased insight into hydration as a function of a number of different parameters,

### **Materials and scope of compositional effects**

Increasing the scope of study to include a range of slags and clinkers of a wider range of compositions would allow for greater quantification of the degree to which PSD and chemical composition affect rate and degree of hydration. Due to a number of external factors, as well as time and resource limitations, it was not possible to expand the project in this manner; doing so would enable a greater understanding of the impacts of changes in supply to be quantified.

### **Testing methods**

This study would be enhanced through the inclusion of more in-depth XRD analysis, in particular quantitative XRD, via the application of PONKCS and Rietveld refinement. Given the constraints with both time and availability of suitable resources it was not deemed feasible to include this area of investigation into the present study. This would become an increasingly significant avenue of study were the study to be extended to include a wider range of powder compositions.

More detailed investigation into the impact of heating on the phase assemblage and degradation of samples would provide insight into resilience. Conducting a more thorough study of heat-damaged samples via SEM-BSE would allow for better understanding of the impact upon the hydrates (in particular the CH and C-S-H) within the bulk of the grouting materials. Conducting subsequent heat-testing in which samples were exposed to designated temperatures (200°C, 400°C and 800°C) for longer durations to allow them to reach equilibrium would provide further insight into the resilience of the various grout formulations and avoid the disparity in temperature profiles that were observed in the results provided herein.

Had access to X-ray  $\mu$ CT facilities been more reliable and readily available, further expanding this area of investigation to include both younger and much older samples would provide a very interesting avenue of enquiry. Similarly, had applications to access synchrotron facilities been successful, this could have expanded the scope of this area of investigation (either through enhancing resolution, increasing throughput or allowing very young samples to be analysed multiple times, to follow early age hydration).

Expanding the range of testing methods to probe pore-structure (MIP, BET etc.) would allow for a wider range of length-scales to be investigated and for a rigorous assessment of the strengths and weaknesses of each technique to be critically analysed.

### **Degradation mechanisms**

Application of long-term engineering performance testing would provide a great deal of insight into the resilience and degradation of different grout formulations. Coupling this with accelerated testing (by means of leaching, carbonation, chloride penetration etc.) would be useful in gaining insight into the very long-term behaviour of conditioned waste packages.

Analysis of grout samples from full-scale waste packages would allow for a great deal of additional insight to be gained. Investigation of samples from a range of positions within a waste package would allow for the impact of heating to be quantified; understanding how this impacts upon hydration and, hence, porosity.

Exposure to elevated temperatures for extended periods would provide further insight into induced degradation. Through heating samples for a sufficient period for a constant temperature profile to establish it would be possible to compare and contrast

performance of samples in a simpler way. Interaction between anhydrous and hydrated phases and the propagation of cracks could be studied and quantified in more detail.

## 7. References

- ABELL, A., WILLIS, K. & LANGE, D. 1999. Mercury intrusion porosimetry and image analysis of cement-based materials. *J Colloid Interface Sci*, 211, 39-44.
- ALARCON-RUIZ, L., PLATRET, G., MASSIEU, E. & EHRLACHER, A. 2005. The use of thermal analysis in assessing the effect of temperature on a cement paste. *Cement and Concrete Research*, 35, 609-613.
- ALIGIZAKI, K. K. 2005. *Pore structure of cement-based materials: testing, interpretation and requirements*, CRC Press.
- ALTENDORF, H. 2011. *3D Morphological Analysis and Modelling of Random Fiber Networks*. PhD, Mines Paris Tech.
- ANGUS, M. J., GODFREY, I. H., HAYES, M. & FOSTER, S. 2010. *Managing Change in Supply of Cement Powders for Radioactive Waste Encapsulation - Twenty Years of Operational Experience*. Waste Management Symposia. Phoenix, AZ.
- ARVANITI, E., JUENGER, M. G., BERNAL, S., DUCHESNE, J., COURARD, L., LEROY, S., PROVIS, J., KLEMM, A. & DE BELIE, N. 2014a. Physical characterization methods for supplementary cementitious materials. *Materials and Structures*, 1-12.
- ARVANITI, E. C., JUENGER, M. C. G., BERNAL, S. A., DUCHESNE, J., COURARD, L., LEROY, S., PROVIS, J. L., KLEMM, A. & DE BELIE, N. 2014b. Determination of particle size, surface area, and shape of supplementary cementitious materials by different techniques. *Materials and Structures*, 48, 3687-3701.
- ATKINS, M., BENNETT, D., DAWES, A., GLASSER, F., KINDNESS, A. & READ, D. 1992. A thermodynamic model for blended cements. *Cement and Concrete Research*, 22, 497-502.
- ATKINS, M. & GLASSER, F. P. 1992. Application of portland cement-based materials to radioactive waste immobilization. *Waste Management*, 12, 105-131.
- ATKINS, M., GLASSER, F. P. & KINDNESS, A. 1990. *Phase Relations and Solubility Modelling in the Cao- SiO<sub>2</sub>- Al<sub>2</sub>O<sub>3</sub>- MgO- SO<sub>3</sub>-H<sub>2</sub>O System: For Application To Blended Cementss*. MRS Online Proceedings Library, 212, null-null.
- BANHART, J. 2008. *Advanced tomographic methods in materials research and engineering*, Oxford, Oxford University Press.
- BAQUERIZO, L. G., MATSCHEI, T., SCRIVENER, K. L., SAEIDPOUR, M. & WADSÖ, L. 2015. Hydration states of AFm cement phases. *Cement and Concrete Research*, 73, 143-157.
- BBC. 2015. SSI Redcar steelworks to be shut [Online]. <http://www.bbc.co.uk/news/uk-england-34509329>: BBC. [Accessed 26 April 2016].
- BECKMANN, F., GRUPP, R., HAIBEL, A., HUPPMANN, M., NÖTHE, M., PYZALLA, A., REIMERS, W., SCHREYER, A. & ZETTLER, R. 2007. In-Situ Synchrotron X-Ray Microtomography Studies of Microstructure and Damage Evolution in Engineering Materials. *Advanced Engineering Materials*, 9, 939-950.

- BEN HAHA, M., LOTHENBACH, B., LE SAOUT, G. & WINNEFELD, F. 2012. Influence of slag chemistry on the hydration of alkali-activated blast-furnace slag — Part II: Effect of Al<sub>2</sub>O<sub>3</sub>. *Cement and Concrete Research*, 42, 74-83.
- BENSTED, J. & BARNES, P. 2002. *Structure and Performance of Cements, Second Edition*, Taylor & Francis.
- BENTZ, D. P. 2007. Transient plane source measurements of the thermal properties of hydrating cement pastes. *Materials and Structures*, 40, 1073-1080.
- BENTZ, D. P., QUENARD, D. A., KUNZEL, H. M., BARUCHEL, J., PEYRIN, F., MARTYS, N. S. & GARBOCZI, E. J. 2000. Microstructure and transport properties of porous building materials. II: Three-dimensional X-ray tomographic studies. *Materials and Structures*, 33, 147-153.
- BENTZ, D. P. & GARBOCZI, E. J. 1991. Percolation of phases in a three-dimensional cement paste microstructural model. *Cement and Concrete Research*. 21. 325-344
- BERGOLD, S. T., GOETZ-NEUNHOEFFER, F. & NEUBAUER, J. 2013. Quantitative analysis of C–S–H in hydrating alite pastes by in-situ XRD. *Cement and Concrete Research*, 53, 119-126.
- BERODIER, E. & SCRIVENER, K. 2014. Understanding the Filler Effect on the Nucleation and Growth of C-S-H. *Journal of the American Ceramic Society*, 97, 3764-3773.
- BERODIER, E. & SCRIVENER, K. 2015. Evolution of pore structure in blended systems. *Cement and Concrete Research*, 73, 25-35.
- BERODIER, E. M. J. 2015. Impact of the Supplementary Cementitious Materials on the kinetics and microstructural development of cement hydration. Ph.D. Thesis, Ecole Polytechnique Federale De Lausanne.
- BHATTY, J. I. 1986. Hydration versus strength in a portland cement developed from domestic mineral wastes — a comparative study. *Thermochimica Acta*, 106, 93-103.
- BNFL 2000. *BNFL Technical Specification for Ordinary Portland cement (OPC), Ground Granulated Blastfurnace Slag (BFS) and Pulverised Fuel Ash (PFA) powders for use in the encapsulation/immobilisation of radioactive waste materials.*
- BORGES, P. H., MILESTONE, N. B., COSTA, J. O., LYNSDALE, C. J., PANZERA, T. H. & CHRISTOPHORO, A. L. 2012. Carbonation durability of blended cement pastes used for waste encapsulation. *Materials and Structures*, 45, 663-678.
- BORGES, P. H., MILESTONE, N. B. & STREATFIELD, R. E. Accelerated weathering of composite cements used for immobilisation. *MRS Proceedings*, 2008. Cambridge Univ Press, 305.
- BORGES, P. H. R., COSTA, J. O., MILESTONE, N. B., LYNSDALE, C. J. & STREATFIELD, R. E. 2010. Carbonation of CH and C–S–H in composite cement pastes containing high amounts of BFS. *Cement and Concrete Research*, 40, 284-292.
- BOSSA, N., CHAURAND, P., VICENTE, J., BORSCHNECK, D., LEVARD, C., AGUERRE-CHARIOL, O. & ROSE, J. 2015. Micro- and nano-X-ray computed-tomography: A step forward in the characterization of the pore network of a leached cement paste. *Cement and Concrete Research*, 67, 138-147.

BRADBURY, M. H. & VAN LOON, L. R. 1997. *Cementitious near-field sorption data bases for performance assessment of a L/ILW repository in a Palfris Marl host rock, Nagra, National Cooperative for the Disposal of Radioactive Waste.*

BROWN, P. E., BARRET, P., DOUBLE, D. D., FROHNSDORFF, G., JOHANSEN, V. & PARROTT, L. J. 1986. *The hydration of tricalcium aluminate and tetracalcium aluminoferrite in the presence of calcium sulfate. Materials and Structures, 19, 137-147.*

BRUNAUER, S., EMMETT, P. H. & TELLER, E. 1938. *Adsorption of gases in multimolecular layers. Journal of the American Chemical Society, 60, 309-319.*

BRUNAUER, S., MIKHAIL, R. S. & BODOR, E. 1967. *Some remarks about capillary condensation and pore structure analysis. J Colloid Interface Sci, 25, 353-358.*

BULLARD, J. W. & FLATT, R. J. 2010. *New insights into the effect of calcium hydroxide precipitation on the kinetics of tricalcium silicate hydration. Journal of the American Ceramic Society, 93, 1894-1903.*

BULLARD, J. W., JENNINGS, H. M., LIVINGSTON, R. A., NONAT, A., SCHERER, G. W., SCHWEITZER, J. S., SCRIVENER, K. L. & THOMAS, J. J. 2011. *Mechanisms of cement hydration. Cement and Concrete Research, 41, 1208-1223.*

BYE, G. C. 1999. *Portland Cement: Composition, Production and Properties, Thomas Telford.*

CABRERA, J. G. & LYNSDALE, C. J. 1988. *A new gas permeameter for measuring the permeability of mortar and concrete. Magazine of Concrete Research, 40, 177-182.*

CARRUTHERS, K. & COLLIER, N. 2013. *Blast Furnace Slag and Pulverised Fuel Ash Reactivity Test Methods. National Nuclear Laboratory.*

CASTELLOTE, M., ALONSO, C., ANDRADE, C., TURRILLAS, X. & CAMPO, J. 2004. *Composition and microstructural changes of cement pastes upon heating, as studied by neutron diffraction. Cement and Concrete Research, 34, 1633-1644.*

CHEN, W. 2006. *Hydration of slag cement - theory, modeling and application. Ph.D. Thesis, University of Twente.*

CHEN, W. & BROUWERS, H. J. H. 2006. *The hydration of slag, part 1: reaction models for alkali-activated slag. Journal of Materials Science, 42, 428-443.*

CODINA, M., CAU-DIT-COUMES, C., LE BESCOP, P., VERDIER, J. & OLLIVIER, J. P. 2008. *Design and characterization of low-heat and low-alkalinity cements. Cement and Concrete Research, 38, 437-448.*

COLLIER, N. C. 2006. *The Encapsulation of Iron Hydroxide FLoc in Composite Cement. Ph.D. Thesis, University of Sheffield.*

COLLIER, N. C. 2010. *Immobilisation matrices for intermediate level nuclear wastes using sulphate activated BFS/OPC and PFA/OPC composite cements. Advances in Applied Ceramics, 109.*

COLLIER, N. C. & MILESTONE, N. B. 2010. *The encapsulation of Mg(OH)<sub>2</sub> sludge in composite cement. Cement and Concrete Research, 40, 452-459.*

COLLIER, N. C., MILESTONE, N. B. & GODFREY, I. H. 2004. *The Encapsulation of Iron Hydroxide Floc in Composite Cement. Cement and Concrete Science. Warwick: University of Sheffield.*

- COLLIER, N. C., MILESTONE, N. B., HILL, J. & GODFREY, I. H. 2006. *The disposal of radioactive ferric floc. Waste Management, 26, 769-775.*
- COLLIER, N. C., MILESTONE, N. B., HILL, J. & GODFREY, I. H. 2009a. *Immobilisation of Fe floc: Part 1, pre-treatment of floc with slaked lime. Journal of Nuclear Materials, 393, 77-86.*
- COLLIER, N. C., MILESTONE, N. B., HILL, J. & GODFREY, I. H. 2009b. *Immobilisation of Fe floc: Part 2, encapsulation of floc in composite cement. Journal of Nuclear Materials, 393, 92-101.*
- COLLIER, N. C., SHARP, J. H., MILESTONE, N. B., HILL, J. & GODFREY, I. H. 2008. *The influence of water removal techniques on the composition and microstructure of hardened cement pastes. Cement and Concrete Research, 38, 737-744.*
- COSTOYA, M. 2008. *Effect of particle size distribution on the hydration kinetics and microstructural development of cement hydration. Ph.D. Thesis, Ecole Polytechnique Federale De Lausanne.*
- COVILL, A., HYATT, N. C., HILL, J. & COLLIER, N. C. 2011. *Development of magnesium phosphate cements for encapsulation of radioactive waste. Advances in Applied Ceramics, 110, 151-156.*
- CROSSLAND, I. & VINES, S. 2001. *Why a Cementitious Repository? Nirex Report N/034.*
- DARMA, I. S., SUGIYAMA, T. & PROMENTILLA, M. A. B. 2013. *Application of X-Ray CT to Study Diffusivity in Cracked Concrete Through the Observation of Tracer Transport. Journal of Advanced Concrete Technology, 11, 266-281.*
- DARQUENNES, A., ESPION, B. & STAQUET, S. 2013. *How to assess the hydration of slag cement concretes? Construction and Building Materials, 40, 1012-1020.*
- DAY, R. L. & MARSH, B. K. 1988. *Measurement of porosity in blended cement pastes. Cement and Concrete Research, 18, 63-73.*
- DE CEUKELAIRE, L. & VAN NIEUWENBURG, D. 1993. *Accelerated carbonation of a blast-furnace cement concrete. Cement and Concrete Research, 23, 442-452.*
- DE SCHUTTER, G. & TAERWE, L. 1995. *Specific heat and thermal diffusivity of hardening concrete. Magazine of Concrete Research, 47, 203-208.*
- DE WEERDT, K., HAHN, M. B., LE SAOUT, G., KJELLEN, K. O., JUSTNES, H. & LOTHENBACH, B. 2011. *Hydration mechanisms of ternary Portland cements containing limestone powder and fly ash. Cement and Concrete Research, 41, 279-291.*
- DECC 2011. *Planning our electric future: a White Paper for secure, affordable and low-carbon electricity.*
- DECC 2014. *Implementing Geological Disposal. In: CHANGE, D. O. E. A. C. (ed.). Crown copyright.*
- DELHOMME, F., AMBROISE, J. & LIMAM, A. 2012. *Effects of high temperatures on mortar specimens containing Portland cement and GGBFS. Materials and Structures, 45, 1685-1692.*
- DIAMOND, S. 2000. *Mercury porosimetry: An inappropriate method for the measurement of pore size distributions in cement-based materials. Cement and Concrete Research, 30, 1517-1525.*

- DINKU, A. & REINHARDT, H. W. 1997. Gas permeability coefficient of cover concrete as a performance control. *Materials and Structures*, 30, 387-393.
- DUXSON, P., FERNÁNDEZ-JIMÉNEZ, A., PROVIS, J. L., LUKEY, G. C., PALOMO, A. & DEVENTER, J. S. J. 2006. Geopolymer technology: the current state of the art. *Journal of Materials Science*, 42, 2917-2933.
- ELSDEN, A. 1984. The management of intermediate level radioactive wastes arising from reprocessing operations. *Progress in Nuclear Energy*, 13, 19-30.
- ESCALANTE-GARCIA, J. I. & SHARP, J. H. 2004. The chemical composition and microstructure of hydration products in blended cements. *Cement and Concrete Composites*, 26, 967-976.
- ESCALANTE, J. I., GÓMEZ, L. Y., JOHAL, K. K., MENDOZA, G., MANCHA, H. & MÉNDEZ, J. 2001. Reactivity of blast-furnace slag in Portland cement blends hydrated under different conditions. *Cement and Concrete Research*, 31, 1403-1409.
- EVANS, N. D. M. 2008. Binding mechanisms of radionuclides to cement. *Cement and Concrete Research*, 38, 543-553.
- FAIRHALL, G., AMWACK, A., MACKRILL, P. & SULLIVAN, P. 1985. Blast furnace slag/ordinary portland cement formulation envelope studies.
- FAIRHALL, G. & PALMER, J. 1987. The evaluation of the properties of immobilised intermediate level wastes. *Radioact. Waste Manage. Nucl. Fuel Cycle*, 9, 51-69.
- FAUCON, P., ADENOT, F., JACQUINOT, J. F., PETIT, J. C., CABRILLAC, R. & JORDA, M. 1998. Long-term behaviour of cement pastes used for nuclear waste disposal: review of physico-chemical mechanisms of water degradation. *Cement and Concrete Research*, 28, 847-857.
- FENG, X., GARBOCZI, E. J., BENTZ, D. P., STUTZMAN, P. E. & MASON, T. O. 2004. Estimation of the degree of hydration of blended cement pastes by a scanning electron microscope point-counting procedure. *Cement and Concrete Research*, 34, 1787-1793.
- FU, Y.-F., WONG, Y.-L., POON, C.-S., TANG, C.-A. & LIN, P. 2004. Experimental study of micro/macro crack development and stress-strain relations of cement-based composite materials at elevated temperatures. *Cement and Concrete Research*, 34, 789-797.
- GALLÉ, C. 2001. Effect of drying on cement-based materials pore structure as identified by mercury intrusion porosimetry: A comparative study between oven-, vacuum-, and freeze-drying. *Cement and Concrete Research*, 31, 1467-1477.
- GALLUCCI, E., SCRIVENER, K., GROSO, A., STAMPANONI, M. & MARGARITONDO, G. 2007. 3D experimental investigation of the microstructure of cement pastes using synchrotron X-ray microtomography ( $\mu$ CT). *Cement and Concrete Research*, 37, 360-368.
- GARBOCZI, E. J. & BENTZ, D. P. 2001. The effect of statistical fluctuation, finite size error, and digital resolution on the phase percolation and transport properties of the NIST cement hydration model. *Cement and Concrete Research*, 31, 1501-1514.
- GARDNER, L. J., BERNAL, S. A., WALLING, S. A., CORKHILL, C. L., PROVIS, J. L. & HYATT, N. C. 2015. Characterisation of magnesium potassium phosphate cements blended with fly ash and ground granulated blast furnace slag. *Cement and Concrete Research*, 74, 78-87.
- GARTNER, E. M., YOUNG, J. F., DAMIDOT, D. A. & JAWED, I. 2002. Hydration of Portland Cement. *Structure and Performance of Cements, Second Edition*. London: Spon Press.

- GEIKER, M. 1983. *Studies of Portland cement hydration by measurements of chemical shrinkage and a systematic evaluation of hydration curves by means of the dispersion method*. Ph.D. Thesis, Technical University of Denmark.
- GEIKER, M. 2016. *Characterisation of development of cement hydration using chemical shrinkage*. *A Practical Guide to Microstructural Analysis of Cementitious Materials*, 75.
- GHATTAS, N. K., ESKANDER, S. B. & BAYOUMI, T. A. 1992. *Improved cement barriers applied in nuclear wastes*. *Cement and Concrete Research*, 22, 311-318.
- GLASSER, F. 1997. *Fundamental aspects of cement solidification and stabilisation*. *Journal of Hazardous Materials*, 52, 151-170.
- GLASSER, F. & ATKINS, M. 1994. *Cements in radioactive waste disposal*. *MRS Bulletin*, 19, 33-38.
- GLASSER, F., TYRER, M. & QUILLIN, K. 1999. *The chemistry of blended cements and backfills intended for use in radioactive waste disposal*. Environment Agency.
- GLASSER, F. P. 1992. *Progress in the immobilization of radioactive wastes in cement*. *Cement and Concrete Research*, 22, 201-216.
- GLASSER, F. P. 2001. *Mineralogical aspects of cement in radioactive waste disposal*. *Mineralogical Magazine*, 65, 621-633.
- GLASSER, F. P. 2011. 4 - *Application of inorganic cements to the conditioning and immobilisation of radioactive wastes*. In: OJOVAN, M. I. (ed.) *Handbook of Advanced Radioactive Waste Conditioning Technologies*. Woodhead Publishing.
- GLASSER, F. P. 2013. *Cements in Radioactive Waste Disposal*. IAEA.
- GLASSER, F. P., DIAMOND, S. & ROY, D. M. 1986. *Hydration Reactions in Cement Pastes Incorporating Fly Ash and Other Pozzolanic Materials*. *MRS Online Proceedings Library*, 85, null-null.
- GOGUEL, R. 1995. *A new consecutive dissolution method for the analysis of slag cements*. *Cement, Concrete and Aggregates*, 17, 84-91.
- GOLDSTEIN, J., NEWBURY, D. E., ECHLIN, P., JOY, D. C., ROMIG JR, A. D., LYMAN, C. E., FIORI, C. & LIFSHIN, E. 2012. *Scanning electron microscopy and X-ray microanalysis: a text for biologists, materials scientists, and geologists*, Springer Science & Business Media.
- GORCE, J.-P. & MILESTONE, N. B. 2007. *Probing the microstructure and water phases in composite cement blends*. *Cement and Concrete Research*, 37, 310-318.
- GORCE, J.-P., MILESTONE, N. B. & MCDONALD, P. J. *Probing the Water Phases and Microstructure in a Model Cement Blend Matrix used for the Encapsulation of Intermediate Level Nuclear Wastes*. *MRS Proceedings*, 2006. Cambridge Univ Press, 37.1.
- GOUGAR, M. L. D., SCHEETZ, B. E. & ROY, D. M. 1996. *Ettringite and C-S-H Portland cement phases for waste ion immobilization: A review*. *Waste Management*, 16, 295-303.
- GRUYAERT, E. 2011. *Effect of blast-furnace slag as cement replacement on hydration, microstructure, strength and durability of concrete*. Ph.D. Thesis, Ghent University.

GRUYAERT, E., ROBEYST, N. & DE BELIE, N. 2010. Study of the hydration of Portland cement blended with blast-furnace slag by calorimetry and thermogravimetry. *Journal of Thermal Analysis and Calorimetry*, 102, 941-951.

GÜNEYISI, E. & MERMERDAŞ, K. 2007. Comparative study on strength, sorptivity, and chloride ingress characteristics of air-cured and water-cured concretes modified with metakaolin. *Materials and Structures*, 40, 1161-1171.

GUTTERIDGE, W. A. & DALZIEL, J. A. 1990. Filler cement: The effect of the secondary component on the hydration of Portland cement: Part 2: Fine hydraulic binders. *Cement and Concrete Research*, 20, 853-861.

HALL, C. 1989. Water sorptivity of mortars and concretes: a review. *Magazine of Concrete Research*, 41, 51-61.

HANDOO, S., AGARWAL, S. & AGARWAL, S. 2002. Physicochemical, mineralogical, and morphological characteristics of concrete exposed to elevated temperatures. *Cement and Concrete Research*, 32, 1009-1018.

HARRISSON, A., WINTER, N. & TAYLOR, H. F. *Microstructure and microchemistry of slag cement pastes*. MRS Proceedings, 1986. Cambridge Univ Press, 213.

HEAFIELD, W. & FAIRHALL, G. 1987. *The conditioning and storage of intermediate level wastes in the UK*. RECOD 87.

HEARN, N. & HOOTON, R. D. 1992. Sample mass and dimension effects on mercury intrusion porosimetry results. *Cement and Concrete Research*, 22, 970-980.

HEARN, N. & MILLS, R. H. 1991. A simple permeameter for water or gas flow. *Cement and Concrete Research*, 21, 257-261.

HELFEN, L., DEHN, F., MIKULIK, P. & BAUMBACH, T. 2005. Three-dimensional imaging of cement microstructure evolution during hydration. *Advances in Cement Research*, 17, 103-111.

HEWLETT, P. 2003. *Lea's Chemistry of Cement and Concrete*, Elsevier Science.

HILL, J. & SHARP, J. 2002. The mineralogy and microstructure of three composite cements with high replacement levels. *Cement and Concrete Composites*, 24, 191-199.

HILL, J. & SHARP, J. *Incorporation of AlCl<sub>3</sub> and As<sub>2</sub>O<sub>3</sub> in Composite Cement Systems*. MRS Proceedings, 2003. Cambridge Univ Press, 353.

HILL, J. & SHARP, J. H. 2005. Encapsulation of Sn (II) and Sn (IV) chlorides in composite cements. *Journal of the American Ceramic Society*, 88, 560-565.

HILL, J., WHITTLE, B., SHARP, J. & HAYES, M. *Effect of Elevated Curing Temperature on Early Hydration and Microstructure of Composite Cements*. MRS Proceedings, 2002. Cambridge Univ Press, II10. 3.

HINRICHS, W. & ODLER, I. 1989. Investigation of the hydration of Portland blastfurnace slag cement: hydration kinetics. *Advances in Cement Research*, 2, 9-13.

HOLMAN, J. P. 1981. *Heat transfer*, New York, McGraw-Hill.

IAEA 2009. *Disposal Approaches for Long Lived Low and Intermediate Level Radioactive Waste*. Vienna, Austria.

IKEDA, S., NAKANO, T. & NAKASHIMA, Y. 2000. Three-dimensional study on the interconnection and shape of crystals in a graphic granite by X-ray CT and image analysis. *Mineralogical Magazine*, 64, 945-959.

INSTITUTE, B. S. 2011. *BS EN 197-1 Cement - Part I: Composition, Specifications and Conformity for Common Cements*. London: BSI.

JAWED, I., GOTO, S. & KONDO, R. 1976. Hydration of tetracalcium aluminoferrite in presence of lime and sulfates. *Cement and Concrete Research*, 6, 441-453.

JUENGER, M. C. G. & JENNINGS, H. M. 2001. The use of nitrogen adsorption to assess the microstructure of cement paste. *Cement and Concrete Research*, 31, 883-892.

JUENGER, M. C. G. & SIDDIQUE, R. 2015. Recent advances in understanding the role of supplementary cementitious materials in concrete. *Cement and Concrete Research*, 78, Part A, 71-80.

JUILLAND, P. 2009. *Early Hydration of Cementitious Systems*. Ph.D. Thesis, Ecole Polytechnique Federale De Lausanne.

JUILLAND, P., GALLUCCI, E., FLATT, R. & SCRIVENER, K. 2010. Dissolution theory applied to the induction period in alite hydration. *Cement and Concrete Research*, 40, 831-844.

KAMALI, S., GÉRARD, B. & MORANVILLE, M. 2003. Modelling the leaching kinetics of cement-based materials—influence of materials and environment. *Cement and Concrete Composites*, 25, 451-458.

KAUFMANN, J., LOSER, R. & LEEMANN, A. 2009. Analysis of cement-bonded materials by multi-cycle mercury intrusion and nitrogen sorption. *Journal of Colloid and interface Science*, 336, 730-7.

KIM, K. Y., YUN, T. S. & PARK, K. P. 2013. Evaluation of pore structures and cracking in cement paste exposed to elevated temperatures by X-ray computed tomography. *Cement and Concrete Research*, 50, 34-40.

KOCABA, V. 2010. *Development and Evaluation of Methods to Follow Microstructural Development of Cementitious Systems Including Slags*. Ph.D. Thesis, Ecole Polytechnique Federale De Lausanne.

KOCABA, V., GALLUCCI, E. & SCRIVENER, K. L. 2012. Methods for determination of degree of reaction of slag in blended cement pastes. *Cement and Concrete Research*, 42, 511-525.

KOLANI, B., BUFFO-LACARRIÈRE, L., SELIER, A., ESCADEILLAS, G., BOUTILLON, L. & LINGER, L. 2012. Hydration of slag-blended cements. *Cement and Concrete Composites*, 34, 1009-1018.

KORPA, A., KOWALD, T. & TRETTIN, R. 2008. Hydration behaviour, structure and morphology of hydration phases in advanced cement-based systems containing micro and nanoscale pozzolanic additives. *Cement and Concrete Research*, 38, 955-962.

KORPA, A. & TRETTIN, R. 2006. The influence of different drying methods on cement paste microstructures as reflected by gas adsorption: Comparison between freeze-drying (F-drying), D-drying, P-drying and oven-drying methods. *Cement and Concrete Research*, 36, 634-649.

LANG, E. 2002. Blastfurnace cements. In: BENSTED, J. & BARNES, P. (eds.) *Structure and Performance of Cements*. Second edition ed. New York: Taylor & Francis.

LE CHATELIER, H. 1905. *Experimental Researches on the Constitution of Hydraulic Mortars.*, New York, McGraw Publishing Company.

LE SAOÛT, G., KOCABA, V. & SCRIVENER, K. 2011. Application of the Rietveld method to the analysis of anhydrous cement. *Cement and Concrete Research*, 41, 133-148.

LOCKINGTON, D., PARLANGE, J.-Y. & DUX, P. 1999. Sorptivity and the estimation of water penetration into unsaturated concrete. *Materials and Structures*, 32, 342-347.

LOOSVELDT, H., LAFHAJ, Z. & SKOCZYLAS, F. 2002. Experimental study of gas and liquid permeability of a mortar. *Cement and Concrete Research*, 32, 1357-1363.

LOTHENBACH, B., LE SAOUT, G., BEN HAHHA, M., FIGI, R. & WIELAND, E. 2012. Hydration of a low-alkali CEM III/B-SiO<sub>2</sub> cement (LAC). *Cement and Concrete Research*, 42, 410-423.

LOTHENBACH, B., SCRIVENER, K. & HOOTON, R. D. 2011. Supplementary cementitious materials. *Cement and Concrete Research*, 41, 1244-1256.

LU, S., LANDIS, E. N. & KEANE, D. T. 2006. X-ray microtomographic studies of pore structure and permeability in Portland cement concrete. *Materials and Structures*, 39, 611-620.

LUKE, K. & GLASSER, F. P. 1987. Selective dissolution of hydrated blast furnace slag cements. *Cement and Concrete Research*, 17, 273-282.

LUMLEY, J. S., GOLLOP, R. S., MOIR, G. K. & TAYLOR, H. F. W. 1996. Degrees of reaction of the slag in some blends with Portland cements. *Cement and Concrete Research*, 26, 139-151.

MAIRE, E. & WITHERS, P. J. 2014. Quantitative X-ray tomography. *International Materials Reviews*, 59, 1-43.

MASSAZZA, F. 1998. 10 - Pozzolana and Pozzolanic Cements. In: HEWLETT, P. C. (ed.) *Lea's Chemistry of Cement and Concrete (Fourth Edition)*. Oxford: Butterworth-Heinemann.

MENDES, A., SANJAYAN, J. & COLLINS, F. 2008. Phase transformations and mechanical strength of OPC/Slag pastes submitted to high temperatures. *Materials and Structures*, 41, 345-350.

MENDES, A., SANJAYAN, J. G. & COLLINS, F. 2009. Long-term progressive deterioration following fire exposure of OPC versus slag blended cement pastes. *Materials and Structures*, 42, 95-101.

MENDES, A., SANJAYAN, J. G., GATES, W. P. & COLLINS, F. 2012. The influence of water absorption and porosity on the deterioration of cement paste and concrete exposed to elevated temperatures, as in a fire event. *Cement and Concrete Composites*, 34, 1067-1074.

MILESTONE, N. B., BAI, Y., BORGES, P. R., COLLIER, N. C., GORCE, J.-P., GORDON, L. E., SETIADI, A., UTTON, C. A. & ZHOU, Q. 2006. Reactions in cemented nuclear waste forms - The need for a toolbox of different cement types. In: VANISEGHEM, P. (ed.) *Scientific Basis for Nuclear Waste Management XXIX*.

MILLER, E. W. 2000. *BNFL Technical Specification for Ordinary Portland Cement (OPC), Ground Granulated Blastfurance Slag (BFS) and Pulverised Fuel Ash (PFA) Powders for use in the encapsulation/immobilisation of radioactive waste materials*. BNFL plc on behalf of Sellafield Ltd.

MOBASHER, N. 2015. *Ba (OH) 2-Na<sub>2</sub>SO<sub>4</sub>-BFS cement composites for the encapsulation of sulphate bearing nuclear waste*. University of Sheffield.

MONTEAGUDO, S. M., MORAGUES, A., GÁLVEZ, J. C., CASATI, M. J. & REYES, E. 2014. The degree of hydration assessment of blended cement pastes by differential thermal and thermogravimetric analysis. Morphological evolution of the solid phases. *Thermochimica Acta*, 592, 37-51.

MORANVILLE-REGOURD, M. 1998. 11 - Cements Made From Blastfurnace Slag. In: HEWLETT, P. C. (ed.) *Lea's Chemistry of Cement and Concrete (Fourth Edition)*. Oxford: Butterworth-Heinemann.

MORO, F. & BÖHNI, H. 2002. Ink-bottle effect in mercury intrusion porosimetry of cement-based materials. *J Colloid Interface Sci*, 246, 135-149.

MYERS, N., BERODIER, E. & SCRIVENER, K. L. 2011. *Nanocem internal study*. Unpublished.

MYERS, R. J. 2015. *Thermodynamic Modelling of CaO-Al<sub>2</sub>O<sub>3</sub>-SiO<sub>2</sub>-H<sub>2</sub>O-Based Cements*. Ph.D. Thesis, University of Sheffield.

NAKASHIMA, Y. & KAMIYA, S. 2007. Mathematica Programs for the Analysis of Three-Dimensional Pore Connectivity and Anisotropic Tortuosity of Porous Rocks using X-ray Computed Tomography Image Data. *Journal of Nuclear Science and Technology*, 44, 1233-1247.

NAKASHIMA, Y., KAMIYA, S. & NAKANO, T. 2008. Diffusion ellipsoids of anisotropic porous rocks calculated by X-ray computed tomography-based random walk simulations. *Water Resources Research*, 44, n/a-n/a.

NAKASHIMA, Y. & NAKANO, T. 2012. Steady-State Local Diffusive Fluxes in Porous Geo-Materials Obtained by Pore-Scale Simulations. *Transport in Porous Media*, 93, 657-673.

NAKASHIMA, Y., NAKANO, T., NAKAMURA, K., UESUGI, K., TSUCHIYAMA, A. & IKEDA, S. 2004. Three-dimensional diffusion of non-sorbing species in porous sandstone: computer simulation based on X-ray microtomography using synchrotron radiation. *Journal of Contaminant Hydrology*, 74, 253-264.

NAKASHIMA, Y. & WATANABE, Y. 2002. Estimate of transport properties of porous media by microfocus X-ray computed tomography and random walk simulation. *Water Resources Research*, 38, 12.

NDA 2010a. *The 2010 UK Radioactive Waste Inventory: Main Report*.

NDA 2010b. *Geological Disposal Steps Towards Implementation*.

NDA 2010c. *Geological Disposal: Waste package accident performance status report*.

NDA 2013a. *2013 UK Radioactive Waste Inventory - A Summary of the 2013 Inventory*.

NDA 2013b. *2013 UK Radioactive Waste Inventory - Radioactive Waste Composition*.

NDA 2013c. *2013 UK Radioactive Waste Inventory - Radioactivity Content of Wastes*.

NDA 2013d. *2013 UK Radioactive Waste Inventory - Scope and Conventions*.

NDA 2015. *An Overview of NDA Higher Activity Wastes*.

NDA 2016a. *Nuclear Decommissioning Authority: Strategy (effective from April 2016)*. Cumbria.

NDA. 2016b. *UK Radioactive Waste Inventory* [Online]. <https://ukinventory.nda.gov.uk/about-radioactive-waste/how-do-we-manage-radioactive-waste/high-level-waste/>. [Accessed 10-05 2016].

NEVILLE, A. M. 1997. *Properties of Concrete*, New York, Wiley.

OCHS, M., MALLANTS, D. & WANG, L. 2015. *Radionuclide and Metal Sorption on Cement and Concrete*, Springer.

ODLER, I. 2003. The BET-specific surface area of hydrated Portland cement and related materials. *Cement and Concrete Research*, 33, 2049-2056.

OGAWA, K., UCHIKAWA, H., TAKEMOTO, K. & YASUI, I. 1980. The mechanism of the hydration in the system C3S-pozzolana. *Cement and Concrete Research*, 10, 683-696.

OGIRIGBO, O. R. 2016. *Influence of Slag Composition and Temperature on the Hydration and Performance of Slag Blends in Chloride Environments*. University of Leeds.

PAGE, C., SHORT, N. & EL TARRAS, A. 1981. Diffusion of chloride ions in hardened cement pastes. *Cement and Concrete Research*, 11, 395-406.

PALMER, J. D. & FAIRHALL, G. A. 1992. *Properties of Cement Systems Containing Intermediate Level Wastes*. *Cement and Concrete Research*, 22, 325-330.

PANE, I. & HANSEN, W. 2005. Investigation of blended cement hydration by isothermal calorimetry and thermal analysis. *Cement and Concrete Research*, 35, 1155-1164.

PAPADAKIS, V. G. 2000. Effect of supplementary cementing materials on concrete resistance against carbonation and chloride ingress. *Cement and Concrete Research*, 30, 291-299.

PATEL, H. H., PRATT, P. L. & PARROTT, L. J. 1988. Porosity In The Microstructure Of Blended Cements Containing Fly Ash. *MRS Online Proceedings Library Archive*, 137, null-null.

PENG, G.-F. & HUANG, Z.-S. 2008. Change in microstructure of hardened cement paste subjected to elevated temperatures. *Construction and Building Materials*, 22, 593-599.

POON, C. S., CLARK, A. I., PERRY, R., BARKER, A. P. & BARNES, P. 1986. Permeability study on the cement based solidification process for the disposal of hazardous wastes. *Cement and Concrete Research*, 16, 161-172.

POWERS, T. 1935. Absorption of Water by Portland Cement Paste during the Hardening Process. *Industrial & Engineering Chemistry*, 27, 790-794.

PROMENTILLA, M., SUGIYAMA, T., HITOMI, T. & TAKEDA, N. Studies on pore structure characterization in hydrated cement system based on 3D micro-geometry technique. *Proceedings of the JCI symposium on Durability Mechanics, Tokyo, Japan, 2007*.

PROMENTILLA, M. A. B., CORTEZ, S. M., PAPEL, R. A. D., TABLADA, B. M. & SUGIYAMA, T. 2016. Evaluation of Microstructure and Transport Properties of Deteriorated Cementitious Materials from Their X-ray Computed Tomography (CT) Images. *Materials*, 9, 388.

PROMENTILLA, M. A. B. & SUGIYAMA, T. 2010. X-ray microtomography of mortars exposed to freezing-thawing action. *Journal of Advanced Concrete Technology*, 8, 97-111.

PROMENTILLA, M. A. B., SUGIYAMA, T., HITOMI, T. & TAKEDA, N. 2008. Characterizing the 3D pore structure of hardened cement paste with synchrotron microtomography. *Journal of Advanced Concrete Technology*, 6, 273-286.

PROMENTILLA, M. A. B., SUGIYAMA, T., HITOMI, T. & TAKEDA, N. 2009. Quantification of tortuosity in hardened cement pastes using synchrotron-based X-ray computed microtomography. *Cement and Concrete Research*, 39, 548-557.

PROVIS, J. L., MYERS, R. J., WHITE, C. E., ROSE, V. & VAN DEVENTER, J. S. J. 2012. X-ray microtomography shows pore structure and tortuosity in alkali-activated binders. *Cement and Concrete Research*, 42, 855-864.

PROVIS, J. L. & VAN DEVENTER, J. S. J. 2009. *Geopolymers: structures, processing, properties and industrial applications*, Elsevier.

PURNELL, P. & BLACK, L. 2012. Embodied carbon dioxide in concrete: Variation with common mix design parameters. *Cement and Concrete Research*, 42, 874-877.

RARICK, R. L., BHATTY, J. I. & JENNINGS, H. M. 1995. Surface area measurement using gas sorption: application to cement paste. *Material Science of Concrete IV*, American Ceramic Society, 1-41.

REY, F., FORNES, V. & ROJO, J. M. 1992. Thermal decomposition of hydrotalcites. An infrared and nuclear magnetic resonance spectroscopic study. *Journal of the Chemical Society, Faraday Transactions*, 88, 2233-2238.

RICHARDSON, I. & GROVES, G. 1992. Microstructure and microanalysis of hardened cement pastes involving ground granulated blast-furnace slag. *Journal of Materials Science*, 27, 6204-6212.

RICHARDSON, I. & GROVES, G. 1997. The structure of the calcium silicate hydrate phases present in hardened pastes of white Portland cement/blast-furnace slag blends. *Journal of Materials Science*, 32, 4793-4802.

RICHARDSON, I., WILDING, C. & DICKSON, M. 1989. The hydration of blastfurnace slag cements. *Advances in Cement Research*, 2, 147-157.

RICHARDSON, I. G. 1999. The nature of C-S-H in hardened cements. *Cement and Concrete Research*, 29, 1131-1147.

RICHARDSON, I. G. 2000. The nature of the hydration products in hardened cement pastes. *Cement and Concrete Composites*, 22, 97-113.

RICHARDSON, I. G. 2008. The calcium silicate hydrates. *Cement and Concrete Research*, 38, 137-158.

RICHARDSON, I. G., BROUGH, A. R., BRYDSON, R., GROVES, G. W. & DOBSON, C. M. 1993. Location of Aluminum in Substituted Calcium Silicate Hydrate (C-S-H) Gels as Determined by  $^{29}\text{Si}$  and  $^{27}\text{Al}$  NMR and EELS. *Journal of the American Ceramic Society*, 76, 2285-2288.

RICHARDSON, J. M., BIERNACKI, J. J., STUTZMAN, P. E. & BENTZ, D. P. 2002. Stoichiometry of slag hydration with calcium hydroxide. *J. Am. Ceram. Soc.*, 85, 947-953.

RIETVELD, H. M. 1969. A profile refinement method for nuclear and magnetic structures. *Journal of Applied Crystallography*, 2, 65-71.

ROSSEN, J. E. 2014. *Composition and morphology of C-A-S-H in pastes of alite and cement blended with supplementary cementitious materials*. Ph.D. Thesis, Ecole Polytechnique Federale de Lausanne.

- ROY, S., POH, K. & NORTHWOOD, D. 1999. *Durability of concrete—accelerated carbonation and weathering studies. Building and environment*, 34, 597-606.
- SAITO, H. & DEGUCHI, A. 2000. *Leaching tests on different mortars using accelerated electrochemical method. Cement and Concrete Research*, 30, 1815-1825.
- SAITO, H., NAKANE, S., IKARI, S. & FUJIWARA, A. 1992. *Preliminary experimental study on the deterioration of cementitious materials by an acceleration method. Nuclear Engineering and Design*, 138, 151-155.
- SCARLETT, N. V. Y. & MADSEN, I. C. 2006. *Quantification of phases with partial or no known crystal structures. Powder Diffraction*, 21, 278-284.
- SCRIVENER, K., SNELLINGS, R. & LOTHENBACH, B. 2016. *A Practical Guide to Microstructural Analysis of Cementitious Materials*, CRC Press.
- SCRIVENER, K. L. 2004. *Backscattered electron imaging of cementitious microstructures: understanding and quantification. Cement and Concrete Composites*, 26, 935-945.
- SCRIVENER, K. L., FÜLLMANN, T., GALLUCCI, E., WALENTA, G. & BERMEJO, E. 2004. *Quantitative study of Portland cement hydration by X-ray diffraction/Rietveld analysis and independent methods. Cement and Concrete Research*, 34, 1541-1547.
- SCRIVENER, K. L., JUILLAND, P. & MONTEIRO, P. J. M. 2015a. *Advances in understanding hydration of Portland cement. Cement and Concrete Research*, 78, Part A, 38-56.
- SCRIVENER, K. L., LOTHENBACH, B., DE BELIE, N., GRUYAERT, E., SKIBSTED, J., SNELLINGS, R. & VOLLPRACHT, A. 2015b. *TC 238-SCM: hydration and microstructure of concrete with SCMs. Materials and Structures*, 48, 835-862.
- SCRIVENER, K. L. & NONAT, A. 2011. *Hydration of cementitious materials, present and future. Cement and Concrete Research*, 41, 651-665.
- SCRIVENER, K. L., PATEL, H. H., PRATT, P. L. & PARROTT, L. J. 1987. *Analysis of Phases in cement Paste Using Backscattered Electron Images, Methanol Absorption and Thermogravimetric Analysis. Materials Research Society Symposium Proceedings*, 85, 67-76.
- SETIADI, A., HILL, J. & MILESTONE, N. B. 2006a. *Corrosion of metals in composite cements. PhD thesis, University of Sheffield, UK.*
- SETIADI, A., MILESTONE, N. B., HILL, J. & HAYES, M. 2006b. *Corrosion of aluminium and magnesium in BFS composite cements. Advances in Applied Ceramics*, 105, 191-196.
- SHARP, J., HILL, J., MILESTONE, N. & MILLER, E. *Cementitious Systems for Encapsulation of Intermediate Level Waste. ASME 2003 9th International Conference on Radioactive Waste Management and Environmental Remediation, 2003. American Society of Mechanical Engineers*, 1425-1433.
- SHORT, N., PURKISS, J. & GUISE, S. 2001. *Assessment of fire damaged concrete using colour image analysis. Construction and Building Materials*, 15, 9-15.
- SINGH, N., SARVAHI, R., SINGH, N. & SHUKLA, A. 1994. *Effect of temperature on the hydration of ordinary Portland cement in the presence of a superplasticizer. Thermochemica Acta*, 247, 381-388.

SKIBSTED, J. R., ANDERSEN, M. D. & JAKOBSEN, H. J. R. 2007. Applications of solid-state Nuclear Magnetic Resonance (NMR) in studies of Portland cements-based materials. *Zement Kalk Gips*.

SNELLINGS, R., BAZZONI, A. & SCRIVENER, K. 2014a. The existence of amorphous phase in Portland cements: Physical factors affecting Rietveld quantitative phase analysis. *Cement and Concrete Research*, 59, 139-146.

SNELLINGS, R., SALZE, A. & SCRIVENER, K. L. 2014b. Use of X-ray diffraction to quantify amorphous supplementary cementitious materials in anhydrous and hydrated blended cements. *Cement and Concrete Research*, 64, 89-98.

SNOECK, D., VELASCO, L. F., MIGNON, A., VAN VLIERBERGHE, S., DUBRUEL, P., LODEWYCKX, P. & DE BELIE, N. 2014. The influence of different drying techniques on the water sorption properties of cement-based materials. *Cement and Concrete Research*, 64, 54-62.

STAUFFER, D. & AHARONY, A. 1994. *Introduction to percolation theory*, CRC press.

STOCK, S. R. 2008a. *Fundamentals. MicroComputed Tomography*. CRC Press.

STOCK, S. R. 2008b. *MicroComputed Tomography: Methodology and Applications*, CRC Press.

SUGIYAMA, T., PROMENTILLA, M., HITOMI, T. & TAKEDA, N. 2010a. Application of synchrotron microtomography for pore structure characterization of deteriorated cementitious materials due to leaching. *Cement and Concrete Research*, 40, 1265-1270.

SUGIYAMA, T., PROMENTILLA, M. A. B., HITOMI, T. & TAKEDA, N. 2010b. Application of synchrotron microtomography for pore structure characterization of deteriorated cementitious materials due to leaching. *Cement and Concrete Research*, 40, 1265-1270.

TAN, Z., DE SCHUTTER, G., YE, G., GAO, Y. & MACHIELS, L. 2014. Influence of particle size on the early hydration of slag particle activated by Ca(OH)<sub>2</sub> solution. *Construction and Building Materials*, 52, 488-493.

TASDEMIR, C. 2003. Combined effects of mineral admixtures and curing conditions on the sorptivity coefficient of concrete. *Cement and Concrete Research*, 33, 1637-1642.

TAYLOR, H. F., MOHAN, K. & MOIR, G. 1985a. Analytical study of pure and extended Portland cement pastes: I, pure Portland cement pastes. *Journal of the American Ceramic Society*, 68, 680-685.

TAYLOR, H. F., MOHAN, K. & MOIR, G. 1985b. Analytical Study of Pure and Extended Portland Cement Pastes: II, Fly Ash-and Slag-Cement Pastes. *Journal of the American Ceramic Society*, 68, 685-690.

TAYLOR, H. F. W. 1997. *Cement Chemistry*, Thomas Telford.

TAYLOR, R., RICHARDSON, I. G. & BRYDSON, R. M. D. 2007. Nature of C-S-H in 20 year old neat ordinary Portland cement and 10% Portland cement-90% ground granulated blast furnace slag pastes. *Advances in Applied Ceramics*, 106, 294-301.

TAYLOR, R., RICHARDSON, I. G. & BRYDSON, R. M. D. 2010. Composition and microstructure of 20-year-old ordinary Portland cement-ground granulated blast-furnace slag blends containing 0 to 100% slag. *Cement and Concrete Research*, 40, 971-983.

TODD, S. S. 1951. *Low-temperature Heat Capacities and Entropies at 298.16°K. of Crystalline Calcium Orthosilicate, Zinc Orthosilicate and Tricalcium Silicate. Journal of the American Chemical Society*, 73, 3277-3278.

U S GEOLOGICAL SURVEY. 2016. *Mineral Commodity Summaries 2016 [Online]. Reston, Virginia. [Accessed 26 April 2016].*

UTTON, C. A. 2006. *The encapsulation of a BaCO<sub>3</sub> waste in composite cement. Ph.D. Thesis, University of Sheffield.*

UTTON, C. A., GALLUCCI, E., HILL, J. & MILESTONE, N. B. 2011. *Interaction between BaCO<sub>3</sub> and OPC/BFS composite cements at 20°C and 60°C. Cement and Concrete Research*, 41, 236-243.

UTTON, C. A. & GODFREY, I. H. 2010. *Review of stability of cemented grouted ion exchange materials, sludges and flocs. Prepared for and on behalf of NDA RWMD.*

UTTON, C. A., HAYES, M., HILL, J., MILESTONE, N. B. & SHARP, J. H. 2008. *Effect of Temperatures up to 90°C on the Early Hydration of Portland–Blastfurnace Slag Cements. Journal of the American Ceramic Society*, 91, 948-954.

UTTON, C. A., MILESTONE, N. B. & HILL, J. 2003. *The Effect of Simulated Barium Carbonate Waste Stream on the Hydration of Composite Cement Systems. Cement and Concrete Science. Leeds.*

VAN DEVENTER, J. S. J., PROVIS, J. L. & DUXSON, P. 2012. *Technical and commercial progress in the adoption of geopolymer cement. Minerals Engineering*, 29, 89-104.

WADSÖ, L. 2010. *Operational issues in isothermal calorimetry. Cement and Concrete Research*, 40, 1129-1137.

WADSÖ, L. & ARNDT, M. 2016. *An international round robin test on isothermal (conduction) calorimetry for measurement of three-day heat of hydration of cement. Cement and Concrete Research*, 79, 316-322.

WALLING, S. A., KINOSHITA, H., BERNAL, S. A., COLLIER, N. C. & PROVIS, J. L. 2015. *Structure and properties of binder gels formed in the system Mg (OH) 2–SiO 2–H 2 O for immobilisation of Magnox sludge. Dalton Transactions*, 44, 8126-8137.

WANG, H. 2008. *The effects of elevated temperature on cement paste containing GGBFS. Cement and Concrete Composites*, 30, 992-999.

WATANABE, Y. & NAKASHIMA, Y. 2002. *RW3D.m: three-dimensional random walk program for the calculation of the diffusivities in porous media. Computers & Geosciences*, 28, 583-586.

WHITTAKER, M. 2014. *The Impact of Slag Composition on the microstructure of Composite Slag Cements Exposed to Sulfate Attack. Ph.D. Thesis, University of Leeds.*

WHITTAKER, M., ZAJAC, M., BEN HABA, M., BULLERJAHN, F. & BLACK, L. 2014. *The role of the alumina content of slag, plus the presence of additional sulfate on the hydration and microstructure of Portland cement-slag blends. Cement and Concrete Research*, 66, 91-101.

WIELAND, E., VAN LOON, L. R. & ENERGY, N. 2003. *Cementitious near-field sorption data base for performance assessment of an ILW repository in Opalinus Clay, Paul Scherrer Institut Villigen, Switzerland.*

WILDING, C. R. 1992. *The performance of cement based systems. Cement and Concrete Research*, 22, 299-310.

WILLIAMS, R. P., HART, R. D. & VAN RIESSEN, A. 2011. *Quantification of the Extent of Reaction of Metakaolin-Based Geopolymers Using X-Ray Diffraction, Scanning Electron Microscopy, and Energy-Dispersive Spectroscopy. Journal of the American Ceramic Society*, 94, 2663-2670.

WILLIS, K. L., ABELL, A. B. & LANGE, D. A. 1998. *Image-based characterization of cement pore structure using wood's metal intrusion. Cement and Concrete Research*, 28, 1695-1705.

WINSLOW, D. & DIAMOND, S. 1969. *A mercury porosimetry study of the evolution of porosity in Portland cement: technical publication.*

WINSLOW, D. N. 1984. *Advances in experimental techniques for mercury intrusion porosimetry. Surface and Colloid Science. Springer.*

WINSLOW, D. N., COHEN, M. D., BENTZ, D. P., SNYDER, K. A. & GARBOCZI, E. J. 1994. *Percolation and pore structure in mortars and concrete. Cement and Concrete Research*, 24, 25-37.

WONG, H. S., ZOBEL, M., BUENFELD, N. R. & ZIMMERMAN, R. W. 2009. *Influence of the interfacial transition zone and microcracking on the diffusivity, permeability and sorptivity of cement-based materials after drying. Magazine of Concrete Research*, 61, 571-589.

YANG, R., GUI, Q., LEMARCHAND, E., FEN-CHONG, T. & LI, K. 2015. *Micromechanical Modeling of Transport Properties of Cement-Based Composites: Role of Interfacial Transition Zone and Air Voids. Transport in Porous Media*, 110, 591-611.

ZHANG, J. & SCHERER, G. W. 2011. *Comparison of methods for arresting hydration of cement. Cement and Concrete Research*, 41, 1024-1036.

ZHANG, L. & GLASSER, F. P. 2000. *Critical examination of drying damage to cement pastes. Advances in Cement Research*, 12, 79-88.

ZHANG, M., HE, Y., YE, G., LANGE, D. A. & BREUGEL, K. V. 2012. *Computational investigation on mass diffusivity in Portland cement paste based on X-ray computed microtomography ( $\mu$ CT) image. Construction and Building Materials*, 27, 472-481.

ZHOU, J., YE, G. & VAN BREUGEL, K. 2010. *Characterization of pore structure in cement-based materials using pressurization–depressurization cycling mercury intrusion porosimetry (PDC-MIP). Cement and Concrete Research*, 40, 1120-1128.